

Mutations, post-translational modifications, and small molecule binding to the  
cardiac troponin complex alter cardiac contractile function

by

Zabed Mahmud

A thesis submitted in partial fulfillment of the requirements for the degree of  
Doctor of Philosophy

Department of Biochemistry  
University of Alberta

## **ABSTRACT**

Ischemic heart disease is the leading cause of death worldwide. It can lead to acute myocardial infarction, commonly known as a “heart attack”, in which heart muscle dies due to disruption of its oxygen and blood supply. Even if patients survive a heart attack and receive the best medical therapy possible, many go on to develop systolic heart failure, in which the heart muscle becomes progressively weaker and more dilated, impairing its ability to pump enough blood to satisfy the needs of the body. It is important to understand how the heart regulates its pumping activity, how it becomes dysregulated in ischemic heart disease and heart failure, and how this might be corrected through novel medical therapies.

Cardiac muscle contraction is turned on and off in a calcium dependent manner through the cardiac troponin complex, which is comprised of three subunits: troponin C (cTnC), troponin I (cTnI) and troponin T (cTnT). cTnI has a C-terminal tail (residues 135-209) that binds to the actin-tropomyosin thin filament to maintain it in a blocked state under low calcium resting conditions. During systole, calcium ions flood the cytoplasm and activate the N-terminal domain of cTnC (cNTnC), allowing it to bind to the switch region of cTnI (residues 146-158), releasing inhibition of cTnI and allowing actin-myosin cross-bridging and muscle contraction to proceed.

cTnI is known to be cleaved in ischemia-reperfusion (I/R) injury. We demonstrate that it remains susceptible to proteolysis even while bound to actin or cTnC. Using *in vitro* proteolysis and mass spectrometry, we demonstrate that the switch region of cTnI is cleaved by matrix metalloproteinase-2 (MMP-2) and calpain, two intracellular proteases implicated in I/R injury. Cleavage in this essential region could account for myocardial stunning, a phenomenon whereby contraction is temporarily depressed in living and apparently structurally intact cardiac muscle.

Physiologic regulation of human cardiac troponin activation occurs via phosphorylation of the cardiac-specific N-terminal tail of cTnI (residues 1-32). Using solution NMR spectroscopy, we

demonstrate that this N-terminal tail interacts with the cNTnC to fix it to the active orientation needed to bind the switch region of cTnI. Phosphorylation of the N-terminal tail disrupts this orientation, as do some mutations in cTnC and cTnI associated with dilated cardiomyopathy. By reconstituting the cardiac troponin complex without the activating N- and C-terminal tails of cTnI, we demonstrate the presence of an alternative “dormant” orientation of the cNTnC domain that competes with its active orientation.

Finally, we have developed RPI-194, a novel small molecule cardiac troponin activator. Using NMR and fluorescence spectroscopy, we demonstrate that it stabilizes the activated calcium-bound complex between cNTnC and cTnI. Moreover, RPI-194 acts as a calcium sensitizer in cardiac muscle, as well as in slow skeletal and fast skeletal muscle fibers. However, it appears to slow down unloaded contraction in muscle fibers as well as in individual mouse cardiomyocytes. In isolated perfused mouse heart, RPI-194 increases cardiac work.

In summary, cardiac function is carefully regulated at the level of the cardiac troponin complex, but can be disrupted by proteolysis or cardiomyopathy-causing mutations. An exciting possibility is the development of drugs to powerfully modulate troponin activity in order to correct cardiac contractile function in disease states.

## PREFACE

A portion of Chapter 1 has been published as: Mahmud, Z. & Hwang, P.M. Cardiac troponin complex: cardiac troponin C (TNNC1), cardiac troponin I (TNNI3), and cardiac troponin T (TNNT2). *Encyclopedia of Signaling Molecules, 2nd Edition. S. Choi (ed.)*.692-701 (2018).

Contributions of authors in chapter 1: Z. Mahmud and P.M. Hwang wrote the original manuscript.

Chapter 2 has been published as: Mahmud, Z., Zahran, S., Liu, P. B., Reiz, B. Chan, B. Y. H. Roczkowsky, A. McCartney, C. E. Davies, P. L. Li, L. Schulz, R. Hwang, P. M. Structure and proteolytic susceptibility of the inhibitory C-terminal tail of cardiac troponin I. *Biochim Biophys Acta Gen Subj* 1863, 661-671 (2019).

Some of the research conducted for chapter 2 forms part of a research collaboration, led by Dr. Peter M. Hwang at the University of Alberta with Dr. Peter L. Davies (Queen's University), Dr. Liang Li (University of Alberta), and Dr. Richard Schulz (University of Alberta).

Contributions of authors in chapter 2: Z. Mahmud and S. Zahran equally contributed to this work. Z. Mahmud did protein expression and purification, *in vitro* proteolysis, NMR and mass spectrometry data analysis, and wrote the original manuscript. S. Zahran did protein expression and purification, NMR data acquisition, and wrote the original manuscript. P.B. Liu did protein expression and purification. B. Reiz did the mass spectrometry data collection. B.Y.H Chan and A. Roczkowsky were involved in developing MMP-2 *in vitro* proteolysis protocol. C.E. McCartney purified recombinant calpain. P. L. Davies provided recombinant calpain, expertise in calpain-mediated proteolysis and reviewed the manuscript. L. Li provided mass spectrometry facility and reviewed the manuscript. R. Schulz was involved in conceptualization, expertise in

MMP-2 mediated proteolysis, supervision, and reviewed the manuscript. P.M. Hwang was involved in conceptualization, funding acquisition, supervision, writing and reviewing the manuscript.

Chapter 3 has been published as: Mahmud, Z., Dhimi, P.S., Rans, C., Liu, P.B. & Hwang, P.M. Dilated cardiomyopathy mutations and phosphorylation disrupt the active orientation of cardiac troponin C. *J Mol Biol* 433, 167010 (2021).

Contributions of authors in chapter 3: Z. Mahmud did protein expression and purification, NMR data acquisition, analysis, and wrote the original manuscript. P.S. Dhimi and C. Rans were involved in NMR data acquisition and analysis. P. B. Liu did protein expression and purification. P.M. Hwang was involved in conceptualization, funding acquisition, NMR data acquisition and analysis, supervision, writing, and reviewing the manuscript.

Chapter 4 will be submitted for publication as: Mahmud, Z., Tikunova, S., Belevych, N., Wagg, C.S., Zhabyeyev, P., Liu, P.B, Rasicci, D.V., Yengo, C.M., Oudit, G.Y., Lopaschuk, G.D., Reiser, P.J., Davis, J.P., and Hwang, P.M. Small molecule RPI-194 stabilizes activated troponin to increase the calcium sensitivity of striated muscle contraction.

Some of the research conducted for chapter 4 forms part of a research collaboration, led by Dr. Peter M. Hwang at the University of Alberta with Dr. Gary D. Lopaschuk (University of Alberta), Dr. Gavin Y. Oudit (University of Alberta), Dr. Peter J. Reiser (The Ohio State University), Dr. Christopher M. Yengo (Pennsylvania State University) and Dr. Jonathan P. Davis (The Ohio State University). The research project, which is part of this thesis, received research ethics approval from the University of Alberta Research Ethics Board, Dr. Gary D. Lopaschuk, “Protection of the ischemic myocardium and breeding colony”, AUP00000288, September 3,

2021, Dr. Gavin Y. Oudit “Cardiac response to pressure overload”, AUP00000306, April 4, 2019, and from The Ohio State University Institutional Animal Care and Use Committee, Dr. Jonathan P. Davis, “Therapeutic interventions for cardiovascular function”, 2013A00000037-R2, May 20, 2019.

Contributions of authors in chapter 4: Z. Mahmud did protein expression and purification, NMR and steady state fluorescence spectroscopy data acquisition and analysis, screening drug compounds, and wrote the original manuscript. S. Tikunova, and J.P. Davis did stopped flow fluorescence data acquisition and analysis and reviewed the manuscript. N. Belevych tested compounds in skinned muscle fibers and trabeculae. C.S. Wagg tested compounds in the isolated perfused mouse hearts. P. Zhabyeyev tested compounds in isolated single cardiomyocytes. P.B. Liu expressed and purified proteins. D.V. Rasicci tested compounds using the myosin ATPase assay. C.M. Yengo, G.Y. Oudit, G.D. Lopaschuk and P.J. Reiser provided their lab facilities, and reviewed the manuscript. P.M. Hwang was involved in conceptualization, funding acquisition, supervision, writing, and reviewing the manuscript.

## **DEDICATION**

*Dedicated with love and affection to my family*

## ACKNOWLEDGEMENTS

Above all, I am grateful to my Almighty Allah for everything in this life, happiness, sorrows, sufferings, and blessings. I seek his forgiveness and help to be an honest, compassionate, and good human being.

First and foremost, I would like to thank my supervisor, Dr. Peter Hwang, for his mentorship, guidance, friendship, and kindness throughout my PhD program. In the last six years, you shaped me as a researcher. You spent countless hours helping me understand my projects, analyse NMR data, teach me the basics of NMR, prepare me for presentations, and hear me out when I was in trouble both in my academic and personal life. I am grateful for your unconditional support that helped me get through this long PhD journey. I cherish all the moments we have had together such as our Friday lunches, yearly golf, and the Banff and Dublin conferences. I will never forget those memories. I will miss you. Thank you, Peter.

I want to thank my co-supervisor Dr. Richard Schulz, for being always there for me. You are a great teacher and an amazing person. You are my source of inspiration. You and your lab accepted me with an open heart, and now I have a life-long relationship with that place. Your patience and advice were crucial to my successful scholarship application and accepted manuscripts. I have so many memorable moments with you that I will never forget. Thank you, Rick.

Many thanks to my supervisory committee member Dr. Olivier Julien, for your valuable suggestions and comments on my projects during the committee meeting and PhD candidacy exam.



Thank you to the members of Hwang and Schulz labs for being amazing lab mates and friends. Dan, thank you for being my best friend. Because of you, my lab life was so enjoyable. You helped me, supported me when I was in distress, and you celebrated with me when I had good news. Phil, thank you so much for your patience and help while teaching me protein purification and other lab techniques. You taught me most of the basics of lab work that I needed to learn to run my projects. You inspired me to think rationally and how to tackle difficult situations. Thank you, Phil.

Thank you to the Department of Biochemistry for giving me an opportunity to make my dream come true. Throughout the time in my PhD program, I met amazing and kind-hearted people in this department. I will miss this place.

I could not say enough to thank my lovely wife and sweetheart, Mimi. You sacrificed a lot for me. You are living far away from your family, and you are not able to see them in the last four years. Your love and care helped me to get through difficulties in my life. Thank you, Mimi, for your love, affection, and patience. Most importantly, you give me the biggest present of my life, our son, Faiyaz.

Nothing is enough to say how grateful I am to my parents. They gave their everything just to ensure I have a better life. It would not be possible where I am now without them. Thank you, Baba and Ma! Thank you, my sister, Mahmuda and brother, Nabed for believing in me and always being there for me.

Last but not least, the most important person in my life, my son Faiyaz. Of all the countless blessings in my life, Faiyaz is the biggest one. When I see him, hold him, I forget every problem, stress, or deadline in my life. Thank you for spreading joy in my life.

## TABLE OF CONTENTS

ABSTRACT.....	ii
PREFACE.....	iv
DEDICATION.....	vii
ACKNOWLEDGEMENTS.....	viii
TABLE OF CONTENTS.....	x
LIST OF FIGURES.....	xiv
LIST OF TABLES.....	xvii
LIST OF APPENDICES.....	xvii
LIST OF ABBREVIATIONS.....	xviii
<b>CHAPTER 1: INTRODUCTION.....</b>	<b>1</b>
1.1    Introduction to the cardiac troponin complex.....	2
1.2    The sarcomere and the troponin complex.....	3
1.3    Structure and function of the cardiac troponin complex.....	6
1.3.1    Structure and function of cardiac troponin C.....	6
1.3.2    Structure and function of cardiac troponin I.....	8
1.3.3    Structure and function of cardiac troponin T.....	11
1.3.4    Post-translational modifications of cTnI regulate troponin activity.....	13
1.4    Troponin C and I in cardiac diseases.....	14
1.4.1    Heritable cardiomyopathies.....	14
1.4.2    Myocardial ischemia-reperfusion injury.....	17
1.4.3    Systolic heart failure.....	25
1.5    Biophysical studies of the troponin complex.....	36
1.5.1    NMR techniques used in this study.....	39
1.6    Thesis hypothesis.....	40

1.7	Objectives .....	40
1.7.1	Chapter 2: Structure and proteolytic susceptibility of the inhibitory C-terminal tail of cardiac troponin I .....	40
1.7.2	Chapter 3: Dilated cardiomyopathy mutations and phosphorylation disrupt the active orientation of cardiac troponin C .....	41
1.7.3	Chapter 3: Small molecule RPI-194 stabilizes activated troponin to increase the calcium sensitivity of striated muscle contraction .....	41
<b>CHAPTER 2: STRUCTURE AND PROTEOLYTIC SUSCEPTIBILITY OF THE INHIBITORY C-TERMINAL TAIL OF CARDIAC TROPONIN I .....</b>		<b>42</b>
2.1	Introduction .....	43
2.2	Materials and methods.....	46
2.2.1	Protein expression and purification .....	46
2.2.2	NMR Spectroscopy.....	46
2.2.3	SDS-PAGE analysis of <i>in vitro</i> proteolysis .....	48
2.2.4	Mass spectrometric analysis of <i>in vitro</i> proteolysis.....	49
2.3	Results .....	51
2.3.1	Structure of free cTnI <sub>135-209</sub> by NMR spectroscopy .....	51
2.3.2	Partial structuring of cTnI <sub>135-209</sub> in the presence of monomeric actin-DNase I .....	54
2.3.3	<i>In vitro</i> proteolysis of cTnI by MMP-2 and calpain-2 .....	57
2.3.4	Mass spectrometric identification of MMP-2 cleavage sites of cTnI .....	58
2.3.5	Mass spectrometric identification of calpain-2 cleavage sites of cTnI.....	61
2.3.6	<i>In vitro</i> proteolysis of cTnI <sub>1-77</sub> in the presence of cTnC .....	63
2.3.7	<i>In vitro</i> proteolysis of cTnI <sub>135-209</sub> in the presence of cTnC .....	65
2.3.8	<i>In vitro</i> proteolysis of cTnI <sub>135-209</sub> in the presence of actin .....	66
2.4	Discussion .....	68

<b>CHAPTER 3: DILATED CARDIOMYOPATHY MUTATIONS AND PHOSPHORYLATION DISRUPT THE ACTIVE ORIENTATION OF CARDIAC TROPONIN C</b> .....		72
3.1	Introduction .....	73
3.1	Materials and methods.....	79
3.1.1	Production and purification of cTnC wild type and mutant constructs .....	79
3.1.2	Production and purification of wild type and mutant cTnI <sub>1-77</sub> constructs, cTnT <sub>223-288</sub> , and cTnT <sub>223-276</sub> .....	80
3.1.3	Production and purification of mutant solubilized cTnI <sub>38-134</sub> .....	81
3.1.4	Production and purification of mutant W237S, Q238D, Y241H, A245S-cTnT <sub>223-288</sub> .....	81
3.1.5	Reconstitution of the cardiac troponin ternary complex.....	83
3.1.6	NMR spectroscopy.....	83
3.2	Results and Discussion.....	85
3.2.1	The N-terminal tail of cTnI stabilizes the active orientation of cTnC .....	85
3.2.2	Phosphomimetic mutants of cTnI disrupt the active orientation of cTnC .....	88
3.2.3	Dilated cardiomyopathy mutations disrupt the active orientation of cTnC .....	91
3.2.4	An alternative “dormant” orientation of the cTnC domain.....	97
<b>CHAPTER 4: SMALL MOLECULE RPI-194 STABILIZES ACTIVATED TROPONIN TO INCREASE THE CALCIUM SENSITIVITY OF STRIATED MUSCLE CONTRACTION</b> .....		106
4.1	Introduction .....	107
4.2	Materials and methods.....	110
4.2.1	Preparation of proteins for NMR studies .....	110
4.2.2	NMR titration of RPI-194 against gChimera and cTnC .....	110
4.2.3	NMR titration of ssTnI against cTnC and cTnC·RPI-194 complex .....	111

4.2.4	NMR spectroscopy.....	111
4.2.5	Determination of binding affinities by steady state fluorescence.....	112
4.2.6	Determination of Ca <sup>2+</sup> dissociation rates by stopped-flow fluorescence.....	113
4.2.7	Measurements of force versus pCa (-log [Ca <sup>2+</sup> ]) in skinned ventricular trabeculae .....	113
4.2.8	Isolation of mouse ventricular myocytes, contractility assays and cAMP measurements .....	115
4.2.9	Isolated working mouse heart perfusion and measurement of metabolic rates ....	116
4.2.10	Impact of RPI-194 on cardiac myosin ATPase activity.....	116
4.3	Results .....	117
4.3.1	Titration of RPI-194 into Ca <sup>2+</sup> saturated gChimera .....	117
4.3.2	Titration of RPI-194 into Ca <sup>2+</sup> saturated cTnC .....	119
4.3.3	Impact of RPI-194 on binding of ssTnI switch peptide to cTnC.....	120
4.3.4	Effects of RPI-194 on the rate of calcium release from trimeric cardiac troponin complex and isolated cTnC .....	123
4.3.5	RPI-194 activates cardiac, slow skeletal, and fast skeletal muscle in isometric contraction, but slows the velocity of unloaded contraction .....	124
4.3.6	RPI-194 decreases velocity and amplitude of contraction in individual mouse cardiomyocytes.....	129
4.3.7	RPI-194 enhances cardiac work in isolated, perfused working mouse hearts .....	130
4.4	Discussion .....	131
<b>CHAPTER 5: CONCLUSIONS .....</b>		<b>134</b>
5.1	Conclusions .....	135
<b>BIBLIOGRAPHY .....</b>		<b>142</b>

## LIST OF FIGURES

<b>Figure 1.1:</b> The cryo electron microscopy structure of cardiac thin filament consists of actin, tropomyosin, and troponin complex. ....	4
<b>Figure 1.2:</b> Striated muscle specific expression of troponin subunits.....	5
<b>Figure 1.3:</b> Amino acid sequence of cTnC and its nine helices are denoted by helix illustration with their corresponding sequences.. ....	7
<b>Figure 1.4:</b> Calcium-saturated cardiac troponin complex (PDB:4Y99). ....	12
<b>Figure 1.5:</b> Illustration of structural and functional domains of cTnT.....	13
<b>Figure 1.6:</b> The structural domains and cardiomyopathy-associated mutations in cTnC.....	15
<b>Figure 1.7:</b> The structural and functional domains of cTnI with interacting binding region of cTnC, cTnT, and actin. ....	17
<b>Figure 1.8:</b> Development of a chimeric protein “gChimera”.....	30
<b>Figure 1.9:</b> The design process of small molecules as troponin modulators.. ....	31
<b>Figure 2.1:</b> The 3D structure and domain orientation of calcium-saturated cTn.....	44
<b>Figure 2.2:</b> Residue-specific secondary structure of cTnI <sub>135-209</sub> calculated by the program $\delta$ 2D using backbone NMR chemical shifts. ....	52
<b>Figure 2.3:</b> 2D <sup>1</sup> H, <sup>15</sup> N HSQC NMR spectra of cTnI <sub>135-209</sub> .....	56
<b>Figure 2.4:</b> Representative Coomassie Blue-stained 16% Tris-Tricine gels illustrating <i>in vitro</i> proteolysis of cTnI <sub>1-77</sub> or cTnI <sub>135-209</sub> by proteases MMP-2 or calpain-2 .....	58
<b>Figure 2.5:</b> Summary of mass spectrometric analysis identifying MMP-2 and calpain-2 cleavage sites within cTnI <sub>1-77</sub> and cTnI <sub>135-209</sub> .....	59
<b>Figure 2.6:</b> Mass spectrometry data of cTnI <sub>1-77</sub> proteolysed by MMP-2 at 10 min incubation time point. ....	60

<b>Figure 2.7:</b> Comparison of in vitro proteolysis of cTnI <sub>1-77</sub> in the presence or absence of cTnC by MMP-2 and calpain-2 in representative Coomassie Blue-stained SDS–PAGE gel .....	64
<b>Figure 2.8:</b> Comparison of in vitro proteolysis of cTnI <sub>135-209</sub> in the presence or absence of cTnC by MMP-2 and calpain-2 in representative Coomassie Blue-stained SDS–PAGE gel .....	66
<b>Figure 2.9:</b> Representative Coomassie Blue-stained SDS–PAGE gels showing in vitro proteolysis of cTnI <sub>135-209</sub> in the presence of MMP-2 or calpain-2 .....	67
<b>Figure 3.1:</b> Three dimensional structure of calcium-saturated human cTn.....	74
<b>Figure 3.2:</b> Backbone overlay of seven Ca <sup>2+</sup> bound and three Ca <sup>2+</sup> free structures of cTn. ....	77
<b>Figure 3.3:</b> Schematics of cTnC, cTnI, and cTnT constructs .....	82
<b>Figure 3.4:</b> <sup>15</sup> N R <sub>2</sub> relaxation rates of free cTnC and cTnC bound to cTnI <sub>1-77</sub> .....	86
<b>Figure 3.5:</b> Comparison of <sup>15</sup> N R <sub>2</sub> relaxation rates of free cTnC, cTnC complexed with wildtype cTnI <sub>1-77</sub> , and cTnC complexed with phosphomimetic cTnI <sub>1-77</sub> S22/23D or cTnI <sub>1-77</sub> S41/43D. ....	87
<b>Figure 3.6:</b> Comparison of <sup>15</sup> N R <sub>2</sub> relaxation rates of free cTnC, cTnC complexed with wildtype cTnI <sub>1-77</sub> , and substituted DCM mutant cTnI <sub>1-77</sub> K35Q, cTnC D75Y, or cTnC G159D. ....	92
<b>Figure 3.7:</b> <sup>1</sup> H and <sup>15</sup> N chemical shift changes between cTnC·cTnI <sub>1-77</sub> versus free cTnC, cTnC·cTnI <sub>38-134</sub> versus free cTnC and cTnC·cTnI <sub>38-134</sub> ·cTnT <sub>223-288</sub> versus cTnC·cTnI <sub>38-134</sub> as a function of cTnC sequence. ....	96
<b>Figure 3.8:</b> <sup>15</sup> N R <sub>2</sub> relaxation rates of free cTnC, cTnT <sub>223-288</sub> and cTnT <sub>223-276</sub> . ....	98
<b>Figure 3.9:</b> Comparison of <sup>15</sup> N R <sub>2</sub> relaxation rates of free cTnC, binary complex (cTnC·cTnI <sub>38-134</sub> ) and ternary complex (cTnC·cTnI <sub>38-134</sub> ·cTnT <sub>223-288</sub> ). ....	102
<b>Figure 4.1:</b> Titration of RPI-194 compound into <sup>15</sup> N labeled gChimera and cNTnC tracked by 2D <sup>15</sup> N HSQC NMR spectra.....	118
<b>Figure 4.2:</b> Fluorescence signal of RPI-194 with titration of gChimera, or cNTnC.....	120

<b>Figure 4.3:</b> The 2D <sup>15</sup> N HSQC of ssTnI titration into <sup>15</sup> N labeled cNTnC.....	122
<b>Figure 4.4:</b> Stopped flow fluorescence measurements of IAANS-labeled gChimera and troponin complex in the presence of 50 μM of RPI-194.....	123
<b>Figure 4.5:</b> Force versus pCa curves for rat skinned cardiac trabeculae, or fast skeletal and slow skeletal muscle fibers in the presence of 50 μM of RPI-194.....	125
<b>Figure 4.6:</b> Impact of RPI-194 on myosin ATPase activity.....	129
<b>Figure 4.7:</b> Measurement of sarcomere length, fractional shortening, rate of contraction and rates of relaxation of isolated single mouse cardiomyocytes. ....	130
<b>Figure 4.8:</b> Effects of RPI-194 in cardiac work, glucose oxidation and oxygen consumption in isolated, perfused working mouse hearts. ....	131



## **LIST OF TABLES**

<b>Table 1.1:</b> List of compounds synthesized by Rane Pharmaceuticals and screened by NMR to identify cardiac troponin activators.....	32
<b>Table 1.2:</b> List of compounds obtained from the National Cancer Institute and screened by NMR to identify cardiac troponin activators.....	35
<b>Table 3.1:</b> Comparison of average $^{15}\text{N}$ $R_2$ relaxation rates between cTnC, cTnC·cTnI <sub>1-77</sub> complex, dilated cardiomyopathy mutations and phosphomimetic variants of cTnC-cTnI <sub>1-77</sub> complexes..	95
<b>Table 4.1:</b> Fundamental properties (sarcomere length, cross-sectional area, maximum isometric force, and shortening velocity) of slow and fast fibers and of cardiac trabeculae, in the absence or presence of 20, 50 and 100 $\mu\text{M}$ RPI-194.....	127

## **LIST OF APPENDICES**

<b>Appendix 1:</b> Mass spectrometry data of cTnI <sub>1-77</sub> and cTnI <sub>135-209</sub> proteolysed by MMP-2 at time points from 0 min to 24 h.....	191
<b>Appendix 2:</b> Mass spectrometry data of cTnI <sub>1-77</sub> proteolysed by calpain-2 at time points from 0 min to 24 h.....	204
<b>Appendix 3:</b> Mass spectrometry data of cTnI <sub>135-209</sub> proteolysed by calpain-2 at time points from 0 min to 24 h.....	225

## LIST OF ABBREVIATIONS

cTn	Cardiac troponin complex
cTnC	Cardiac troponin C
cNTnC	N-domain of cTnC
cCTnC	C-domain of cTnC
cTnI	Cardiac troponin I
cTnT	Cardiac troponin T
DPA	Diphenylamine
DCM	Dilated cardiomyopathy
HCM	Hypertrophic cardiomyopathy
HFrEF	Heart failure with reduced ejection fraction
HFpEF	Heart failure with preserved ejection fraction
HSQC	Heteronuclear single quantum coherence
IDP	Intrinsically disordered protein
IPTG	Isopropyl $\beta$ -D- thiogalactopyranoside
I/R	Ischemia-reperfusion
$K_D$	Dissociation constant
MMP-2	Matrix metalloproteinase-2
NMR	Nuclear magnetic resonance
NOE	Nuclear overhauser enhancement
PKA	Protein kinase A
RCM	Restrictive cardiomyopathy

RONS	Reactive oxygen and nitrogen species
R <sub>1</sub>	Longitudinal relaxation rate
R <sub>2</sub>	Transverse relaxation rate
SDS-PAGE	Sodium dodecyl sulfate polyacrylamide gel electrophoresis
TIMP	Tissue inhibitor of metalloproteinases

# **CHAPTER 1**

## **INTRODUCTION**

A portion of this chapter has been published as a book chapter in:

Mahmud, Z. & Hwang, P.M. Cardiac troponin complex: cardiac troponin C (TNNC1), cardiac troponin I (TNNI3), and cardiac troponin T (TNNT2). *Encyclopedia of Signaling Molecules, 2nd Edition*. S. Choi (ed.). pp. 692-701 (2018). Adapted by permission from Springer Nature Customer Service Centre GmbH: Springer Nature, Cardiac troponin complex: cardiac troponin C (TNNC1), cardiac troponin I (TNNI3), and cardiac troponin T (TNNT2) by Mahmud, Z. & Hwang, P.M. 5118631015424, (2018).

## 1.1 Introduction to the cardiac troponin complex

The 1950s and 1960s were a golden era of striated muscle research. Several fundamental discoveries from that period shaped our existing knowledge of the mechanism of striated muscle regulation. It all started even prior to that, with the discovery of a sticky protein extracted from muscle in salt solution by Kühne in 1864<sup>1,2</sup>. It was named “myosin”<sup>1</sup>. During the Second World War years of 1941-1943, Albert Szent-Györgyi and his colleagues identified two forms of myosin (A, B)<sup>2,3</sup>. In 1942, it was discovered that the difference between myosin A and B is the presence of another protein, named “actin”<sup>4</sup>. One of the most significant discoveries that revolutionized the study of striated muscle is the sliding filament theory by Hugh Huxley<sup>5</sup>. In 1952, he described two filamentous structures by electron microscopy: thick filaments and thin filaments<sup>6</sup>. Tropomyosin, a part of the thin filament, was discovered by Bailey in 1946 and isolated by him in 1948<sup>7,8</sup>. Unknown at the time, this purified tropomyosin also contained troponin and regulated the thin filament by inhibiting the actin-myosin ATPase activity in a calcium-dependent manner. The troponin complex was first discovered and characterized by Ebashi in 1963<sup>9,10</sup>. Initially it was named “native tropomyosin”, but later Greaser and Gergely proposed the name of a separate troponin complex made up of three subunits<sup>11</sup>. Troponin C binds to  $\text{Ca}^{2+}$  and belongs to the calmodulin superfamily, Troponin I is an inhibitory subunit, and Troponin T binds to tropomyosin<sup>12</sup>. In 2003, the crystal structure of the human cardiac troponin complex (cTn) was published and serves as a tool for the fundamental structural understanding of each troponin subunit<sup>13</sup>. In 2020, the cryo-EM structure of the cardiac thin filament showcases each of the troponin subunits in relation to the other thin filament proteins<sup>14</sup>.

## 1.2 The sarcomere and the troponin complex

Sarcomeres are the primary contractile units of striated muscles, e.g., cardiac and skeletal muscles, which are linked in series and wrapped bundled together to form the organelles of contraction, myofibrils<sup>15</sup>. An individual sarcomere is composed of overlapping motor protein myosin-containing thick filaments (15 nm in diameter) and thin filaments (7 nm in diameter), which are comprised of actin monomers, tropomyosin, and the troponin complex<sup>16</sup>. Activation of myosin ATPase by the interaction between actin and myosin powers muscle contraction by sliding actin thin filaments against myosin thick filaments<sup>17</sup>. Thin filaments are organised into repeating structural units (38.5 nm)<sup>18</sup>, each containing fourteen twisted “double string of beads” actin monomers, one tropomyosin dimer and one troponin complex associated with seven helically arranged actin monomers. Each thick filament of striated muscle is comprised of a bundle of highly organised myosin molecules (more than 200)<sup>19</sup>. Cross-bridges between thin and thick filaments are formed when the globular head of myosin binds to actin. At low  $\text{Ca}^{2+}$  concentration, the tropomyosin-troponin complex blocks the interaction between myosin and actin, so the muscle does not contract (Figure 1.1). The release of  $\text{Ca}^{2+}$  from the sarcoplasmic reticulum increases the cytoplasmic concentration of  $\text{Ca}^{2+}$ , and  $\text{Ca}^{2+}$  binding to troponin results in a conformational change within the troponin complex that releases tropomyosin into a position that allows for actin-myosin interaction and muscle contraction.

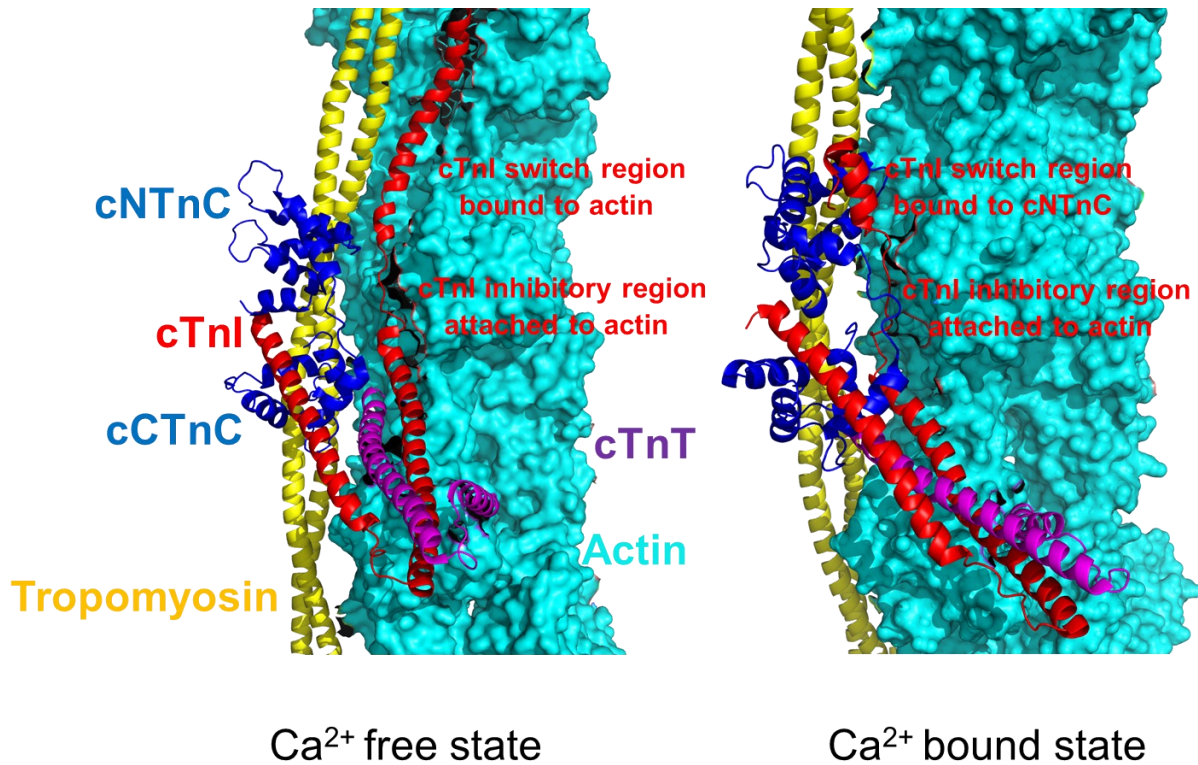


**Figure 1.1:** The cryo-EM structure of reconstituted thin filament consists of recombinantly expressed and purified rabbit skeletal muscle actin, human cardiac tropomyosin, human cardiac troponin complex (cTnC-blue, cTnI-red and cTnT-magenta) in calcium-free and bound states. Presence of calcium results in conformational changes in cTn (switch region of cTnI comes off from actin (cyan) and binds to cNTnC (blue), moving tropomyosin (yellow) from the blocked position to a closed position and exposing actin-binding sites for myosin. Myosin from the thick filament is not shown in this figure. A three-dimensional illustration of this thin filament was prepared by PyMOL using PDB structures, 6KN8 and 6KN7<sup>14</sup>.

Troponin subunits are encoded by separate homologous genes for each muscle type: cardiac, slow skeletal (type 1) and fast skeletal (type 2) muscle. Both TnI and TnT have three muscle type-specific isoforms, whereas TnC is expressed in two isoforms. Cardiac and slow skeletal muscle share one isoform encoded by *TNNC1*, while fast TnC expressed in fast skeletal muscle is encoded by *TNNC2*<sup>20</sup>. Both cardiac TnC (cTnC) and fast skeletal TnC (sTnC) isoforms are expressed in embryonic skeletal muscle during development (Figure 1.2). However, gene

expression of cTnC is switched off during the transition to fast skeletal muscle. The three isoforms of TnI are encoded by slow skeletal muscle (*TNNI1*), fast skeletal muscle (*TNNI2*), and cardiac TnI (*TNNI3*)<sup>21</sup>. During embryonic and fetal development, the slow skeletal isoform is expressed in the heart, but it is completely replaced by cardiac isoform shortly after birth (Figure 1.2). *TNNI3* is the sole isoform throughout adult life, and this does not change through pathologic states such as heart failure. There are three muscle type-specific homologous genes encoded by TnT present in vertebrates: slow skeletal (*TNNT1*), cardiac muscle (*TNNT2*) and fast skeletal muscle (*TNNT3*)<sup>22</sup>. Their expression is fiber specific, with *TNNT1* and *TNNT3* expressed in slow and fast skeletal muscle, respectively. *TNNT2* is expressed in cardiac muscle, but it is also expressed in embryonic skeletal muscle (Figure 1.2).

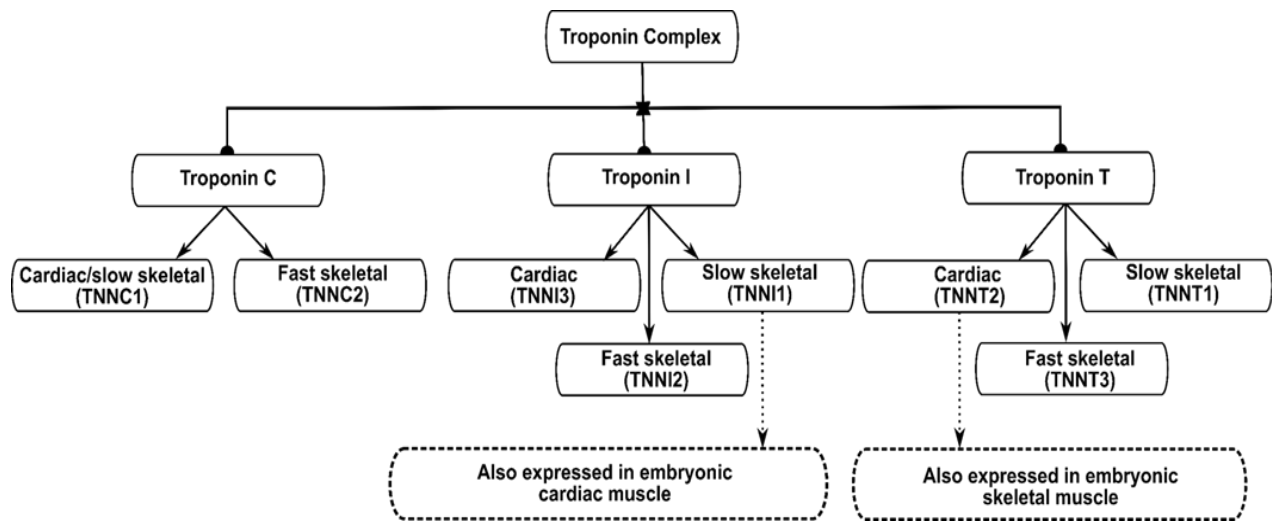


**Figure 1.2:** Striated muscle specific expression of troponin subunits. Figure adapted from Mahmud & Hwang<sup>23</sup>.

The presence of tissue-specific isoforms is clinically important. The measurement of elevated cTnI and cTnT levels in serum is a very specific marker for myocardial damage. Detection of cTnI or cTnT in blood has thus become the gold standard for diagnosing non-ST segment elevation myocardial infarction. More recently, the detection of cTnI and cTnT has become so



sensitive that low levels can now be detected even in healthy individuals, and chronically elevated levels indicate increased cardiovascular risk<sup>24</sup>.

### **1.3 Structure and function of the cardiac troponin complex**

#### **1.3.1 Structure and function of cardiac troponin C**

cTnC is a calcium binding subunit of the cTn belonging to the EF hand superfamily. It consists of 161 amino acid residues with a molecular mass of 18 kDa, containing four EF hand helix-loop-helix metal ion binding signature motifs. X-ray and NMR studies revealed that cTnC adopts a dumbbell shaped structure with N- and C-terminal globular domains connected by a central linker. In X-ray structures, the central linker forms a rigid nine turn  $\alpha$ -helix, whereas it is very flexible and intrinsically disordered in solution NMR structures. NMR studies also show that the two domains of cTnC tumble separately and are able to adopt various domain orientations<sup>25</sup>. There are eight helices (A-H) in four EF hands and one additional 9-residue N helix at the N terminus (Figure 1.3). The  $\text{Ca}^{2+}$  binding loop consists of 12 amino acid residues rich in aspartate and glutamate. Six residues 1(X), 3(Y), 5(Z), 7(-X), 9(-Y) and 12(-Z) in the loop provide oxygen ligands to coordinate the  $\text{Ca}^{2+}$  ion (EF hand I\*, II, III, and IV calcium-coordinating residues colored as green in Figure 1.3). The C-terminal domain (cCTnC) is also called the structural domain, and it anchors the whole troponin complex to the thin filament by interacting with other subunits of the troponin complex, troponin I (TnI) and troponin T (TnT). It has two high affinity  $\text{Ca}^{2+}$  or  $\text{Mg}^{2+}$  binding sites (EF III and EF IV), which are always occupied by either one of these ions, even in the resting muscle cell. On the other hand, the regulatory domain or the N-terminal domain (cNTnC) plays a major role in muscle contraction and relaxation through its two low affinity  $\text{Ca}^{2+}$  binding sites (EF I and EF II). The  $\text{Ca}^{2+}$  binding site properties of the structural C domain are similar in both fast skeletal and cardiac/slow skeletal isoforms but differ in the

regulatory N domain. In cTnC, the N domain EF I calcium binding site is inactive because of a Val28 single residue insertion and two chelating residue D29L and D31A substitutions. Therefore, only the binding site EF II in the N-domain maintains the crucial calcium-sensitive regulatory function for cardiac/slow skeletal muscle.

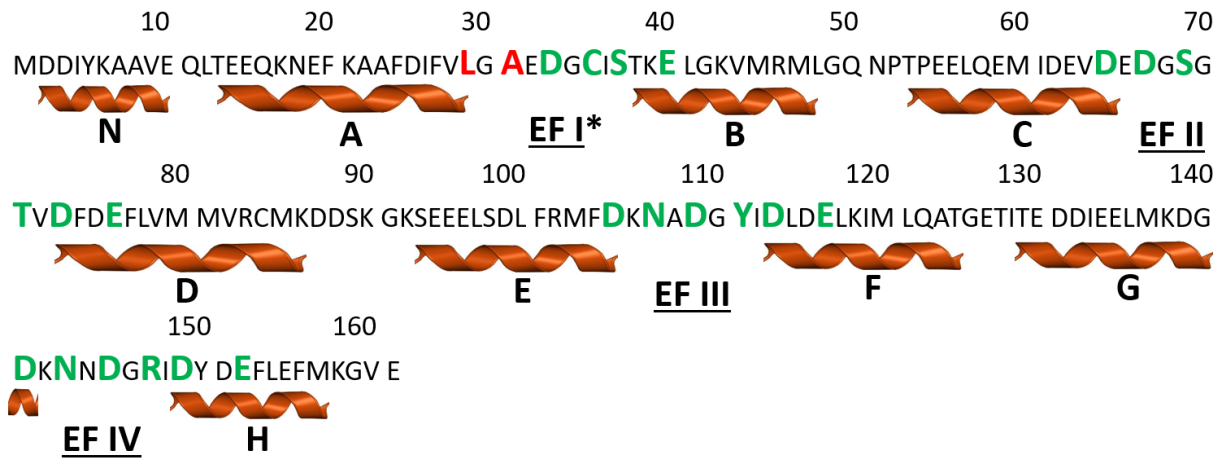


**Figure 1.3:** Amino acid sequence of cTnC and its 9 helices are denoted by helix illustration with their corresponding sequences. Calcium-coordinating EF-hand positions 1(X), 3(Y), 5(Z), 7(-X), 9(-Y), and 12(-Z) are marked in green. EF-hand I in cTnC is inactive denoted with an asterisk due to two chelating residue substitutions at position 29 and 31 highlighted in red. Figure adapted from Mahmud & Hwang<sup>23</sup>.

The mechanism of striated muscle contraction by the transient rise of cytosolic  $Ca^{2+}$  in both isoforms (sTnC and cTnC) is dependent on the N-domain.  $Ca^{2+}$  binding to the N-domain initiates a cascade of conformational changes in the troponin complex as well as in the thin filament<sup>26</sup>. This phenomenon switches the N-domain from a closed to open state by moving away helices B, and C from helices N, A and D, exposing a hydrophobic pocket<sup>27</sup> that interacts with the switch region of troponin I (cTnI<sub>148-158</sub>)<sup>28</sup> (Figure 1.4). Binding of cTnC to the switch region promotes the detachment of its adjacent cTnI inhibitory regions from their binding sites on actin, which releases actin-myosin inhibition and turns on muscle contraction by activating myofilament sliding. In

contrast, although having significant homology to sTnC, the structural transition in the cardiac isoform (cTnC) is different because cNTnC remains predominately closed in the absence or presence of calcium, most likely the consequence of inactive calcium binding site I (EF I)<sup>29</sup>. It has been demonstrated that binding of Ca<sup>2+</sup> alone in the EF II site of cNTnC does not bring any large conformational changes, but it increases the binding affinity of cTnI<sub>148-158</sub> for cNTnC. The NMR structure of Ca<sup>2+</sup> bound cNTnC in the presence of cTnI<sub>148-158</sub> revealed that binding of cTnI<sub>148-158</sub> stabilizes the open conformation by inserting Ile 148 and Met 153 residues into the large hydrophobic patch<sup>20</sup>. It is apparent that cNTnC exists in dynamic equilibrium between closed and open forms in the presence of Ca<sup>2+</sup>, which favors the subsequent binding of the cTnI switch region as well as increasing its Ca<sup>2+</sup> binding affinity. During development and pathological adaptations, there are no alternative splicing or post-translational modifications of cTnC observed that modulate its calcium binding activity<sup>17</sup>.

### **1.3.2 Structure and function of cardiac troponin I**

cTnI, the inhibitory subunit of the cTn, is a 24 kDa highly flexible protein that can adopt different conformations to interact with other thin filament proteins. There are six functional segments of cTnI according to *in vitro* structure-function studies. For consistent numbering and explanation of these segments we will use the first alanine as residue 1 because the N-terminal methionine residue is removed and replaced by an acetyl group.

The cardiac specific N-terminal extension (cTnI<sub>1-31</sub>), which is absent in both fast and slow skeletal TnI, contains two protein kinase dependent phosphorylation sites, Ser-22 and Ser-23<sup>30,31</sup>. The structure of this segment was studied by solution NMR techniques in both phosphorylated and

non-phosphorylated states<sup>32</sup>, showing that it is intrinsically disordered, explaining why it is not visible in crystal structures<sup>13</sup>.

The N-terminal extension interacts with the N-domain of cTnC when it is not phosphorylated. According to a study<sup>33</sup> from our lab of cTnI<sub>1-73</sub> in complex with cTnC.3Ca<sup>+</sup>, cTnI<sub>19-37</sub> has an electrostatic interaction with the negatively charged cNTnC in which the N terminal extended region remains disordered even in complex with cNTnC. This interaction stabilizes the activated orientation of the cNTnC domain relative to the rest of the cTn, thereby promoting calcium-activated cardiac muscle contraction. Cyclic AMP-activated protein kinase A phosphorylation of Ser-22, and Ser-23 weakens the electrostatic interaction, thus destabilizing the activated orientation of the cNTnC domain and shifting the contractile balance more towards relaxation.

The IT arm region consists of cTnI<sub>39-136</sub> and cTnT<sub>225-276</sub> binding to the C domain of cTnC. cTnI<sub>39-136</sub> has two  $\alpha$  helices, cTnI<sub>39-79</sub> and cTnI<sub>88-136</sub>. cTnI<sub>39-60</sub> has been demonstrated to bind with the hydrophobic cleft of cCTnC (Figure 1.4). cTnT<sub>225-276</sub> is positioned between cCTnC and cTnI<sub>88-136</sub><sup>28</sup>. This IT arm region dominates the overall core domain structure of the troponin complex and plays a structural role by bringing the three subunits of troponin together.

The inhibitory-peptide region cTnI<sub>128-147</sub> (or rather the corresponding homologous segment in rabbit fast skeletal TnI) was originally found to inhibit actin-myosin ATPase activity on its own<sup>34</sup>. This inhibitory peptide showed 90% inhibition of actin-myosin ATPase activity in the presence of tropomyosin<sup>34</sup>. An NMR study prior to the publication of the X-ray crystal structure of cTn suggested a potential interaction between cTnI<sub>128-147</sub> and cCTnC<sup>35</sup>. That interaction could be possible when cTnI<sub>128-147</sub> and cCTnC are studied separately but in the context of intact cTn, it is unlikely to happen because when cTnI<sub>41-60</sub> binds to cCTnC it will displace cTnI<sub>128-147</sub> from the

cTnC binding sites (Figure 1.4). The X-ray structure of cTn clearly shows that the second  $\alpha$ -helix of cTnI, cTnI<sub>90-135</sub> is a part of the IT arm and forms a coiled-coil structure with the cTnI<sub>226-271</sub>. According to the X-ray structure of cTn<sup>13</sup>, the inhibitory region of cTnI that inhibits actin-myosin interaction is cTnI<sub>137-148</sub><sup>13</sup>. It was originally thought to come off of actin with activation (cNTnC bound to Ca<sup>2+</sup>), but the cryo-EM structure shows that this inhibitory region stays tethered to actin during activation<sup>14</sup>.

The switch region cTnI<sub>148-158</sub> plays an important role in the cNTnC dynamic equilibrium between closed and open states. The position of the switch region is just next to the inhibitory peptide region (Figure 1.4). During relaxation (Ca<sup>2+</sup> free state), the switch region cTnI<sub>148-158</sub> binds to actin and promotes inhibition of actin-myosin interaction. During contraction, it comes off from actin and binds to the hydrophobic cleft of cNTnC and stabilizes the open conformation in the presence of calcium<sup>14</sup>.

The C-terminal actin binding site cTnI<sub>159-209</sub> is the second actin-tropomyosin binding site which is intrinsically disordered (may adopt secondary structure when it binds to actin-tropomyosin) and is the most conserved region among cTnI isoforms across species.

The recently solved cryo-EM structure of cardiac thin filament illustrates the activation of cTn in the context of other thin filament proteins (Figure 1.1)<sup>14</sup>. The most widely accepted hypothesis of muscle contraction is that which includes the presence of calcium, cNTnC binds to the switch region of cTnI, dragging the adjacent inhibitory region (cTnI<sub>135-147</sub>) away from its actin-tropomyosin binding sites. Tropomyosin shifts from the blocked position<sup>36</sup> along the actin filament to the closed position<sup>36</sup>, which allows the myosin head to bind to the exposed actin-binding site and further shift tropomyosin to the open position<sup>36</sup>. In the cryo-EM structure of the low calcium form of the thin filament, the C-terminal tail of cTnI including the inhibitory region (cTnI<sub>135-147</sub>),

the switch region (cTnI<sub>148-158</sub>), and the C-terminal actin-tropomyosin binding site (cTnI<sub>159-209</sub>) can be seen adopting an elongated shape that spans several actin monomers as it maintains tropomyosin and puts tropomyosin in the blocked state<sup>14</sup>. Surprisingly, in the high calcium state, the inhibitory region in fact remains bound to actin even though cTnI binds to the switch region<sup>14</sup>, so that it remains bound to actin throughout the cardiac cycle, in contrast to pre-existing models of its role<sup>37,38</sup>. Instead, the cTnI domain appears to form interactions with tropomyosin that displace it from the blocked position, and the cTnI switch region and the segments C-terminal to it, cTnI<sub>146-209</sub>, are displaced from their binding sites on actin.

### 1.3.3 Structure and function of cardiac troponin T

cTnT is a striated muscle specific myofilament protein with a molecular weight of 31-36 kDa that contains 250-300 amino acids, depending on variable alternative splicing. cTnT anchors the troponin complex to tropomyosin on the thin filament. Based on proteolysis and binding studies, cTnT is divided into two functionally and structurally distinct regions; one is the tropomyosin binding site 1 (T1) which is at the N-terminal end of the middle conserved region of cTnT that binds to the head-to-tail junction of tropomyosin, and the second tropomyosin binding site (T2) is a more C-terminal region of cTnT that interacts with cTnC, cTnI and F-actin and anchors the whole troponin complex in the thin filament<sup>39-45</sup> (Figure 1.5). The cryo-EM structure of the cardiac thin filament also shows a long alpha-helix structure of T1 region of cTnT (cTnT<sub>87-150</sub>) which binds to tropomyosin in a head-to-tail manner, in agreement with previously published studies<sup>14,39-42,46</sup>. This region is not present in the cTn X-ray structure<sup>13</sup>. The second tropomyosin binding site (T2), cTnT<sub>199-272</sub> is present in both X-ray and cryo-EM structures and is a part of the cTn core. cTnT is comparatively longer than slow and fast skeletal muscle isoforms because of a long N-terminal hypervariable region. Structural and functional diversity of the three isoforms of

cTnT is due to the N-terminal variable region, whereas the middle and C-terminal regions are present in highly conserved form in all the isoforms across different species<sup>17</sup>. The X-ray structure of the human troponin complex<sup>13</sup> revealed that the interaction between cTnT<sub>224-274</sub> and cTnI<sub>89-135</sub> is a  $\alpha$ -helical coiled-coil bundle interface, referred to as the IT arm region, which is highly conserved in all the TnT isoforms<sup>22</sup>. cTnT<sub>275-288</sub>, the C-terminal segment of cardiac troponin T is just next to the cTnI<sub>135-147</sub> inhibitory region and both are crucial for blocking the actin-tropomyosin interaction. Therefore, the IT arm and this adjacent region are important to maintain the interaction of the troponin complex with tropomyosin and balance the active open or inactive blocked state of troponin-tropomyosin on actin.

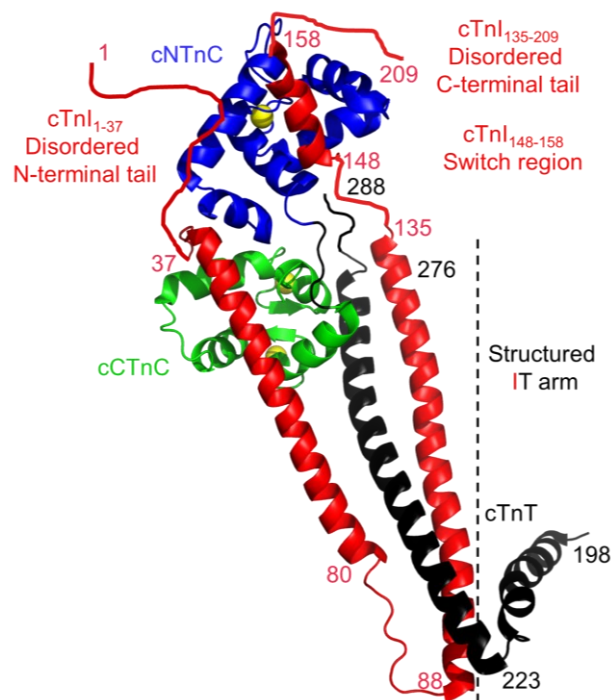


**Figure 1.4:** Calcium-saturated reconstituted human cardiac troponin complex (PDB:4Y99). Cardiac troponin C (cTnC) consists of two domains, an N-terminal domain, cNTnC (blue) and a C-terminal domain, cCTnC (green). Cardiac troponin I (cTnI) is shown in red, The N- and C-terminal tails of cTnI, with intrinsically disordered drawn manually as squiggles. The region of cardiac troponin T (cTnT) that is bound to the rest of the troponin complex is shown in black.

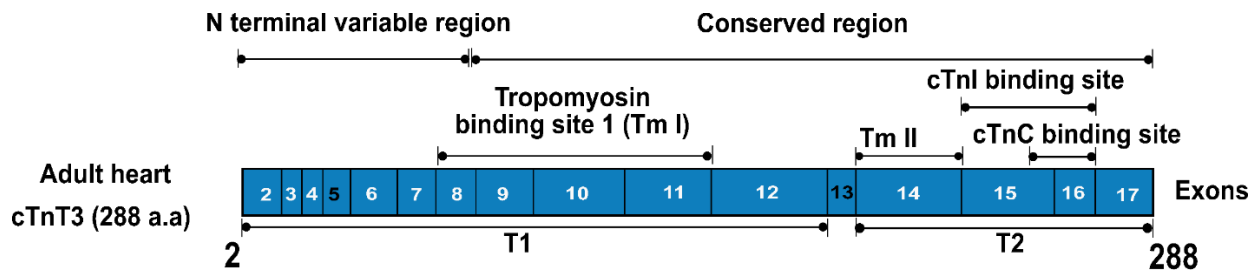


**Figure 1.5:** Illustration of structural and functional domain of human cTnT. Figure adapted from Mahmud & Hwang<sup>23</sup>.

### 1.3.4 Post-translational modifications of cTnI regulate troponin activity

Post translational modifications of cTnI play a major role in regulating the interaction of cTnI with cTnC and actin to impact cardiac muscle contractility. cTnI contains 3 tyrosine, 12 serine and 8 threonine residues as potential phosphorylation sites. There are several phosphorylation sites in cTnI that are phosphorylated by different protein kinases (Figure 1.7)<sup>15</sup>. The most studied and best understood phosphorylation sites of cTnI are Ser-22/Ser-23, originally found to be phosphorylated by cyclic AMP-dependant protein kinase A during  $\beta$ -adrenergic signaling cascades, impacting cardiac muscle contractility by decreasing the  $\text{Ca}^{2+}$  sensitivity of the sarcomere<sup>30,31,47</sup>. These two phosphorylated sites weaken the interaction between cTnI and the N-domain of cTnC and promote cardiac muscle relaxation by increasing  $\text{Ca}^{2+}$  dissociation from cTnC<sup>48</sup>. However, these two serine residues can be phosphorylated by several other protein kinases *in vitro* including protein kinase C<sup>49</sup>, protein kinase D<sup>50</sup> and cyclic GMP-dependant protein kinase<sup>51</sup>. Bisphosphorylation of these sites impedes muscle relaxation and reduces myofilament sliding velocity in a motility assay<sup>52</sup>. It also lowers the maximal tension as well as decreases cross



bridge cycling kinetics<sup>15</sup>. It has been reported that Ser-149 also can be phosphorylated by P21 activated kinase or AMPK activated protein kinase which prolongs muscle relaxation and increases the Ca<sup>2+</sup> sensitivity of cardiac myofibrils. Several novel phosphorylation sites in cTnI have also been reported in a proteomic survey of phosphorylation sites, and interestingly, phosphorylation sites present in cardiac specific N-terminal extension region showed a lower extent of phosphorylation in heart failure patients whereas the IT arm and C terminal region showed a higher extent<sup>53</sup>. Several in vitro studies showed mammalian sterile 20 like 1 (Mst1)-mediated phosphorylation of Thr-30, Thr-50 and Thr-180 in cTnI, among them Thr-30 being a preferred site. Proper understanding of the physiological roles of cTnI phosphorylation in both normal and pathological states will require further research.

## **1.4 Troponin C and I in cardiac diseases**

### **1.4.1 Heritable cardiomyopathies**

Mutations in the cardiac isoforms of troponin give rise to heritable cardiomyopathies, all of which are associated with an enhanced risk of arrhythmias and progression to heart failure<sup>54</sup>. Hypertrophic cardiomyopathy is the most common, with an estimated prevalence of 1:500<sup>55</sup>. Its most prominent feature is abnormal hypertrophy of the ventricles, particularly in the ventricular septum. This process can lead to left ventricular outflow tract obstruction. There is some overlap between mutations causing hypertrophic cardiomyopathy and restrictive cardiomyopathy, with restrictive cardiomyopathy being a rarer, severe condition characterized by impaired relaxation and filling of the ventricles, leading to right-sided heart failure. Dilated cardiomyopathy is associated with enlarged thin walled ventricles, generally leading to left-sided heart failure. A better understanding of the functioning of the cardiac troponin complex is needed to explain the

pathogenesis of the cardiomyopathies. One complicating factor is that the evidence linking some mutations to cardiomyopathies is poor, with some mutations only having been observed in a single individual. However, with genome sequencing becoming standard-of-care and vast amounts of sequence information being generated, it should in theory be possible to determine which mutations are truly disease-causing alterations or just incidental benign polymorphisms.

For cTnC, there are several mutations linked with HCM (A8V, L29Q, A31S, C84Y, Q122AfsX30, E134D, D145E,) and DCM (Y5H, Q50R, E59D/D75Y, M103I, D145E, I148V, G159D) have been reported (Figure 1.6)<sup>20</sup>. As cTnC has two different states, resting and active, it would make sense that mutations destabilizing these two different states gives rise to HCM and DCM, respectively. However, the exact mechanism by which mutations in the cardiac troponin complex give rise to cardiomyopathies is still being worked out.

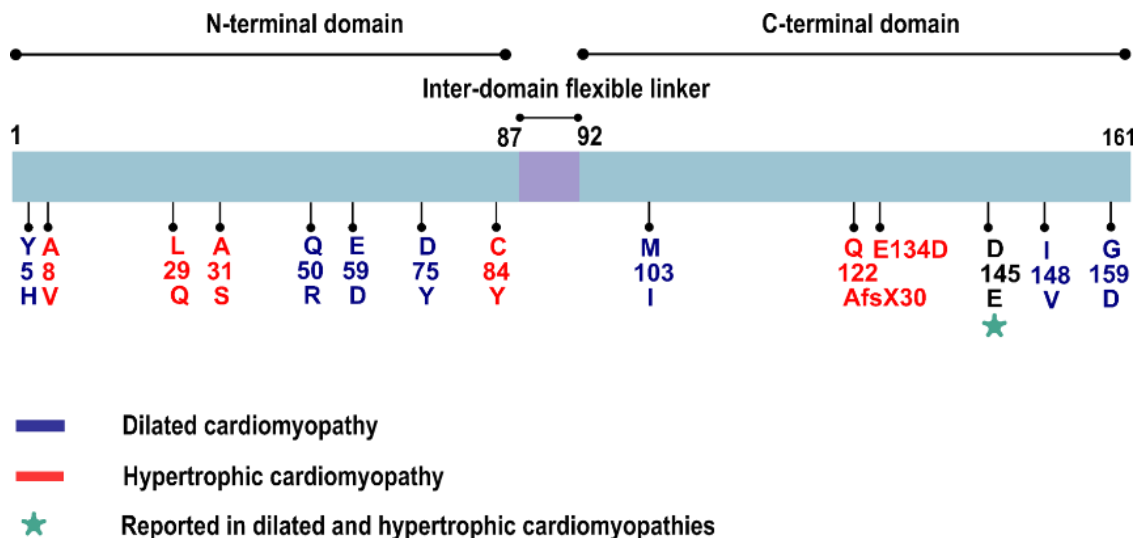


**Figure 1.6:** The structural domains of cTnC and cardiomyopathy-associated mutations reported in cTnC. Figure adapted from Mahmud & Hwang<sup>23</sup>.

Approximately 95% of the disease-causing mutations in cTnI are located in its C-terminal region, spanning residues 135 to 209<sup>54</sup> (Figure 1.7). Almost all of these are associated with

hypertrophic or restrictive cardiomyopathy (with the exception of N184K). This is consistent with the main physiologic role of this region, binding to actin-tropomyosin to maintain the thin filament in an inactive state. When this function is disrupted by mutation, the result is a hyper-activated thin filament with an associated increase in calcium sensitivity. Several cTnI mutations (L143Q, R144W, A170T, K177E, D189G and R191H) in restrictive cardiomyopathy (RCM) patients showed greater  $\text{Ca}^{2+}$  sensitizing effects in cardiac muscle force generation compared to HCM mutations in cTnI<sup>56</sup>. At low  $\text{Ca}^{2+}$  concentration, these mutations also increased the force generation of cardiac muscle in the resting state. Interestingly, many of the mutations associated with RCM and HCM involve positively charged residues, underscoring the importance of electrostatic interactions, perhaps a recurrent theme for the intrinsically disordered segments of troponin.

Several mutations have also been found in the N-terminal of cTnI. One of these, R20C, has been linked to HCM<sup>57</sup>. The mutation abolishes the phosphorylation consensus sequence, RRXS, of protein kinase A, abolishing the phosphorylation of Ser-22 and Ser-23. An additional four mutations (A1V, K35Q, N184K and P15T) have been identified that are associated with DCM in an autosomal dominant manner<sup>54</sup>.

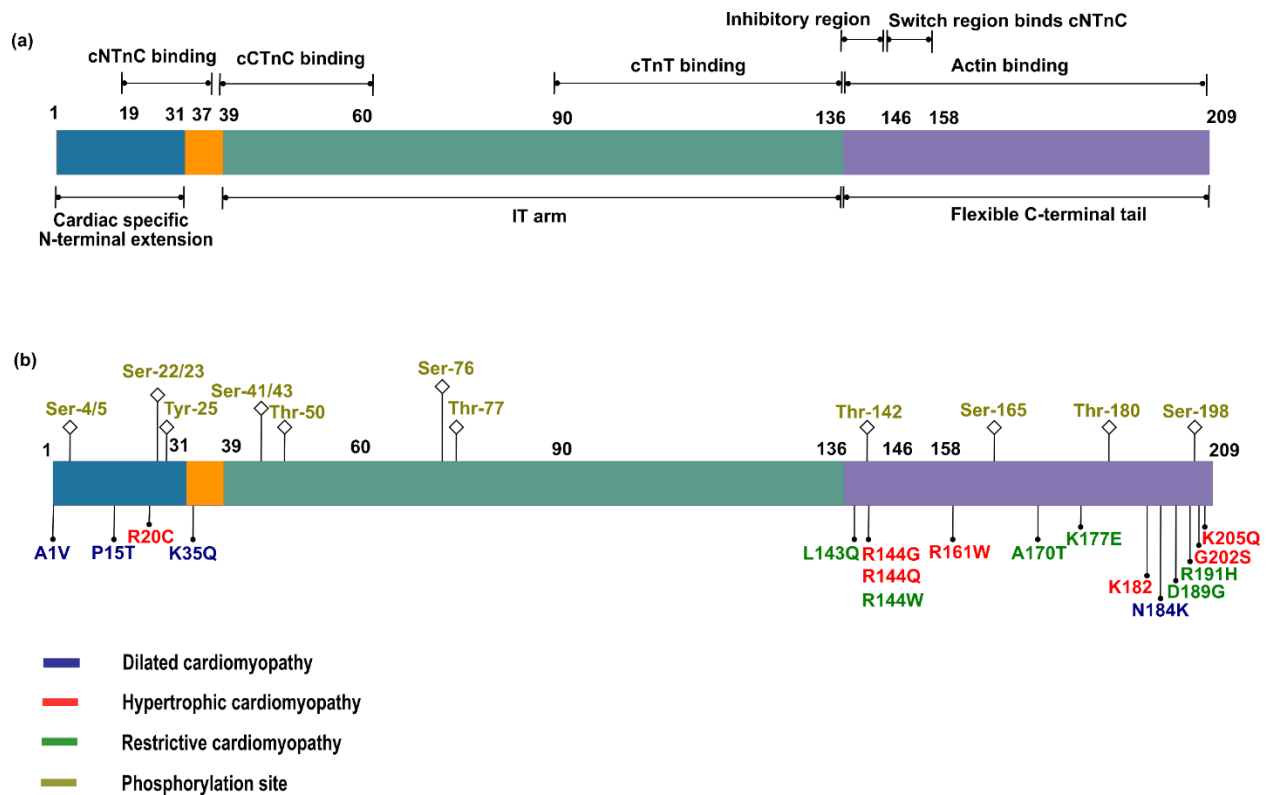


**Figure 1.7:** The structural and functional domains of human cTnI with interacting binding region of cTnC, cTnT and actin (a). Cardiomyopathy-associated mutations and phosphorylated residues are also mentioned in the figure (b). Numbering excludes Met-1 from the cTnI sequence. Figure adapted from Mahmud & Hwang<sup>23</sup>.

## 1.4.2 Myocardial ischemia-reperfusion injury

### 1.4.2.1 Ischemia reperfusion injury

According to the World Health Organization, cardiovascular disease is responsible for 17.1 million deaths worldwide each year, representing ~31% of all deaths<sup>58</sup>. It is the second leading cause of death after cancer among Canadians<sup>59</sup>. An estimated cost of 22 billion dollars (direct and indirect costs) associated with cardiovascular diseases was reported in 2009 by the Canadian Heart Health Strategy and Action Plan committee<sup>60</sup>. In Canada, over 51,500 deaths reported in 2015

were due to heart disease, mainly ischemic heart disease (IHD) or coronary heart disease<sup>61</sup>. Ischemic heart disease was found in 71% of diagnosed heart failure patients aged over 40 among Canadians<sup>62</sup>. It is a clinical and financial burden for the Canadian health care sector.

In IHD, the heart muscle cannot meet the metabolic demands of the body (by pumping blood at a sufficient rate) because of restricted oxygenated blood supply to the heart muscle via the coronary circulation, known as myocardial ischemia<sup>63</sup>. Blocked or narrowed coronary arteries cause this condition due to the presence of atherosclerotic plaques, accumulated over long periods of cholesterol and calcium deposition. These plaques prevent the heart muscle from receiving oxygenated and nutrient-rich blood to sufficiently perfuse heart muscle. Acute myocardial infarction (AMI)<sup>64</sup> occurs due to rupture or erosion of an atherosclerotic plaque causing thrombus (blood clot) formation in a coronary artery that leads to an acute disruption of blood supply<sup>65</sup>. The primary therapeutic intervention of AMI is to restore blood supply to the heart, also known as reperfusion<sup>66</sup>. Timely reperfusion is essential to protect the myocardium from permanent damage (necrosis) and myocardial contractile dysfunction (systolic heart failure).

Reperfusion techniques developed over time to treat ischemic heart patients are either thrombolytic therapy (use of intravenous thrombolysis drugs) or percutaneous coronary intervention (a minimally invasive procedure of opening an obstructed artery by either a balloon catheter or stent placement)<sup>66</sup>. Surprisingly, in addition to salvaging ischemic myocardium, reperfusion also induces further injury, which is now known as myocardial ischemia-reperfusion (I/R) injury<sup>66</sup>. In 1960 Jennings et al. first observed reperfusion-induced necrosis in an ischemic canine heart in a coronary artery ligation experiment<sup>67</sup>. They reported using histological studies that the degree of necrosis after 30-60 minutes of ischemia followed by reperfusion is similar to necrosis typically found in 24 hours of prolonged acute myocardial ischemia<sup>68</sup>. This study stirred

a debate among scientists over a decade whether reperfusion actually causes further damage to an ischemic heart until Murray *at el.* in 1986 first discovered that myocardial preconditioning can mitigate reperfusion injury and help to differentiate the independent effects of ischemia and reperfusion in myocardial injury<sup>69</sup>.

Reperfusion-induced injury can result in reversible or irreversible cell damage. Myocardial stunning is a form of reversible injury with impaired contractile function of the myocardium<sup>70</sup>. The myocardium is still viable and metabolically intact but may takes hours to days to completely regain its contractile ability<sup>71</sup>. It was reported in several canine models that despite rapid reperfusion after 5-15 minutes of temporary coronary artery obstruction where no necrosis was present, cardiac function still showed left ventricular abnormalities (contractile dysfunction), that persisted for days<sup>72-76</sup>. Substantial progress has been made in understanding and deciphering underlying mechanisms of I/R mediated injury. Among them, oxidative stress due to generation of reactive oxygen nitrogen species (RONS) and intracellular calcium overload are the two most studied and widely accepted mechanisms<sup>77</sup>.

#### **1.4.2.2 Mechanisms of I/R injury**

A normal heart produces RONS (superoxide, hydroxyl, peroxy, nitrogen dioxide radicals, and peroxynitrite anion)) during the process of cellular metabolism<sup>78</sup>. A certain low concentration of RONS is optimal for the heart and involved in many cellular signaling systems<sup>79</sup>. Inside cells, free radical scavenger enzymes such as superoxide dismutase, glutathione peroxidase delicately balanced the level of RONS<sup>80</sup>. Reperfusion in a post-ischemic heart tips the scale of RONS, resulting in pathologic oxidative stress. Within minutes of reperfusion, a burst of RONS generated in the heart favours the production of highly reactive peroxynitrite (ONOO<sup>-</sup>) utilizing an excess

amount of superoxide and nitric oxide present at that time<sup>81</sup>. Products of peroxynitrite ( $\text{OH}^\cdot$ ,  $\text{NO}_2^\cdot$ ) can react with cellular proteins, causing cellular damage and activating intracellular proteases like matrix metalloproteinases-2 (MMP-2)<sup>81-83</sup>. In I/R injury, MMP-2 targets the myocardial contractile apparatus and cleaves several sarcomeric proteins that lead to contractile dysfunction<sup>84-86</sup>.

In the ischemic heart, oxygen depletion (hypoxia) and restricted nutrient supply through occluded arteries causes a cascade of biochemical, metabolic, and cellular changes within cells<sup>87</sup>. Hypoxia shuts down mitochondrial oxidative phosphorylation and causes lower ATP production in the cell. It also activates anaerobic glycolysis, which causes intracellular acidosis<sup>77,87</sup>. As a result, an excess amount of intracellular  $\text{H}^+$  accumulates inside the cell<sup>88</sup>. To normalize intracellular pH, upon reperfusion, the  $\text{Na}^+$ - $\text{H}^+$  exchanger pump imports extracellular  $\text{Na}^+$  into the cell in exchange for  $\text{H}^+$ . The excess intracellular  $\text{Na}^+$  activates the  $\text{Na}^+$ - $\text{Ca}^{2+}$  exchanger pump to export  $\text{Na}^+$  to bring calcium inside the cell (under normal physiological condition the opposite exchange happens)<sup>89-91</sup>. This exchange gives rise to intracellular calcium overload<sup>66,92</sup> and activation of calcium-dependent-proteases like calpains<sup>93</sup>. Activated unregulated calpains can cause impaired contractile function by degrading sarcomeric proteins<sup>94</sup>.

### **1.4.2.3 Activation of intracellular proteases in ischemia-reperfusion injury**

MMPs are a group of 25 endopeptidases (23 in humans) which are zinc-dependent and ubiquitously distributed<sup>95</sup>. They degrade the fibrillar collagen matrix and were first discovered in tadpole tails during morphogenesis<sup>96</sup>. They are best known for their role in extracellular matrix remodeling, and scientists quickly realized their significance and contribution to several physiological processes including angiogenesis, wound healing, inflammation, metastasis and apoptosis<sup>97</sup>.

MMP-2 (type IV collagen or gelatinase A) is commonly found in all cardiac cells. MMP-2 has a multi-domain structure (72 kDa)<sup>98</sup> starting with an N-terminal signal sequence that helps MMP-2 translocate from the endoplasmic reticulum to the outside of the cell. Next to the signal sequence is an inhibitory propeptide domain, which prevents the catalytic domain from becoming active<sup>98,99</sup>. The propeptide domain contains a conserved cysteine switch motif (PRCGXPD) that binds to the active site zinc and blocks catalytic activity. The catalytic domain has a conserved zinc-binding motif (HEXGHXXGXXH) which is required for MMP-2 proteolytic activity<sup>98</sup>. Only MMP-2 and MMP-9 have an additional three fibronectin repeat domains within the catalytic domain that help them to degrade gelatin. An additional hemopexin domain is connected to the catalytic domain by a flexible hinge region<sup>98</sup>.

MMP-2 activities are highly regulated at multiple levels, namely subcellular localization, post-translational modifications, natural and synthetic inhibitors, proteolytic digestion and transcription factors<sup>100-104</sup>. Among them, there are three primary mechanisms of MMP-2 activation<sup>105</sup>: 1) Proteolytic cleavage of inhibitory propeptide domain by a proenzyme, membrane-type MMP (MT-MMP)<sup>106,107</sup>. Deleting the propeptide domain produces a shorter form of MMP-2 (~64 kDa) and disengages an inhibitory cysteine thiol group from the active zinc binding site, allowing the catalytic domain to be activated<sup>106,107</sup>. 2) MMPs are naturally inhibited by endogenous tissue inhibitors of metalloproteinases (TIMPs)<sup>108,109</sup>. There are four TIMPs and they inhibit MMPs activity by interacting with the catalytic active site. The stoichiometry ratio of MMP and TIMPs is 1:1. Of the four TIMPs, TIMP-4 is localized within cardiac myocytes, and excessive secretion of MMP-2 and TIMP-4 during I/R injury creates an imbalance in the MMP-2: TIMP-4 ratio, which promotes unregulated MMP-2 activity<sup>110</sup>. 3) Post-translational modification of MMP-2 by acetylation, S-glutathiolation, nitrosylation and phosphorylation also regulates its activity. In



I/R injury, peroxynitrite (ONOO<sup>-</sup>) is able to activate intracellular MMP-2 without removal of the propeptide domain. Peroxynitrite causes S-glutathiolation within the propeptide conserved motif that disrupts the interaction between catalytic zinc and the inhibitory thiol group of conserved cysteine 102 residue, activating the zinc-containing catalytic site of MMP-2<sup>111-113</sup>.

Initial studies related to MMP-2 substrate identification focused mainly on the extracellular space as MMPs were originally believed to be only as secreted proteases acting upon extracellular matrix proteins. However, they have now been found in nearly every cellular compartment including the nucleus, mitochondria, cytosol, and sarcomere, where they are involved in physiologic and pathologic states<sup>95</sup>. In 1999, the intracellular activity of gelatinases (MMP-2 and MMP-9) was first discovered in both normal and dilated cardiomyopathy hearts<sup>114</sup>. Both were shown to cleave myosin heavy chain *in vitro* and *in vivo*. They concluded that MMP-2 and MMP-9 might have a role in damaging the myocardial contractile apparatus to cause dilated cardiomyopathy. MMP-2 was found to proteolyze the contractile protein cTnI during ischemia-reperfusion injury in 2002<sup>85</sup>. It was successfully demonstrated for the first-time that MMP-2 contributed to acute myocardial contractile dysfunction after I/R injury. Using confocal microscopy and immunoblot analysis, MMP-2 was found to co-localize with cTnI. In isolated rat hearts subjected to ischemia-reperfusion injury, the use of MMP inhibitors including an MMP-2 neutralizing antibody, showed reduced MMP-2 activity, reduced cTnI proteolysis, and improved contractile function<sup>83,85</sup>. Later, unregulated MMP-2 activity and proteolysis of other contractile apparatus proteins such as titin, and myosin light chain 1 were identified in I/R injury<sup>84,86</sup>.

Calpains are a group of 15 cysteine proteases that depend upon calcium for activation<sup>115,116</sup>. Most of them are ubiquitously expressed and found in almost all mammalian cells, while some calpains have tissue-specific expression. Two calpain isoforms, calpain 1, also known as  $\mu$ -calpain

(encoded by *Capn1*), and calpain 2 (m-calpain, encoded by *Capn2*) are expressed ubiquitously in the cell<sup>117-119</sup>. They are heterodimers with a large 80 kDa catalytic domain and a small 28 kDa regulatory domain (encoded by *Capn4*)<sup>119,120</sup>. Both calpains possess 60% sequence homology and have very similar substrate specificity. As their name suggests, micromolar and millimolar concentrations of calcium are required for the full activation of calpains 1 and 2, respectively, which are higher than the normal calcium concentrations in a healthy beating heart<sup>121</sup>.

The proposed and most accepted hypothesis regarding calpain activation is that inactive calpain is initially located in the cytosol bound to its endogenous inhibitor calpastatin, but it then translocates to the membrane where calpain becomes attached to phospholipids. Phospholipids lower the calcium concentration required for calpain activation<sup>118,122</sup>. During I/R injury, downregulation of calpastatin also contributes to calpain activation<sup>123,124</sup>. There are other possibilities related to calpain activation such as post-translational modifications and calpain activator-proteins<sup>125,126</sup>.

A large number of studies of simulated I/R reported the involvement of calpains in the derangement of cardiac contractile and structural proteins (cTnI<sup>127</sup>, cTnT<sup>128</sup>, titin<sup>129</sup>, and desmin<sup>130</sup>). In isolated rat hearts subjected to I/R injury, overexpression of the inhibitor calpastatin by gene transfer showed improved contractile function and inhibition of cTnI proteolysis<sup>131</sup>. Also, low pH/low Ca<sup>2+</sup> conditions during reperfusion protects isolated rat heart from myocardial stunning and cTnI degradation<sup>132</sup>. The calpain inhibitor MDL-28170 showed protection against myocardial stunning by inhibiting cTnI proteolysis in rat hearts<sup>133</sup> though another study reported MDL-28170 also inhibits MMP-2<sup>134</sup>.

#### 1.4.2.4 Proteolysis of cTnI in ischemia-reperfusion injury

Selective and partial proteolysis of cTnI has been observed in moderate to severe ischemic conditions (15-60 minutes) followed by 45 minutes of reperfusion<sup>135</sup>. Immunologic studies using monoclonal antibodies against cTnI identified a cut site between cTnI<sub>188-199</sub><sup>135</sup>. Selective proteolysis of cTnI, also reported in myocardial stunning, resulted in the truncation of 17 amino acid residues from the C-terminal tail of cTnI<sup>136</sup>. Mass spectrometry analysis identified a band of 22 kDa corresponding to cTnI<sub>1-192</sub> in the reperfusion effluent. More degradation products cTnI<sub>63-132</sub> and cTnI<sub>73-192</sub> were detected with more prolonged ischemic times<sup>136</sup>. Higher molecular weight products were eluted in reperfusion effluent corresponding to covalent complexes of either cTnI·cTnC or cTnI·cTnT<sup>136</sup>. The 17-residue truncated cTnI fragment was also responsible for myocardial stunning when overexpressed in transgenic mouse hearts<sup>137</sup>. Partially proteolyzed cTnI<sub>1-193</sub> was later identified in coronary artery bypass graft patients presenting with a myocardial stunning phenotype<sup>138</sup>.

In contrast, some studies did not find convincing evidence that proteolysis of cTnI is responsible for myocardial stunning due to I/R injury<sup>139</sup>. An *in vivo* study in swine hearts subjected to I/R did not identify a cTnI degradation product<sup>140</sup>. In conscious dogs undergoing reversible cardiac ischemia, only minor cTnI degradation was present<sup>17,141,142</sup>. No cTnI degradation product was found in a study of stunned pig hearts. Instead, dephosphorylation of phospholamban was identified as a potential cause of stunning<sup>143</sup>.

Scientists have debated over the years about the significance of cTnI proteolysis in myocardial I/R injury. One hypothesis is that cTnI degradation depends on preload rather than ischemia. In one study, preventing increased preload independent of ischemia led to increased  $\mu$ -calpain-mediated proteolysis of cTnI in isolated rat hearts which was prevented by the calpain

inhibitor calpastatin. It was suggested that preventing increased preload protects against cTnI proteolysis in I/R injury and improves contractile function<sup>144</sup>. Thus, the exact mechanism of myocardial stunning remains controversial.

### **1.4.3 Systolic heart failure**

Heart failure is an end stage of cardiac disease and an important cause of mortality, morbidity, and hospitalizations around the world. It is a global problem and a severe financial burden for health care systems around the world as treatment of heart failure requires complex and costly medical care and frequent hospitalizations.

Heart failure occurs when cardiac muscle exhibits impaired relaxation and contraction causing reduced ventricular filling or ejection of blood, respectively<sup>145</sup>. It is generally categorized based on the left ventricular ejection fraction: 1) heart failure with reduced ejection fraction (HFrEF), and 2) heart failure with preserved ejection fraction (HFpEF)<sup>146</sup>. In HFrEF (ejection fraction less than 40%), also known as systolic heart failure, the left ventricle has reduced ability to eject blood to the rest of the body due to impaired cardiac muscle contraction. Over time, the heart muscle becomes increasingly thinned, dilated and too weak to pump sufficient blood to satisfy the requirements of the body<sup>147</sup>. Many diseases contribute to this state, such as ischemic heart disease, metabolic diseases, familial dilated cardiomyopathy, tachycardia, and hypertension<sup>147</sup>. In HFpEF (ejection fraction 50% or more), also known as diastolic heart failure, the ventricular cavity is unable to expand properly to fill with blood during relaxation. In this condition, hypertrophied heart muscle cannot relax properly resulting in increased ventricular filling pressures. Reduced blood filling during diastole thus compromises cardiac output<sup>147</sup>.

Often heart failure is the result of a gradual deterioration of heart function. It is classified as chronic or acute decompensated heart failure. Acute decompensations occur in the setting of chronic heart failure with a rapid worsening of signs and symptoms like low blood pressure, shortness of breath, and leg swelling.

Significant advancement has been made in the last decades for the treatment of heart failure. Numerous clinical trials have been conducted to identify better treatment strategies for systolic heart failure. Fewer positive trials and data are available for diastolic heart failure<sup>148,149</sup>. Regardless, the main treatment plan for systolic heart failure patients includes the use of angiotensin-converting enzyme-I inhibitors or angiotensin-II receptor blockers, beta-blockers, aldosterone antagonists, and diuretics. Angiotensin-converting enzyme-I inhibitors improve mortality in systolic heart failure, and they also reduce the number of hospitalizations<sup>150-152</sup>. Angiotensin-II receptor blockers are an alternative to the angiotensin-converting enzyme-I inhibitors<sup>153</sup> that are less likely to cause angioedema (cough, hypotension, laryngeal edema). Beta-blockers are used as a polytherapy with angiotensin-converting enzyme-I and/or diuretics. Beta-blockers have been shown in a large number of clinical trials to reduce morbidity and mortality rate in systolic heart failure<sup>148,154,155</sup>. Diuretics are also used for treating symptomatic heart failure patients. There are no clinical trials that reported effects of diuretics in improved mortality or morbidity in heart failure patients, likely because they are so essential to treatment that withholding them in a clinical trial would be unjustifiable. They improve hemodynamics by removing excess fluid, also improving cardiac function<sup>148</sup>. The positive inotropic drug digoxin is also effective in improving symptoms<sup>156</sup> but has shown no benefit in reducing mortality<sup>157</sup>.

The aforementioned treatments have been established into medical practice by a large number of clinical trials, but no treatments have been shown to be beneficial in acute,

decompensated systolic heart failure. Positive inotropes are used in clinical practice to treat acute decompensated systolic heart failure, but clinical trials have failed to show any correlation with improving mortality rate. This class of drugs has adverse side effects, which also contribute to increasing the mortality rate<sup>158</sup>. There are two types of positive inotropes: calcium mobilizers and calcium sensitizers<sup>159</sup>. Dopamine, dobutamine, and Phosphodiesterase 3 (PDE3) inhibitors are calcium mobilizers that increase myocardial contractility and cardiac output by increasing calcium fluxes in and out of cardiac muscle. Dopamine and dobutamine are  $\beta$ -adrenergic receptor agonists, and they increase cAMP synthesis from ATP by adenylyl cyclase<sup>160</sup>. PDE3 inhibitors like milrinone inhibit the breakdown of PDE3 and the conversion of cAMP to AMP. As a result, cAMP levels go up, and activates more PKA. Activated PKA phosphorylates L-type  $\text{Ca}^{2+}$  channels which results in increased intracellular calcium flow into the cell during systole<sup>161</sup>. Calcium mobilizers are sarcomeric modulators that indirectly improve cardiac contraction. All of these calcium mobilizers have unwanted side effects such as increased heart rate, increased oxygen consumption, and vasodilation, which are less likely to be tolerated in acute decompensated systolic heart failure patients<sup>162-165</sup>.

#### **1.4.3.1 Existing calcium sensitizers to treat systolic heart failure**

To avoid adverse side effects by indirect modulators, it was proposed in 1980 that a direct sarcomeric modulator or calcium sensitizer would be a better approach to correct contractile dysfunction<sup>166,167</sup>. Pimobendan was the first direct sarcomeric modulator that was discovered in 1984<sup>168</sup>. Pimobendan increased calcium sensitivity by binding with cTnC but also by inhibiting PDE3 as a dual action mechanism<sup>169</sup>. Despite increasing calcium sensitization and improved contractility, a large clinical study showed increased mortality with pimobendan<sup>169</sup>. It is only approved in Japan but is can be used worldwide in treating congestive heart failure in animals<sup>170</sup>.

Levosimendan is a cTnC-targeted calcium sensitizer that can directly increase cardiac contraction without mobilizing cellular calcium<sup>171,172</sup>. However, it is not a pure cTnC activator<sup>170</sup>. It also a selective PDE3 inhibitor which might explain results of phase III clinical trials that revealed undesirable side effects like hypotension and cardiac arrhythmias, resulting in no improvement in overall mortality<sup>173,174</sup>. It has been extensively studied to date and is currently used in systolic heart failure in some South American and European countries<sup>175</sup>. Levosimendan increases muscle contraction by binding to the N-domain of cTnC in the presence of cTnI. It can bind to both domains without cTnI, however, the presence of cTnI displaces levosimendan from the C-domain but not from the N-domain<sup>176</sup>. Levosimendan's exact binding orientation in the N-domain is still unknown because a three-dimensional structure of the cTnC-levosimendan complex is lacking.

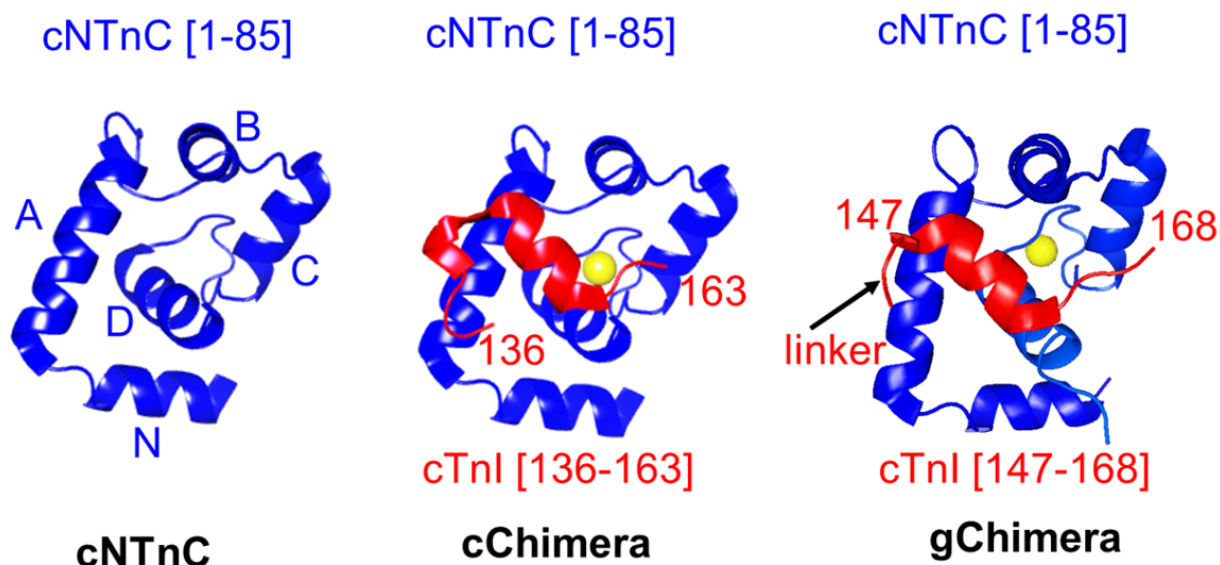
Omecamtiv mecarbil was first introduced in 2010 as a myosin activator that increases muscle contraction in both animals and humans, independent of cytosolic calcium concentration or increasing oxygen consumption<sup>177,178</sup>. Its mode of action involves binding to the pre-power stroke state of myosin, increasing the actin-myosin duty ratio (proportion of myosin heads bound to actin) while keeping the rate of shortening unaffected<sup>178</sup>. Omecamtiv mecarbil improved systolic function in a dose dependent manner<sup>179</sup>. With great anticipation, Omecamtiv mecarbil entered into a phase III clinical trial for systolic heart failure patients but failed to produce any improvement in the mortality rate<sup>180</sup>. This trial did not report any significant improvement in the primary outcome (Omecamtiv mecarbil group, 37% vs. placebo group, 39.1%) and secondary outcome (Omecamtiv mecarbil group, 19.6% vs. placebo group, 19.4%) of heart failure or death from cardiovascular causes compared to the placebo group<sup>180</sup>.

### 1.4.3.2 Design and development of a calcium sensitizer by targeting cTnC

Tirasemtiv, a fast skeletal muscle specific troponin activator, was developed by Cytokinetics Inc.<sup>181</sup>. In 2019, the company completed phase III clinical trials in amyotrophic lateral sclerosis patients but failed to show any significant improvement because of poor tolerability<sup>182</sup>. Tirasemtiv specifically targets fast skeletal troponin C and increases the calcium sensitivity of skeletal muscle. Solution NMR structure of tirasemtiv with fsTnC·fsTnI chimera (sChimera) revealed that tirasemtiv binds to the interface between the N-domain of fsTnC and the switch peptide of fsTnI and increases their binding affinity by tenfold<sup>183</sup>.

Bepridil<sup>184</sup> is a drug that targets calcium channels. It is too non-specific for cTnC to be used for this purpose, but bepridil provides valuable insights to understand the calcium sensitization mechanism of cTnC. A crystal structure of bepridil bound to cTnC showed that it binds to the central hydrophobic cavity of cTnC to stabilize its calcium-bound open state<sup>185</sup>. It binds to cTnC with a binding affinity of ~20  $\mu\text{M}$ . However, bepridil competes with the cTnI switch region for binding to the hydrophobic cleft of cTnC. Bepridil has two aromatic rings in its structure. The NMR structure showed that most of the nuclear overhauser effects (NOEs) are from the two aromatic rings of bepridil when bound to cTnC<sup>186</sup>. Thus, our lab started designing small molecules based on two aromatic rings to screen against a new chimeric protein cTnC-cTnI [136-163] we developed and named as cChimera (Figure 1.8). The lab has screened hundreds of compounds by a NMR titration method and identified that 3-methyldiphenylamine (3-Cl-DPA, a diphenylamine (DPA) based compound, binds to cChimera with a  $K_D$  of ~ 10  $\mu\text{M}$ <sup>187</sup> which was about an order of magnitude tighter binding than bepridil.

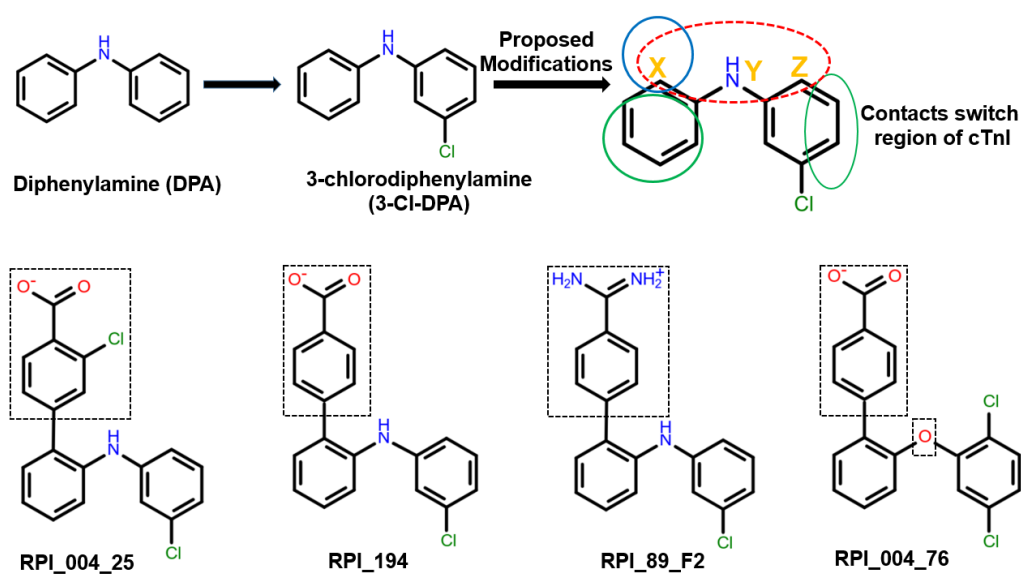




**Figure 1.8:** The N-domain of cardiac troponin complex (cNTnC<sub>1-85</sub>) in blue with 5 helices (A-D, N) and residues 136-163 of cardiac troponin I in red bound to calcium (yellow) activated cNTnC named as cChimera mimicking Ca<sup>2+</sup> bound activated conformation of cNTnC. The newly developed gChimera contains cNTnC<sub>1-85</sub> and cTnI<sub>147-168</sub> with a linker. Both cNTnC and gChimera will be used to screen many compounds to for binding to the activated cNTnC-cTnI complex.

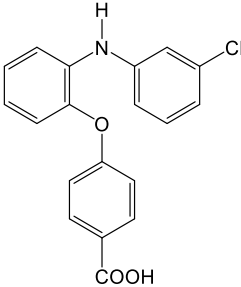
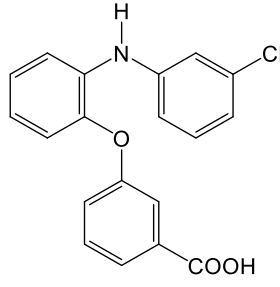
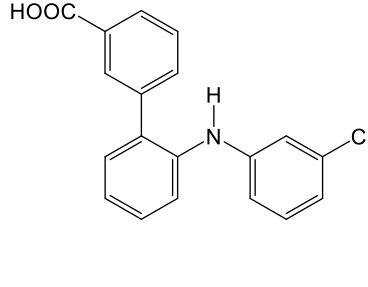
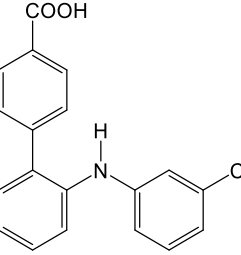
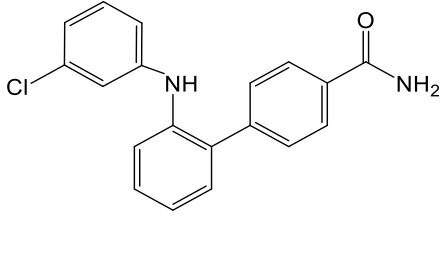
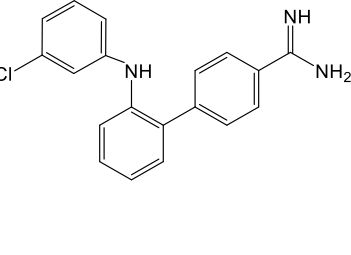
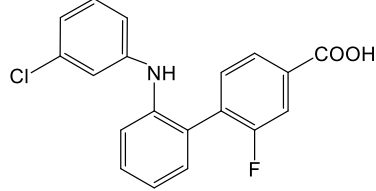
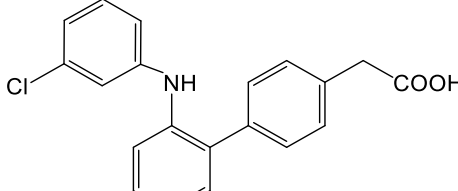
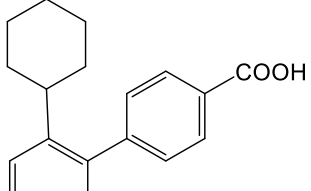
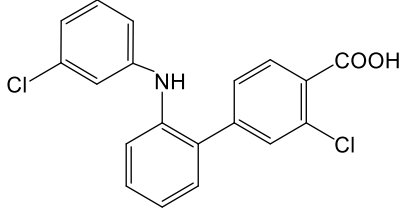
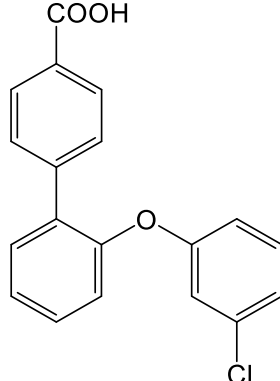
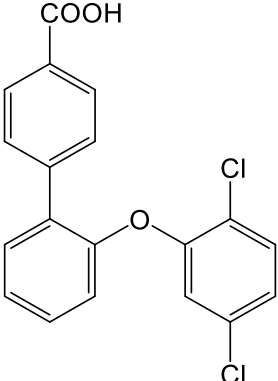
Calcium release rates of the cardiac troponin complex with bepridil and 3-Cl-DPA were measured and compared using T53C-IAANS-labeled cTnC by stopped-flow fluorescence spectroscopy. 3-Cl-DPA slowed calcium release from the troponin complex, suggesting that 3-Cl-DPA is better than bepridil when it comes to stabilizing the calcium bound open conformation of cTnC in the context of the full complex, that is, when cNTnC is bound to the switch region of cTnI. In contrast, 3-Cl-DPA was ineffective in slowing calcium release from isolated cNTnC in the absence of cTnI and cTnT, whereas bepridil significantly increased calcium affinity of isolated cTnC. An ideal troponin activator would stabilize calcium binding both before and after cTnI binding to cNTnC.

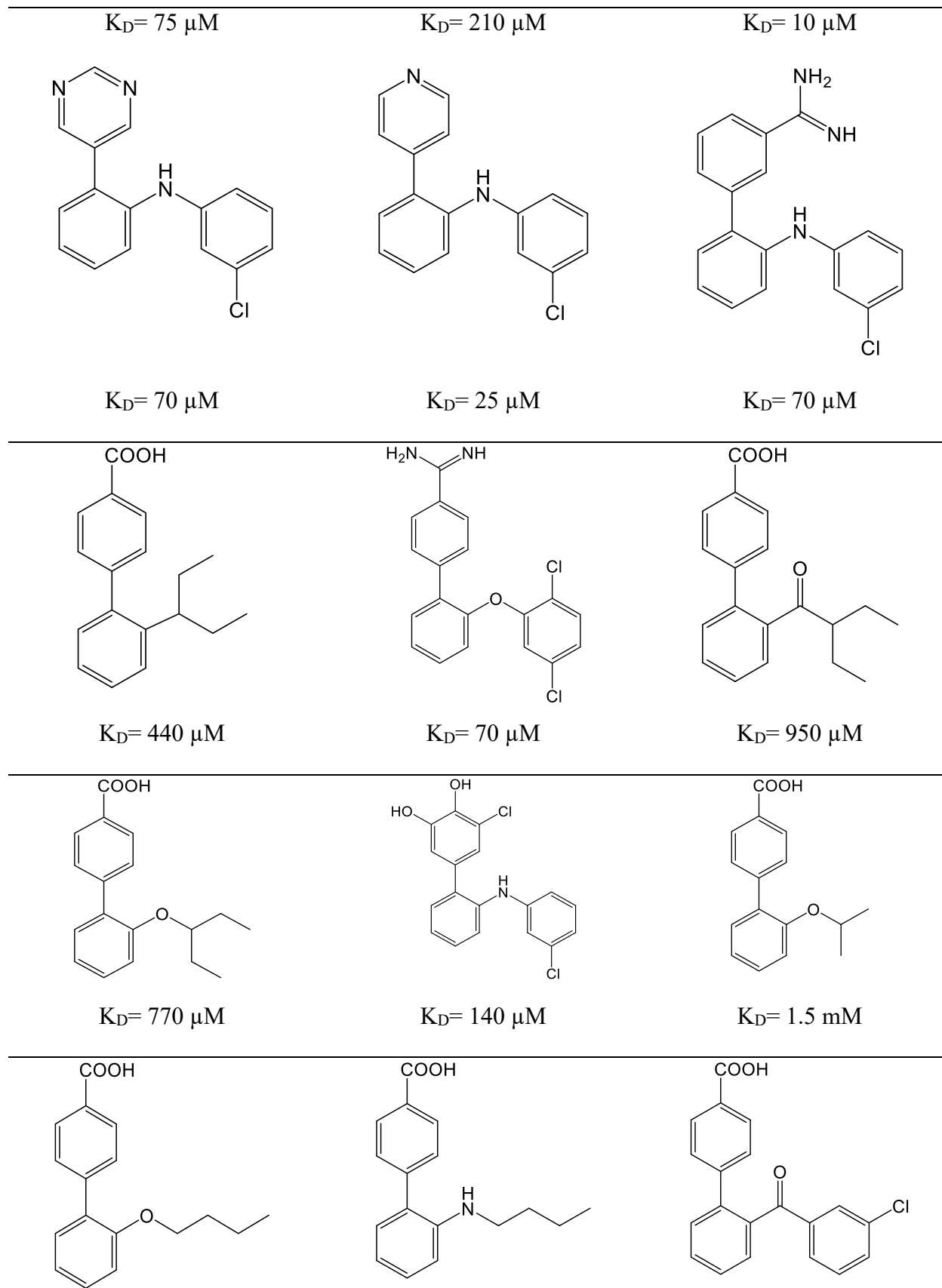
There are two phenyl rings in 3-Cl-DPA, one is an unsubstituted phenyl ring, and the other is a chloro-substituted phenyl ring. Figure 1.9 shows the details of our rational drug design process based on 3-Cl-DPA. The 3-Cl-DPA structure has three key positions (X, Y, and Z), where modifications are tolerated (does not cause steric clash). It was determined that hydrophilic substituents were better tolerated than any other site at the ortho-position (X) on the unsubstituted phenyl ring in 3-Cl-DPA. The X position was substituted with various charged residues that could potentially interact with the cNTnC-cTnI interface. All three positions in X, Y and Z were also altered for cyclization in multiple synthesized compounds. The green circles represent areas that are restricted to any substitution or modification to prevent steric clash with the cNTnC binding pocket or cTnI switch region. Table 1.1 and Table 1.2 listed a total of 47 compounds based on 3-Cl-DPA that we screened by NMR to identify potential troponin activators.



**Figure 1. 9:** The design process for small molecules as troponin modulators. 3-Cl-DPA is used as a base structure for rational drug design. X, Y and Z position of 3-Cl-DPA show where modifications or substitutions were done. Green circles indicate no modification zones to avoid steric clash with cNTnC and interference with the cTnI switch region. Four synthesized compounds are illustrated at the bottom with different modifications.

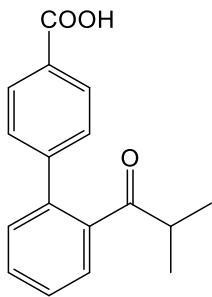
**Table 1.1:** List of compounds synthesized by the Rane pharmaceuticals and screened by NMR to identify cardiac troponin activators. Dissociation constant ( $K_D$ ) of respective compound was calculated by NMR titration experiments against gChimera.

 <p><math>K_D = 600 \mu\text{M}</math></p>	 <p><math>K_D = 125 \mu\text{M}</math></p>	 <p><math>K_D = 95 \mu\text{M}</math></p>
 <p><math>K_D = 20 \mu\text{M}</math></p>	 <p><math>K_D = 180 \mu\text{M}</math></p>	 <p><math>K_D = 40 \mu\text{M}</math></p>
 <p><math>K_D = 140 \mu\text{M}</math></p>	 <p><math>K_D = 40 \mu\text{M}</math></p>	 <p><math>K_D = 900 \mu\text{M}</math></p>
		

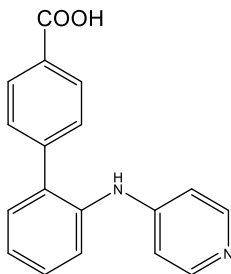


---

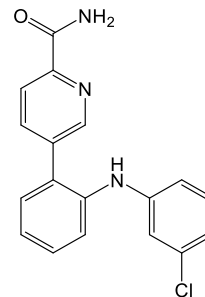
$K_D = 1.5 \text{ mM}$



$K_D = 440 \text{ } \mu\text{M}$



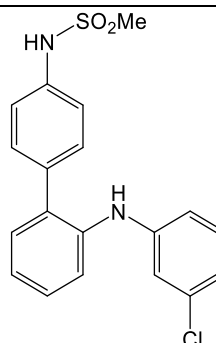
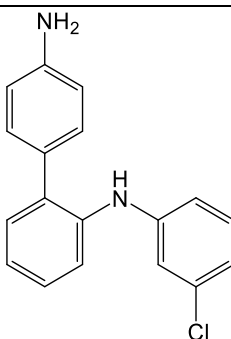
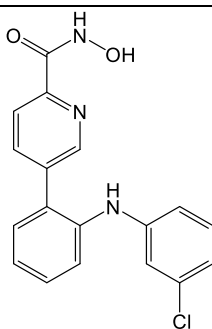
$K_D = 950 \text{ } \mu\text{M}$



$K_D = 600 \text{ } \mu\text{M}$

No binding

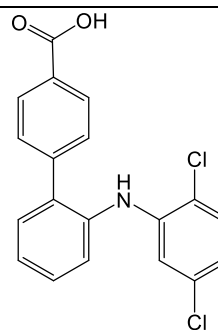
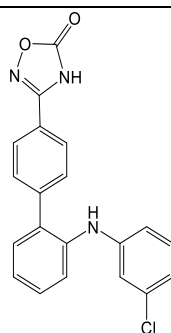
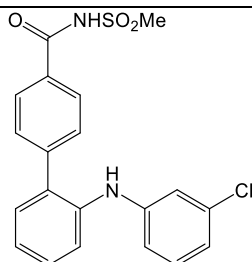
$K_D = 270 \text{ } \mu\text{M}$



$K_D = 510 \text{ } \mu\text{M}$

$K_D = 40 \text{ } \mu\text{M}$

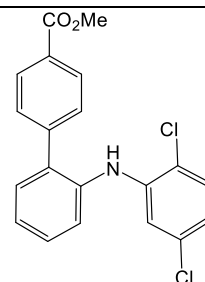
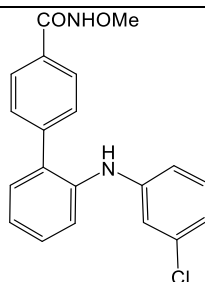
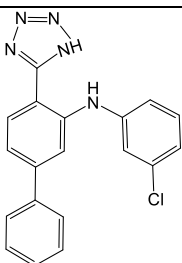
$K_D = 115 \text{ } \mu\text{M}$



$K_D = 95 \text{ } \mu\text{M}$

$K_D = 30 \text{ } \mu\text{M}$

$K_D = 20 \text{ } \mu\text{M}$

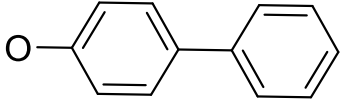
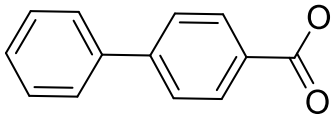
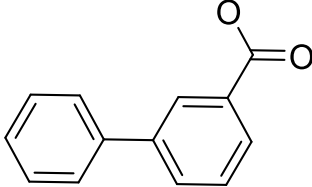
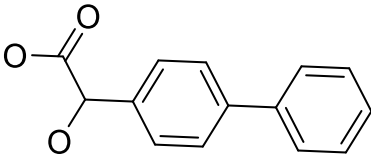
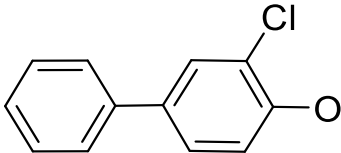
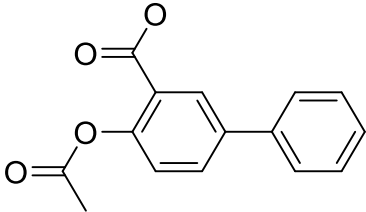
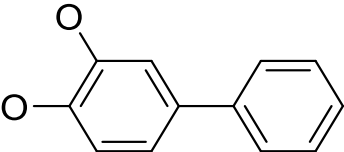
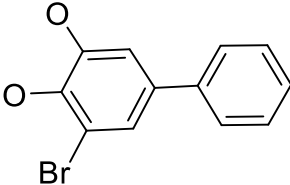
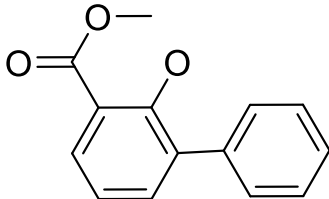
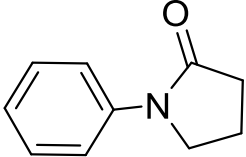
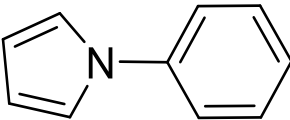


No binding

No binding

$K_D = 55 \text{ } \mu\text{M}$

**Table 1.2:** List of compounds obtained from the national cancer institute and screened by NMR to identify cardiac troponin activators. Dissociation constant ( $K_D$ ) of respective compound was calculated by NMR titration experiments against gChimera.

		
$K_D = 310 \mu\text{M}$	$K_D = 1.2 \text{ mM}$	No binding
		
No binding	$K_D = 155 \mu\text{M}$	No binding
		
$K_D = 490 \mu\text{M}$	$K_D = 110 \mu\text{M}$	No binding
		
No binding	$K_D = 1 \text{ mM}$	

## 1.5 Biophysical studies of the troponin complex

The X-ray crystal structure of cTn in 2003 revealed the structured core domains of cTn and the relative arrangement of its subunits in the absence of actin and tropomyosin<sup>13</sup>. The recent cryo-EM structure (2020) of the cardiac thin filament provides extraordinary details of the orientations and interactions of thin filament proteins, including cTn in the presence or absence of calcium<sup>14</sup>. Before that, structural and functional details within cTn were identified piece by piece using two mainstream structure determination techniques, X-ray crystallography and NMR.

Since the birth of X-ray crystallography in 1912, it became the method of choice for protein molecular structure determination<sup>188</sup>. It requires a high-quality crystallized form of a purified target protein. The crystal is then placed on a goniometer and rotated against a shooting X-ray beam and diffraction patterns of that crystal are recorded from different directions. Electron density maps of every single atom within the unit cell of a crystal are generated from diffraction patterns using Fourier transform<sup>189</sup>. Electron density maps can determine the location and orientation of each atom in the crystal and collectively generates a three-dimensional structure of the target protein. X-ray crystallography can produce a high atomic resolution of protein structure and the size of the protein does not matter that much except for large macromolecules and membrane proteins. The caveat is that the crystallizing form of a target protein represents it as a static form (fixed in one orientation) rather than a native form where it might have multiple orientations. This is what happened in the crystal structure of the troponin complex. A big piece of this complex is missing from the crystal structure because it contains regions which are intrinsically disordered or flexible in nature, which are absent in the crystallized form. These include the N and C-terminal tails of troponin I, the C-terminal tail of cTnT and the interdomain flexible linker of cTnC. These intrinsically disordered regions are vital to the structural and functional role of the troponin

complex. Unlike folded globular proteins, these regions do not have fixed three-dimensional structures and they may or may not adopt structural conformation when binding to their partners. They can also act as a flexible linker between globular domains, such as in cNTnC and cCTnC. Intrinsically disordered regions are complex entities involved in many physiological roles like transcription, translation, signaling pathways, post translational modifications such as phosphorylation, and mutations. Knowing the functions of the intrinsically disordered regions of cTn is important for elucidating the exact mechanism of muscle function. X-ray crystallography is limited for this purpose. However, it can be overcome by using a complementary low-resolution technique called small-angle X-ray scattering (SAXS)<sup>190</sup>. SAXS can be used to read biological molecules in solution in order to identify the size, shape and plasticity of flexible and unstructured parts of the proteins. In SAXS, solubilized target proteins are excited by an X-ray beam and the scattered intensity from the solution is recorded by a detector. Solvent scattering is subtracted from the sample scattering to get only scattering that is from the solubilized target protein<sup>190</sup>. Now a days, SAXS is now a days very commonly used to study the structure and dynamics of intrinsically disordered regions.

NMR is another major tool to determine three-dimensional protein structure and conformational dynamics. This is a structure determination technique that can provide atomic-scale resolution and information on structural and dynamic properties of proteins including disordered regions. It studies biological molecules in solution which is nearer to their original state. Unlike X-ray crystallography, the three-dimensional structure generated by NMR spectroscopy is an ensemble of multiple structures which can provide invaluable structural information for proteins that adopt multiple conformations<sup>191</sup>. Using solution NMR, it was identified that the linker between two domains of fast skeletal troponin C is not a rigid  $\alpha$ -helix structure but a flexible, unstructured



region in solution<sup>25,192</sup>. Even before this, the NMR structure of calmodulin (a calcium regulatory protein in smooth muscle tissue) revealed similar findings that it has two dumbbell shape domains that are connected by a flexible linker rather than an  $\alpha$ -helical structure<sup>193-196</sup>. A significant number of studies later confirmed that the two domains of fast skeletal troponin C connected by a flexible linker tumble independently when they are isolated in solution. NMR <sup>15</sup>N relaxation experiments were used to measure the tumbling rate of these two domains<sup>25,192</sup>. The first NMR structure of calcium saturated cardiac troponin C was published in 1997<sup>29</sup> and showed that both domains are connected by a flexible linker. It also revealed a surprising result that, unlike fast skeletal troponin C where both domains stay in an open conformation in the calcium saturated state, the N-domain of cTnC remains closed in both apo and calcium saturated states<sup>29,197</sup>. Later it was found that inactive calcium-binding site I is responsible for this predominant closed conformation of cTnC<sup>198</sup> (see Figure 1.3), and it required the switch peptide of cTnI to stabilize its open conformation<sup>13</sup>. Until now, this is the most critical interaction within the troponin complex that is targeted exclusively to develop troponin activators or calcium sensitizers.

The major obstacle for solution NMR is the rapid decay of signal with increasing high molecular weight systems. Thus, it is a considerable technical challenge to study the whole troponin complex using solution NMR. However, NMR can provide detailed information about the domain orientation and intrinsically disordered region interactions by using <sup>15</sup>N relaxation rates. It can detect nanosecond to picosecond timescale conformational changes within a protein<sup>33</sup>. The binding of an interaction partner can decrease these internal motions. The relaxation rate  $R_2$  ( $1/T_2$ ) is proportional to the effective correlation time, which increases with the size of the protein but decreases with greater internal flexibility. All positions in a protein domain tumble according

to a global correlation time, except for flexible segments, which have a shorter effective correlation time.

Another application for the NMR technique is to screen small molecules against a target protein. Solution NMR can monitor the binding of small molecules to the target protein. Titration of unlabeled small molecules into  $^{15}\text{N}$  labeled target protein at each time point can be monitored by two-dimensional  $^1\text{H}$ ,  $^{15}\text{N}$  HSQC. The titration curves of many residues with concentration-dependent chemical shift perturbations can be used to calculate binding affinity based on the global fitting method developed by Hoffman and Sykes<sup>199</sup>. One difficulty of NMR drug titration is that the drug binding affinity is not accurate when the drug precipitates before saturating the protein. Also, in order to get a good 2D HSQC spectrum, the protein concentration needs to be at least 100  $\mu\text{M}$ . Another major concern is the solubility issue as the compounds get more hydrophobic in order to bind them more tightly to the hydrophobic pocket of the target protein.

### **1.5.1 NMR techniques used in this study**

In all three chapters of this thesis, we used different NMR techniques in addition to other molecular biology, biochemical and biophysical techniques. In Chapter 2 of this thesis, we used multiple 2D and 3D experiments ( $^1\text{H}$ - $^{15}\text{N}$  HSQC, HNCACB and CBCA(CO)NH) to get backbone ( $^1\text{H}$ ,  $^{15}\text{N}$ ,  $^{13}\text{C}$ ) chemical shift assignments of the intrinsically disordered C-terminal tail of cTnI, and the free versus actin-Dnase1 bound state. The side chain  $^1\text{H}$ ,  $^{13}\text{C}$  chemical shift assignments were also carried out by using (H)C(CO)NH-TOCSY and H(C)(CO)NH-TOCSY experiments. Other 3D experiments were performed to determine the secondary structure of the unstructured tail and include  $^{15}\text{N}$ -edited and  $^{13}\text{C}$ -edited homonuclear  $^1\text{H}$ - $^1\text{H}$  NOESY experiments. In Chapter 2, we used the NMR relaxation measurement technique ( $^{15}\text{N}$   $R_2$  relaxation rate) to determine the

tumbling rate of cTnC domains when they are in free form, in activated orientation, or in the presence of DCM mutations and phosphorylation. In Chapter 3, we used the NMR titration method to screen 47 compounds against cNTnC and gChimera. NMR titration results identified the best compound based on the rate of dissociation constant of the compound and its solubility which was further tested using different experimental models such as by stopped flow fluorescence, in skinned ventricular trabeculae, the isolated-perfused mouse heart, and mouse ventricular cardiomyocytes.

## **1.6 Thesis hypothesis**

The key interaction that turns cardiac muscle contraction on and off is the calcium-dependent binding of cTnI<sub>146-158</sub> by the regulatory N-terminal domain of cTnC. We hypothesize that this interaction is regulated by phosphorylation in other regions of the troponin complex to control the contractile balance of the healthy heart, but disruption of this regulation by cardiomyopathy-associated mutations, or proteolysis, gives rise to contractile dysfunction. Importantly, the interaction can also be modulated by drug-like small molecules to compensate for abnormal heart function in disease.

## **1.7 Objectives**

### **1.7.1 Chapter 2: Structure and proteolytic susceptibility of the inhibitory C-terminal tail of cardiac troponin I**

- 1 To gain structural understanding of the C-terminal tail of troponin I and its interaction with actin. This region was absent in the 2003 X-ray crystal structure.
- 2 To map cleavage sites of this region with respect to MMP-2 and calpain.

**1.7.2 Chapter 3: Dilated cardiomyopathy mutations and phosphorylation disrupt the active orientation of cardiac troponin C**

- 1 To reconstitute binary and ternary complexes of cTn to understand the active orientation of the N-domain of cTnC.
- 2 To determine how phosphorylation and DCM-associated mutations found in cTnI and cTnC disrupt its active orientation.

**1.7.3 Chapter 4: Small molecule RPI-194 stabilizes activated troponin to increase the calcium sensitivity of striated muscle contraction**

- 1 Designing new drug compounds for cNTnC using existing knowledge of calcium sensitizers, screening and the selecting best candidate compound.
- 2 Determining binding affinity of the selected compound against cNTnC and gChimera.
- 3 Measuring the activity of the selected compound in different *ex vivo* experimental models.

## CHAPTER 2

### STRUCTURE AND PROTEOLYTIC SUSCEPTIBILITY OF THE INHIBITORY C- TERMINAL TAIL OF CARDIAC TROPONIN I

Chapter 2 has been published in:

Mahmud, Z., Zahran, S., Liu, P. B., Reiz, B. Chan, B. Y. H. Roczkowsky, A. McCartney, C. E. Davies, P. L. Li, L. Schulz, R. Hwang, P. M. Structure and proteolytic susceptibility of the inhibitory C-terminal tail of cardiac troponin I. *Biochim Biophys Acta Gen Subj* **1863**, 661-671 (2019).

## 2.1 Introduction

Cardiac troponin (cTn) links cyclic  $\text{Ca}^{2+}$  fluctuations to cardiac muscle contraction and relaxation<sup>200,201</sup>. It is comprised of three subunits<sup>12</sup>: cTnC binds calcium; cTnT anchors the complex to tropomyosin; and cTnI is the inhibitory subunit (Figure 2.1). Cardiac troponin I (cTnI) has two flexible tails that are critical to its function. The N-terminal tail, cTnI<sub>1-38</sub>, interacts with the regulatory domain of cTnC (cNTnC) to enhance its calcium affinity. This effect is attenuated by phosphorylation of cTnI at Ser22/Ser23<sup>202</sup>, the primary post-translational modification regulating the calcium sensitivity of cardiac muscle contraction in humans<sup>203</sup>.

The C-terminal tail, cTnI<sub>135-209</sub>, binds actin to anchor the troponin-tropomyosin complex to a “blocked” position that prevents actin-myosin cross-bridging during diastole (the ventricular relaxation phase of the cardiac cycle). During systole (the ventricular contraction phase), cNTnC binds the cTnI switch region, cTnI<sub>146-158</sub>, in a calcium-dependent manner, to release the inhibitory effect of cTnI<sub>135-209</sub>. Thus, the cTnI<sub>135-209</sub> C-terminal tail cycles back and forth between actin and cTnC during diastole and systole, respectively, driving the cardiac cycle. The interactions between cTnI and cTnC have been well established by X-ray crystallography and NMR spectroscopy<sup>13,187,204</sup>, but very little is known about the interaction between cTnI and actin.

The N-terminal and C-terminal tails of cTnI are flexible, solvent-exposed, and susceptible to post-translational modifications like proteolysis<sup>205,206</sup>. Western blot analysis of serum cTnI in myocardial infarction patients demonstrates multiple cut sites within the cTnI N- and C-terminal tails<sup>207</sup>. In animal hearts, proteolytic digestion of cTnI has been demonstrated to occur in myocardial ischemia-reperfusion injury<sup>85,136,208</sup>. Two major mechanisms are known to contribute to ischemia-reperfusion injury: generation of excess RONS<sup>80,209</sup> and calcium overload<sup>210,211</sup>. Both

processes activate downstream proteases that can compromise structural integrity and promote cell death.

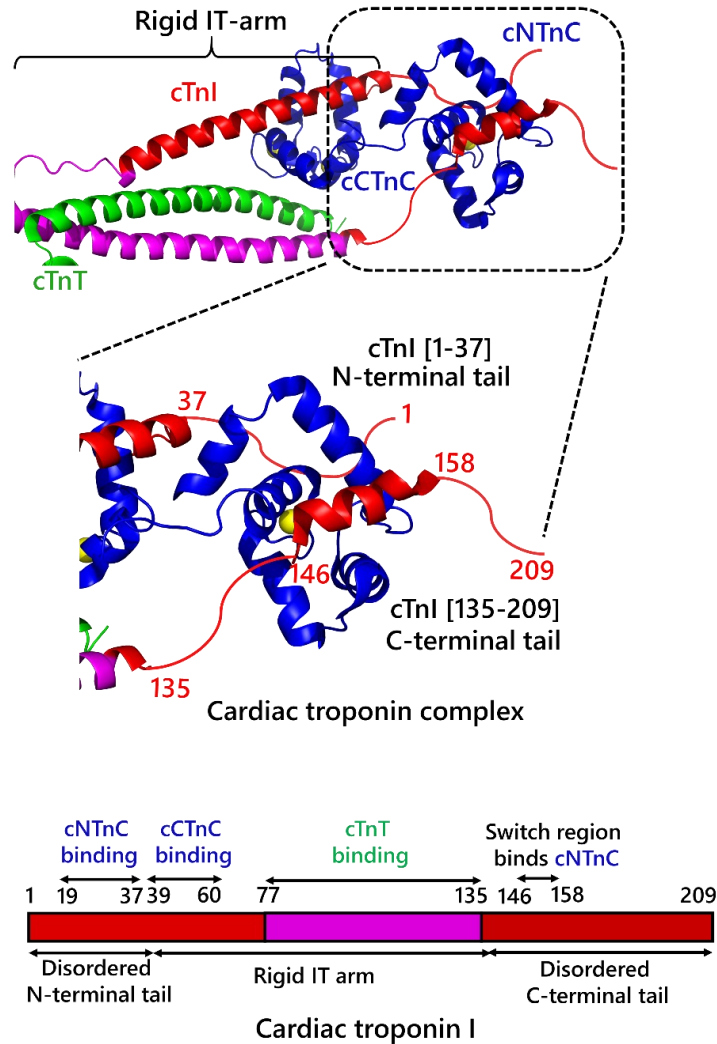


**Figure 2.1:** Calcium-saturated cTn (partial structure shown). cTnC is shown in blue and consists of cNTnC and cCTnC. cTnI is shown in magenta and red, with the red regions corresponding to the two constructs used in this study: cTnI<sub>1-77</sub> and cTnI<sub>135-209</sub>. The inset highlights the N- and C-terminal tails of cTnI, with intrinsically disordered regions drawn manually as squiggles. Figure prepared using PyMOL and structure 4Y99 (PDB code). At resting calcium concentrations, cNTnC releases calcium (yellow sphere), adopts a closed conformation, and cTnI<sub>135-209</sub> binds to actin. Bar diagram at the bottom shows domain organization and different functional region of cTnI with its binding partners.

MMPs were originally identified as extracellular proteases but were subsequently found to localize to intracellular compartments as well<sup>85,212</sup>, with MMP-2 being the predominant isoform in cardiomyocytes. MMPs are synthesized as inactive zymogens, with an inhibitory cysteine residue in the pro-peptide domain complexing the catalytic zinc ion. MMPs are activated by proteolytic removal of the pro-peptide domain or by chemical modification of the inhibitory cysteine sulfhydryl group, as occurs when RONS, particularly peroxynitrite<sup>113</sup>, are generated during ischemia-reperfusion injury<sup>81,213,214</sup>.

Calpains are a family of calcium-dependent cysteine proteases that are involved in cytoskeletal remodeling, signal transduction, and cell death<sup>215,216</sup>. Calpain-1 ( $\mu$ -calpain) and calpain-2 (m-calpain) are ubiquitously expressed and are activated by elevated intracellular  $\text{Ca}^{2+}$  concentrations<sup>116,210,211,217,218</sup>. These calpains have nearly indistinguishable substrate specificities<sup>219,220</sup> but differ in the concentration of calcium required for activation. Both MMP-2 and calpain have been shown to cleave cTnI in animal models of ischemia-reperfusion injury<sup>85,131</sup>. Small molecule inhibition of MMP-2<sup>83,85</sup> or calpain<sup>121,221,222</sup> has been shown to attenuate ischemia-reperfusion injury in animal models.

The structured core of cTnI (residues 39-134) is known to be relatively resistant to proteolytic digestion<sup>223</sup>. Moreover, since full-length cTnI misfolds and aggregates on its own, we generated two soluble fragments of cTnI containing its flexible protease-susceptible N- and C-terminal tails, cTnI<sub>1-77</sub> and cTnI<sub>135-209</sub>, respectively. Using purified proteins and mass spectrometry, we have mapped out the precise cTnI cleavage sites for MMP-2 and calpain-2. Since cTnI interacts primarily with cTnC and actin *in vivo*, we also examine its proteolysis in the presence of these binding partners.



Given the extensive biophysical characterization of the troponin complex over the past six decades, it is possible to understand the proteolytic susceptibility of cTnI in terms of its structure. However, relatively little is known about the structure of the critical C-terminal tail bound to the actin, because the intrinsic disorder of the tail, combined with the filamentous nature of actin, is difficult for any one biophysical technique to tackle comprehensively. In the current study, we use solution NMR spectroscopy to probe the structure of the C-terminal cTnI<sub>135-209</sub> tail without actin and in the presence of actin maintained in a monomeric form by its complex with DNase I (so that it can be studied by solution NMR)<sup>224</sup>.

## **2.2 Materials and methods**

### **2.2.1 Protein expression and purification**

Soluble recombinant human cTnI proteins, cTnI<sub>1-77</sub> and cTnI<sub>135-209</sub>, were expressed in *Escherichia coli* and purified as described previously<sup>225,226</sup> (see 3.1.2 for protocol in detail). Briefly, both recombinant proteins were expressed as fusions to the  $\beta$ -barrel membrane protein, PagP. This causes the fusion protein to accumulate in insoluble inclusion bodies, which can be harvested by centrifugation, solubilized in 6 M guanidine-HCl, and then purified by nickel affinity chromatography. cTnI<sub>1-77</sub> was separated from PagP via cyanogen bromide cleavage in 0.1 M HCl<sup>33,225</sup>, while cTnI<sub>135-209</sub> was separated using nickel ion-catalyzed cleavage<sup>226</sup>. cTnI<sub>135-209</sub> was also produced with <sup>15</sup>N- and/or <sup>13</sup>C-isotope enrichment for solution NMR studies. Purity of produced proteins were confirmed by SDS-PAGE gel.

### **2.2.2 NMR Spectroscopy**

All NMR data used in this study were generated at 30°C using a Varian Inova 500 MHz spectrometer equipped with a triple resonance probe and pulsed field gradients. NMR samples

contained 500  $\mu$ l of aqueous NMR buffer consisting of 10 mM imidazole, 0.5 mM 2,2-dimethyl-2-silapentane-5-sulfonate-d6 sodium salt ( $d_6$ -DSS), and 0.01 %  $\text{NaN}_3$  in 90%  $\text{H}_2\text{O}$ : 10%  $\text{D}_2\text{O}$  or 100%  $\text{D}_2\text{O}$  at pH 6.8. Three-dimensional HNCACB and CBCA(CO)NH experiments were carried out to obtain backbone  $^1\text{H}$ ,  $^{15}\text{N}$ ,  $^{13}\text{C}$  chemical shift assignments for a sample of 2.8 mg cTnI<sub>135-209</sub> dissolved in NMR buffer. In addition, both (H)C(CO)NH-TOCSY and H(C)(CO)NH-TOCSY experiments were conducted to obtain side-chain  $^1\text{H}$  and  $^{13}\text{C}$  chemical shift assignments. 3D  $^{15}\text{N}$ -edited and  $^{13}\text{C}$ -edited homonuclear  $^1\text{H}$ - $^1\text{H}$  NOESY experiments were also performed and analyzed to obtain Nuclear Overhauser effect (NOE) information. All two- and three-dimensional NMR data were processed using NMRPipe/NMRDraw software<sup>227</sup>. NMRViewJ<sup>228</sup> from One Moon Scientific was used to further visualize and analyse spectra. The  $\delta$ 2D program<sup>229</sup> (<http://www-mvsoftware.ch.cam.ac.uk/>) was used to quantitate secondary structure propensities ( $\alpha$ -helix,  $\beta$ -strand and random coil) using backbone chemical shift assignments<sup>230</sup>.

Recombinant bovine cardiac muscle actin (>99% pure) was purchased from Cytoskeleton, Inc. (Denver, Colorado, USA). RNase-free and protease-free deoxyribonuclease I (DNase I) was purchased from Worthington Biochemical Corporation. Actin was maintained in a monomeric form through its tight binding to DNase I, thereby inhibiting polymerization<sup>231</sup>.

$^{15}\text{N}$ -labeled cTnI<sub>135-209</sub> (1.1 mg) was dissolved in 500  $\mu$ l NMR buffer supplemented with 10 mM DTT. A baseline ( $^1\text{H}$ ,  $^{15}\text{N}$ )-HSQC spectrum was recorded of this sample. Next, 1 mg of actin was dissolved in 100  $\mu$ l NMR buffer + 10 mM DTT and then added to 1 mg DNase I, and this mixture was added to the 500  $\mu$ l solution of  $^{15}\text{N}$ -labeled cTnI<sub>135-209</sub>. The ( $^1\text{H}$ ,  $^{15}\text{N}$ )-HSQC spectrum was repeated, and a comparison of peak intensities before and after addition of monomeric actin-DNase I was obtained, after correcting for dilution. The mathematical equation for calculating errors is as follows:

$$\Delta\left(\frac{I}{I_0}\right) = \frac{\sqrt{I^2 N_0^2 + I_0^2 N^2}}{I_0^2}$$

Here,

$$\Delta\left(\frac{I}{I_0}\right) = \text{Estimated error in signal intensity ratio}$$

$I$  = Signal intensity in the presence of actin – DNase I

$I_0$  = Signal intensity before adding actin – DNase I

$N$  = Noise level in the presence of actin – DNase I

$N_0$  = Noise level before adding actin – DNase I

### 2.2.3 SDS-PAGE analysis of *in vitro* proteolysis

Purified human recombinant MMP-2 (72 kDa) (200 µg/ml) was activated chemically by 1 mM of 4-aminophenylmercuric acetate (APMA) in activation buffer (100 mM Tris-HCl, 10 mM CaCl<sub>2</sub>, pH 7.6), as previously described<sup>232</sup>. Recombinant rat calpain-2 was expressed and purified as previously described<sup>233</sup>. APMA-activated recombinant human MMP-2 was incubated with cTnI<sub>1-77</sub> (0.1 µg/µl) or cTnI<sub>135-209</sub> (0.1 µg/µl) in incubation buffer I (50 mM Tris-HCl, 5 mM CaCl<sub>2</sub>, 150 mM NaCl, pH 7.6) for 2 h at 37°C. Similarly, recombinant rat calpain-2 was also incubated with cTnI<sub>1-77</sub> (0.1 µg/µl) or cTnI<sub>135-209</sub> (0.1 µg/µl) in incubation buffer II (50 mM Tris-HCl, 5 mM CaCl<sub>2</sub>, 150 mM NaCl, 10 mM beta mercaptoethanol, 10 mM DTT, pH 7.6) for 2 h at 37 °C. Proteolytic assays were carried out with enzyme-to-substrate molar ratios ranging from 1:500 to 1:10000 and 1:250 to 1:5000 for MMP-2:cTnI and calpain-2:cTnI, respectively. As controls, 2-[[[(1, 1'-Biphenyl)-4-ylsulfonyl)-(1-methylethoxy) amino]-N-hydroxyacetamide (ARP-100) and

MDL-28170 inhibitors [Cayman Chemical, Ann Arbor, Michigan, USA] were used to block MMP-2 and calpain-2 activity, respectively. The products of all proteolysis assays were separated by electrophoresis in 16% Tris-Tricine gels and visualized by Coomassie Blue staining.

In an additional set of experiments, activated MMP-2 or calpain-2 were incubated with cTnI<sub>1-77</sub> or cTnI<sub>135-209</sub> in the presence or absence of cTnC or actin. cTnC binds to cTnI with a 1:1 stoichiometry, so 0.32 µg/µl cTnC was used, corresponding to a 1.5:1 cTnC:cTnI ratio (excess cTnC). For actin, a 1:1 stoichiometry was suspected (discussed further in the Results section 2.3), therefore actin was added at a concentration of 0.50 µg/µl, corresponding to a 1:1 molar ratio. The actin concentration was then serially diluted two-fold to yield molar ratios ranging from 1:1 to 0.0625:1. Note that under these conditions, actin is predominantly in the filamentous F-actin form, though at the lowest concentrations used, there would be a more significant proportion of monomeric G-actin<sup>234</sup>.

#### **2.2.4 Mass spectrometric analysis of *in vitro* proteolysis**

A cocktail of MMP-2 (1 ng/µl) with cTnI<sub>1-77</sub> (0.43 µg/µl) or MMP-2 (1 ng/µl) with cTnI<sub>135-209</sub> (0.44 µg/µl), each at 1:5000 molar ratio, was incubated at 37°C for a time course study from 0 min to 24 h. The same time course study was applied to calpain-2 (4 ng/µl) with cTnI<sub>1-77</sub> (0.43 µg/µl) and calpain-2 (4 ng/µl) with cTnI<sub>135-209</sub> (0.44 µg/µl), each incubated at 1:1000 molar ratio at 37°C. Formic acid (1% v/v) was used to denature the proteins and stop the reaction, and the samples were immediately flash frozen with liquid nitrogen. For protein molecular weight determination reverse phase high performance liquid chromatography followed by mass spectrometry (RP-HPLC-MS) was performed using an Agilent 1200 SL HPLC System with a Poroshell 300SB-C8, 5 µm particle size, 75x0.5 mm column (Agilent Technologies, Santa Clara,

CA, USA), with Opti-pak trap cartridge kit, 5  $\mu$ l BED, C8, thermostated at 60°C or a Phenomenex Aeris 3.6  $\mu$ m, WIDEPORE XB-C8, .02  $\mu$ m, 2.1x50 mm with guard column, thermostated at 50°C.

For the Poroshell column a buffer gradient system composed 0.1% formic acid in water as mobile phase A and 0.1% formic acid in acetonitrile as mobile phase B was used. An aliquot of 5  $\mu$ l of sample was loaded onto the column at a flow rate of 0.15 ml/min and an initial buffer composition of 95% mobile phase A and 5% mobile phase B. After injection, the column was washed using the initial loading conditions for 3 min to effectively remove salts. Elution of the proteins was done by using a linear gradient from 5% to 50% mobile phase B for 10 min, 50% to 95% mobile phase B for 2 min, 95% to 98% mobile phase B for 4 min and back to 5% mobile phase B for of 1 min.

For the Phenomenex Aeris column the following gradient was used: the column was washed after loading of the sample using a 0.4 ml/min flow rate and 5% mobile phase B for 2 min to effectively remove salts. Elution of the proteins was done by using a linear gradient from 5% to 65% mobile phase B for 8 min, 65% to 98% mobile phase B over a period of 2 minute, kept at 98% mobile phase B for 2 min and back to 5% mobile phase B for 1 min.

Mass spectra were acquired in positive mode of ionization using an Agilent 6220 Accurate-Mass TOF HPLC/MS system (Santa Clara, CA, USA) equipped with a dual sprayer electrospray ionization source with the second sprayer providing a reference mass solution. Mass correction was performed for every individual spectrum using peaks at  $m/z$  121.0509 and 922.0098 from the reference solution. Mass spectrometric conditions were in drying gas 10 l/min at 325 °C, nebulizer 20 psi, mass range 100-3000 Da, acquisition rate of  $\sim$ 1.03 spectra/sec, fragmentor 200 V, skimmer 65 V, capillary 3200 V, instrument state 4 GHz High Resolution. Data analysis was performed using the Agilent MassHunter Qualitative Analysis software package version B.03.01 SP3. From

the masses, the proteolysis fragments from both recombinant proteins were determined by using the online bioinformatics tool FindPept from the ExPASy , <sup>235</sup> (<http://web.expasy.org/findpept/>). SequenceEditor (Build 5.65) from Bruker Daltonics Biotools 3.2 SR3 was also used to analyse the peptide masses.

## 2.3 Results

### 2.3.1 Structure of free cTnI<sub>135-209</sub> by NMR spectroscopy

The <sup>1</sup>H-<sup>15</sup>N HSQC spectrum of cTnI<sub>135-209</sub> alone in solution (see Figure 2.3A below) shows narrow and intense peaks with poor chemical shift dispersion, suggestive of intrinsically disordered regions. Some peaks are weak due to rapid backbone amide-solvent exchange (becoming more visible at more acidic pH due to the slowing of base-catalyzed solvent exchange), especially peaks corresponding to inhibitory region residues 135-147. Near-complete chemical shift assignments of backbone and side chain resonances were obtained (deposited in the Biological Magnetic Resonance Bank, BMRB# 27476).

Secondary structure analysis showed predominantly random coil structure, using the chemical shift analysis program  $\delta$ 2D, which determines the percentage of secondary structure based on HN, N, H $\alpha$ , C $\alpha$ , CO, and C $\beta$  chemical shifts on a per residue basis. cTnI residues 150-159 are known to form an alpha helix when the switch region binds cTnC, and  $\delta$ 2D indicates that this region has the highest helical propensity (up to 50%) in cTnI<sub>135-209</sub> in the absence of cTnC (Figure 2.2A). Some helical character extends beyond the switch region out to residue 172, though this is not observed in X-ray or NMR structures <sup>13,204</sup>. Slight helical propensity is also observed from residues 189 to 202 (though only up to ~10%). There is no significant  $\beta$ -sheet propensity anywhere in the cTnI<sub>135-209</sub> sequence.

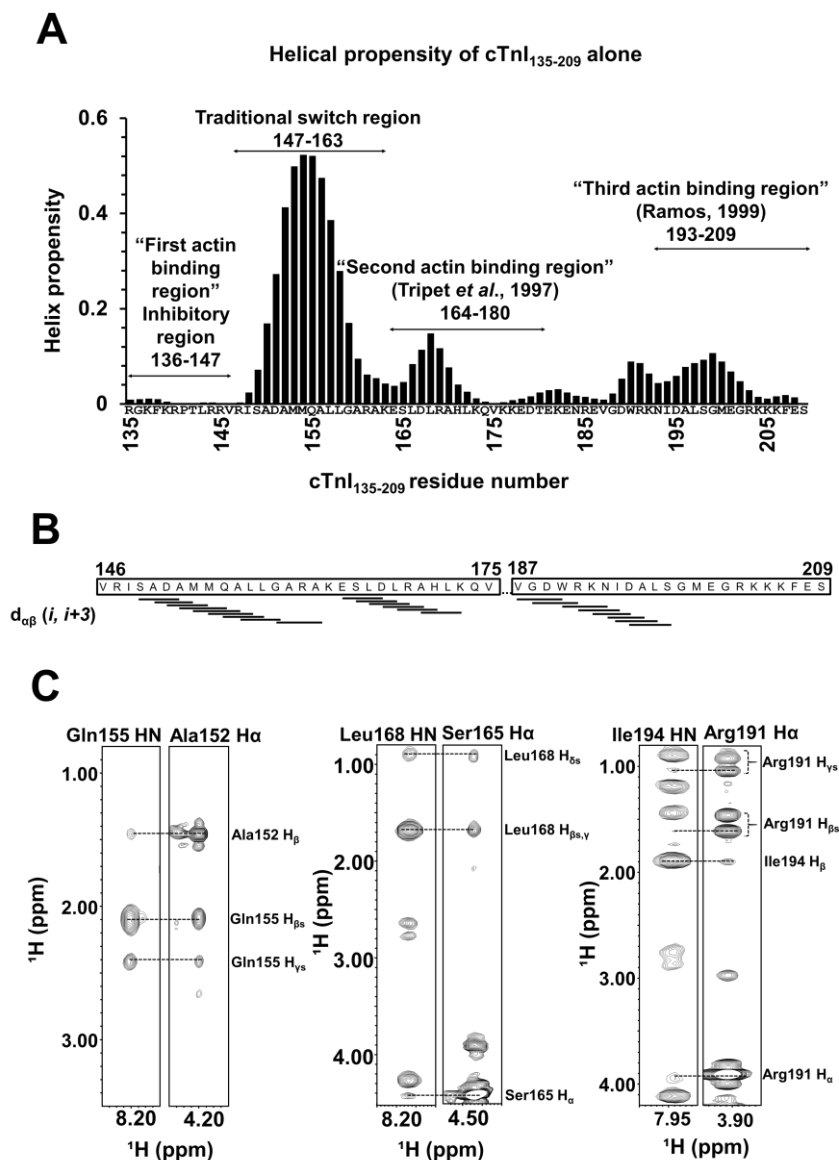


**Figure 2.2:** (A) Residue-specific secondary structure of cTnI<sub>135-209</sub> calculated by the program  $\delta 2D$  using backbone NMR chemical shifts. The functional regions shown highlight the results of limited binding studies in the past, rather than exact boundaries determined from structure. (B) Summary of medium-range NOE connectivities  $d_{\alpha\beta}(i, i+3)$  that are specific for alpha helix. (C) Representative strip plots showing helical medium-range NOEs from 3D  $^{15}\text{N}$ - edited NOESY-HSQC and 3D  $^{13}\text{C}$  edited NOESY-HSQC. Section 2.3.2 describes the second actin-binding region (Tripet *et al.* 1997<sup>236</sup>) and the third actin-binding region (Ramos, 1999<sup>237</sup>) in detail.

Regions with helical propensity indicated by  $\delta 2D$  also had corroborating NOEs obtained from  $^{13}C$ - and  $^{15}N$ -edited NOESY-HSQC experiments. Figure 2.2B shows medium range NOEs  $d_{\alpha\beta}(i, i + 3)$  that correspond to the helical regions identified by chemical shift analysis. The strongest helical NOEs were observed in the switch region, as shown in Figure 2.2C, which shows 6 strip plots extracted from  $^{15}N$ - and  $^{13}C$ -edited NOESY spectra. The NOE pattern confirms nascent helix formation in residues 149-159, 164-172 and 187-197.

Our analysis of the cardiac troponin I C-terminal region is consistent with that of Blumenschein et al.<sup>238</sup>, who documented primarily disordered random coil in the corresponding region in fast skeletal troponin I. However, this study did not include an analysis of the helical switch region (unobservable due to the high molecular weight of the fast skeletal troponin complex), nor did it consider nascent helical structure via  $^1H$ - $^1H$  NOEs or backbone chemical shifts. In contrast to the Blumenschein et al. study, Murakami et al.<sup>239</sup> describe a “mobile domain” in the C-terminal region of fast skeletal troponin I made up of a small anti-parallel  $\beta$ -sheet extending from residues V143 to L154 (corresponding to V175 to N184 in cardiac troponin I, though according to sequence alignment, D153-L154 in fast skeletal troponin I are deleted in the cardiac isoform, precluding formation of a similar anti-parallel  $\beta$ -sheet in cTnI), packed against a helix extending from V157 to K167 (V187 to L197 in cTnI). It is important to note that the backbone chemical shifts obtained by Murakami et al. agree with those obtained by Blumenschein, but these are not supportive of a rigid mobile domain structure. Thus, the “mobile domain” of Murakami et al. could be at most a transiently structured domain, which the authors support by the presence of many weak long range NOEs. In this regard, we note that our chemical shift and NOE data are in agreement with Murakami et al. with respect to the presence of nascent helical structure in residues cTnI 164-172 and 187-197. However, there is no evidence of  $\beta$ -sheet formation in our



construct, either by chemical shift or NOE analysis. As well, Murakami et al. note the presence of an additional C-terminal helix that we do not observe in our construct, likely because of sequence differences between the fast skeletal and cardiac isoforms of troponin I.

### **2.3.2 Partial structuring of cTnI<sub>135-209</sub> in the presence of monomeric actin-DNase I**

Many intrinsically disordered segments of proteins acquire structure upon binding to a protein partner. However, we previously found that cTnI<sub>1-37</sub> does not acquire any rigid secondary structure upon binding the cTnTnC domain through predominantly electrostatic interactions<sup>33</sup>. In contrast, the hydrophobic binding of cTnI<sub>146-158</sub> to cTnTnC is associated with formation of a rigid alpha helix comprising cTnI residues 150-158<sup>13,204</sup>.

When we added cTnI<sub>135-209</sub> to filamentous F-actin, all NMR signals broadened out beyond detection, consistent with a molecular tumbling rate too slow to allow the use of solution NMR spectroscopy (data not shown). We, therefore, added DNase I to actin to maintain it in a monomeric form, with the total molecular weight of the complex ~74 kDa. Addition of a 10% molar ratio of actin-DNase I to cTnI<sub>135-209</sub> caused sequence-specific broadening of cTnI<sub>135-209</sub> (Figure 2.3A), indicating that the kinetics of cTnI<sub>135-209</sub> binding to actin-DNase I occur within the fast exchange regime with respect to the NMR signal frequency differences between free and bound states. (If binding were in the slow exchange regime, binding of a 1:10 ratio actin-DNase I to cTnI<sub>135-209</sub> could at most obliterate 10% of the signal.) The degree of signal attenuation provides a rough estimate of which regions of cTnI<sub>135-209</sub> acquire the greatest structural changes upon interacting with actin-DNase I. More tightly bound residues will experience a greater degree of signal broadening caused by the relatively slow tumbling of the ternary complex, whereas this effect is lessened by rapid internal motions in less restricted residues. Signal broadening additionally occurs

due to conformational exchange between free and actin-bound cTnI<sub>135-209</sub> states. In the fast exchange regime, the residues that broaden most will be those that most frequently occupy bound states and/or those with the largest chemical shift differences between free and bound states (thus moving towards an intermediate exchange regime). In any case, the regions of cTnI<sub>135-209</sub> that broaden most will be those that experience the largest structural dynamic changes upon interaction with actin.

In the 2D <sup>1</sup>H-<sup>15</sup>N spectrum of cTnI<sub>135-209</sub> in the absence of actin-DNase I, the inhibitory region, residues 135-147, contain weak signals that became undetectable upon addition of actin-DNase I, confirming that the region interacts with actin, as expected (Figure 2.3A). A small peptide consisting of only cTnI residues 136-147 alone is capable of completely inhibiting actin-myosin cross-bridging, demonstrating this to be the minimal actin-binding inhibitory region<sup>240</sup>. Residues 147-177, which includes the switch region, broaden considerably upon addition of actin-DNase I, suggesting substantial structuring upon binding to actin-DNase I. This finding is consistent with the work of Tripet et al.<sup>236</sup>, which showed a “second actin-binding region” within a region corresponding to cTnI residues 164-180. In summary, our data indicate that residues 135-177, comprising the inhibitory, switch, and second actin-binding regions, acquire rigid structure upon interaction with actin-DNase I.

The rest of the C-terminal tail of cTnI, residues 178-209, appear to be more loosely tethered to actin-DNase I than residues 135-177 (Figure 2.3B). However, the helical C-terminal region from residues 190-198 appears to be more tightly bound than adjacent segments. This is consistent with the study of Ramos<sup>237</sup>, who found that the last 17 residues of chicken skeletal troponin I (corresponding to residues 193-209 in the current construct) also contribute to a third actin-interacting region in cTnI.

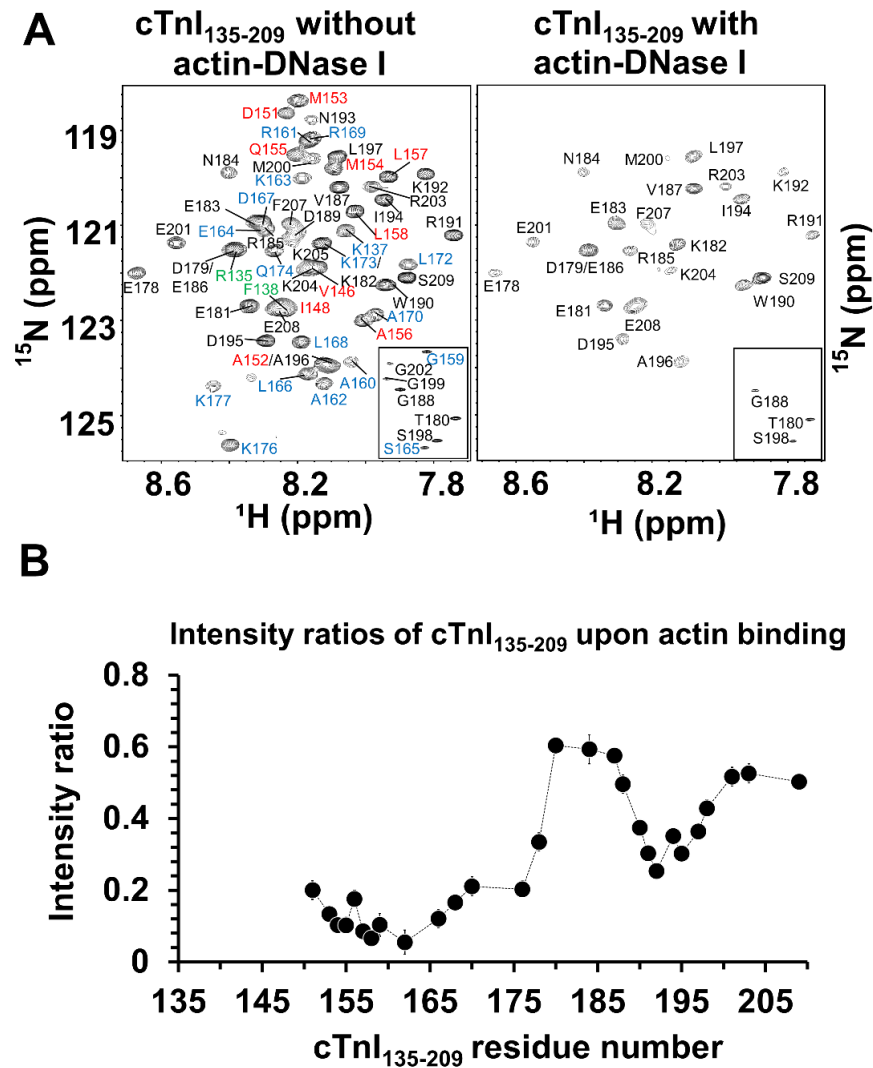


**Figure 2.3:** 2D [ $^1\text{H}$ ,  $^{15}\text{N}$ ]-HSQC NMR spectra of cTnI<sub>135-209</sub>. (A) cTnI<sub>135-209</sub> without actin-DNase I (left) or with actin-DNase I (right). The insets show the  $^{15}\text{N}$ -upfield region of the spectrum containing, Gly, Ser, and Thr residues. Addition of a small amount of monomeric actin-DNase I complex into cTnI<sub>135-209</sub> causes differential signal broadening (right). Residues belongs to inhibitory region (green), switch region (red) and second actin binding region (blue) are undetectable upon addition of actin-DNase I. (B) The observed reduction in signal intensity ratio in the 2D [ $^1\text{H}$ ,  $^{15}\text{N}$ ]-HSQC signals of cTnI<sub>135-209</sub> when actin-DNase I complex is added. Overlapped signals or signals with weak intensity were excluded.

It is noteworthy that the regions of cTnI<sub>135-209</sub> that become the most structured upon binding actin-DNase I are the same regions found to possess alpha-helical propensity (Figure 2.3B), with the exception of the inhibitory region cTnI<sub>135-147</sub>. It is therefore quite possible that the same regions acquire helical structure when bound to actin. In contrast, residues 178-192 and 201-209 have negligible intrinsic helical propensity and do not appear to become as structured upon binding actin (which suggests that the folded “mobile domain” detected by Murakami et al.<sup>239</sup> could be formed by cTnI residues 135-177, rather than 164-209, as originally proposed). Nevertheless, it is important to note that all residues in cTnI<sub>135-209</sub> broaden upon binding actin-DNase I, including the less structured regions, which may represent flexible loops that bind to actin through predominantly electrostatic interactions. In fact, mutations associated with hypertrophic or restrictive cardiomyopathy are found throughout the sequence of cTnI<sub>135-209</sub><sup>241</sup>, suggesting that residues along its entire length are important to interactions with the actin thin filament.

### **2.3.3 *In vitro* proteolysis of cTnI by MMP-2 and calpain-2**

Proteolytic cleavage of purified recombinant human cardiac troponin constructs, cTnI<sub>1-77</sub> and cTnI<sub>135-209</sub>, was monitored by SDS-PAGE (Figure 2.4). cTnI<sub>1-77</sub> runs as a single 16 kDa band, which is higher than its actual (mass spectrometry-confirmed) weight of 8.6 kDa, likely due to its high proportion of positively charged residues. cTnI<sub>135-209</sub> similarly runs slower than predicted on SDS-PAGE. cTnI<sub>1-77</sub> and cTnI<sub>135-209</sub> were readily proteolysed by MMP-2, and this was almost entirely abolished by the MMP inhibitor, ARP-100 (Figure 2.4A, Figure 2.4B). Similarly, calpain-2 readily cleaved cTnI<sub>1-77</sub> and cTnI<sub>135-209</sub>, and this was blocked by the calpain inhibitor, MDL-28710. (Figure 2.4C, Figure 2.4D).

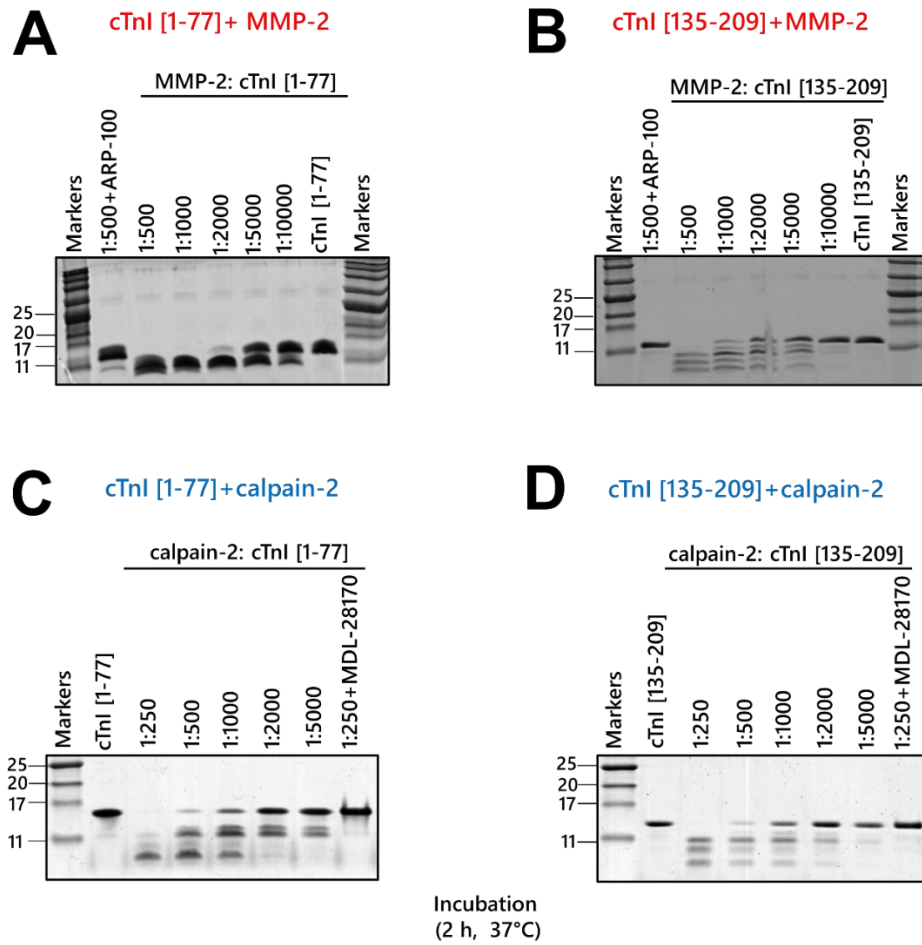


**Figure 2.4:** Representative Coomassie Blue-stained 16% Tris-Tricine gels illustrating in vitro proteolysis of cTnI<sub>1-77</sub> or cTnI<sub>135-209</sub> by proteases MMP-2 or calpain-2 (representative of N=3 independent experiments). Molar protease-to-substrate ratios are shown above each lane in the gel. 2 µg of cTnI was loaded in every reaction lane. Incubations were 2 h at 37 °C. Inhibition of MMP-2 and calpain-2 activities by ARP-100 and MDL-28710, respectively, is also shown.

### 2.3.4 Mass spectrometric identification of MMP-2 cleavage sites of cTnI

Reverse-phase high-performance liquid chromatography-mass spectrometry was used to identify MMP-2-derived cleavage sites in cTnI<sub>1-77</sub> and cTnI<sub>135-209</sub>. We observed cleavage products after incubation with MMP-2 for 10 min, 30 min, 2 h, 6 h and 24 h (Figure 2.5 and Appendix 1).

At 0 min, intact cTnI<sub>1-77</sub> appeared at its expected molecular weight, 8627 Da. Within 10 min of incubation, cleavage products were formed corresponding to cTnI<sub>1-17</sub> (1663.8 Da) and cTnI<sub>18-77</sub> (6980.9 Da) (Figure 2.6 and Appendix 1), and these continued to predominate even after 24 h of digestion. Thus, there appears to be a single main cleavage site for MMP-2 within cTnI<sub>1-77</sub> at <sup>12</sup>RPAPAP-IRRRSS<sup>23</sup>.

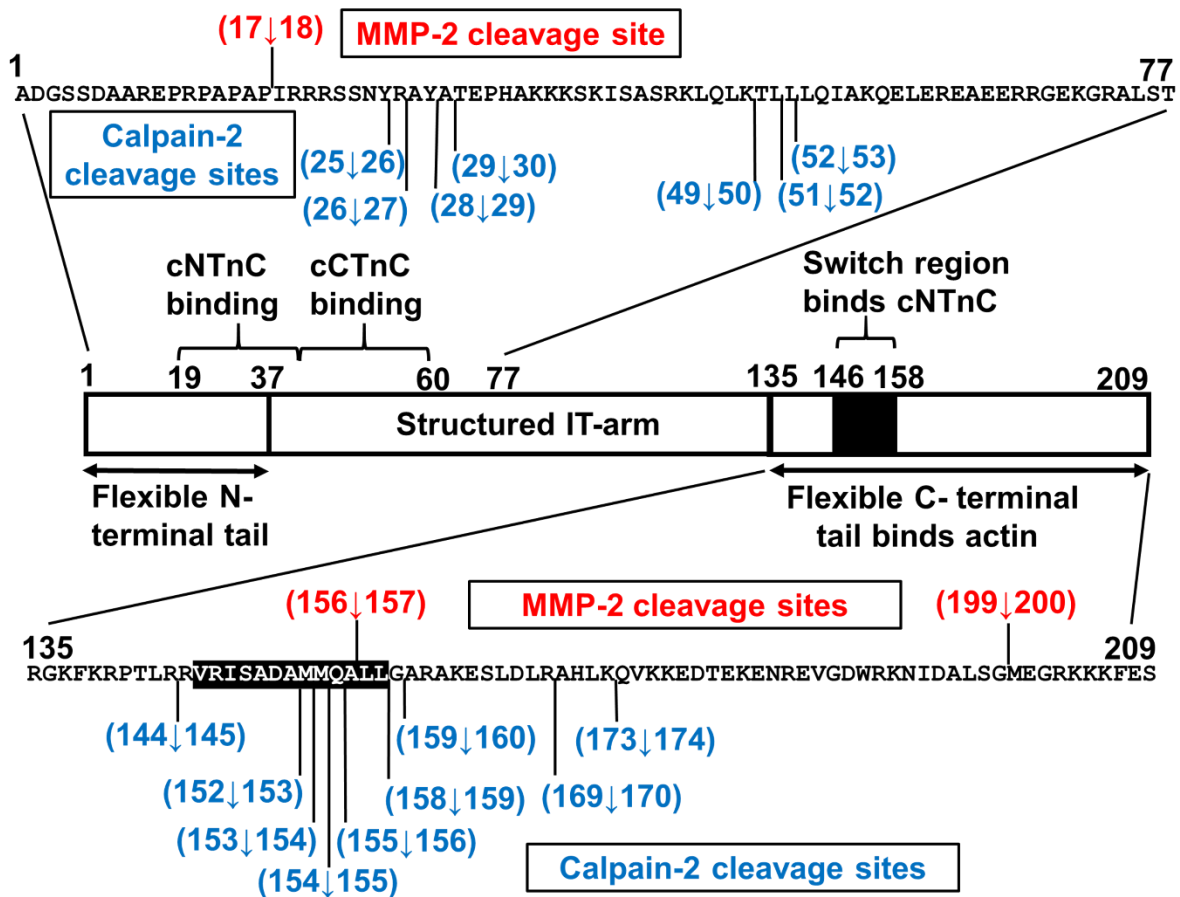


**Figure 2.5:** Summary of mass spectrometric analysis identifying MMP-2 and calpain-2 cleavage sites within cTnI<sub>1-77</sub> and cTnI<sub>135-209</sub> (included in Supplementary Data). Note that our numbering of cTnI excludes the N-terminal methionine, which is removed and replaced by an acetyl group in post-translational processing.

## MMP-2 proteolysis of cTnI [1-77] at 10 min

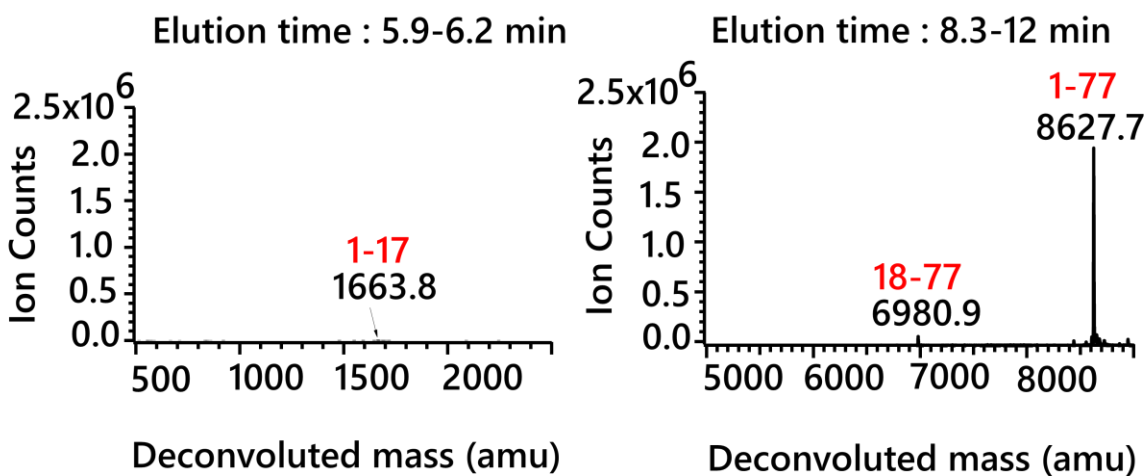


**Figure 2.6:** Mass spectrometry data of cTnI<sub>1-77</sub> proteolysed by MMP-2 at 10 min incubation time point. Proteolysed fragments of cTnI<sub>1-77</sub> were eluted at different retention time and the molecular weight of fragments were determined by reverse phase high performance liquid chromatography followed by mass spectrometry.

MMP-2-mediated cleavage of cTnI<sub>135-209</sub> occurs at two sites that were apparent after 10 min of digestion: <sup>151</sup>DAMMQA-LLGARAK<sup>163</sup> and <sup>194</sup>IDALSG-MEGRKK<sup>205</sup> (Appendix 1). The cleavage site at A156-L157 is preferred, because it is entirely cleaved at 2 h, whereas the more C-terminal site at G199-M200 is not entirely cleaved, even after 24 h. (Note that cTnI<sub>135-209</sub> was <sup>15</sup>N-labeled for NMR studies, so its molecular mass was increased by the amount expected from replacing the naturally occurring <sup>14</sup>N isotope with <sup>15</sup>N).

The MMP-2 cleavage sites identified within cTnI<sub>1-77</sub> and cTnI<sub>135-209</sub> are consistent with computer-aided prediction of MMP-2 cleavage sites <http://cleavpredict.sanfordburnham.org/><sup>242</sup> and consensus sequences derived from MMP-2-catalyzed cleavage of peptide libraries using a high throughput PICS (proteomic identification of protease cleavage sites) technique and biotinylated

peptide library cleavage assay<sup>243-245</sup>, which show a strong preference for a hydrophobic residue (particularly leucine, isoleucine, methionine) in the P1' site (the residue immediately C-terminal to the cleavage site), as well as a proline or hydrophobic  $\beta$ -branched residue (valine or isoleucine) at P3 (the third residue N-terminal to the cleavage site)<sup>243,246</sup>. A feature that is somewhat unique to MMP-2 is its predilection for small amino acid residues like glycine, alanine, or serine at positions P1, P2, and P3'.

### **2.3.5 Mass spectrometric identification of calpain-2 cleavage sites of cTnI**

We also mapped calpain-2 specific cleavage sites within cTnI<sub>1-77</sub> and cTnI<sub>135-209</sub> using mass spectrometry (Appendix 2). We identified calpain-2-mediated cTnI<sub>1-77</sub> and cTnI<sub>135-209</sub> cleavage products after 0 min, 10 min, 2 h, 6 h and 24 h (See Appendices 2 and 3). At 0 min, intact cTnI<sub>1-77</sub> is observed at its expected molecular weight 8627 Da (See Appendix 2), though cleavage products have already appeared, with the most prominent fragments being cTnI<sub>1-28</sub> (3088 Da), cTnI<sub>1-29</sub> (3159 Da), cTnI<sub>29-77</sub> (5557 Da), cTnI<sub>30-77</sub> (5486 Da), and cTnI<sub>50-77</sub> (3225 Da), suggesting rapid proteolysis even before the reaction is immediately stopped by adding 1% v/v formic acid and the reaction vial frozen in liquid nitrogen. Thus, calpain-2-mediated proteolysis of cTnI occurs at a much faster rate than that observed with MMP-2. By 10 min (see Appendix 2), intermediate cleavage products like cTnI<sub>1-49</sub> (5419.9 Da) and cTnI<sub>30-77</sub> (5486.1 Da) are disappearing, while smaller cleavage fragments begin to predominate: cTnI<sub>1-25</sub> (2697.4 Da), cTnI<sub>1-28</sub> (3087.6 Da), cTnI<sub>1-29</sub> (3158.6 Da), cTnI<sub>27-49</sub> (2583 Da), cTnI<sub>26-49</sub> (2739.6 Da), cTnI<sub>50-77</sub> (3224.8 Da), and cTnI<sub>53-77</sub> (2897.6 Da). These terminal products are still present after 24 h, suggesting that the major cleavage sites for calpain are all clustered around cTnI residues 25-30 and 49-53.



For calpain-2 digestion of cTnI<sub>135-209</sub>, we identified intact <sup>15</sup>N-labelled cTnI<sub>135-209</sub> with expected molecular weight 8964.4 Da at 0 min (See Appendix 3). Similar to cTnI<sub>1-77</sub>, the major cleavage products of cTnI<sub>135-209</sub> can also be detected from 0 min. After 10 min incubation, numerous major cleavage sites are apparent. Strikingly the calpain-2 activity localizes predominantly to the hydrophobic switch region, with a total of 6 different sites located between residues 152 and 160 (Figure 2.5). This is consistent with the known sequence preferences of calpains-1 and -2<sup>247</sup>. Of note is the cleavage site at <sup>156</sup>ALL-GAR<sup>161</sup>, which has a striking similarity to the optimal calpain cleavage sequence PLF-AAR determined by peptide library analysis<sup>247</sup> and alanine scanning mutagenesis<sup>220</sup>, with hydrophobic residues on either side of the central scissile bond. Additional calpain cleavage sites are located N-terminal to residues R145, A170, and Q174.

In contrast to the very specific cut sites of MMP-2, calpain-2 appears to possess much broader substrate specificity, having multiple cleavage sites within cTnI<sub>1-77</sub> and cTnI<sub>135-209</sub> (Figure 2.5). Remarkably, calpain cut sites occur in all cTnI segments that are involved in protein-protein interactions. It seems as though calpain targets protein regions above a certain threshold of hydrophobicity, and these tend to be the same segments involved in protein-protein interactions: cTnI<sub>25-30</sub> contains four calpain cleavage sites and is the most hydrophobic segment of cTnI<sub>19-37</sub>, which binds electrostatically to the N-terminal domain of cTnC; cTnI<sub>49-53</sub> contains three calpain cleavage sites and is the most hydrophobic segment of cTnI<sub>39-60</sub>, which forms an alpha helix that binds tightly to C-terminal domain of cTnC; and cTnI<sub>152-160</sub> contains six calpain cleavage sites and includes the most hydrophobic segment of the cTnI switch region, cTnI<sub>146-158</sub>. Full activation of MMP-2 and calpain would have a devastating effect on cardiac troponin I function, severely disabling calcium-mediated excitation-contraction coupling. However, it is necessary to determine

which physiologic protein-protein interactions protect cTnI from proteolysis, as detailed in the sections below.

### **2.3.6 *In vitro* proteolysis of cTnI<sub>1-77</sub> in the presence of cTnC**

We therefore examined proteolysis of cTnI<sub>1-77</sub> in the presence of its only known binding partner, cTnC. cTnI<sub>1-77</sub> interacts with both globular domains of cTnC in two distinct ways. cTnI residues 39-60 bind tightly to the C-terminal domain of cTnC (cCTnC) as a well-structured alpha helix that extends down to residue 79<sup>13</sup>. In contrast, cTnI<sub>1-37</sub> is intrinsically disordered in nature, with cTnI<sub>19-37</sub> interacting with the cNTnC domain through predominantly electrostatic interactions<sup>33</sup>.

There was no observable proteolysis of cTnC itself in the presence of MMP-2 or calpain-2 (Figure 2.7). cTnC binding had virtually no effect on MMP-2-mediated digestion of cTnI<sub>1-77</sub> (Figure 2.7A), which occurs between residues 17 and 18 (Figure 2.5). This cut site lies just N-terminal to cTnI<sub>19-37</sub>, which interacts with cNTnC<sup>33</sup>. Calpain-2-mediated digestion of cTnI<sub>1-77</sub> yields two partially digested intermediate fragments at 11 and 12 kDa on SDS-PAGE corresponding roughly to fragments cTnI<sub>30-77</sub> and cTnI<sub>1-49</sub>, respectively. Upon addition of cTnC, the larger fragment, corresponding to residues 1-49, disappears completely (Figure 2.7B), this makes sense because the cut sites between residues 49 and 53 lie exactly in the middle of the alpha helix (cTnI residues 39-60) that binds very tightly to cCTnC. Thus, formation of a rigid alpha helix precludes calpain-mediated proteolysis at this site in its native biologic context. In contrast, when cTnI<sub>19-37</sub> binds electrostatically to the cTnC N-terminal domain, cTnI residues 25-31 display a partial restriction in mobility, but retain an intrinsically disordered random coil state<sup>33</sup>. Apparently, this interaction provides only partial protection from calpain-mediated proteolysis, as suggested

by Figure 2.7B (that is, digestion at this site still produces a prominent 11 kDa band in the presence of cTnC).

Based on earlier biophysical studies, proteolytic removal of the first 17 residues of cTnI by MMP-2 would be expected to slightly decrease the calcium sensitivity of the troponin complex, but not to the same extent as the physiologic phosphorylation of Ser22 and Ser23<sup>248</sup>. Hence, while cTnI is vulnerable to MMP-2 digestion at residues 17-18 when in complex with cTnC, proteolytic cleavage at this site would not be expected to have a devastating impact on cardiac function. In contrast, cleavage at cTnI residues 25-30 by calpain would remove more of the N-terminal tail and have a much larger calcium desensitizing effect<sup>248</sup>.

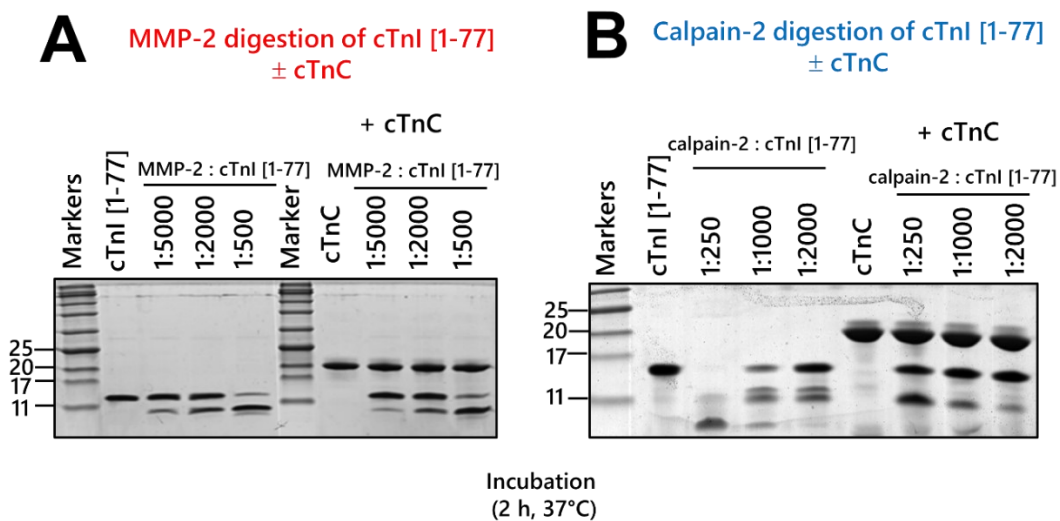


**Figure 2.7:** Comparison of in vitro proteolysis of cTnI<sub>1-77</sub> in the presence or absence of cTnC by MMP-2 (A) and calpain-2 (B) in representative Coomassie Blue-stained SDS-PAGE gel (representative of N=3 independent experiments). Cardiac troponin C is not susceptible to either MMP-2 or calpain-2 proteolysis and appears intact as a single band at ~21 kDa. 2 µg of cTnI was loaded in every reaction lane. Molar cTnI-to-cTnC ratio was 1 to 1. The incubation period was 2 h at 37°C.

### 2.3.7 *In vitro* proteolysis of cTnI<sub>135-209</sub> in the presence of cTnC

Note that MMP-2 has only two cut sites (between residues 156-157 and 199-200) in cTnI<sub>135-209</sub>, leading to the production of five different degradation products, producing a surprisingly complex appearance on the SDS-PAGE gels for so few cut sites (Figure 2.4). cTnC binding to cTnI<sub>135-209</sub> resulted in proteolytic protection against MMP-2 (Figure 2.8A) primarily at the cut site between residues 156 and 157. This results from the binding of the switch region, cTnI<sub>146-158</sub>, to cTnC, with an alpha helix extending from residues 150-159<sup>13</sup>. In contrast, the C-terminal cut site between cTnI residues 199 and 200, which is not known to form any interaction with cTnC, remains exposed to MMP-2 cleavage. Thus, in the presence of cTnC, this C-terminal locus becomes the preferred MMP-2 cut site in cTnI<sub>135-209</sub>.

Binding of cTnI<sub>135-209</sub> to cTnC significantly changes its proteolysis pattern by calpain (Figure 2.8B). In the absence of cTnC, the most favoured cut sites are distributed throughout the switch region, between residues 152 and 160, yielding a fragment at about 11 kDa (cTnI<sub>153-209</sub>) on the SDS-PAGE gel and a smaller fragment that runs at the bottom (cTnI<sub>135-152</sub>). However, binding of the cTnI<sub>146-158</sub> switch region to cTnC shields it from cleavage, making the cut sites flanking the switch region more probable and altering the pattern of SDS-PAGE-visible proteolytic fragments.

Cleavage of the switch region would be expected to have a devastating effect on cardiac function, making it impossible to activate cardiac muscle contraction. However, it is apparent that binding of cTnI<sub>135-209</sub> to cTnC specifically protects the switch region against proteolytic digestion, though adjacent segments are still susceptible to MMP-2 and calpain-mediated proteolysis.

### 2.3.8 *In vitro* proteolysis of cTnI<sub>135-209</sub> in the presence of actin

We next examined the proteolysis of cTnI<sub>135-209</sub> in the presence of actin. The current NMR study of cTnI<sub>135-209</sub> suggests a partial rigidification throughout its entire length upon interaction with actin. Incubation of cTnI<sub>135-209</sub> with actin showed pronounced concentration-dependent inhibition of MMP-2 proteolytic activity, almost completely inhibiting cTnI proteolysis at the highest concentration of actin studied, at a molar ratio of cTnI<sub>135-209</sub> to actin of 1:1 (Figure 2.9A). However, even at this concentration of actin, some residual proteolysis at both MMP-2 cut sites is still evident.

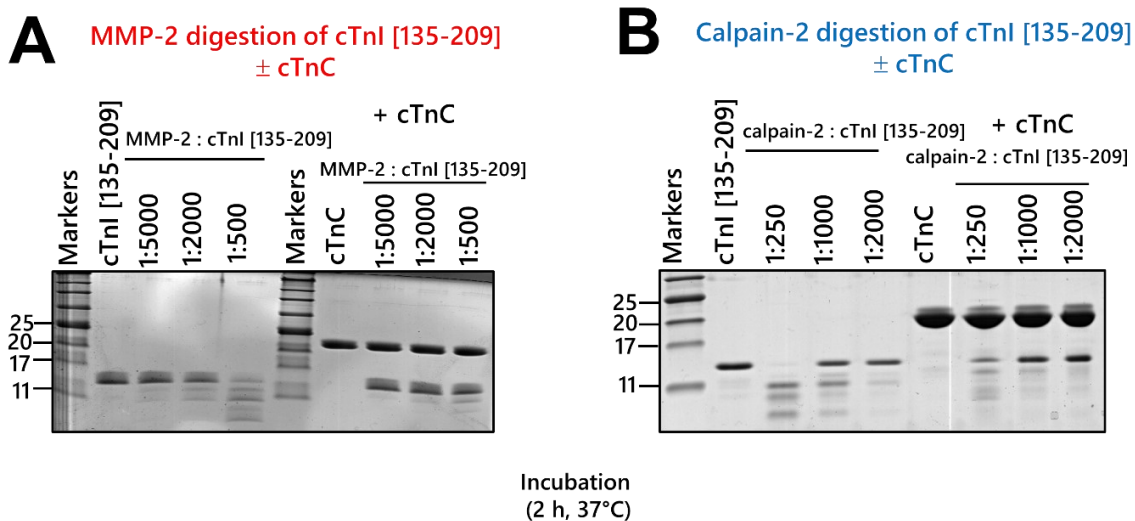


**Figure 2.8:** Comparison of *in vitro* proteolysis of cTnI<sub>135-209</sub> in the presence or absence of cTnC by MMP-2 (A) and calpain-2 (B) in representative Coomassie Blue-stained SDS-PAGE gel (representative of N=3 independent experiments). Cardiac troponin C is not susceptible to either MMP-2 or calpain-2 proteolysis and appears intact as a single band at ~21 KDa. 2 µg of cTnI was loaded in every reaction lane. Molar cTnI-to-cTnC ratio was 1 to 1. The incubation period was 2 h at 37°C.

Calpain-2-mediated digestion of cTnI<sub>135-209</sub> in the presence of actin at a 1:1 molar ratio showed partial proteolytic protection of all cut sites, leading to significant preservation of intact cTnI<sub>135-209</sub> (Figure 2.9B). The degradation band at 11 kDa, corresponding to cleavage of the switch region, remains prominent in the presence of actin. This suggests that actin binding does not protect the switch region to the same extent as binding to cTnC.

It should be noted that within the sarcomere, the stoichiometry of actin:cTnI is 7:1. However, this is the result of a single troponin complex being associated with a single tropomyosin coiled-coil that lies along seven actin monomers. Presumably, in the absence of tropomyosin, the binding site for cTnI is limited to a single actin monomer. The protection of cTnI<sub>135-209</sub> by a 1:1 molar ratio of actin is suggestive of a 1:1 stoichiometry of binding, as expected.

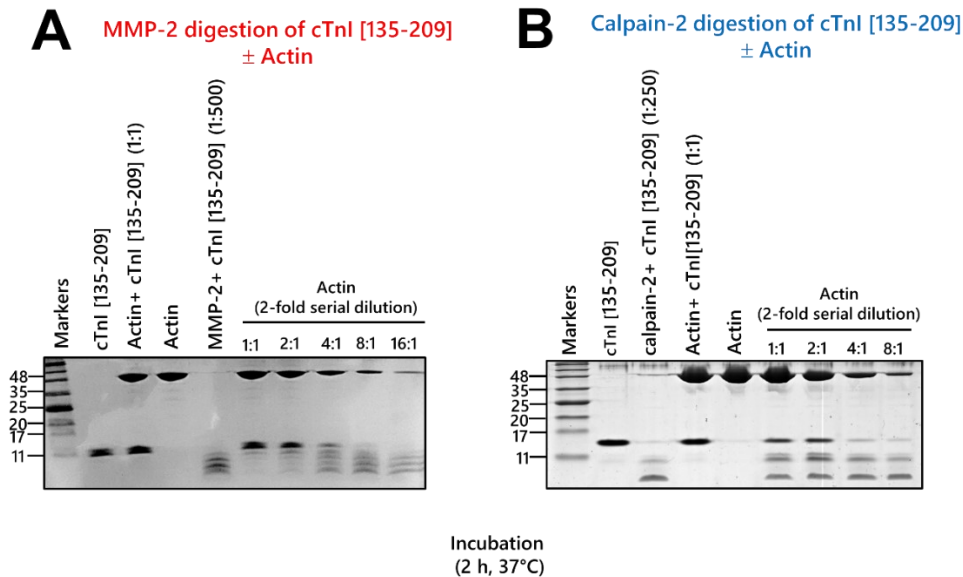


**Figure 2.9:** Representative Coomassie Blue-stained SDS-PAGE gels showing in vitro proteolysis of cTnI<sub>135-209</sub> in the presence of A) MMP-2 (representative of N=3 independent experiments) or B) calpain-2 (representative of N=3 independent experiments). Molar actin:cTnI ratios are indicated above the gel. Incubation duration was 2 h at 37°C. 2 µg of cTnI was loaded in every reaction lane. MMP-2-to-cTnI ratio was 1:500, and calpain-2-to-cTnI ratio was 1:250.

## 2.4 Discussion

Our study demonstrates that the C-terminal tail of cTnI contains three regions with intrinsic helical propensity, corresponding to the critical switch region that binds to cNTnC, the “second actin binding region”<sup>236</sup>, and the “third actin binding region”<sup>237</sup>. We further show that all of these regions exhibit structural changes in the presence of actin, and it would not be unreasonable to postulate that they acquire more helical character. Finally, we demonstrate that the N and C-terminal tails of cTnI are susceptible to cleavage by MMP-2 and calpain-2, two intracellular proteases that are activated in ischemia-reperfusion injury<sup>85,121,212,218,222</sup>.

Numerous studies in different animal model systems have attempted to address the issue of cTnI proteolysis in ischemia-reperfusion injury<sup>85,131,132,136,137,143,249-251</sup>. A fundamental question is which proteases are activated, and at what degree of ischemic injury. One can envision a full spectrum of ischemia-reperfusion injury ranging from immediate recovery of function to irreversible cell death. Even with cell death, there is a spectrum of functional impairment ranging from ventricular wall akinesis to aneurysm to wall rupture. Central to the understanding of structural damage is the activation of intracellular proteases, of which MMP-2, calpains, and caspases have been identified as major players. (Caspase, however, was found to not digest cTnI in an earlier study<sup>252</sup>).

Myocardial stunning is a form of reversible injury<sup>253</sup> in which restoration of blood flow relieves ischemia, but the viable, post-ischemic myocardium does not recover full contractile function immediately, sometimes requiring hours to days for full restoration<sup>73,254</sup>. The exact mechanism behind stunning remains a mystery, though the stunned cardiomyocyte is believed to be structurally and metabolically intact<sup>209,255</sup>. Most investigations have indicated that calcium

handling is unperturbed, but there is decreased maximum force generation and either decreased or unchanged calcium sensitivity<sup>135,256-259</sup>.

Proteolytic digestion of cTnI has previously been proposed as an explanation for myocardial stunning. Past studies focused on a 17-residue C-terminal truncation of cTnI, cTnI<sub>1-193</sub>, that was associated with decreased Ca<sup>2+</sup> sensitivity and myocardial stunning<sup>260</sup>. Separate biochemical analyses of this cleavage product demonstrated increased, rather than decreased, Ca<sup>2+</sup> sensitivity<sup>37,260</sup>. We found no evidence to suggest that cTnI<sub>1-193</sub> is generated by either MMP-2- or calpain cleavage. On the other hand, we have determined that within the C-terminal tail of cTnI, the critical switch region is most susceptible to cleavage, both by MMP-2 and calpain, and cleavage at this site would provide the simplest possible explanation for the phenomenon of myocardial stunning.

The cTnI switch region is partially protected from proteolytic cleavage as it cycles between cTnI and actin to control cardiac contraction, although severe myocardial ischemia creates additional factors that could release it from both: 1) formation of the actomyosin “rigor” state due to depletion of ATP<sup>261</sup>; and 2) intracellular acidosis causing calcium desensitization of the cTnI domain. (It should however be noted that acidosis would also compromise the calcium-dependent activity of calpains.) The necessary convergence of multiple factors under sub-lethal conditions is a possible explanation for why myocardial stunning is not universally observed in all experimental and clinical settings involving ischemia-reperfusion injury.

The proteolytic cleavage of cTnI residues C-terminal to the switch region would likely also have a negative impact on cardiac function. The importance of C-terminal residues is underscored by the existence of many hypertrophic cardiomyopathy-associated mutations that extend all the way to Glu208<sup>241</sup>. A recent case study of a patient with progressive heart failure associated with



restrictive cardiomyopathy identified a 15-residue (D195-S209) deletion from the C-terminus of cTnI<sup>262</sup>.

There is a complex interplay between cTnI proteolysis, phosphorylation, cardiomyopathy-associated mutations, and different disease states. The most consistently observed phosphorylation sites in human are cTnI at S22 and S23, which modulates the calcium sensitivity of cardiac muscle<sup>202,203</sup>. The phosphorylation state of cTnI S22/S23 is impacted by the presence of heart failure<sup>263</sup> or cardiomyopathy-related mutations<sup>57,264</sup>. Phosphorylation at S22 and S23 by protein kinase A<sup>265</sup> or just S23 by protein kinase D<sup>133</sup> has also been shown to decrease calpain-mediated proteolysis. Phosphorylation at this site likely interferes with calpain cleavage at its preferred sites between Y25 and R26 or between R26 and A27, identified in the current study.

More recently, phosphorylation of S198 by protein kinase C has been shown to increase the calcium sensitivity of cardiac muscle contraction<sup>127</sup>. Further studies in transgenic mice found that the pseudophosphorylation mutation S198D decreased formation of a proteolyzed form of cTnI following 30 min of global ischemia and 1 h of reperfusion<sup>249</sup>. An S198A mutation did not attenuate proteolytic digestion. The simplest explanation is that the cTnI S198D mutation abolishes the MMP-2 cleavage site at G199-M200, whereas the S198A mutation does not, as suggested by MMP-2 cleavage site amino acid preferences at position P2<sup>243</sup>.

Proteolytic digestion of cTnI during myocardial ischemia has clinical consequences beyond impairment of cardiac function. Proteolytic cleavage results in the generation of heterogeneous fragments of cTnI that are released into the bloodstream and used in the detection and diagnosis of myocardial infarction<sup>266,267</sup>. In a recently published study, we demonstrate that the degree of proteolysis in cTnI depends on the severity of ischemic injury, with the highest degree of digestion observed in patients with ST-elevation myocardial infarct and lesser degrees

of digestion seen in supply-demand ischemia<sup>268</sup>. It is thus quite possible that the pattern of cTnI proteolysis could be used to differentiate between different mechanisms of myocardial injury.

In summary, cTnI contains intrinsically disordered tails that are key to its function, but are also sensitive to proteolysis by the proteases purported to be active during ischemia-reperfusion injury. Proteolytic digestion of cTnI has important implications for cardiac muscle function, as well as for the clinical diagnosis of myocardial infarction via the detection of cTnI fragment.

## **CHAPTER 3**

### **DILATED CARDIOMYOPATHY MUTATIONS AND PHOSPHORYLATION DISRUPT THE ACTIVE ORIENTATION OF CARDIAC TROPONIN C**

Chapter 3 has been published in:

Mahmud, Z., Dhami, P.S., Rans, C., Liu, P.B. & Hwang, P.M. Dilated cardiomyopathy mutations and phosphorylation disrupt the active orientation of cardiac troponin C. *J Mol Biol* **433**, 167010 (2021).

### 3.1 Introduction

Cardiomyopathies are associated with abnormal growth of heart muscle, heart failure, and fatal arrhythmias. Some cardiomyopathies are heritable, with sequencing to detect causative mutations becoming standard clinical care<sup>269</sup>. DCM is characterized by impaired systolic contraction of the left ventricle or both ventricles. The phenotypic prevalence of familial DCM is 1/5,000 to 1/10,000<sup>270</sup>. Over time, the ventricular walls get thinned, and the ventricular chambers become progressively dilated and impaired in their ability to pump blood.

Although rare, some DCM mutations localize to the cardiac troponin complex<sup>271</sup>, which adorns the actin-tropomyosin thin filament at specific sites where it helps to translate cytoplasmic calcium spikes into muscle contraction<sup>272</sup>. The cardiac troponin complex is made up of three subunits<sup>12,200,201</sup>: cTnC binds to calcium, cTnI reversibly binds to actin to inhibit contraction, and cTnT anchors the whole complex to tropomyosin (Figure 3.1A). In 2003, the X-ray crystal structure of the cardiac troponin complex (PDB ID: 1J1D,1J1E) delineated for the first time the structural core of the complex, with the 3 subunits coming together to form the so-called “IT-arm”<sup>13</sup>. The structural C-terminal domain of cTnC (cCTnC<sub>93-161</sub>) has two calcium-binding EF-hands (EF-III and EF-IV) that remain occupied and structurally invariant throughout the cardiac cycle due to very high- affinity Ca<sup>2+</sup>/ Mg<sup>2+</sup> binding. The cCTnC domain is the hub of the IT-arm, which resembles a meatball grasped by two helical chopsticks, with one chopstick consisting of cTnI<sub>41-79</sub> and the other, a helical coiled coil made up of cTnT<sub>223-272</sub> and cTnI<sub>89-134</sub><sup>28</sup> (Figure 3.1A).

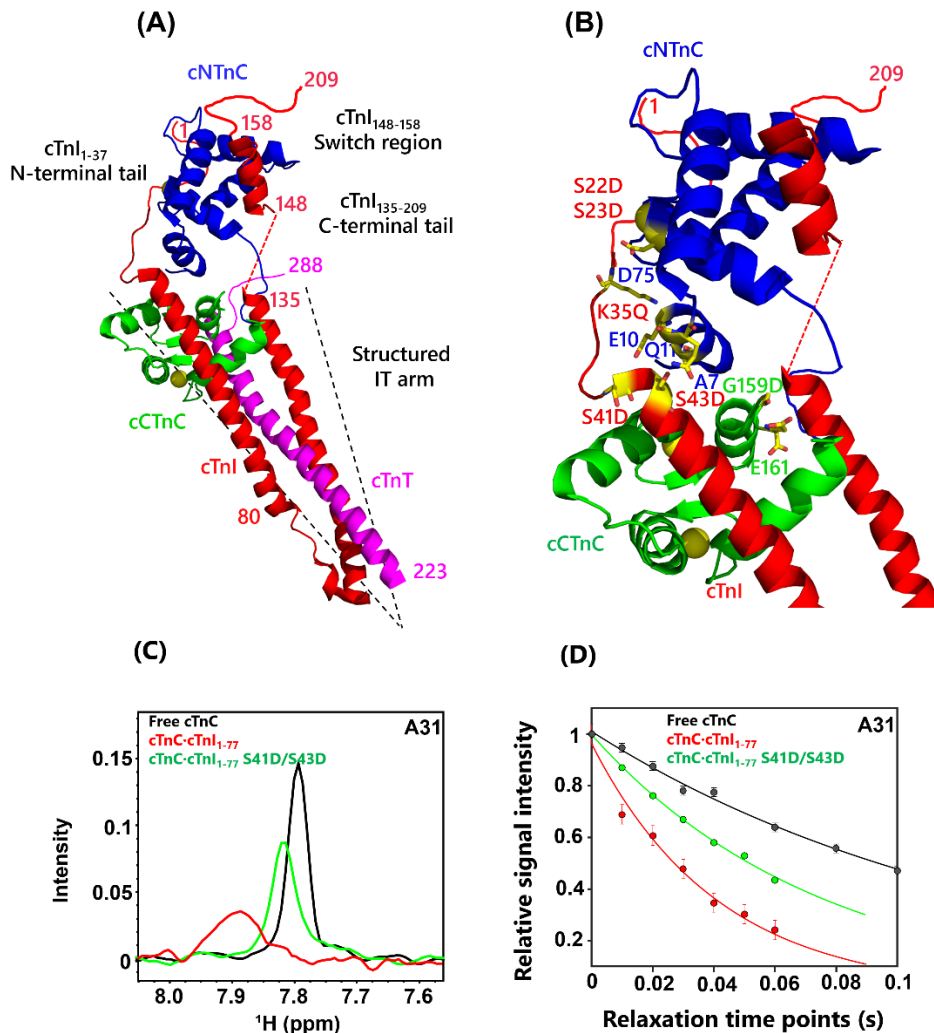


**Figure 3.1:** (A) Calcium-saturated human cTn. cTnC consists of two domains, cNTnC (blue) and cCTnC (green). cTnI is shown in red, The N- and C-terminal tails of cTnI, with intrinsically disordered regions that were invisible in the X-ray crystal structure drawn manually as squiggles. cTnT is shown in magenta. Figure prepared using PyMOL and structure 1J1E (PDB code). (B) Calcium-saturated cTnC bound to N-terminal tail of cTnI<sub>1-77</sub> in the active orientation. The key interaction sites for the active orientation and DCM and phosphomimetic variants are colored as yellow. (C) Residue A31 of cTnC shows different NMR signal lineshapes in free cTnC, cTnC·cTnI<sub>1-77</sub> and cTnC·cTnI<sub>1-77</sub> S41/43D. (D) Representative T1 $\rho$  relaxation decay curves for the residue A31 in free cTnC, cTnC·cTnI<sub>1-77</sub> and cTnC·cTnI<sub>1-77</sub> S41/43D. T1 $\rho$  relaxation delays were varied from 0 to 100 ms.

The structural rigidity of the IT-arm revealed by X-ray crystallography contrasts with the mobility of the regulatory N-terminal domain of cTnC (cNTnC<sub>1-85</sub>) observed by solution nuclear magnetic resonance (NMR) spectroscopy<sup>29</sup>. The cNTnC domain has only one functional low-affinity calcium-binding EF-hand, EF-II, while EF-I is defunct. During diastole, the cNTnC domain is in a closed conformation, but in response to calcium influx during systole, it binds a single calcium ion and enters a dynamic equilibrium between closed and open states, with the closed state still predominating<sup>29,197</sup>. However, the open state is stabilized by binding to the switch region of cTnI, cTnI<sub>146-158</sub>, and this removes the inhibitory effect of the cTnI<sub>135-209</sub> tail. The removal of cTnI<sub>135-209</sub> from its binding site on actin allows the actin-tropomyosin filament to transition from a blocked state to one that is conducive to actin-myosin cross-bridging and force generation<sup>14</sup>. Binding to the cTnI switch region also increases the apparent calcium affinity of the cNTnC domain<sup>28</sup>, suggesting that the open state has a higher calcium affinity (a slower calcium off-rate) than the closed state.

Solution NMR relaxation studies have revealed additional flexibility of the cNTnC domain. Solution transverse magnetization  $R_2$  relaxation rates of backbone amide <sup>15</sup>N nuclei are proportional to the effective correlation time at each site. The correlation time is dominated by the nanosecond timescale tumbling of the entire protein in solution, though it can be locally decreased by rapid nanosecond-picosecond timescale fluctuations typically in flexible tails or large loops. NMR <sup>15</sup>N relaxation analysis has revealed that the two domains of cTnC are connected by an intrinsically disordered linker (cTnC<sub>86-92</sub>) displaying rapid nanosecond-picosecond timescale fluctuations<sup>25</sup>. This means that the cNTnC domain can sample a wide range of positions relative to the rigid IT-arm of the cardiac troponin complex.

However, it turns out that the positioning of the cNTnC domain is regulated by additional interactions with other parts of the cardiac troponin complex. We previously demonstrated that binding of cTnC to a soluble fragment of cTnI, cTnI<sub>1-71</sub>, fixes the two domains of cTnC so that the complex tumbles as a single unit<sup>33</sup>. cTnI<sub>1-71</sub> is comprised of the flexible cardiac muscle-specific N-terminal tail of cTnI, cTnI<sub>1-37</sub>, followed by a helical region, cTnI<sub>39-60</sub>, that binds with tight nanomolar affinity to the cCTnC domain<sup>273</sup>. cTnI<sub>1-37</sub> is intrinsically disordered, even when the cTnI<sub>19-37</sub> binds to cNTnC via electrostatic interactions. The interaction fixes the cNTnC domain into an orientation relative to the cCTnC domain that is consistent with the 2003 X-ray crystal structure of the calcium-bound activated cardiac troponin complex. We verified that the activated orientation observed in the X-ray crystal structure was also present in solution (via nuclear Overhauser enhancement-derived distance restraints), and this did not require binding of cNTnC to the switch region, cTnI<sub>146-158</sub>. We therefore proposed that the interaction between cTnI<sub>19-37</sub> and the cNTnC domain stabilizes a “primed orientation”, which is compatible with cNTnC binding to the cTnI switch region, cTnI<sub>146-158</sub>.

Recently determined cryo-EM structures of the cardiac thin filament have shown that the orientation that we previously highlighted as the “primed” orientation is in fact exactly the same as that in the activated calcium-bound form of the cardiac thin filament (Figure 3.2)<sup>14</sup>. Previously undocumented interactions between the cNTnC domain and tropomyosin are also observed in the cryo-EM structure, suggesting that active orientation of the cNTnC domain also helps to promote the active conformation of the thin filament.

### Cardiac troponin complex

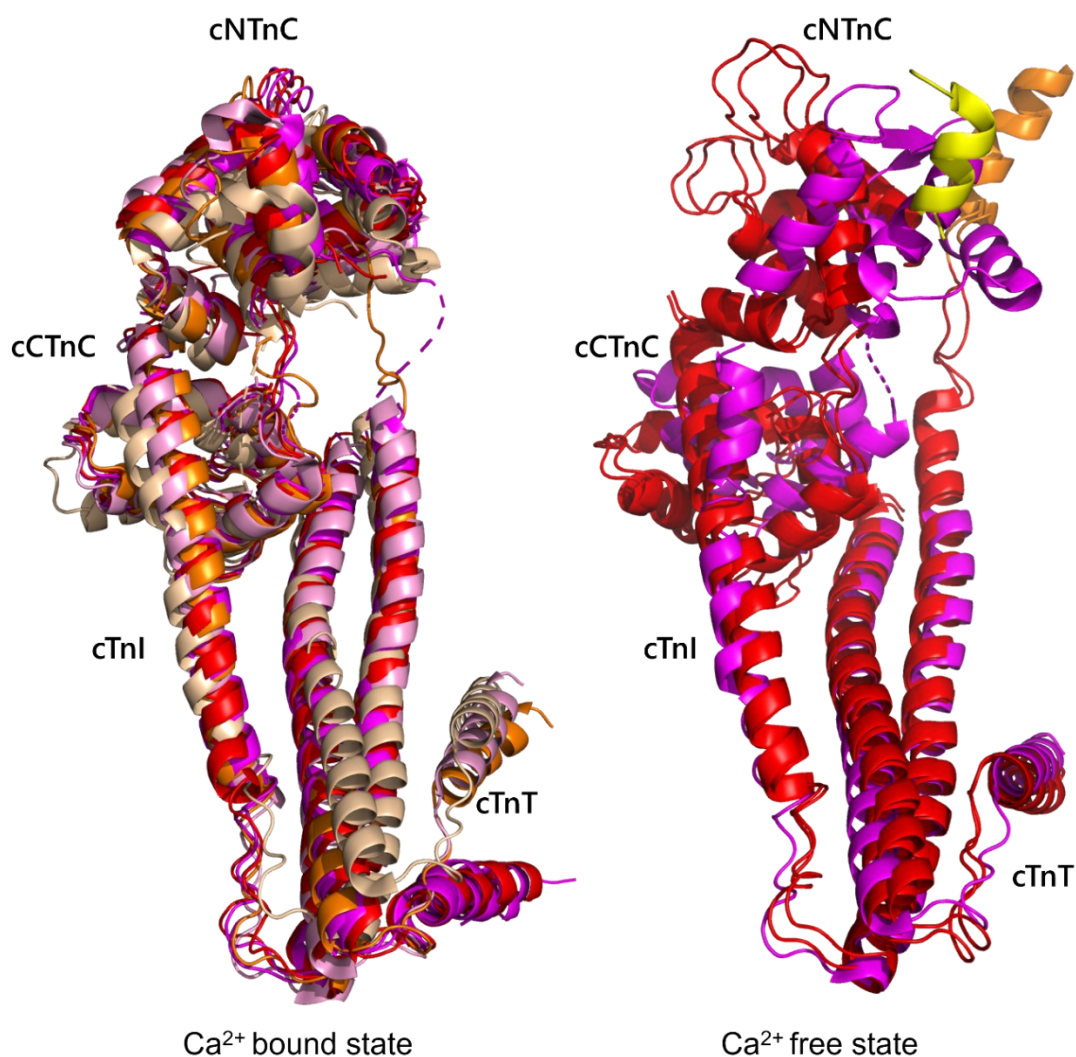


**Figure 3.2:** (A) Backbone overlay of 7 Ca<sup>2+</sup> bound structures of the cardiac troponin complex. The coloring scheme is as follows, PDB: 1J1E (red), PDB: 1J1D (magenta), PDB: 6KN8 (orange), PDB: 6KLU (tint), and PDB: 4Y99 (pink). Both 1J1E and 1J1D have two structures in each unit cell. Both 6KN8 and 6KLU are cryo-EM structures, but 6KN8 has two different troponin complexes in the structure. (B) Backbone overlay of 3 Ca<sup>2+</sup> free structures of the cardiac troponin complex. The coloring scheme is as follows, PDB: 6KN7 (red) and PDB: 6KLT (magenta). Both 6KN7 and 6KLT are cryo-EM structures, but 6KN7 has two different troponin complexes in the structure. The switch peptides (cTnI<sub>148-158</sub>) are colored as orange and yellow for 6KN7 and 6KLT, respectively. The Ca<sup>2+</sup> ions are not visible in this figure due to superimposition of these structures.



The orientation of the cNTnC domain shifts slightly in the low calcium diastolic state of the thin filament. In this state the cNTnC domain is forced to rotate somewhat to accommodate binding of the essential inhibitory region of cTnI, cTnI<sub>135-147</sub>, to actin and tropomyosin. Binding of the inhibitory region is key to the formation of the blocked state of the cardiac thin filament, and the cTnI switch region, cTnI<sub>146-158</sub>, is also bound to actin and unavailable for binding to cNTnC. Activation of cardiac muscle contraction, then, requires not only binding of calcium to cNTnC, but also weak myosin-actin-tropomyosin interaction to shift the position of tropomyosin and displace cTnI<sub>135-158</sub> from its binding site on actin, so that the cNTnC domain can bind to the cTnI switch region and rotate into its active orientation.

The current study focuses on interactions within the cardiac troponin that promote the active orientation of the cNTnC domain. We propose that disruption of the active orientation through phosphorylation of cTnI is the main mechanism by which the calcium sensitivity of cardiac muscle contraction is regulated. Moreover, point mutations that disrupt the active orientation of the cNTnC domain give rise to dilated cardiomyopathy (DCM). To test these structural hypotheses, we produced phosphomimetic mutant forms of cTnI fragments (cTnI<sub>1-77</sub> S22D/S23D and cTnI<sub>1-77</sub> S41D/S43D) along with DCM-associated mutants (cTnC G159D, cTnC D75Y and cTnI K35Q). We then used solution NMR <sup>15</sup>N relaxation studies to compare the mobility of the cTnC domains in the wildtype versus mutant forms of the cTnC-cTnI<sub>1-77</sub> complex.

Finally, we also reconstituted the IT-arm of the cardiac troponin complex and present evidence using <sup>15</sup>N relaxation analysis that the cNTnC domain can participate in a previously undescribed interaction with the IT-arm. We call this new position the “dormant” orientation, because it competes with the active orientation of the cNTnC domain in its calcium-loaded state. We therefore propose that a balance between active and dormant orientations is carefully regulated

to control access of the cTnC domain to the cTnI switch region and consequently, the calcium sensitivity of cardiac muscle contraction.

### **3.1 Materials and methods**

#### **3.1.1 Production and purification of cTnC wild type and mutant constructs**

The expression and purification strategies for cTnC and cTnI constructs are different because of the different natures of these two protein subunits. cTnC is a well-behaved soluble subunit, whereas cTnI is intrinsically disordered and prone to aggregate. Expression plasmids for wild type and mutant forms of cTnC were created by ATUM (formerly DNA 2.0) and designed to incorporate IsoPropyl-beta-d-ThioGalactopyranside (IPTG)-inducible expression, T5 promoters (compatible with endogenous *E. coli* RNA polymerase), codon optimization for *E. coli*, and ampicillin selection. The cTnC constructs begin with the native sequence, followed by a nickel (II)-catalyzed peptide bond cleavage motif SRHW and a polyhistidine tag, (His<sub>6</sub>-tag) (Figure 3.3). Cleavage N-terminal to the SRHW sequence leaves behind the native protein C-terminus. Isotope-labeled <sup>15</sup>N cTnC wild type and mutant constructs were expressed in *E. coli* BL21(DE3) cells using M9 minimal media supplemented with <sup>15</sup>N-labeled ammonium chloride. Cells from a 2 liter culture were grown to an absorbance between 0.5 and 1.0 at 600 nm wavelength and induced with IPTG. Subsequently, cells were harvested by centrifugation. Cells were resuspended at room temperature with 40 ml buffer containing 50 mM Tris at pH 8, 10 mM MgSO<sub>4</sub>, 0.01 mg/ml DNase, and 1 mM CaCl<sub>2</sub>. After resuspension, cells were lysed with the addition of 20 mg lysozyme and 200 mg sodium deoxycholate per liter of growth. Cells were further dispersed using a Kontes Glass Duall tissue grinder followed by high-speed centrifugation to remove cell debris. The supernatant was filtered through a 0.45- $\mu$ m PVDF Millipore syringe filter before being applied to a nickel affinity column. The binding buffer contained 20 mM Tris-HCl, 300 mM NaCl, 10 mM imidazole. The

wash and elute buffers contain the same recipe except 20-80 mM and 250 mM imidazole, respectively. The eluted fractions were collected and dialyzed against 5 mM HEPES at pH 7.5, and 1 mM CaCl<sub>2</sub>. Ni (II)-catalyzed cleavage was used to cleave the His<sub>6</sub> affinity tag from the cTnC previously described in<sup>226</sup>. The cleavage reaction was done in 1 mM NiSO<sub>4</sub>, 50 mM CHES buffer, pH 9.5, incubated for 1-2 days (construct-dependent) at 45°C. The reaction was quenched by adding 10 mM EDTA, 20 mM CaCl<sub>2</sub> and 100 mM imidazole, pH 5.5. After dialyzing the sample against nickel column binding buffer, the tag was removed from cTnC by passing the mixture through a second nickel affinity column and collecting the purified tagless cTnC in the flowthrough, which was then dialyzed against 5 mM HEPES at pH 7.5 once and then 3 times against 5 mM ammonium bicarbonate and 1 mM CaCl<sub>2</sub>. In the last (5<sup>th</sup>) dialysis, the concentration of CaCl<sub>2</sub> was lowered to 0.01 mM, and then the sample was lyophilized. The yield for wildtype and mutant cTnC constructs was around 70 mg per liter of culture.

### **3.1.2 Production and purification of wild type and mutant cTnI<sub>1-77</sub> constructs, cTnT<sub>223-288</sub>, and cTnT<sub>223-276</sub>**

For wild type and mutant cTnI<sub>1-77</sub> constructs, as well as cTnT<sub>223-288</sub> and cTnT<sub>223-276</sub>, expression with a PagP-based fusion partner was utilized. PagP is a Gram-negative bacterial outer membrane protein (Figure 3.3). Note that the N-terminal methionine of cTnI is removed and replaced by an acetyl group during post-translational modification, so we begin numbering at the next amino acid residue so that the last C-terminal residue is Ser209. Although a similar modification occurs in cTnT, we are not aware of anyone who numbers it accordingly.

Deleting the signal sequence of PagP causes it (and the fused target protein partner) to accumulate into cytoplasmic inclusion bodies<sup>274</sup>. Guanidine hydrochloride was used as a denaturant to solubilize inclusion bodies and facilitate purification under denaturing conditions, as

previously published<sup>274</sup>. All target proteins were separated from PagP via cyanogen bromide cleavage and then purified using nickel affinity chromatography under denaturing conditions, as previously published<sup>225</sup>.

### **3.1.3 Production and purification of mutant solubilized cTnI<sub>38-134</sub>**

Our initial attempts to work with cTnI<sub>38-134</sub> were unsuccessful because the construct was highly insoluble. We were able to dissolve it in urea or guanidine denaturant, but all attempts to reconstitute into a complex with cTnC and cTnT were unsuccessful. We therefore introduced a number of mutations into cTnI<sub>38-134</sub> to increase its solubility: C79A, C96S, I121T, T122R, A125K, T128K, and F132N. Cysteine mutations were previously used for the 2003 X-ray crystal structure of the cardiac troponin complex<sup>13</sup>. The other 5 mutations are found in other troponin homologs, and none are involved in known contacts to the rest of the troponin complex. When we introduced these mutations into full length cTnI, overexpression with PagP as a C-terminal fusion partner failed, as the fusion construct did not accumulate sufficiently in inclusion bodies. Therefore, we created new constructs in which the N-terminus of cTnI was fused to a short TrpLE tag, also known to direct proteins to inclusion bodies, while the C-terminus of cTnI was fused to PagP (Figure 3.3). The dual TrpLE and PagP fusion tags were designed to be removed via nickel (II) cleavage of the motif SRHW. The N-terminal SRHW tag and His6-tag could be further cleaved off by TEV protease cleavage using standard protocols<sup>275</sup>. This approach was successful for producing engineered cTnI<sub>38-134</sub>.

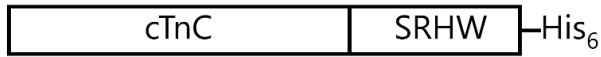
### **3.1.4 Production and purification of mutant W237S, Q238D, Y241H, A245S-cTnT<sub>223-288</sub>**

We also produced a mutant variant of cTnT<sub>223-288</sub> fused with PagP in which four mutations (W237S, Q238D, Y241H, and A245S) corresponding to human slow skeletal troponin T, were

introduced. Like tail-less cTnI<sub>38-134</sub>, this construct also begins with TrpLE and has two His<sub>6</sub>-tags and two nickel (II) cleavage motifs SRHW at both N and C-terminal sites of the target sequence (Figure 3.3).

**Cardiac troponin C constructs**

1. cTnC wild type
2. cTnC G159D
3. cTnC D75Y



**Cardiac troponin I constructs**

1. cTnI<sub>1-77</sub> wild type
2. cTnI<sub>1-77</sub> K35Q
3. cTnI<sub>1-77</sub> S41/43D
4. cTnI<sub>1-77</sub> S22/23D



**Tailless cardiac troponin I construct**

1. cTnI<sub>38-134</sub>



*\*C79A, C96S, I121T, T122R, A125K, T128K, F132N*

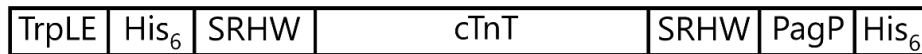
**Cardiac troponin T constructs**

1. cTnT<sub>223-288</sub>
2. cTnT<sub>223-276</sub>



**Mutated cardiac troponin T construct**

1. cTnT<sub>223-288</sub>



*\*W237S, Q238D, Y241H, A245S*

**Figure 3.3:** Schematics of all cTnC, cTnI, and cTnT constructs used in this study.

### 3.1.5 Reconstitution of the cardiac troponin ternary complex

Cardiac troponin ternary complex was reconstituted at 4°C using cTnC, engineered soluble cTnI<sub>38-134</sub> mutant, and cTnT<sub>223-288</sub> constructs. <sup>2</sup>H, <sup>15</sup>N, <sup>13</sup>C labeled cTnC (18 kDa, 500 μM) was dissolved into 500 μl of buffer containing 0.1 mM Tris-HCl at pH 7.5, 200 mM MgCl<sub>2</sub> and 10 mM CaCl<sub>2</sub>. The cTnC was diluted into 24.5 ml of the same buffer, and the pH was brought down to 5.5 from 7.5 by adding sodium acetate to 10 mM, pH 5.5. In a separate vial, unlabeled cTnI<sub>38-134</sub> (11 kDa, 500 μM) was dissolved into 500 μl of 4.6 M urea and 10 mM sodium acetate at pH 5.5. cTnI<sub>38-134</sub> was added dropwise to continuously stirred 24.5 ml solution of cTnC, producing a total of 25 ml reconstituted binary complex. Unlabeled cTnT<sub>223-288</sub> (8 kDa, 500 μM) was dissolved into 500 μl of the same buffer that was used to dissolve cTnC and 10 mM sodium acetate was added to maintain a pH 5.5. The 500 μl of cTnT<sub>223-288</sub> was then diluted into 25 ml of the same buffer. The 25 ml of cTnT<sub>223-288</sub> was added dropwise to the continuously stirred 25 ml of binary complex to produce a total of 50 ml of the ternary complex (5 μM). To prepare a ternary complex sample for the NMR experiment, 50 ml 5 μM ternary complex was exchanged with NMR buffer (10 mM Imidazole, 200 mM MgCl<sub>2</sub>, and 10 mM CaCl<sub>2</sub>, pH 6.5) and then concentrated to 500 μM in 500 μL by using MilliporeSigma™ Amico Ultra Centrifugal Filter (molecular weight cut off =30 kDa) at 4500 xg centrifugation. Finally, 50 μl of 0.5 mM DSS in D<sub>2</sub>O was added to make a 550 μl NMR sample.

### 3.1.6 NMR spectroscopy

All 2D <sup>1</sup>H, <sup>15</sup>N HSQC spectra were acquired from Varian Inova 500 MHz spectrometer equipped with a triple resonance probe and pulsed field gradients. cTnC and its variants were <sup>15</sup>N-

labeled for  $^{15}\text{N}$  relaxation experiments. For experiments examining the troponin ternary complex, cTnC was  $^2\text{H}$ ,  $^{13}\text{C}$ ,  $^{15}\text{N}$ -labeled. All cTnI and cTnT constructs were unlabeled.

NMR samples contained 0.3 - 0.5 mM protein dissolved in NMR buffer (100mMKCl, 10mM imidazole, 10 mM  $\text{CaCl}_2$ , pH 6.5), to which 10% volume of 0.5 mM 3-(trimethylsilyl)-1-propanesulfonate (DSS) solution in  $\text{D}_2\text{O}$  was added with 0.1% sodium azide. cTnI<sub>1-77</sub> was titrated into the  $^{15}\text{N}$  cTnC sample while monitoring the disappearance of free cTnC peaks to ensure 1:1 complexation. All NMR experiments were performed at 30°C. 2D  $^{15}\text{N}$  gradient enhanced-sensitivity HSQC and  $T_1$  and  $T_{1\rho}$   $^{15}\text{N}$  relaxation variants of the HSQC experiment were as supplied by VnmrJ BioPack.  $^{15}\text{N}$   $T_1$  and  $T_{1\rho}$  relaxation experiments were performed as previously described<sup>33</sup> and time delays for  $T_1$  and  $T_{1\rho}$  relaxation experiments were in the range of 0.010–1.0s and 0 - 0.1 s respectively. All 2D HSQC spectra were processed using NMRPipe<sup>227</sup> software.

For  $T_1$  and  $T_{1\rho}$  relaxation analysis, decay curves were fitted using a monoexponential decay function using a simplex minimization algorithm in MATLAB (version R2015b, The Mathworks, Inc. Natick, Massachusetts, USA), courtesy of Lewis Kay, University of Toronto. Error estimates for calculated  $T_1$  and  $T_{1\rho}$  values were calculated as previously described<sup>33</sup>.  $T_{1\rho}$  ( $1/R_{1\rho}$ ) values were converted to  $T_2$  ( $1/R_2$ ) values using the formula<sup>276</sup> :

$$R_2 = \frac{R_{1\rho}}{\sin^2 \theta} - \frac{R_1}{\tan^2 \theta}$$

Here  $\theta = \frac{\omega_1}{\Delta\Omega}$ ,  $\theta$  = tilt angle in the rotating frame,  $\omega_1$ = spin-lock radio frequency field strength and  $\Delta\Omega$ = offset difference between corresponding resonance and the  $^{15}\text{N}$  carrier frequency.  $R_2$ ,  $R_{1\rho}$  and  $R_1$  relaxation rates are the reciprocal of  $T_2$ ,  $T_{1\rho}$  and  $T_1$  relaxation times, respectively.

## 3.2 Results and Discussion

We are proposing that the domain orientation of the regulatory cNTnC domain is a decisive factor regulating the calcium sensitivity of cardiac muscle contraction. Domain positioning is typically ignored in most solution NMR studies that focus on individual protein domains. Alternative orientations can also be readily missed by X-ray crystallographic and cryo-EM studies in which the domains can become fixed by crystal contacts, sub-zero temperatures, or other manipulations needed to ensure a homogeneous ensemble of conformations. Solution NMR  $^{15}\text{N}$  relaxation has proven to be a powerful method for studying localized structural disorder as well as the global tumbling of protein domains. Figures 3.1C and 3.1D show that fixation or release of the domains in cTnC has a profound impact on the lineshape of NMR signals in the protein (Figure 3.1C), and this can be readily quantitated using  $^{15}\text{N}$  relaxation analysis (Figure 3.1D).

### 3.2.1 The N-terminal tail of cTnI stabilizes the active orientation of cTnC

The two domains of cTnC are connected by a flexible linker, allowing them to move independently of one other. The average  $R_2$  rates of the cNTnC ( $10\text{ s}^{-1}$ ) and cCTnC domains ( $9\text{ s}^{-1}$ ) at  $30^\circ\text{C}$  (Table 3.1)<sup>277,278</sup> are higher than the average  $R_2$  rate of the homologous fast skeletal muscle NTnC domain in isolation ( $7\text{ s}^{-1}$ )<sup>279</sup>, but lower than would be expected if the two domains were tumbling as a single unit. ( $R_2$  rates scale linearly with molecular weight for similarly shaped proteins.) The  $R_2$  rates of the cNTnC and cCTnC domains are slightly different, because the molecular weight of the cNTnC domain (9.6 kDa) is slightly larger than that of the cCTnC domain (8.0 kDa), further supporting the notion that the domains can tumble in solution somewhat independently of each other due to the increased internal mobility of the inter-domain linker, which has an average  $R_2$  relaxation rate of  $5\text{ s}^{-1}$ . Other regions of cTnC that show marked flexibility are



some of the larger inter-helical loops and the ends of the protein, which show decreasing  $R_2$  values towards the N- and C-termini, particularly the C-terminal residue E161 (Figure 3.4A).

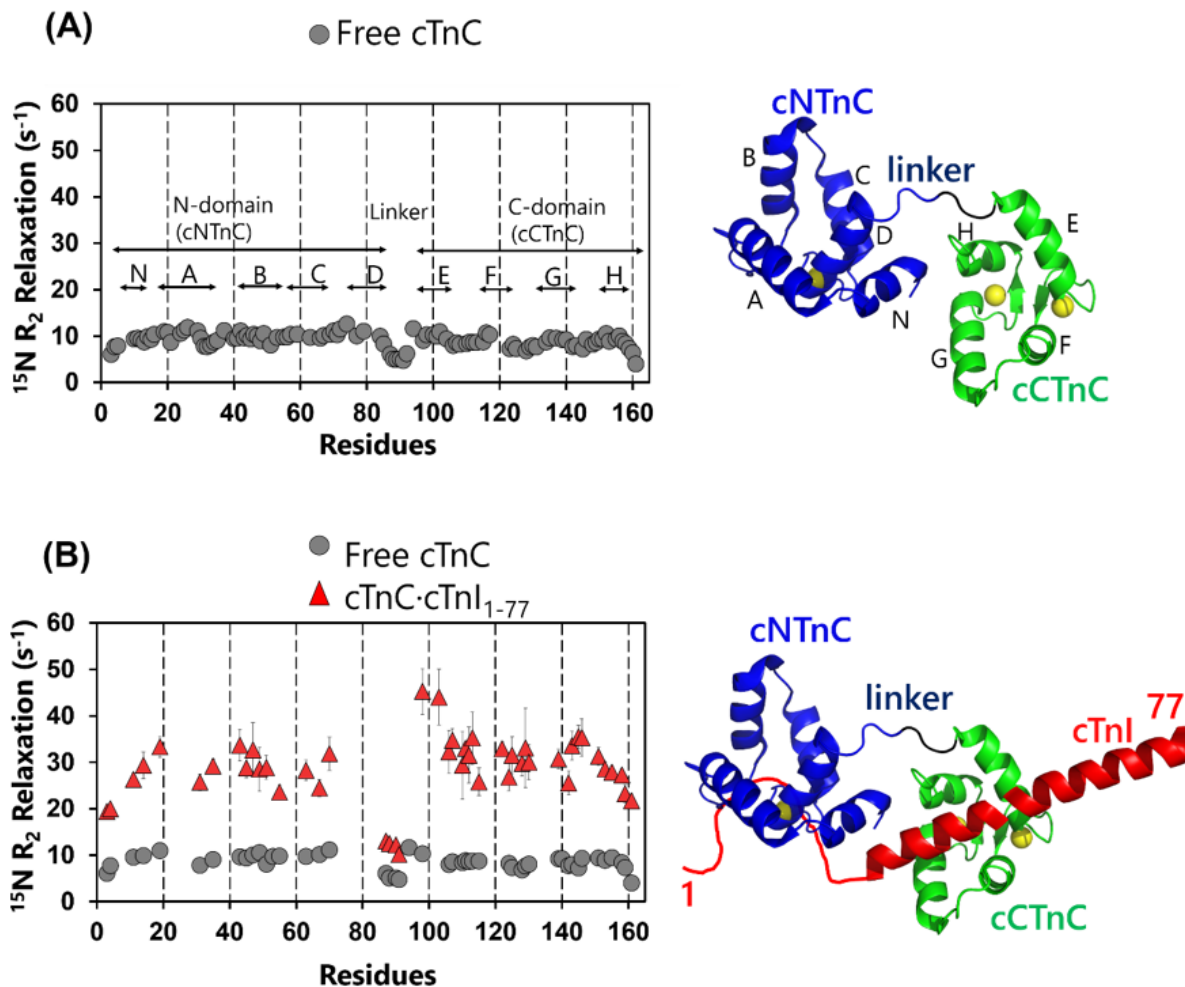


**Figure 3.4:**  $^{15}\text{N}$   $R_2$  relaxation rates of (A) free cTnC and (B) cTnC bound to cTnI<sub>1-77</sub>.

Addition of cTnI<sub>1-77</sub> has a dramatic effect on the NMR spectrum of cTnC. The largest chemical shift perturbations are observed in the cCTnC domain (residues I128, T129, E155, K158, G159, and V160) (Figure 3.5C and Figure 3.7A), consistent with high nanomolar affinity binding between large hydrophobic surfaces within the helical cTnI residues 39-60 and the cCTnC domain. In contrast, binding between the cNTnC domain and cTnI residues 19-37 occurs largely through

electrostatic interactions. Besides the chemical shift perturbations observed throughout cTnC, the most dramatic change to the NMR spectrum is pervasive signal broadening (see Figure 3.1C).  $R_2$  relaxation rates throughout the entire cTnC increase markedly upon addition of cTnI<sub>1-77</sub>, rising to an average  $\sim 31 \text{ s}^{-1}$  (Table 3.1, Figure 3.2B), more than 3 times what is seen in cTnC when it is alone. The global shift indicates a change in the overall tumbling of the protein complex as a whole, which has a combined molecular weight of 26 kDa and has a dumbbell-like structure.

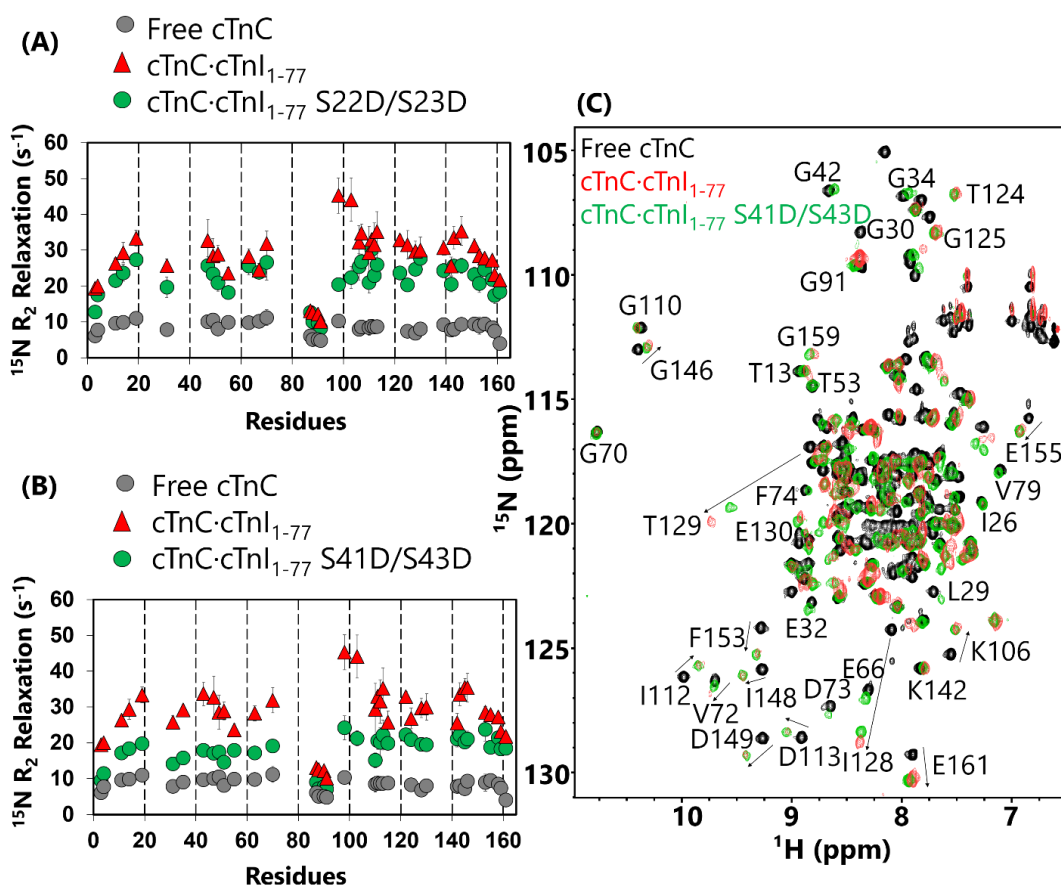


**Figure 3.5:** Comparison of  $^{15}\text{N}$   $R_2$  relaxation rates of free cTnC, cTnC complexed with wildtype cTnI<sub>1-77</sub>, and cTnC complexed with phosphomimetic cTnI<sub>1-77</sub> S22/23D (A) or cTnI<sub>1-77</sub> S41/43D (B). (C) The 2D  $^1\text{H}$ ,  $^{15}\text{N}$  HSQC spectrum of free cTnC (black) superimposed with cTnC bound to wildtype cTnI<sub>1-77</sub> (red) or cTnI<sub>1-77</sub> S41/43D (green).

cTnI<sub>1-77</sub> binds to both domains and fixes the inter-domain orientation between cNTnC and cCTnC. It is interesting to note that many flexible regions of cTnC are involved in the interactions that stabilize this inter-domain orientation: the N-terminal helix of cNTnC, the inter-domain linker, and the C-terminal tail of cCTnC (see structure in Figure 3.1B). Each of these contacts is disrupted by a different DCM-associated mutation or post-translational modification (see below). All of the contacting regions in cTnC display some degree of rigidification upon interaction with cTnI<sub>1-77</sub>, contributing to the global increase in NMR  $R_2$  relaxation rates seen throughout the cTnC protein. The active orientation is stabilized through the formation of three different weak interactions that are accompanied by a loss of conformational entropy, making for a delicate balance that is sensitive to regulatory changes.

### **3.2.2 Phosphomimetic mutants of cTnI disrupt the active orientation of cTnC**

Phosphorylation of cTnI S22/S23 is an important regulatory control of the calcium sensitivity of cardiac muscle contraction<sup>47,280,281</sup>. The N-terminal tail of cTnI contains many residues that can be phosphorylated to impact the calcium sensitivity of heart muscle<sup>282,283</sup>. Of all these S22 and S23 are most consistently phosphorylated in humans<sup>284,285</sup>. Although several kinases seem to converge on these residues, they were originally found to be phosphorylated by cyclic AMP (cAMP)-dependent protein kinase A (PKA) during  $\beta$ -adrenergic stimulation<sup>286</sup>. High levels of phosphorylation of S22 and S23 are observed in healthy hearts, where they appear to contribute to length dependent activation (Frank-Starling mechanism) and improve diastolic relaxation<sup>287-289</sup>. Decreased levels of phosphorylation have been observed in diseased states<sup>290</sup>. Selective proteolytic removal of cTnI N-terminal extension (cTnI<sub>1-31</sub>) or its deletion in a transgenic mouse model appears to recapitulate many of the beneficial functional effects of phosphorylation, suggesting

that the impact of phosphorylation of S22 and S23 has an effect similar to removing the cTnI N-terminal tail<sup>291,292</sup>.

Several functional studies (isolated perfused rabbit and rat hearts<sup>293,294</sup>, hyperpermeable rat myocardium<sup>295</sup>, rat ventricular myocytes<sup>296</sup>, and porcine cardiac skinned muscle<sup>48</sup>) reported decreased calcium sensitivity in the presence of cTnI S22 and S23 phosphorylation or phosphomimetic mutation to aspartate. In this study, we mimicked phosphorylation of cTnI<sub>1-77</sub> by mutating serine to aspartate at both S22 and S23 positions.

When complexed to the S22D/S23D-cTnI<sub>1-77</sub> phosphomimetic double mutant, both cNTnC and cCTnC domains display increased <sup>15</sup>N R<sub>2</sub> values (R<sub>2</sub> ~ 24 s<sup>-1</sup>) relative to what is seen in cTnC on its own, but not to the same degree as seen in complex with wildtype cTnI<sub>1-77</sub> (Figure 3.5A). This indicates that the two domains are still tethered together, but the association is somewhat loosened relative to the wildtype complex (Table 3.1). Phosphomimetic cTnI S22/S23D mutation would be expected to attenuate the electrostatic interactions between positively charged cTnI<sub>19-37</sub> and negatively charged cNTnC. The decrease in electrostatic attraction therefore partially releases the cNTnC domain from its active orientation, making it more mobile.

Phosphorylation of cTnI S41/S43 by protein kinase C (PKC) is also detected in mice, but it occurs to a lesser degree in humans<sup>53,281</sup>. Phosphorylation at these two sites is also known to reduce cardiac myofilament calcium sensitivity and ATPase activity<sup>52,297,298</sup>. In the active orientation, cTnI S43 forms a contact with the cNTnC helix N (A7, E10, and Q11)<sup>33</sup> that would be disrupted by phosphorylation (see Figure 3.1B).

Addition of mutant S41D/S43D-cTnI<sub>1-77</sub> to cTnC had an intermediate effect on the NMR spectrum of cTnC compared with wildtype cTnI<sub>1-77</sub> (see Figures 3.1D and Figure 3.5C).

Examining  $^{15}\text{N}$   $R_2$  relaxation measurements, we determined that the incorporation of phosphomimetic mutations S41D and S43D into cTnI<sub>1-77</sub> increased the average  $R_2$  relaxation rate in cTnC to  $18\text{ s}^{-1}$ , though this is significantly slower than what is observed for cTnC complexed with wildtype cTnI<sub>1-77</sub> ( $R_2=31\text{ s}^{-1}$ ) or S22D/S23D-cTnI<sub>1-77</sub> ( $R_2 \sim 24\text{ s}^{-1}$ ) (Figure 3.5B, Table 3.1). This suggests that the S41D/S43D dual mutation is more disruptive to the active orientation of cTnC than the S22D/S23D dual mutation. Interestingly, the  $R_2$  values for the cCTnC domain are consistently greater for the cTnC domain, suggesting that the motion of the cTnC domain has been uncoupled from the cCTnC domain in the S41D/S43D-cTnI<sub>1-77</sub>-cTnC complex. Under these circumstances, the smaller cCTnC domain tumbles more slowly than cTnC because of the added mass of tightly bound cTnI.

A previous 2014 study examined the contractile properties of cardiomyocytes taken from human donor hearts and how they changed when native cTnI was exchanged with phosphomimetic mutant S22D/S23D-cTnI or S41D/S43D-cTnI. Incorporation of S22D/S23D-cTnI caused the calcium sensitivity,  $p\text{Ca}_{50}$ , to decrease from  $5.55 \pm 0.05$  (wildtype cTnI) to  $5.37 \pm 0.01$ . Incorporation of S41D/S43D-cTnI had an even greater effect, causing  $p\text{Ca}_{50}$  to drop further to  $p\text{Ca}_{50} = 5.26 \pm 0.01$ <sup>299</sup>. Thus, S41D/S43D phosphorylation has a greater calcium desensitizing effect than S22D/S23D in cardiac muscle, as might be predicted from the structure (because it involves the only contact between two structured elements in cTnC and cTnI, see Figure 3.1B), as well as from the greater disruption of the active orientation, as observed in our  $^{15}\text{N}$  relaxation analysis. It is interesting to speculate that perhaps phosphorylation of S41 and S43 is not observed to a large extent in humans because it would shift the contractile balance too far towards relaxation. Perhaps phosphorylation of the corresponding residues in mice is better tolerated because of the much smaller size of the heart, contributing to lower muscle wall tension (that contraction must

overcome) and the fact that the mouse heart has to beat at a much faster rate, necessitating more efficient cardiac muscle relaxation.

### 3.2.3 DCM mutations disrupt the active orientation of cTnC

Since there are several dilated cardiomyopathy-associated mutations in the troponin complex that are associated with decreased calcium sensitivity of cardiac muscle contraction, we surmised that they may also cause a disruption of the active orientation of the cNTnC domain, much like the phosphomimetic modifications examined above. We therefore examined three DCM-associated mutations (cTnI K35Q, cTnC D75Y, and cTnC G159D)<sup>300-302</sup> to determine if this was the case.

The DCM mutation cTnI K35Q was first reported in 2009, segregating with DCM in a single family in an autosomal dominant manner<sup>300</sup>. Both father (the proband) and a younger son exhibited severe DCM necessitating early cardiac transplantation. An older son was also found to have DCM as well as carry the K35Q mutation. Functional studies reported that the cTnI K35Q mutation significantly decreased the calcium-binding affinity of cNTnC in reconstituted cardiac thin filaments (wildtype  $pCa_{50}=6.39 \pm 0.02$  vs cTnI K35Q  $pCa_{50}= 6.00 \pm 0.03$ )<sup>300</sup>. In the X-ray crystal structure of the cardiac troponin complex<sup>13</sup>, cTnI K35 is in a cluster of lysine residues that come into close proximity of the negatively charged calcium binding EF-hand-II of the cNTnC domain.

For the complex between cTnC and K35Q-cTnI<sub>1-77</sub>, the average <sup>15</sup>N R<sub>2</sub> rate of cNTnC and cCTnC was 22 s<sup>-1</sup> compared to 31 s<sup>-1</sup> while in complex with cTnI<sub>1-77</sub> wild type (Figure 3.6A). This suggests that the K35Q mutation disrupts the active orientation of the cNTnC domain as

postulated, perhaps a little bit more than the S22D/S23D mutation, but not as much as the S41D/S43D mutation (Table 3.1).

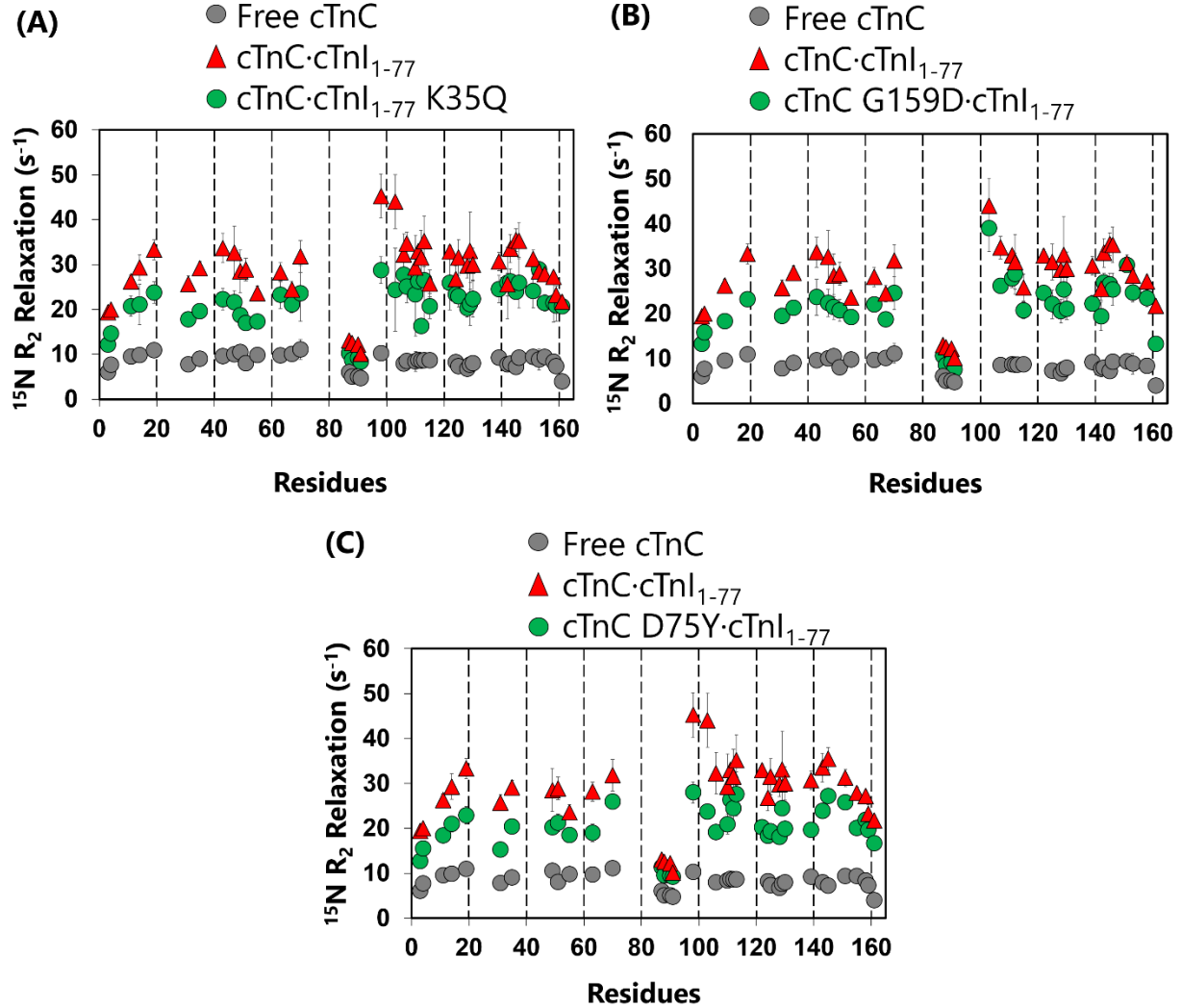


**Figure 3.6:** Comparison of  $^{15}\text{N}$   $R_2$  relaxation rates of free cTnC, cTnC complexed with wildtype cTnI<sub>1-77</sub>, and substituted (A) DCM mutant cTnI<sub>1-77</sub> K35Q, (B) cTnC D75Y, or (C) cTnC G159D.

The DCM-associated cTnC mutation D75Y was found in a double mutation E59D/D75Y in a patient with idiopathic DCM<sup>301</sup>. No further human genetic evidence for these double mutants is available to study co-segregation of the disease with the mutation. In rat cardiomyocytes, expression of the cTnC E59D/D75Y double mutations caused impaired myofilament contractility

and decreased calcium responsiveness in both intact and Triton X-100 permeabilized cells. Reconstitution with a lone D75Y-cTnC mutant in rabbit psoas fibers was able to recapitulate the same phenotype as the double mutant and showed a 50% decrease in maximal force compared to the wildtype cTnC. The single mutant also significantly lowered the calcium responsiveness of myofilaments in a force-pCa relationship analysis (wild type  $pCa_{50} = 6.2 \pm 0.04$  vs cTnC D75Y  $pCa_{50} = 5.9 \pm 0.10$ )<sup>301</sup>. In contrast, the E59D mutation did not appear to have any functional effect.

In cTnC D75 is part of the same EF-hand-II that interacts electrostatically with cTnI<sub>19-37</sub>, but it is not a calcium-binding residue and is not conserved in EF-hand proteins. As such, we predicted that the D75Y interaction would disrupt the active orientation of the cTnC domain. In our <sup>15</sup>N relaxation analysis, cTnC D75Y decreased the average R<sub>2</sub> relaxation rate of both domains from 31 s<sup>-1</sup> to ~ 21 s<sup>-1</sup> (Figure 3.6C), which was consistent with our expectations. The effect is of a similar magnitude to that of the cTnI K35Q mutation.

To date, the DCM linked mutation G159D is the cTnC mutation best supported by genetic evidence<sup>302</sup>. A total of six family members were identified carrying this mutation, including the proband who developed heart failure and required heart transplantation at the age of 23 years, and all family members carrying the mutation eventually developed DCM. The cTnC G159D mutant construct did not show any changes in calcium-binding affinity when the cTnC protein was examined in isolation, but the mutation did decrease the calcium-binding affinity of cTnC in the reconstituted thin filament<sup>303</sup>. The G159D mutation also blunted the effect of PKA-mediated phosphorylation of S22, S23 in the N-terminal tail of cTnI<sub>1-37</sub><sup>304-306</sup>.

G159 is involved in a type II turn structure involving M157, K158, G159, and V160, which places the C-terminal residue E161 in a position to form salt bridges with residues of inter-domain



flexible linker, K90 and K92. While the inter-domain linker of cTnC is very flexible, it becomes partially ordered in the active orientation of the cardiac troponin complex. We hypothesized that the presence of the small glycine amino acid residue at position 159 stabilizes the type II turn, whereas DCM-associated cTnC mutation G159D destabilizes the turn and makes the salt bridges between E161 and K90/K92 less likely to form, thus destabilizing the active orientation of the cardiac troponin complex<sup>302</sup>.

<sup>15</sup>N R<sub>2</sub> relaxation experiments reveal that the cTnC G159D mutation, like the DCM-associated mutations D75Y and cTnI K35Q, decreases the average R<sub>2</sub> values of both cTnC domains (R<sub>2</sub> = 23 s<sup>-1</sup>) (Figure 3.6B). Interestingly, the mutation also significantly mobilizes the C-terminal region of cTnC, particularly residue E161 (The R<sub>2</sub> value is considerably lower in the G159D construct than all of the other constructs), in agreement with our proposal that the G159D mutation disrupts the tight turn in residues 157-160. Moreover, the inter-domain linker also appears to be more mobile for this mutant complex, further supporting the importance of the ionic interactions between E161 and the inter-domain linker. We thus conclude that DCM-associated cTnC G159D mutation, along with cTnC D75Y and cTnI K35Q, destabilizes the active orientation of the cTnC domain, and all of these correlates with decreased calcium sensitivity of cardiac muscle.

**Table 3.1:** Comparison of average  $^{15}\text{N}$   $R_2$  relaxation rates between cTnC, cTnC·cTnI<sub>1-77</sub> complex, DCM and phosphomimetic variants of cTnC-cTnI<sub>1-77</sub> complexes. Average  $R_2$  values of cNTnC, cCTnC and inter-domain linker are reported. Average  $R_2$  values of the cNTnC domain were used to estimate the percentage tethering of the cNTnC domain to the rest of the complex relative to the wildtype cTnC·cTnI<sub>1-77</sub> complex (assuming that the complex exists in an equilibrium between fully tethered and fully free states).

Constructs	cNTnC	Linker	cCTnC	Mean $R_2$ relaxation rate $\text{s}^{-1}$
				% of cNTnC tethered
cTnC	$10 \pm 1$	5	$9 \pm 1$	0
cTnC·cTnI <sub>1-77</sub>	$29 \pm 3$	$12 \pm 1$	$32 \pm 4$	100
cTnC·cTnI <sub>1-77</sub> Ser22D/23D	$23 \pm 3$	$10 \pm 2$	$24 \pm 3$	68
cTnC·cTnI <sub>1-77</sub> Ser41D/43D	$17 \pm 2$	$8 \pm 1$	$21 \pm 2$	37
cTnC·cTnI <sub>1-77</sub> K35Q	$21 \pm 2$	$9 \pm 1$	$24 \pm 2$	58
cTnC D75Y·cTnI <sub>1-77</sub>	$20 \pm 3$	$10 \pm 1$	$23 \pm 3$	53
cTnC G159D·cTnI <sub>1-77</sub>	$21 \pm 2$	$9 \pm 1$	$25 \pm 4$	58

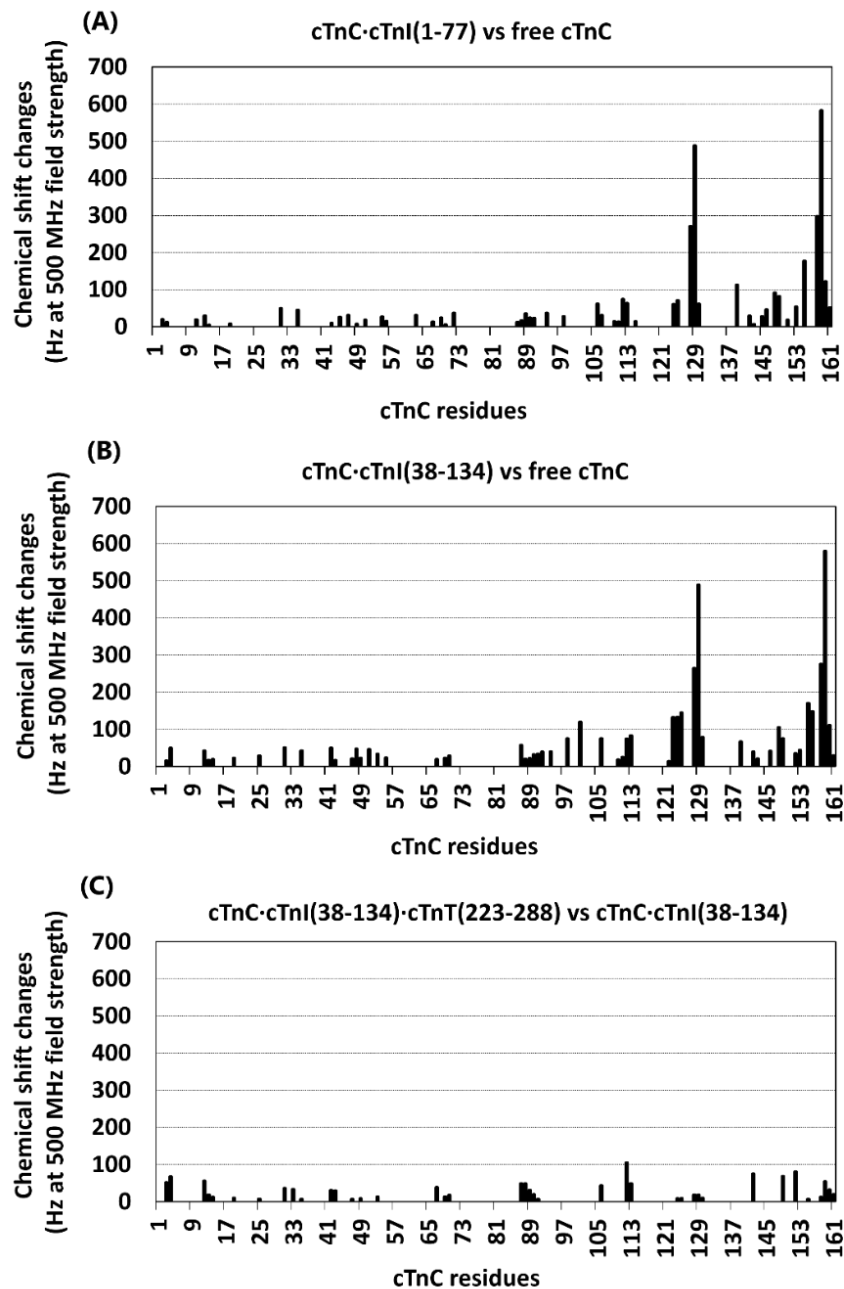


**Figure 3.7:** (A)  $^1\text{H}$  and  $^{15}\text{N}$  chemical shift changes between cTnC·cTnI<sub>1-77</sub> versus free cTnC, (B) cTnC·cTnI<sub>38-134</sub> (binary complex) versus free cTnC and (C) cTnC·cTnI<sub>38-134</sub>·cTnT<sub>223-288</sub> (ternary complex) versus cTnC·cTnI<sub>38-134</sub> (binary complex) as a function of cTnC sequence. Total chemical shift changes in Hz for  $^1\text{H}$  and  $^{15}\text{N}$  dimensions were calculated using the expression

$$\sqrt{(\text{ppm}\Delta\delta * 499.85)^2 + (\text{ppm}\Delta\delta * 50.65)^2}$$

### 3.2.4 An alternative “dormant” orientation of the cNTnC domain

We have demonstrated that certain modifications in cTnC or cTnI can disrupt the active orientation of the cNTnC domain within the cardiac troponin complex. The question arises whether the cNTnC domain becomes completely mobile when it is not tethered to the active orientation. As shown by  $^{15}\text{N}$  relaxation studies, the cNTnC domain can rotate with an angular period on the order of nanoseconds (the typical correlation time of a single domain protein) when it is restricted only by the flexible inter-domain linker. One would think that a transition from a freely mobile cNTnC domain to the active orientation would therefore not present a significant barrier to thin filament activation, since rotational diffusion would quickly allow it to move into an orientation conducive to binding the cTnI switch region.

We therefore postulated that the cNTnC domain is able to adopt an alternative orientation, possibly by interacting with other segments of the cardiac troponin complex, like the IT-arm. We thus sought to reconstitute cTnC with other fragments of the IT-arm: 1) cTnT<sub>223-288</sub>, 2) cTnI<sub>38-134</sub>, and 3) cTnT<sub>223-288</sub>-cTnI<sub>38-134</sub> complex.

Addition of cTnT<sub>223-288</sub> to cTnC revealed some unexpected changes in the NMR spectrum (Figure 3.8A). The most striking change is that the NMR signals of many residues in the cNTnC domain become broadened beyond detection (L29, G30, A31, E32, G42, E66, V72, D73, and V79). This is unexpected because the cNTnC domain was not previously known to interact with cTnT<sub>223-288</sub>. The residues most affected lie around the A-B and C-D loops, suggesting either that these loops are involved in binding cTnT or that binding to cTnT alters the closed-to-open conformational equilibrium in which these inter-helical loops move like hinges. In contrast, NMR signals from the cCTnC domain change minimally, even though cCTnC is known to interact with

residues 259-267 in cTnT. The small changes in the cCTnC NMR spectrum are consistent with a weaker and more superficial interaction compared to the strong cTnI<sub>39-60</sub>-cCTnC interaction (compare NMR spectra in Figure 3.8A versus Figure 3.5C) that involves more hydrophobic surface area.

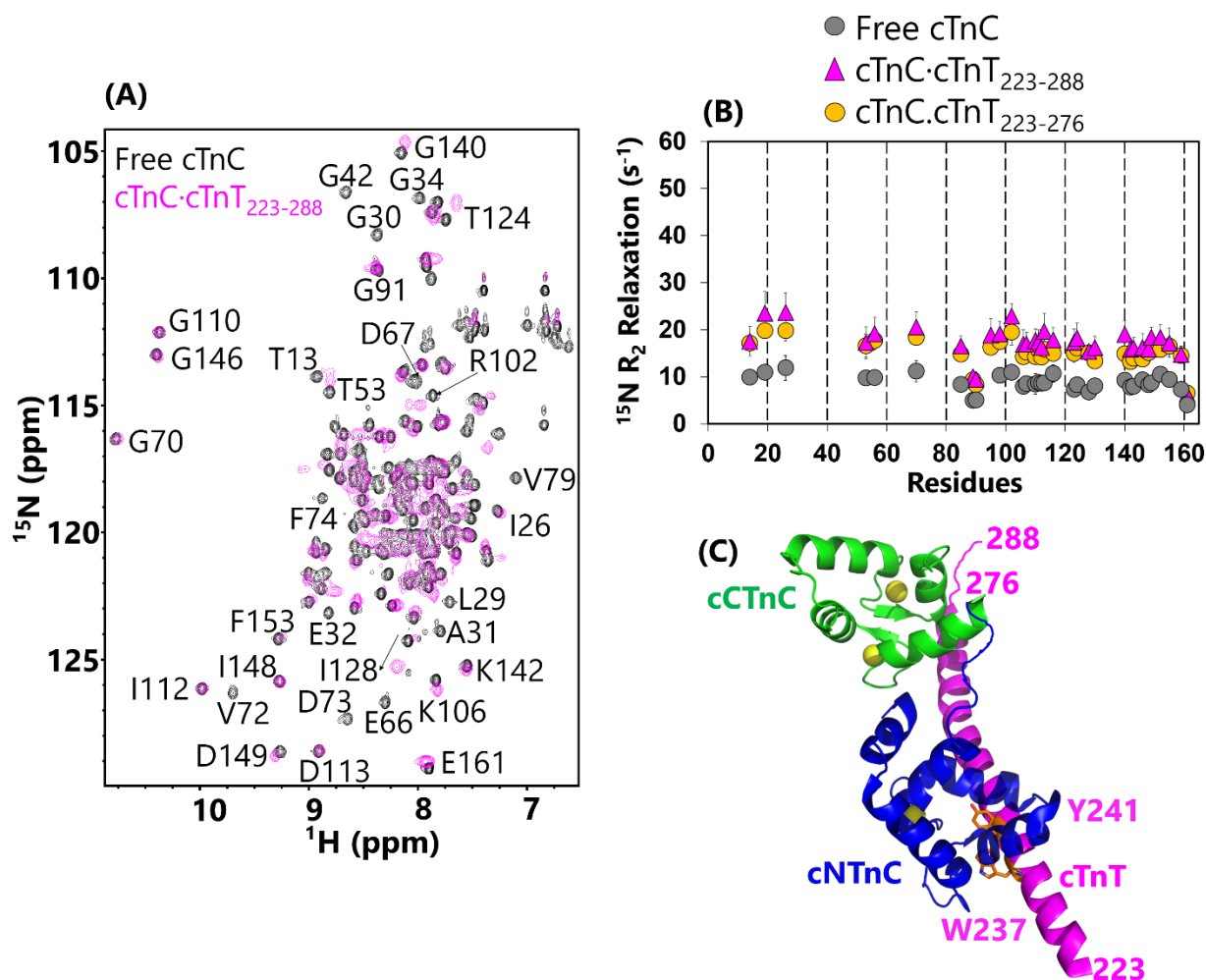


**Figure 3.8:** (A) The 2D <sup>1</sup>H, <sup>15</sup>N HSQC spectrum of free cTnC (black) superimposed with cTnC bound to cTnT<sub>223-288</sub> (magenta). (B) <sup>15</sup>N R<sub>2</sub> relaxation rates of free cTnC, cTnT<sub>223-288</sub> and cTnT<sub>223-276</sub>. (C) Theoretical 3D model of the binary complex cTnC and cTnT<sub>223-288</sub>. Hydrophobic residues that are potentially involved in binding cTnT are colored as magenta. Yellow spheres represent calcium ion.

$^{15}\text{N}$   $R_2$  relaxation measurements confirmed that the cTnT<sub>223-288</sub> fragment interacts with both cTnC domains. The average  $R_2$  relaxation rate of the entire cTnC protein increases from  $10\text{ s}^{-1}$  to  $18\text{ s}^{-1}$  (Figure 3.8B). Although the interaction sites between the cCTnC domain and cTnT are known (see Figure 3.1A), they are unknown for the cNTnC domain. It is possible that the positively charged C-terminal tail of cTnT, cTnT<sub>276-288</sub>, could extend away from the cCTnC domain to interact with the cNTnC domain, in a manner analogous to the electrostatic interaction between the N-terminal tail of cTnI and cNTnC. This has recently been suggested<sup>307</sup>. We therefore produced a cTnT fragment lacking the flexible C-terminal tail, cTnT<sub>223-276</sub>, and formed a binary complex between it and cTnC.  $^{15}\text{N}$   $R_2$  relaxation studies showed that even without the flexible tail, cTnT was still interacting with both domains, with little difference between the  $R_2$  relaxation rates of the cTnC-cTnT<sub>223-276</sub> complex versus cTnC-cTnT<sub>223-288</sub> (Figure 3.8B). Perhaps unexpectedly, deletion of the C-terminal tail of cTnT had slightly more of an impact on the relaxation rate of the cCTnC domain than the cNTnC domain, suggesting that it may interact electrostatically with the cCTnC domain rather than with the cNTnC domain.

A number of studies have suggested that the C-terminal tail of cTnT plays an important role in promoting cardiac muscle relaxation. Point mutations in residues R278 and R286 in the C-terminal tail are associated with hypertrophic cardiomyopathy<sup>308-311</sup>. Moreover, recent studies have demonstrated that deletion or mutation of positive charges in the tail increases the calcium sensitivity of thin filaments and shifts them away from the inactive B-state at low calcium concentrations and towards the activated M-state at high calcium concentrations<sup>307,312</sup>. Unfortunately, the C-terminal tail of cTnT is intrinsically disordered and not visible in any of the X-ray or cryo-EM structures. However, our relaxation data suggests that it may be interacting electrostatically with cCTnC, though it does not appear to be fixing domain orientations in the

manner of the N-terminal tail of cTnI. It may be that as a positively charged tail interposed between the negatively charged cCTnC domain and the positively charged cTnI inhibitory region, it is preventing the electrostatic association between cCTnC and cTnI, which has been shown to occur *in vitro*<sup>313</sup>. Such an unproductive interaction would prevent the cTnI inhibitory region from fulfilling its physiologic role of binding to actin-tropomyosin and promoting the B-state of the thin filament.

We concluded that the interaction surface for the cNTnC domain in cTnT must reside N-terminal (and not C-terminal) to the interaction surface for the cCTnC domain (residues 259-267 in cTnT). Examining the helical structure of cTnT from residues 223-258, we noticed a cluster of aromatic residues along one exposed face of cTnT that is not conserved in slow skeletal cTnT: <sup>237</sup>WQxxYxxxA<sup>245</sup>, which bears some resemblance to a half-face of an IQ-motif alpha helix [where the “I” (Isoleucine) preceding the Q (Glutamine) can be any hydrophobic residue]. We therefore introduced mutations to these residues, W237S, Q238D, Y241H, and A245S to make cTnT more resemble slow skeletal muscle TnT. When this mutant cTnT<sub>223-288</sub> was titrated into free cTnC, there was no change observed in the NMR spectrum (data not shown). This indicates that these mutated residues were indeed necessary for the interaction between the cNTnC domain and cTnT<sub>223-288</sub> (see Figure 3.8C).

Next, we produced an engineered soluble form of cTnI<sub>38-134</sub> (see Materials and Methods section 3.1.3) to form a binary complex with cTnC. As expected, the NMR spectrum of the complex was consistent with tight binding of cTnI residues 39-60 to the cCTnC domain (Figure 3.9B). <sup>15</sup>N R<sub>2</sub> relaxation analysis showed that the average R<sub>2</sub> value (R<sub>2</sub>= 23 s<sup>-1</sup>) of both cNTnC and cCTnC increased compared to free cTnC (Figure 3.9A), suggesting that cTnI<sub>38-134</sub> interacts with both domains of cTnC. Consistent with this, we also observed chemical shift perturbations in both

domains of cTnC (see Figure 3.7B). This was another unexpected result, given that we deleted both N and C-terminal tails of cTnI known to interact with cNTnC. Even if cTnI<sub>38-134</sub> were to interact with cNTnC one would expect that most of cTnI<sub>38-134</sub> would be intrinsically disordered in the absence of cTnT, which would still allow cNTnC to tumble independently of cCTnC. It is possible that in our binary complex the alpha helix of cTnI that is bound to the cCTnC domain extends beyond residue 60 all the way to residue 79 as it does in the X-ray crystal structure<sup>13</sup>, stabilized by binding to cTnC. Note that residue 79 in cTnI is cysteine but we mutate it to alanine, as in the X-ray study<sup>13</sup>. L75, A79, and P81 form an exposed and contiguous hydrophobic patch with W237, Q238, and Y241 from cTnT in the X-ray crystal structure, and we postulate that this hydrophobic patch of residues could bind to the cNTnC domain (Figure 3.9C).

Of course, cTnT<sub>223-288</sub>, cTnI<sub>38-134</sub>, and cCTnC come together to form a ternary complex, which would conceal potential binding sites in cTnI and cTnT, so the interactions that we observe in the binary cTnC-cTnT<sub>223-288</sub> and cTnC-cTnI<sub>38-134</sub> complexes may not be present in the ternary complex. Therefore, we reconstituted the cTnC-cTnT<sub>223-288</sub>-cTnI<sub>38-134</sub> ternary complex (see Materials and Methods section 3.1.5). The NMR spectrum of the ternary complex is distinct from that of any of the binary complexes, indicating successful reconstitution (Figure 3.9B). In particular, the largest chemical shift perturbations are observed in the cCTnC domain, particularly in residues K106, N107, Y111, I112, D113, K142, N143, I148, and D149 (see Figure 3.7C). These residues are located in the EF and GH loops that interact with cTnT. There are also nearby residues whose NMR signals are broadened beyond detection. These changes are only observed in the ternary complex, suggesting that the formation of the alpha helix in cTnT and subsequent binding to the cCTnC domain as depicted in the X-ray crystal structure (Figure 3.1A) are fully



achieved only in the ternary complex. Small chemical shift perturbations in the cTnC domain suggest that it is also involved in binding (see Figure 3.7C).

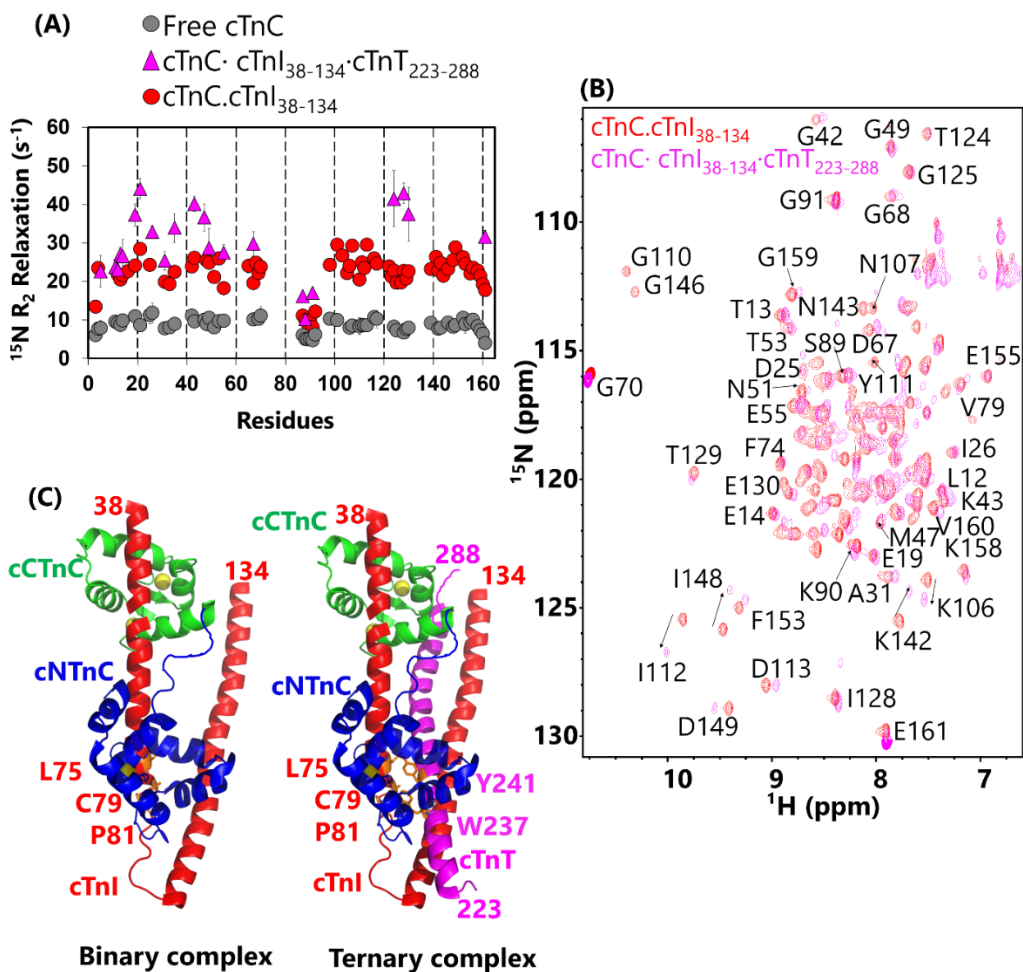


**Figure 3.9:** (A) Comparison of  $^{15}\text{N}$   $R_2$  relaxation rates of free cTnC, binary complex (cTnC·cTnI<sub>38-134</sub>) and ternary complex (cTnC·cTnI<sub>38-134</sub>·cTnT<sub>223-288</sub>). (B) The 2D  $^1\text{H}$ ,  $^{15}\text{N}$  HSQC spectrum binary complex (red) superimposed with ternary complex (magenta). (C) Theoretical 3D structures of the binary (left) and ternary (right) complex. Hydrophobic residues of both cTnI and cTnT subunits located in the IT arm are labeled in red and magenta, respectively. Yellow spheres represent calcium ion.

All of the NMR signals in the ternary complex are very weak, making it difficult to record 2D spectra and relaxation experiments. Nevertheless, we were able to record  $^{15}\text{N}$   $R_2$  relaxation

experiments with longer acquisition times, with some peaks having adequate signal-to-noise for relaxation analysis, though far fewer than were available in the smaller complexes. Relaxation analysis revealed a significant increase in the average  $R_2$  value to about  $35\text{ s}^{-1}$  in the ternary complex, and this value is greater than any observed for the smaller binary complexes in this study, as would be expected due to the higher combined molecular weight (Figure 3.9A). Since the  $R_2$  values are consistently high across both cNTnC and cCTnC domains, this suggests that the cNTnC domain is in fact immobilized in the ternary complex.

Thus, we provide evidence from NMR relaxation experiments that while the active orientation is disrupted by removing the N-terminal and C-terminal tails of cTnI, the cNTnC domain is yet immobilized by binding to the IT-arm. The relaxation experiments do not reveal where the binding site is, but the possible binding sites are limited by the reach of the inter-domain linker of cTnC, residues 86-92. In the active orientation, the linker “flips up” to a position stabilized by the cTnI N-terminal tail away from the IT-arm. If the linker instead “flips down” towards the IT-arm (compare Figure 3.1A with Figure 3.9C), the cNTnC domain encounters a hydrophobic patch comprised of cTnT W237, Q238, Y241 and cTnI L75, C79, P81, which we have been proposing as the potential interaction site. Unfortunately, the mutant cTnT fragment we made lacking these residues could not form a ternary complex for us to test. Small aromatic compounds are known to interact with the cNTnC domain in the same hydrophobic surface that binds the cTnI switch region<sup>187,314,315</sup>. Titration of the switch region into cTnC reverses the spectral changes observed when cTnT<sub>223-288</sub> is added to cTnC, suggesting that the same hydrophobic surface in cNTnC may be involved in binding both.

We thus observe that the cNTnC domain can bind the IT-arm when it is not in the active orientation, and we term this alternative position the “dormant” orientation, similar to when

myosin S1-ATPase heads are maintained in a “super-relaxed” orientation that is not conducive to actin-myosin cross-bridge cycling<sup>316-318</sup>. We have provided evidence that many different modifications known to reduce the calcium sensitivity of cardiac muscle contraction disrupt the active orientation. This suggests that the alternative dormant orientation of the cNTnC domain is not as conducive to binding the switch region of cTnI. In the recent cryo-EM structures of the cardiac thin filament<sup>14</sup>, the “dormant” binding site for the cNTnC domain is well exposed and not obstructed by actin or tropomyosin, far removed from the active position of cNTnC next to tropomyosin. Reduced access to the cTnI switch region decreases the calcium affinity of the cNTnC domain, because the cTnI switch region stabilizes the calcium-bound state by slowing the rate of calcium release.

It is interesting to note that in contrast to cardiac muscle troponin complex, slow skeletal muscle troponin complex does not have the cardiac-specific N-terminal extension of cTnI that stabilizes the active orientation in the cardiac troponin complex. The human cTnI sequence <sup>19</sup>RRRSSNYRAYATEPHAKKK<sup>37</sup> previously shown to interact electrostatically with the cNTnC domain<sup>33</sup> is replaced by <sup>1</sup>PEVERK<sup>6</sup> in slow skeletal TnI. Thus, one might expect that slow skeletal muscle would have a lower calcium sensitivity than cardiac muscle because of the lack of stabilization of the active state of cTnC (the isoform of TnC used in slow skeletal muscle is exactly the same as that used in cardiac muscle). However, the opposite is true, with slow skeletal muscle having a much higher calcium sensitivity than cardiac muscle. One possible explanation for this is the lack of corresponding hydrophobic residues in slow skeletal TnT that promote the dormant orientation in cardiac troponin (cTnT W237 and Y241). Hence, we predict that in the slow skeletal muscle troponin complex the cNTnC domain may be relatively mobile, with the interactions that

stabilize the active versus dormant orientations in the cardiac complex missing in the slow skeletal muscle complex.

The heart must maintain a carefully regulated balance between contraction and relaxation. If the balance is shifted too far towards contraction, over the long term excessive cardiac muscle hypertrophy and inadequate filling can result, leading to diastolic heart failure. On the other hand, if the balance is shifted too far towards relaxation, inadequate contraction leads to thinned dilated ventricles that can no longer generate sufficient force leading to systolic heart failure. We have demonstrated that the contractile balance can be regulated by post-translational modifications to the N-terminal region of cTnI, impacting the equilibrium between active and dormant orientations of the troponin complex. If a given mutation shifts the balance beyond the range that can be corrected for by compensatory post-translational modifications, cardiomyopathies can result.

Varying degrees of inter-domain tethering and release thus explain the regulation of cardiac muscle calcium sensitivity via the cardiac troponin complex, structural effects that are readily detected by solution NMR relaxation techniques but missed by other biophysical methods. Many eukaryotic proteins contain multiple domains attached to flexible linkers and tails that are susceptible to post-translational modifications and protein binding events. Solution NMR spectroscopy may thus play an important role in understanding inter-domain orientations and how they can be exploited to regulate biologic function.

## **CHAPTER 4**

### **SMALL MOLECULE RPI-194 STABILIZES ACTIVATED TROPONIN TO INCREASE THE CALCIUM SENSITIVITY OF STRIATED MUSCLE CONTRACTION**

Chapter 4 will be submitted for publication as:

Mahmud, Z., Tikunova, S., Belevych, N., Wagg, C.S., Zhabyeyev, P., Liu, P.B, Rasicci, D.V., Yengo, C.M., Oudit, G.Y., Lopaschuk, G.D., Reiser, P.J., Davis, J.P., and Hwang, P.M. Small molecule RPI-194 stabilizes activated troponin to increase the calcium sensitivity of striated muscle contraction.

## 4.1 Introduction

Heart failure is a common disease condition in which the heart is unable to pump enough blood to satisfy the metabolic demands of the body. Systolic heart failure, also known as reduced ejection fraction (HFrEF), occurs when the heart is unable to contract with adequate force, resulting in an ejection fraction of less than 40%<sup>319</sup>. Over time, the heart becomes increasingly thinned and dilated, which further increases muscle wall tension and impairs contraction. Atherosclerotic ischemic heart disease is the most common etiology causing HFrEF<sup>159,320</sup>. In decompensated heart failure, blood pressure is often low, the perfusion of vital organs is barely adequate, and fluid accumulates in the body due to maladaptive sodium retention response of the kidneys. The most well-established drug therapies in heart failure are diuretics to reverse volume overload and blood pressure medications that attenuate long term pathologic remodeling of the heart. What is missing from the therapeutic arsenal is an effective positive inotrope, a drug that increases the contractility of the heart, because to date no existing positive inotrope has been shown to improve survival.

The oldest therapy for heart failure, digoxin, inhibits cellular  $\text{Na}^+$ ,  $\text{K}^+$ -ATPase function and increases cardiac muscle contraction through an increase in cytoplasmic calcium concentration. Digoxin therapy improves symptoms and reduces hospitalization rates for heart failure<sup>321</sup>, but a narrow therapeutic index has limited its use so that it is no longer recommended therapy. The most commonly used positive inotropes in the intensive care unit,  $\beta_1$ -agonists like dobutamine and downstream type 3/4-phosphodiesterase (PDE3/PDE4) inhibitors increase cardiac output, but they also increase oxygen consumption, confer a risk of tachyarrhythmias, and promote peripheral vasodilation and hypotension, and it may be due to these side effects that they do not provide a survival benefit in chronic or acute decompensated heart failure<sup>163</sup>.

In theory, directly targeting the sarcomeric proteins that generate cardiac muscle contraction could enhance cardiac output with fewer side effects<sup>185,322-324</sup>. Omecamtiv mecarbil is a compound that binds to myosin to stabilize its pre-powerstroke conformation<sup>325</sup>. This increases the number of strong actin-myosin cross-bridges, enhancing cooperative activation of the cardiac thin filament. However, though it increases actin-myosin cross-bridging, it was also found to suppress the myosin working stroke<sup>326</sup>, giving a mixed activation/inhibition mechanism of action. Omecamtiv mecarbil prolongs the systolic phase of the cardiac cycle and increases the ejection fraction of the left ventricle, though it does not enhance the speed or force of contraction<sup>178</sup>. Phase III clinical trials of omecamtiv mecarbil have not shown a survival benefit in chronic<sup>180</sup> or acute decompensated heart failure<sup>327</sup>.

It may be more advantageous to enhance activation of the thin filament without modulating the force-generating ATPase cycle of myosin. The thin filament is activated by cTn<sup>328,329</sup>, which consists of three protein subunits: calcium-binding cTnC, actin binding inhibitory cTnI, and tropomyosin binding cTnT<sup>12,200,201</sup>. X-ray crystallography<sup>13</sup> and NMR<sup>29</sup> studies revealed that the cTnC subunit is a dumbbell-shaped protein with two globular domains, the cNTnC and cCTnC. The cNTnC domain has two calcium-binding hands, EF-I and EF- II, but only EF-II is active and binds calcium with micromolar affinity, attuned to sense cytoplasmic calcium influxes during systole (the contractile phase of the cardiac cycle). Calcium ions come on and off cNTnC very rapidly (rate of exchange,  $k_{ex} > 5000 \text{ s}^{-1}$ ), with the calcium-bound state experiencing a rapid equilibrium between closed and partially open conformations<sup>29,197</sup>. Binding of the switch region of cTnI (cTnI<sub>148-158</sub>) to cNTnC stabilizes its calcium-bound open state<sup>330</sup>. Cryo-EM<sup>14,331</sup> structures of cTn showed that residues 135-209 of cTnI bind to actin to maintain it in a blocked state, but cNTnC-cTnI<sub>148-158</sub> binding relieves this inhibition to facilitate strong actin-myosin cross-bridging.

The formation and dissociation of the cTnC-cTnI<sub>148-158</sub> complex is also rapid ( $k_{ex} > 5000 \text{ s}^{-1}$ ), establishing an equilibrium that is sensitive to regulatory control<sup>20,330</sup>.

Troponin exists in three different isoforms found in fast skeletal, slow skeletal, and cardiac muscles. For troponin I and troponin T, there are three different isoforms for each muscle type, but cardiac muscle and slow skeletal muscle share the same isoform for troponin C (*i.e.*, cTnC = ssTnC)<sup>20</sup>. The fast skeletal isoform of TnC (fsTnC) has been specifically targeted by the drugs tirasemtiv and reldesemtiv from the company Cytokinetics, which completed clinical trials using them for the treatment of amyotrophic lateral sclerosis, although the benefit was limited<sup>182,332</sup>. Reldesemtiv is currently undergoing clinical trials for the treatment of spinal muscular atrophy<sup>333</sup>. These fsTnC-targeting drugs bind to a hydrophobic cavity in fsTnC that lies beneath the binding site for the fsTnI switch region<sup>183</sup>. In theory, it should be possible to develop a compound that targets the homologous binding cavity in cTnC/ssTnC, though it would be active against both cardiac and slow skeletal muscle. Cytokinetics has developed a cardio-selective troponin activator, CK-136, formerly known as AMG 594, but they have not published data on its structure or binding site, or the results of its phase 1 clinical trial.

Previous attempts to design positive inotropes targeting cardiac troponin have resulted in compounds that bind to other targets in cardiomyocytes, such as levosimendan, pimobendan, MCI-154, and EMD 57033. Of these, levosimendan<sup>334</sup>, pimobendan<sup>335</sup>, and MCI-154<sup>314,336</sup> were found to have potent PDE3-inhibitory activity, whereas EMD 57033 was found to interact with cardiac myosin<sup>323</sup>. These compounds have lower affinity for cTnC than for these other proteins.

We therefore screened compounds for binding to the cardiac troponin complex using a unique cTnC-cTnI chimeric construct, named gChimera. We developed a novel small molecule cardiac troponin modulator, RPI-194, and measured its binding to purified cTnC and gChimera, as well



as its activity in skinned cardiac muscle trabeculae, individual cardiomyocytes, and isolated perfused working mouse hearts. Since cardiac muscle shares the same troponin C isoform as slow skeletal muscle, we have also examined its activity in skinned skeletal muscle fibers. Slow skeletal muscle has a distinct isoform of troponin I [ssTnI], but the switch region of ssTnI is still very similar to that of cTnI. Our goal was to develop a compound that can be used as a positive inotropic agent in the treatment of systolic heart failure, but such a compound would also cross-react with slow skeletal muscle and could have utility in treating neuromuscular conditions.

## **4.2 Materials and methods**

### **4.2.1 Preparation of proteins for NMR studies**

Three human protein constructs were used in the NMR study: 1) recombinant  $^{15}\text{N}$  isotope labeled human  $\alpha\text{Cys-cTnC}$  (C35S, C84S double mutant), 2) recombinant  $^{15}\text{N}$  isotope labeled chimeric construct (gChimera) which mimics the cTnTnC and cTnI switch peptide, cTnTnC<sub>1-85</sub> - linker-cTnI<sub>147-168</sub> and 3) unlabeled slow skeletal troponin I switch peptide (ssTnI). The protocol used to express and purify both cTnTnC and gChimera in *Escherichia coli* was as previously described<sup>187</sup>. The ssTnI was purchased from GL Biochem (Shanghai) Ltd, China.

### **4.2.2 NMR titration of RPI-194 against gChimera and cTnTnC**

RPI-194 was synthesized by Rane Pharmaceuticals, Inc. in Edmonton, Alberta, Canada. Chemical structure was confirmed by NMR. For each NMR titration experiment, recombinant  $^{15}\text{N}$  labeled gChimera or cTnTnC was dissolved into 500  $\mu\text{L}$  NMR buffer (90%  $\text{H}_2\text{O}/10\%$   $\text{D}_2\text{O}$ ) consisting of 100 mM KCl, 10 mM imidazole, and 0.5 mM 4, 4-dimethyl-4-silapentane-1-sulfonic acid as a chemical shift reference. Purified lyophilized forms of gChimera or cTnTnC were dissolved in NMR buffer. A correction factor was applied to calculate the actual protein

concentration because protein quantification by acid hydrolysis followed by amino acid quantitation showed the lyophilized form was 54% pure protein by weight. The pH of each NMR sample was maintained at a slightly acidic pH ~ 6.7 by adjusting with either 1 M NaOH or 1 M HCl. The RPI-194 was dissolved into  $d_6$ -DMSO to make a 68 mM stock solution, which was then diluted ten-fold to perform titrations. For both cNTnC and gChimera, the starting concentration were 115  $\mu$ M. For cNTnC-RPI-194 titration, RPI-194 was titrated to 0.1, 0.2, 0.3, 0.4, 0.6, 0.8, 1, 1.5, 2, 2.5, 3, 3.5, 4, 5, 6 and 8 equivalents of cNTnC. For gChimera-RPI-194 titration, RPI-194 was titrated to 0.2, 0.4, 0.6, 0.8, 1, 1.2 and 1.4 equivalents of gChimera. Each titration point was monitored by recording a two dimensional  $^1\text{H}$ ,  $^{15}\text{N}$  heteronuclear single quantum coherence (HSQC) spectrum. Dilution factors were applied at each titration point to calculate the final concentration of cNTnC and RPI-194 in the calculation of binding affinities.

#### **4.2.3 NMR titration of ssTnI against cNTnC and cNTnC·RPI-194 complex**

Titration of ssTnI was performed against free cNTnC and against cNTnC complexed with RPI-194. A 10 mM stock concentration of ssTnI was made by dissolving it into  $d_6$ -DMSO. ssTnI was titrated to 0.5, 1, 1.5, 2, 2.5, 3, 3.5, 4, 5, 6, 8, 10, 13, 16, 20, 25 and 30 equivalents of cNTnC. For titrating ssTnI into cNTnC·RPI-194 complex, RPI-194 was first titrated into free cTnC (115  $\mu$ M) until both protein and drug were 1:1 equivalent. Then ssTnI was titrated with 0.1, 0.2, 0.4, 0.6, 0.8, 1, 1.5, 2, 2.5, and 3 equivalents of cNTnC·RPI-194 complex (115  $\mu$ M).

#### **4.2.4 NMR spectroscopy**

All titrations were performed on a Varian Inova 500 MHz NMR spectrometer equipped with triple resonance  $^1\text{H}$ ,  $^{13}\text{C}$ ,  $^{15}\text{N}$  probe. 2D  $^1\text{H}$   $^{15}\text{N}$  HSQC spectra were collected for each titration point at 30° C. All titration data were processed using NMRPipe<sup>227</sup>. A MATLAB runtime-based

two dimensional lineshape analysis program called TITAN was used to calculate the dissociation constant ( $K_D$ ) from titration experiments<sup>337</sup>. TITAN can be used for different binding models like two-state, three-state, conformational selection, and induced fit. First, the protein and ligand concentration of each titration points were specified in the program. Next, a specific pulse program HSQC was selected to simulate the actual HSQC experiments that were ran on the NMR spectrometer. Individual NMR spectrum of each titration point was imported into TITAN. When all NMR spectra were imported and superimposed, a specific region of interest was selected for each selected peak showing a chemical shift perturbation. TITAN only considers chemical shift changes within the selected region of interest for fitting and calculating the dissociation constant. For a two-state binding model, it followed a two-stage fitting process. In the initial stage, chemical shift and line widths of free protein were extracted from the first spectrum. In the second stage, remaining spectra were used for calculating chemical shift and line widths of ligand bound protein state, along with rate constants and the dissociation constant. Error calculation for the entire dataset was calculated by residual sampling using 200 replicas and a 5×5 block size.

#### **4.2.5 Determination of binding affinities by steady state fluorescence**

All steady-state fluorescence measurements were obtained on a SpectraMax i3x multi-mode microplate reader at 15°C. RPI-194 has intrinsic fluorescence with peak excitation and emission wavelengths at 335 nm and 470 nm, respectively. The same cNTnC and gChimera proteins (0-297  $\mu$ M) used for NMR were titrated into a solution containing 5-6  $\mu$ M RPI-194, 50 mM HEPES, 150 mM KCl, 5 mM MgCl<sub>2</sub>, 1 mM DTT and 10 mM CaCl<sub>2</sub>. Binding affinities were calculated using GraphPad Prism version 9.0.2 (San Diego, California, USA).

#### **4.2.6 Determination of Ca<sup>2+</sup> dissociation rates by stopped-flow fluorescence**

Recombinant human cTnC (T53C, C35S, and C84S), cTnI and cTnT were used for stopped flow fluorescent studies. Expression, purification, production and labeling of cTnC T53C with 2-(4'-(iodoacetamido) anilino) naphthalene-6-sulfonic acid (IAANS) were previously published<sup>261</sup>. Expression and purification of recombinant cTnI, cTnT and reconstitution of the cardiac troponin complex (cTnC·cTnI·cTnT) were as previously described<sup>261</sup>.

Calcium release rates of IAANS-labeled, reconstituted cardiac troponin complex and isolated cTnC T53C as a function of RPI-194 concentration were measured in a stopped-flow spectrometer (Applied Photophysics model SX.18MV). IAANS excitation and emission were monitored at 330 nm and 420-470 nm, respectively. The calcium release rate was monitored by mixing calcium saturated cardiac troponin complex (500  $\mu\text{M}$  Ca<sup>2+</sup>) with a stopped flow buffer containing calcium chelating solution (EGTA 10 mM, 10 mM MOPS and 150 mM KCl), pH 7.0 with a dead mixing time  $\sim$ 1.4 ms. EGTA 10 mM was used to release calcium from reconstituted cardiac troponin complex (0.3  $\mu\text{M}$ ) or isolated IAANS labeled cTnC T53C (1  $\mu\text{M}$ ) in the absence or presence of RPI-194. Increasing concentrations of RPI-194 were used in both reactions. P.J. King data analysis software developed by Applied Photophysics (Leatherhead, Surrey, UK) was used to calculate stopped flow data. It uses a nonlinear Levenberg–Marquardt algorithm for data fitting.

#### **4.2.7 Measurements of force versus pCa ( $-\log [\text{Ca}^{2+}]$ ) in skinned ventricular trabeculae**

The heart and soleus and tibialis anterior muscles were isolated from each of 8 male Sprague-Dawley rats, ranging in age from 6-9 months. The rats were euthanized (anesthesia induced by isoflurane, followed by rapid cardiectomy) in accordance with a protocol approved by

Institutional Animal Care and Use Committee of The Ohio State University. The soleus and anterior tibialis muscles were immediately placed in cold relaxing solution containing 50% glycerol (v/v)<sup>338</sup>. A single large cut was made through the free wall of the right and left ventricles of the heart, which was then placed in ice cold relaxing solution with 1% Triton X-100 for 30 minutes. The heart was removed from this solution, gently compressed, and blotted and transferred to cold glycerinating solution<sup>338</sup>.

Single trabeculae were isolated and studied as previously described<sup>315</sup>. Briefly, a trabecula was mounted in the experimental chamber that was maintained at 15°C. In the chamber, one end of the trabecula is attached to a motor and another end is attached to a transducer. Using a motor or transducer, the trabecula was set to the resting striation spacing, the equivalent of sarcomere length. Striation spacing was determined using a digital camera that was mounted on the microscope and the measurement tool in SPOT image analysis software (<https://www.spotimaging.com>).

The force versus pCa relationship was studied in six trabeculae for each concentration of RPI-194 (20, 50 and 100 µM), first without, then with RPI-194 (100 mM stock dissolved in DMSO). RPI-194 was added to all of the solutions to which the trabeculae were exposed during the measurements of the force/pCa relationship – pCa 9.0 solution, HDTA pre-activating solution and each of the submaximal activating solutions. The trabeculae were soaked in pCa 9.0 solution with RPI-194 at 15 °C for 30 minutes before initiating the second series of force measurements. We reported that DMSO had no effect on the force/pCa relationship. We initially determined, in three skeletal muscle fibers, that the control (no added compound) force/pCa relationship is essentially identical when measured twice in a given preparation. The trabecula was treated with series of pCa solutions. The composition and preparation of the solutions were as previously

described<sup>338</sup>. The force versus pCa data were fit with the logistic sigmoid function, which is mathematically equivalent to the Hill equation<sup>339,340</sup>.

The sarcomere length in slow and fast fibers was measured using the Fast Fourier Transform in ImageJ (<https://imagej.nih.gov/ij/>). The fiber type (slow or fast) of each studied skeletal muscle fiber was determined from an analysis of the myosin heavy chain isoform composition using SDS-PAGE, as described<sup>341</sup>. The maximal velocity of shortening ( $V_o$ ) was measured, using the slack test<sup>342</sup>, in slow and fast fibers when activated in pCa 4.0 solution (every third activation in the force/pCa measurements series).

#### **4.2.8 Isolation of mouse ventricular myocytes, contractility assays and cAMP measurements**

Adult ventricular cardiomyocytes were isolated and perfused as previously described<sup>343</sup>. Contractility assays from isolated cardiomyocytes were conducted as previously described<sup>344</sup>. Briefly, we used a Grass S44 stimulator with a pulse duration of 3 milliseconds at 1 Hz to stimulate cardiomyocytes and tracked myocyte contraction at 240 Hz by using a video edge detector. In addition, we also recorded myocyte steady state contraction at 1 Hz and subsequent equilibrium period for 4 min at 240 Hz. We determined fractional shortening, shortening ( $+dL/dT$ ) and relaxation rate ( $dL/dT$ ) from the isolated cardiomyocytes. We were unable to collect data from the calcium transient experiments because of the intrinsic fluorescence of RPI-194, which causes a high background signal when FURA-2 was used as a fluorophore in the calcium transient experiment. FURA-2 is excited at 340 and 380 nm and emission taken at 510 nm.

#### **4.2.9 Isolated working mouse heart perfusion and measurement of metabolic rates**

All animals used in isolated working heart perfusion experiments were treated in accordance with the guidelines of the Canadian Council of Animal Care and approved by the University of Alberta Health Sciences Animal Welfare Committee. All animal experiments were conducted on male C57BL/6 mice (7-10 weeks) obtained from Charles River Laboratories (Wilmington, MA, USA) and regularly fed with chow diet (Harlan Teklad, Madison, WI, USA). Animals were anesthetized with 60 mg kg<sup>-1</sup> isoflurane administered through the peritoneum. Isolated working heart perfusions were performed as previously described<sup>345</sup>. Rapidly excised hearts were immediately placed on an ice-cold Krebs-Henseleit solution. A recirculating perfusate solution was used for the isolation of working hearts. It consists of a modified Krebs-Henseleit solution (100 ml) which is a mixture of 1.2 mM KH<sub>2</sub>PO<sub>4</sub>, 1.2 mM MgSO<sub>4</sub>, 2.5 mM CaCl<sub>2</sub>, 4.7 mM KCl, 25 mM NaHCO<sub>3</sub> and 118 mM NaCl. We supplemented the perfusate with 1.2 mM palmitate prebound to 3% bovine serum albumin and 5 mM glucose as energy substrates. Glycolysis and glucose oxidation rates were calculated from the perfused heart by adding a small amount of radiolabeled [5-<sup>3</sup>H] glucose and [U-<sup>14</sup>C] glucose in the Krebs-Henseleit solution<sup>345,346</sup>. The perfusate was continuously supplied with a gas mixture of 95% O<sub>2</sub>, 5% CO<sub>2</sub>. Cardiac output, cardiac work, cardiac efficiency, heart rate and peak systolic pressure were also assessed from the perfused hearts.

#### **4.2.10 Impact of RPI-194 on cardiac myosin ATPase activity**

The ATPase activity of human beta-cardiac myosin subfragment 1 (amino acids 1-843) containing a C-terminal green fluorescent protein tag (M2β-S1 GFP) was examined using the NADH coupled assay<sup>347,348</sup>. Purified M2β-S1 GFP was generated using the C2C12 cell expression

system<sup>347,348</sup>. The ATPase activity was examined in the presence of 40  $\mu$ M actin and varying RPI-194 concentrations with 1% DMSO present.

## 4.3 Results

### 4.3.1 Titrations of RPI-194 into Ca<sup>2+</sup> saturated gChimera

During systole, cardiac muscle contraction is triggered by the calcium dependent binding of the cTnI switch region to the regulatory cNTnC. A cardiac troponin activator drug promotes and stabilizes formation of this activated complex. In last five years, we produced multiple cNTnC-cTnI chimeras with different linkers<sup>187,349</sup>, and with the most recent version (gChimera) utilizing a linker containing multiple Ser and Gly residues for maximum flexibility and solubility while maintaining charge neutrality (amino acid sequence shown in Figure 4.1A).

Based on our previous work, 3-chlorodiphenylamine is a promising starting compound to develop a cardiac troponin activator<sup>187</sup>. Addition of hydrophobic substituents to the aryl rings of 3-chlorodiphenylamine improves binding affinity but greatly reduces solubility, whereas more polar substituents are not well tolerated. We aimed to add at least one hydrophilic group to enhance solubility and specificity of binding. We designed a total of 54 3-chlorodiphenylamine-based compounds that were synthesized by Rane Pharmaceutical Inc., Edmonton, AB, Canada. The compounds were assessed for binding to gChimera by NMR, and we identified a compound, RPI-194, which has an additional *p*-benzoic acid in the ortho position of the aniline group which caused large chemical shift perturbations, with a measured dissociation constant,  $K_D$ , of 24  $\mu$ M (see Figure 4.1A). Linear migration of the NMR signals suggests binding kinetics in the rapid exchange regime and 1:1 binding. We also calculated the binding affinity by titrating gChimera into RPI-194, monitoring the steady state intrinsic fluorescence of the RPI-194 compound with a measured dissociation constant,  $K_D$ , of RPI-194 of 14  $\mu$ M (see Figure 4.2).



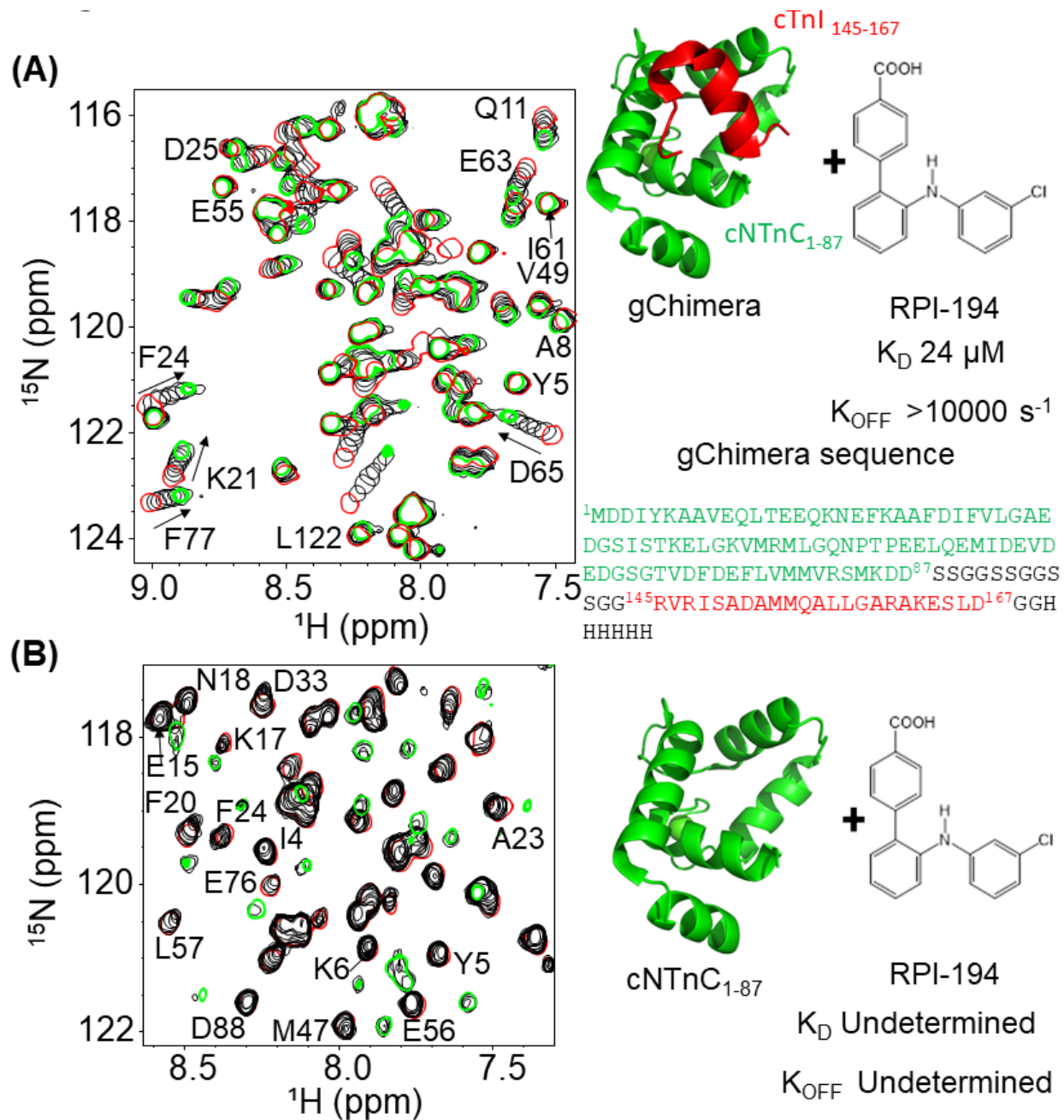


**Figure 4.1:** (A) Titration of RPI-194 compound into  $^{15}$ N labeled gChimera tracked by 2D  $^{15}$ N HSQC NMR spectra (left). Starting and ending points colored as red and green, respectively. Direction of chemical shift perturbation is marked with arrows. A 3D representation of gChimera structure with construct sequence is shown in the right panel. (B) RPI-194 titration into  $^{15}$ N labeled cNTnC domain causes signal broadening after adding an excess amount of RPI-194 (left). A 3D representation of cNTnC is shown in the right panel.

### 4.3.2 Titrations of RPI-194 into Ca<sup>2+</sup> saturated cNTnC

Compared to gChimera, RPI-194 binds to the isolated cNTnC domain with a lower affinity ( $K_D = 300 \mu\text{M}$ , as calculated by the steady state fluorescence) (see Figure 4.2). The weaker affinity could be due to the absence of the cTnI switch region, which binds to small molecules via Ile148 and Met153, as well cNTnC is in a predominantly closed conformation in the absence of the switch region. NMR titration experiments show a complex equilibrium when RPI-194 is titrated into the cNTnC domain that precludes affinity measurements from binding studies as were done for gChimera. Prior to addition of RPI-194, the NMR spectrum of isolated cNTnC domain demonstrates signal broadening due to fast timescale conformational exchange between closed and open states<sup>29,197</sup>, undergoing a closed-to-open transition with a  $k_{\text{ex}}$  of about  $30,000 \text{ s}^{-1}$ , with the more open conformation representing a minor population of about 5%<sup>350,351</sup>. Peaks shift and then rapidly disappear upon addition of RPI-194, indicating intermediate timescale binding, consistent with selective binding of RPI-194 to the less populated open state and its stabilization (see Figure 4.1B). As more RPI-194 is added, new NMR signals corresponding to RPI-194-cNTnC complex abruptly re-appear, but in some cases (for example, for residues G30, G40, and V72) they appear in a different position than one would expect based on the start of the titration. This suggests a new conformational process occurring different from the initial 1:1 binding of cNTnC to RPI-194. Other peaks in the spectrum that do not shift become visibly reduced in intensity, suggesting a large increase in molecular weight consistent with dimerization. Similar changes occur when the drug trifluoperazine is titrated into calmodulin, a protein homologous to troponin C<sup>337,352</sup>. Each homologous domain of calmodulin binds to two molecules of Trifluoperazine, and this promotes association of the N-terminal domain with the C-terminal domain through hydrophobic interactions. We propose that two molecules of RPI-194 are needed to stabilize the open

conformation of the cNTnC domain, which then has a tendency to dimerize. Physiologically, the cNTnC domain does not dimerize because cTnI is tethered to fixed positions along the thin filament. Moreover, the cNTnC domain is predominantly in the closed state unless the cTnI switch region is bound. Thus, while the behaviour of free cNTnC domain in the presence of RPI-194 (and many other compounds) is interesting in terms of its tendency to dimerize, it may not be physiologically relevant, except to note that RPI-194 does bind to calcium-saturated cNTnC domain in the absence of cTnI switch region, though binding is more effective in its presence. This suggests that RPI-194 is more effective at stabilizing the activated troponin complex once it is formed, rather than promoting the formation of the activated complex.

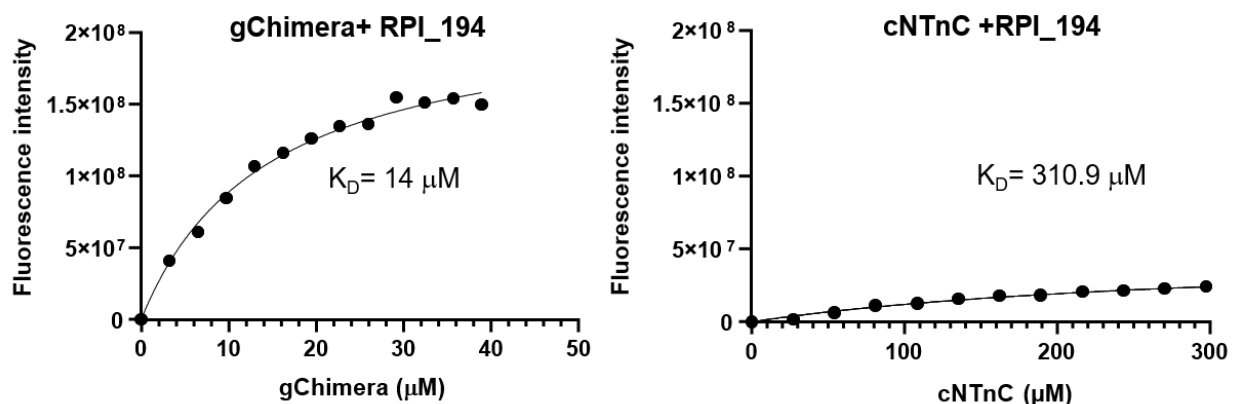


**Figure 4.2:** Fluorescence signal of 5  $\mu\text{M}$  RPI-194 with titration of gChimera (left), or titration of cNTnC (right). Representative number of experiments,  $N=3$ .

### 4.3.3 Impact of RPI-194 on binding of ssTnI switch peptide to cNTnC

Cardiac muscle troponin C (cTnC) is the exact same isoform as slow skeletal muscle troponin C (ssTnC), though slow skeletal muscle uses different isoforms for troponin I (ssTnI) and troponin T (ssTnT). We used a ssTnI switch peptide instead of the cardiac isoform because of its improved solubility. NMR spectral changes are very different when ssTnI switch peptide (as

opposed to small molecule RPI-194) is titrated into cNTnC. Signals that were broad at the start of the titration progressively become narrower as the switch peptide shifts the cNTnC conformational equilibrium to a fully open state (see Figure 4.3A), indicating very fast kinetics of binding (faster than can be detected by NMR line broadening,  $k_{ex} > 30,000 \text{ s}^{-1}$ ). Thus, the ssTnI switch peptide appears able to bind cNTnC via a rapid induced fit, whereby it stimulates the transition of cNTnC from a closed to an open state, whereas RPI-194 may bind through conformational selection, requiring stochastic transition to the open state prior to binding. Using a two-dimensional lineshape analysis tool, TITAN, we calculated the ssTnI switch peptide binding affinity for cNTnC ( $K_D$  652  $\mu\text{M}$ ) that was weaker than that for the corresponding cTnI switch peptide ( $K_D$  150  $\mu\text{M}$ )<sup>330</sup>.

We then titrated ssTnI switch peptide into cNTnC domain in the presence of RPI-194 (Figure 4.3B). The presence of one equivalent of RPI-194 significantly enhances the binding of ssTnI switch peptide to cNTnC. The binding affinity of ssTnI switch peptide for the cNTnC: RPI-194 complex is  $K_D$  22  $\mu\text{M}$  as calculated by TITAN, which is significantly tighter than the value of 652  $\mu\text{M}$  determined for cNTnC-ssTnI binding in the absence RPI-194, over an order of magnitude change. Improved binding of the TnI switch peptide is consistent with previous NMR studies of the cardiac troponin activator dfbp-o<sup>353,354</sup>.

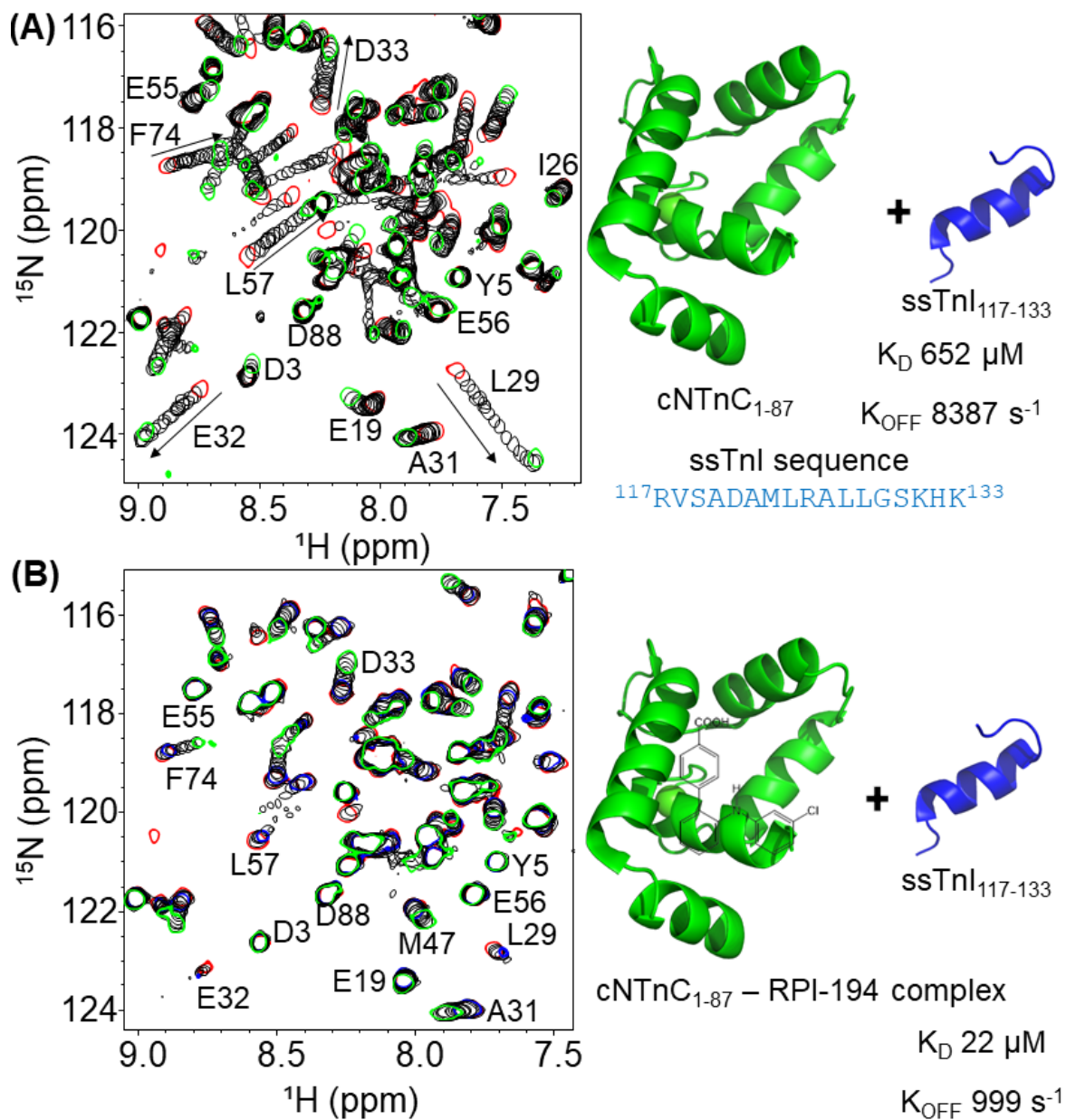


**Figure 4.3:** (A) The 2D  $^{15}\text{N}$  HSQC spectra of ssTnI titration into  $^{15}\text{N}$  labeled cNTnC (left). Titration starting and ending points are colored as red and green, respectively. Chemical shift perturbation is marked with an arrow. A 3D representation of cNTnC and ssTnI construct sequences is shown in the right panel. (B) The 2D  $^{15}\text{N}$  HSQC spectra of ssTnI titration into  $^{15}\text{N}$  labeled cNTnC and unlabeled RPI-194 complex (left). cNTnC·RPI-194 titration start, and end points colored as red and blue. End of cNTnC·RPI-194·ssTnI titration is colored blue. A 3D representation of cNTnC·RPI-194 and ssTnI is shown in the right panel.

#### 4.3.4 Effects of RPI-194 on the rate of calcium release from trimeric cardiac troponin complex and isolated cTnC

We used stopped flow fluorescence of IAANS-labeled protein to measure the impact of RPI-194 on calcium release rates in troponin. RPI-194 binding to reconstituted heterotrimeric cardiac troponin complex slowed the rate of calcium release from  $40 \text{ s}^{-1}$  to  $10 \text{ s}^{-1}$  (Figure 4.4), with an apparent dissociation constant,  $K_D$ , of  $12 \text{ }\mu\text{M}$ , in agreement with NMR and steady state fluorescence measurements. This is consistent with our NMR studies demonstrating that RPI-194 stabilizes the calcium-saturated activated troponin complex.

RPI-194 does not slow the rate of calcium release from isolated cTnC (data not shown). This is somewhat surprising, as RPI-194 binds to the interior hydrophobic patch of cTnT, which is only exposed in the calcium bound state. However, this is consistent with our previously published results that show that some troponin modulators slow the rate of calcium release from cTnT (like bepridil and trifluoperazine), whereas others (like 3-chlorodiphenylamine) do not<sup>315</sup>.

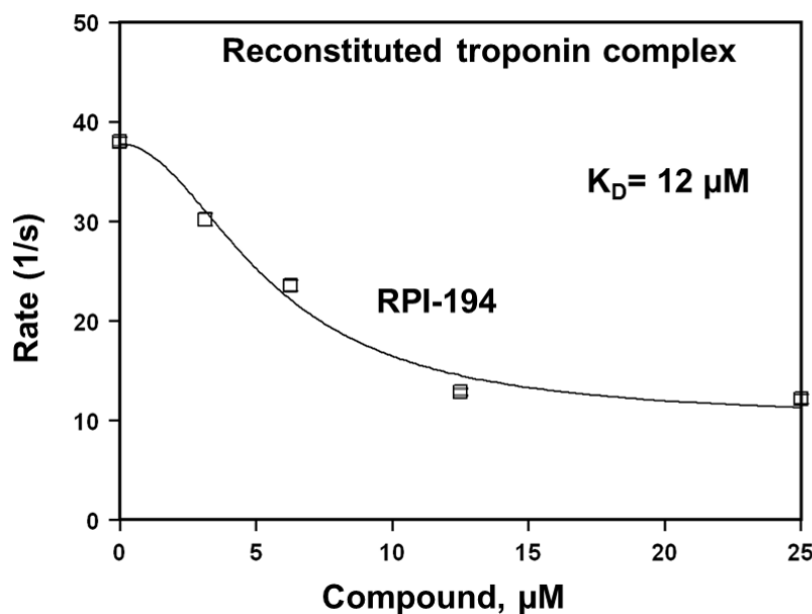


**Figure 4.4:** Stopped flow fluorescence measurements of IAANS-labeled reconstituted troponin complex in the presence of RPI-194. Representative number of experiments,  $N=10$ .

#### **4.3.5 RPI-194 activates cardiac, slow skeletal, and fast skeletal muscle in isometric contraction, but slows the velocity of unloaded contraction**

The inherent calcium sensitivity, i.e., the mean  $pCa_{50}$  in the absence of RPI-194, was not different between limb slow ( $6.32 \pm 0.03$ ) and fast ( $6.28 \pm 0.03$ ) fibers but was significantly different between both types of limb fibers and trabeculae, with the latter having much lower sensitivity ( $5.67 \pm 0.02$ ). Slow skeletal muscle has a higher calcium affinity than cardiac muscle, even though muscle types utilize the same cTnC/ssTnC isoform, the difference in pCa may be due to differences in binding to TnI. It is somewhat unexpected given that the switch region of cTnI appears to bind more tightly to cTnC than that of ssTnI. Thus, the effective concentration of the ssTnI switch region must be higher than that of the cTnI switch region, perhaps due to cTnC being maintained in a dormant orientation or myosin maintained more in a super-relaxed orientation in cardiac muscle<sup>355</sup>. Since the calcium sensitizing activity of RPI-194 depends on the presence of the TnI switch region, one might expect that RPI-194 would have a greater effect on slow skeletal muscle than cardiac muscle, and this is indeed the case.

The effects of RPI-194 were tested at 20, 50 and 100  $\mu$ M concentrations. Six cardiac trabeculae, six slow fibers and six fast fibers were studied at each concentration and each trabecula/fiber was used to study one concentration of the compound. The shift in the  $pCa_{50}$  (i.e.,  $\Delta pCa_{50}$ ) was significant between each tested concentration of RPI-194 within each muscle group. The shift in the  $pCa_{50}$  at each concentration was also significantly different between fast and slow fibers and was not different at any of the tested concentrations, between fast fibers and trabeculae. At 50  $\mu$ M RPI-194, the  $pCa_{50}$  of slow fibers shifted +0.35 units, while the fast fibers and trabeculae shifted +0.14 and +0.16, respectively (Figure 4.5, and Table 4.1). Therefore, limb slow fibers are markedly more sensitive to RPI-194, compared to cardiac trabeculae and limb fast fibers. There is

likely some cross-reactivity of RPI-194 with fast skeletal muscle, but effect is not nearly as large as that observed with tirasemtiv (+0.89)<sup>356</sup>, which was designed to be specific for fast skeletal muscle.

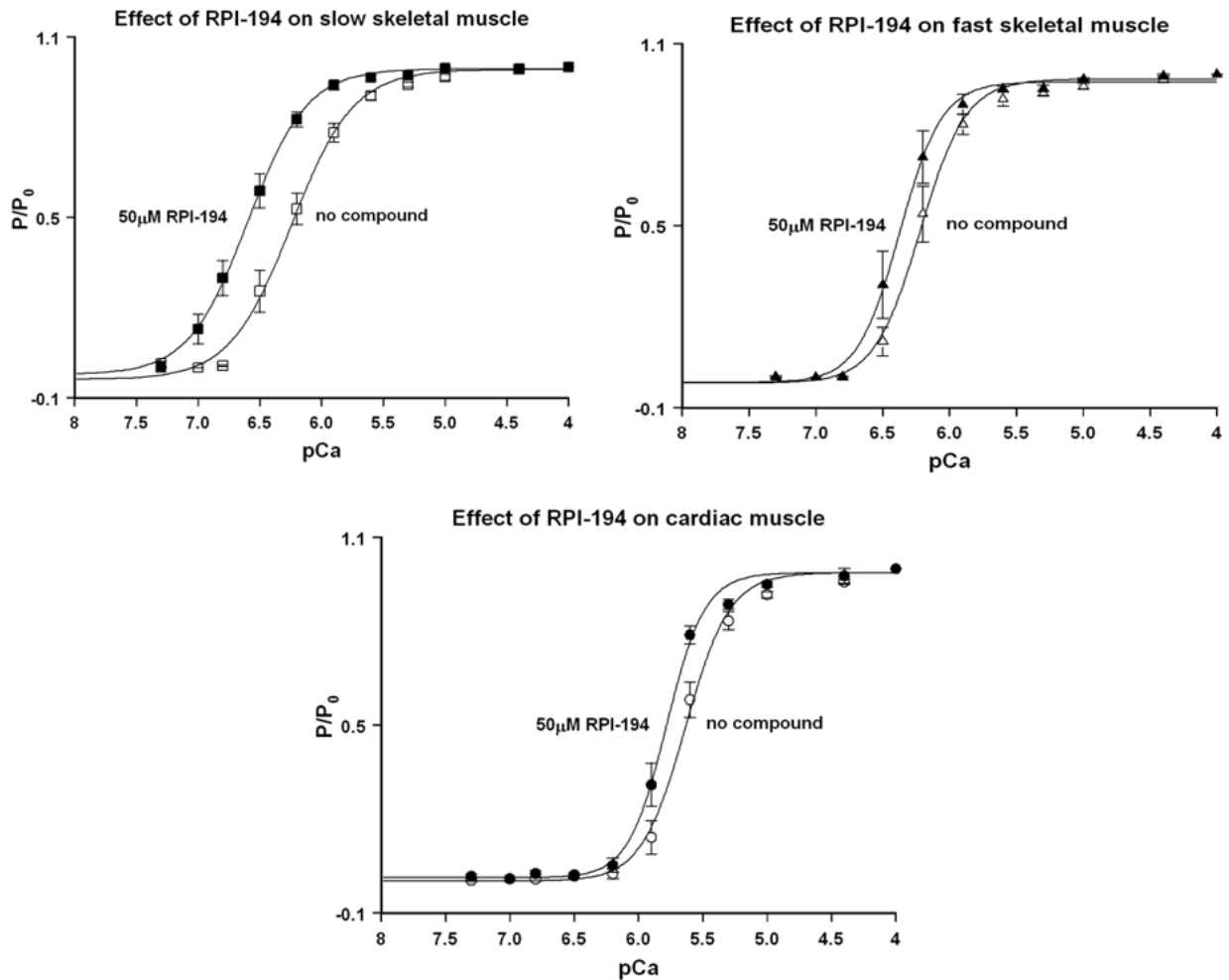


**Figure 4.5.:** Force versus pCa curves for rat skinned cardiac trabeculae, fast skeletal and slow skeletal muscle fibers in the presence of 50 μM concentrations of RPI-194.  $P/P_0$  denotes relative force. Representative number of experiments,  $N=6$  for each type of fiber.

There was a marked effect of RPI-194 on maximal shortening velocity in unloaded slow and fast fibers, with velocity generally decreasing with high concentrations of RPI-194. The overall slowing effect of RPI-194 was similar in slow and fast fibers, but the concentration-



dependency differed, with fast fibers differing significantly only between 20 and 100  $\mu\text{M}$  RPI-194 and slow fibers differing between all three concentrations (Table 4.1). This is somewhat surprising, since the velocity is thought to be related to  $k_{\text{TR}}$ , the rate of actin-myosin cross-bridge cycling. We therefore proceeded to examine the effect of RPI-194 on human beta-cardiac myosin S1 ATPase activity in the presence of 40  $\mu\text{M}$  actin and found that it had no effect (see Figure 4.6).

The first and last activations, of each fiber or trabecula, for all of the measurements of calcium sensitivity (with or without RPI-194) were in a pCa 4.0 solution (maximally activating). To assess the maximal force generating ability of each preparation during measurements, the ratio of the force during the last activation to the force during the first activation was calculated. The average ratio was 0.98 in slow fibers, 1.05 in fast fibers and 0.91 in trabeculae. The average value of the same ratio, in the presence of RPI-194, was  $\sim 1.03$ , independent of the concentration of RPI-194 in slow and fast fibers. Interestingly, the average value of this ratio increased significantly from 20 to 100  $\mu\text{M}$  RPI-194 in trabeculae and was significantly greater with 100  $\mu\text{M}$  RPI-194 in trabeculae, compared to slow and fast fibers (see Table 4.1). The cause of this phenomenon is uncertain, though it does indicate that RPI-194 does not appear to be deleterious to cardiac muscle contraction and force generation.

**Table 4.1:** Fundamental properties of slow and fast fibers and of cardiac trabeculae, in the absence or presence of 20, 50 and 100  $\mu\text{M}$  RPI-194. Values are mean  $\pm$  SEM (range in parentheses). Here,  $P_o$ = maximum isometric force, CSA= cross-sectional area, SL= sarcomere length,  $V_o$ = maximal shortening velocity, and FL=fiber length.

<b>Properties</b>	<b>Slow Fibers</b>	<b>Fast Fibers</b>	<b>Cardiac Trabeculae</b>
Cross-sectional Area ( $\mu\text{m}^2$ ), N = 18 of each	7,114 $\pm$ 335 (4,885-10,282)	10,676 $\pm$ 619 (6,175-18,271)	40,656 $\pm$ 3,129 (25,573-71,409)
Resting SL ( $\mu\text{m}$ ), N = 18 of each	2.48 $\pm$ 0.01 (2.39-2.57)	2.47 $\pm$ 0.01 (2.41-2.55)	2.06 $\pm$ 0.02 (1.93-2.18)
$P_o$ /CSA ( $\text{kN}/\text{m}^2$ ), N = 18 of each	104.5 $\pm$ 3.2 (66.6-121.1)	91.6 $\pm$ 4.1 (56.0-118.7)	14.3 $\pm$ 0.8 (6.4-19.6)
$p\text{Ca}_{50}$ in the absence of RPI-194, N = 18 of each	6.32 $\pm$ 0.03 (6.10-6.58)	6.28 $\pm$ 0.03 (6.03-6.46)	5.67 $\pm$ 0.02 (5.49-5.80)
$\Delta p\text{Ca}_{50}$ with 20 $\mu\text{M}$ RPI-194, N = 6 of each	0.14 $\pm$ 0.02 (0.10-0.24)	0.04 $\pm$ 0.02 (-0.01-0.12)	0.03 $\pm$ 0.02 (-0.01-0.10)
$\Delta p\text{Ca}_{50}$ with 50 $\mu\text{M}$ RPI-194, N = 6 of each	0.35 $\pm$ 0.02 (0.30-0.42)	0.14 $\pm$ 0.02 (0.07-0.19)	0.16 $\pm$ 0.02 (0.09-0.20)
$\Delta p\text{Ca}_{50}$ with 100 $\mu\text{M}$ RPI-194, N = 6 of each	0.71 $\pm$ 0.05 (0.58-0.84)	0.25 $\pm$ 0.02 (0.14-0.27)	0.28 $\pm$ 0.02 (0.21-0.32)
$V_o$ (FL/s), in the absence of RPI-194, N = 18 of each*	1.32 $\pm$ 0.04 (1.04-1.66)	4.67 $\pm$ 0.2 (3.42-6.46)	-
$V_o$ ratio with 20 $\mu\text{M}$ RPI-194, N = 6 of each*	0.75 $\pm$ 0.03 (0.69-0.86)	0.67 $\pm$ 0.06 (0.51-0.82)	-
$V_o$ ratio with 50 $\mu\text{M}$ RPI-194, N = 6 of each	0.58 $\pm$ 0.04 (0.51-0.68)	0.61 $\pm$ 0.06 (0.49-0.85)	-

V <sub>o</sub> ratio with 100 μM RPI-194, N = 6 of each	0.50 ± 0.01 (0.48-0.52)	0.52 ± 0.04 (0.42-0.64)	-
Last P <sub>o</sub> /first P <sub>o</sub> , in the absence of RPI-194, N = 18 of each	0.98 ± 0.01 (0.91-1.11)	1.05 ± 0.02 (0.89-1.17)	0.91 ± 0.01 (0.84-1.04)
First P <sub>o</sub> with 20 μM RPI-194/last P <sub>o</sub> without RPI-194, N = 6 of each	0.85 ± 0.02 (0.81-0.91)	0.91 ± 0.01 (0.87-0.95)	0.89 ± 0.01 (0.84-0.93)
First P <sub>o</sub> with 50 μM RPI-194/last P <sub>o</sub> without RPI-194, N = 6 of each	0.84 ± 0.02 (0.81-0.91)	0.92 ± 0.06 (0.84-1.03)	0.87 ± 0.03 (0.81-0.98)
First P <sub>o</sub> with 100 μM RPI-194/last P <sub>o</sub> without RPI-194, N = 6 of each	0.85 ± 0.02 (0.78-0.92)	0.90 ± 0.01 (0.85-0.94)	0.92 ± 0.02 (0.86-1.00)
Last P <sub>o</sub> with RPI-194/First P <sub>o</sub> with RPI-194, 20 μM, N = 6 of each	1.02 ± 0.01 (0.97-1.05)	1.03 ± 0.02 (0.95-1.07)	0.97 ± 0.03 (0.86-1.07)
Last P <sub>o</sub> with RPI-194/First P <sub>o</sub> with RPI-194, 50 μM, N = 6 of each	1.03 ± 0.02 (0.96-1.07)	1.06 ± 0.02 (0.99-1.12)	1.01 ± 0.04 (0.84-1.09)
Last P <sub>o</sub> with RPI-194/First P <sub>o</sub> with RPI-194, 100 μM, N = 6 of each	1.04 ± 0.02 (0.95-1.09)	1.01 ± 0.02 (0.97-1.07)	1.11 ± 0.02 (1.04-1.18)

\*The V<sub>o</sub> measurements for one fast fiber were not reliable and were not included.

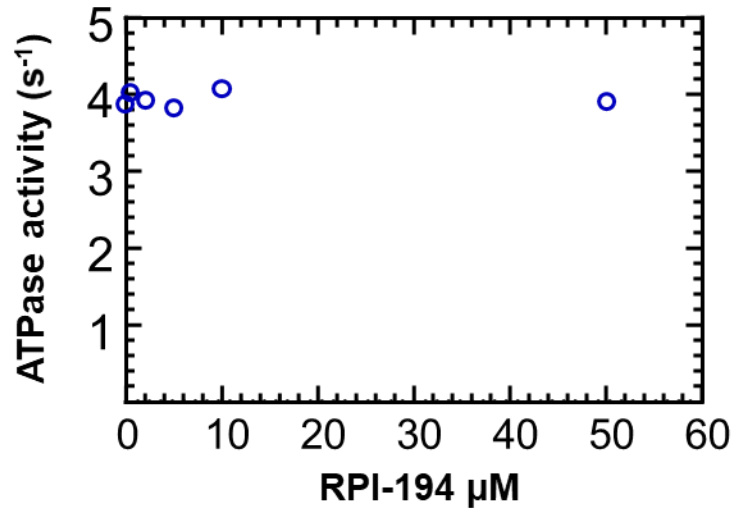


**Figure 4.6:** Impact of RPI-194 on myosin ATPase activity. The ATPase activity of human beta-cardiac myosin subfragment 1 ( $0.1 \mu\text{M}$ ) was measured in the presence of  $40 \mu\text{M}$  actin and varying concentrations of drug (RPI-194P). The ATPase activity is reported as moles of Pi per mole of myosin per second. Number of experiments,  $N=1$ .

#### 4.3.6 RPI-194 decreases velocity and amplitude of contraction in individual mouse cardiomyocytes

In individual cardiomyocytes, RPI-194 appears to exert an inhibitory effect. At  $10 \mu\text{M}$  concentration, the velocity and amplitude of shortening was reduced by about 30% (Figure 4.7). At a concentration of  $100 \mu\text{M}$ , cardiomyocyte contractions were completely inhibited. It is possible that the inhibitory effect of RPI-194 on cardiomyocyte contraction could be due to off-target effects, for instance, inhibition of calcium ion channels. We attempted to measure calcium transients, but the strong intrinsic fluorescence of RPI-194 created too much background signal.

It is also possible that the inhibition of individual cardiomyocytes is analogous to the slowing of unloaded contraction in skinned muscle fibers that we observed. At this stage it is impossible to rule out every possible off-target interaction. However, as more cardiac troponin

activators are tested, it should be possible to conclude whether the inhibition of individual cardiomyocyte contraction is an intrinsic property of cardiac troponin activators or not.

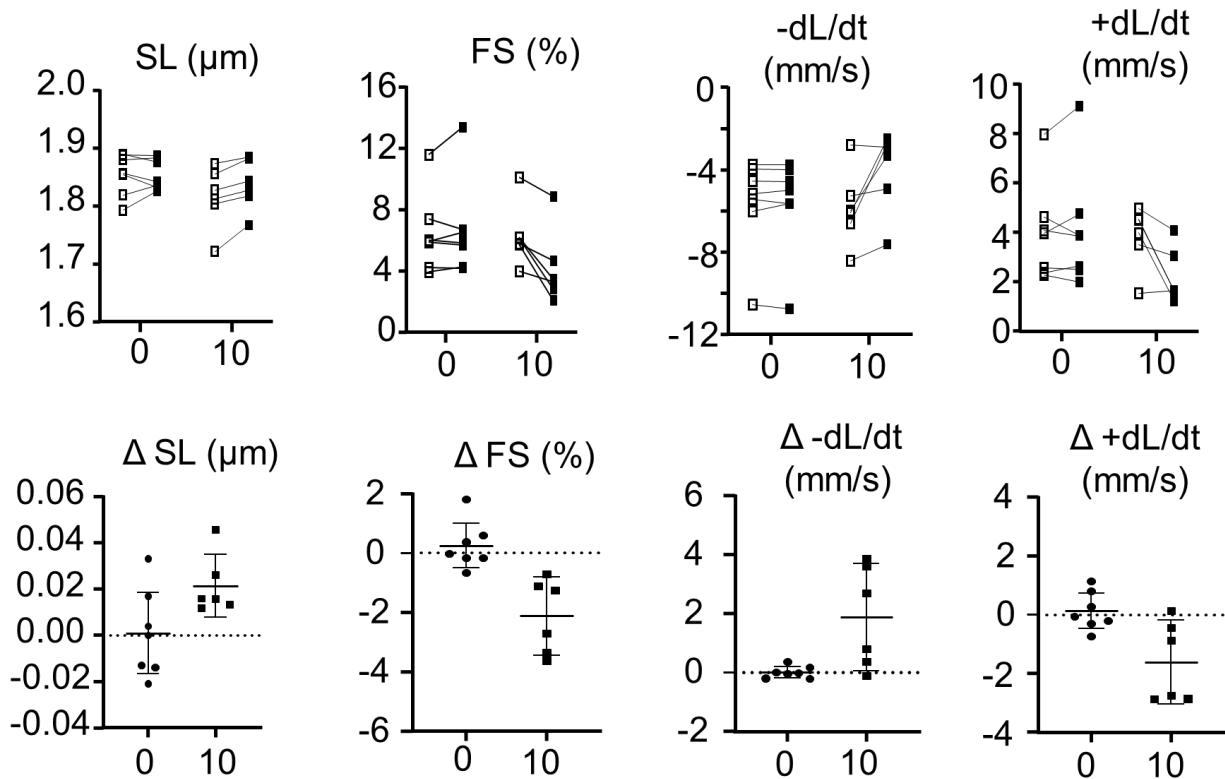


**Figure 4.7:** Top panel shows measurement of sarcomere length (SL), fractional shortening (FS), rate of contraction ( $-dL/dt$ ) and rate of relaxation ( $+dL/dt$ ) of isolated single cardiomyocytes. Open box represents wildtype and filled box represents either placebo (0) or 10  $\mu\text{M}$  of RPI-194 (10). Bottom panel shows absolute changes of measurements from wild type values.

#### 4.3.7 RPI-194 enhances cardiac work in isolated, perfused working mouse hearts

In our preliminary experiments in isolated perfused working mouse hearts, RPI-194 showed positive inotropic activity. As RPI-194 was introduced, cardiac output increased from a baseline of 9.4 mL/min up to 12.4 mL/min at 20  $\mu\text{M}$  RPI-194 (see Figure 4.8). As well, glucose utilization and oxygen consumption also increased, as expected when cardiac work increases. The

severe inhibitory effect of RPI-194 seen in cardiomyocytes did not appear to occur in isolated perfused working hearts. This suggests that calcium ion influxes and oxidative metabolism are still intact in the working heart.

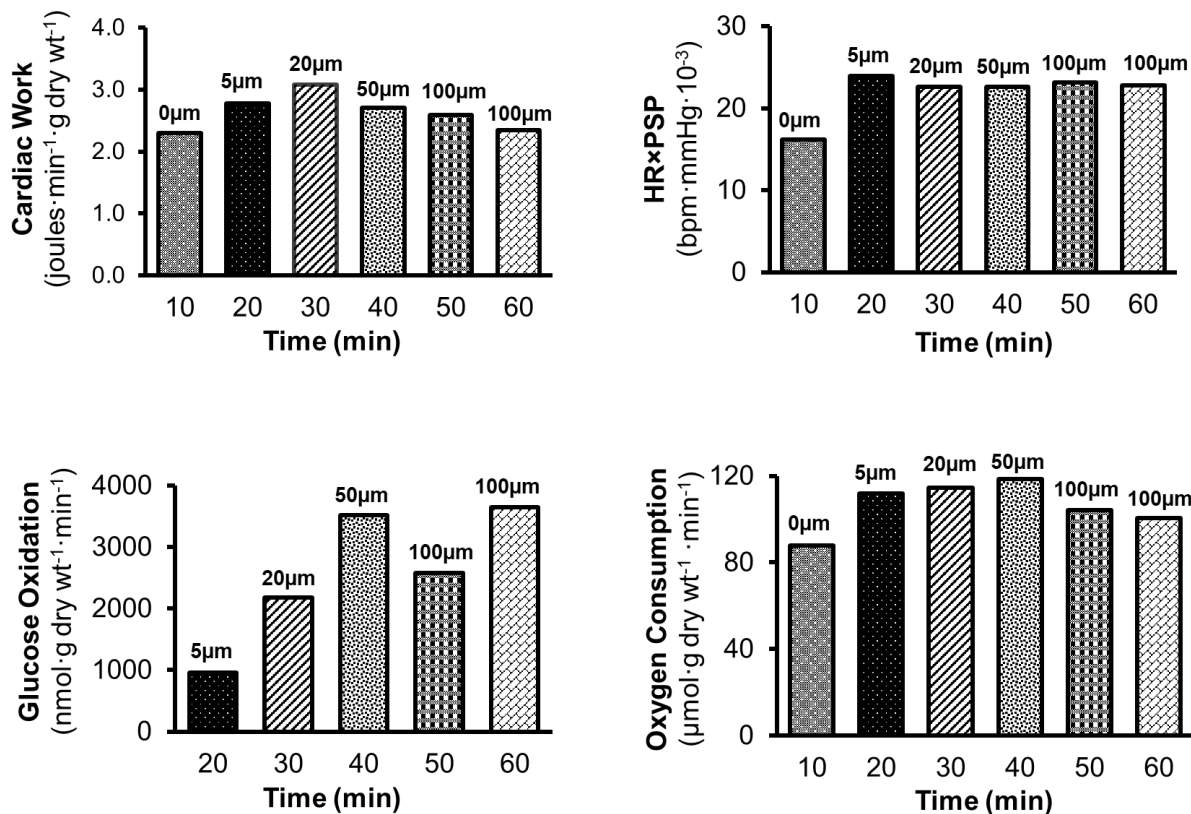


**Figure 4.8:** Effects of RPI-194 in cardiac work, heart rate×peak systolic pressure (HR×PSP), glucose oxidation and oxygen consumption in isolated, perfused working mouse hearts. The bars represent different concentrations of RPI-194. Number of experiments, N=1.

#### 4.4 Discussion

We demonstrate that the small molecule RPI-194 is able to bind to cardiac and slow skeletal muscle troponin and enhance the stability of its calcium-saturated activated form. We also confirm that RPI-194 acts as a calcium sensitizer in cardiac muscle, though it also cross reacts with slow and fast skeletal muscle. This raises the question of whether similar compounds could be used to

enhance muscle strength in neuromuscular conditions, as is being assessed for fast skeletal muscle troponin activators, tirasemtiv and reldesemtiv<sup>356-359</sup>. Whether or not cross-reactivity with skeletal muscle, particularly slow skeletal muscle, would limit potential use of a cardiac troponin activator, remains to be seen. On the other hand, it is also unknown whether the cardiac effects of a general troponin activator would limit its use as slow skeletal muscle activator. Animal studies examining the impact of cardiac/slow skeletal troponin activating compounds are needed.

Another important question is whether cardiac troponin is the most appropriate target for development of a positive inotrope, particularly in light of its known homology to other striated muscle troponins as well as to other EF hand binding proteins like calmodulin. Related to this is the question of whether calcium sensitization would be an effective therapy for systolic heart failure. Increased calcium sensitivity is a feature of cardiac troponin mutations associated with heritable hypertrophic cardiomyopathy and restrictive cardiomyopathy<sup>23,241,360</sup>. However, there is reason to believe that the changes wrought by RPI-194 would be effective and beneficial in systolic heart failure. First of all, post-translational modifications in heart failure increase calcium sensitivity<sup>355</sup>, and this would increase the overall activation of the thin filament (likely by increasing the effective concentration of the cTnI switch region presented to cTnC) to further promote the activating effect of RPI-194. Moreover, the thinned, dilated ventricular walls seen in systolic heart failure increase the wall tension that must be overcome for contraction to occur. The increase in afterload would be expected to convert super-relaxed myosin to its active form, resulting in more actin-myosin cross-bridging, more activation of thin filaments, increasing the effective concentration of the cTnI switch region and enhancing the activating effect of RPI-194. These factors should in theory enhance the positive inotropic effect of RPI-194 in systolic heart failure. Further studies in whole animal models of heart failure are needed to test this.

Perhaps the most puzzling result in the current study is the effect of RPI-194 on the velocity of unloaded shortening, both in skinned muscle fibers and in isolated cardiomyocytes. This could be due to an unknown off-target effect, although it is reassuring that cardiac function was preserved in mouse isolated perfused working hearts. It is also possible that the decreased velocity of unloaded shortening seen with RPI-194 is an effect of troponin activation. One could imagine that the ideal duty ratio (proportion of myosin heads strongly bound to actin) would be dependent on load, with excessive myosin-actin interactions contributing to drag. In isometric muscle contraction, actin-myosin interaction is maximal, with a duty ratio of about 0.25 (the proportion of myosin heads interacting with actin). This value decreases to  $<0.05$  in unloaded shortening, and perhaps excessive formation of actin-myosin cross-bridges beyond this duty ratio slows unloaded contraction<sup>361,362</sup>. It is also possible that extensive cTnI interactions with actin, recently highlighted in a cryo-EM-derived model of the thin filament<sup>14</sup>, plays a role in promoting actin release from myosin, thus speeding up the rate of actomyosin cross-bridge cycling. Reconstitution of hypertrophic cardiomyopathy-associated R95H cardiac troponin T mutant into guinea pig muscle fibers resulted in decreased cross-bridge cycling rate,  $k_{TR}$ <sup>363</sup>, suggesting that troponin may be able to impact actomyosin cross-bridge kinetics. Further studies with small molecules that are structurally distinct from RPI-194 should resolve whether the effect on unloaded contraction is an intrinsic property of cardiac troponin activators or due to an off-target effect.

We conclude that RPI-194 has expected activities as a cardiac/slow skeletal muscle troponin activator, and further studies are needed to optimize its binding affinity and assess the suitability of similar compounds for clinical use.



## **CHAPTER 5**

### **CONCLUSIONS**

## 5.1 Conclusions

This thesis focuses on the structure and function of cTn, fundamental to the control of contraction and relaxation of heart muscle. As such, it touches upon three fundamental questions about myocardial contractile function that are impacted by changes in the cTn; 1) What is the exact mechanism behind myocardial stunning in I/R injury? 2) How does a simple point mutation in cTn cause DCM? and 3) Despite having a well-understood drug target (cNTnC), why are there no approved cardiac troponin activators for the treatment of systolic heart failure?

Although troponin has been known since the 1960s, many fundamental questions about its function at the molecular level have remained enigmatic because of technical difficulties associated with reconstituting it and studying it at an atomic level of detail. In particular, cTn contains large segments of intrinsically disordered regions that are difficult to work with both in terms of production, purification, and reconstitution due to their propensity to be susceptible to proteolysis and aggregate<sup>364</sup>. Chapters 2 and 3 of this thesis represent significant achievements for our laboratory in overcoming these obstacles.

Our lab has developed new ways of producing IDRs of proteins, and we have used them to produce large quantities of pure cTnI and cTnT. We developed an expression system in *E. coli* whereby an IDR is fused to the bacterial membrane protein PagP and accumulates in dense cytoplasmic inclusion bodies where it is protected from active cellular proteases<sup>365</sup>. The inclusion bodies can be solubilized in guanidine hydrochloride denaturant, which further denatures all endogenous proteases. Guanidine hydrochloride interacts with proteins minimally and is suitable for immobilized metal ion chromatography for protein purification<sup>364</sup>. The IDR can be separated from its PagP fusion partner via nickel ion-catalyzed peptide bond cleavage and an engineered linker sequence (SRHW) or by cyanogen bromide-mediated peptide bond cleavage at methionine

residues<sup>226,274</sup>. This methodology for producing and purifying IDRs is widely applicable to other protein systems.

Within cTn, very little is known about the C-terminal tail of cTnI (cTnI<sub>135-209</sub>) from the structural perspective. Part of this flexible tail, the switch region, toggles between cNTnC and actin during muscle contraction and relaxation, respectively, though the exact details of its interaction with actin remain unknown. Although the recently solved cryo-EM structure of what showed a large segment of the tail stretched out across several actin monomers, the electron density of this was poor and the exact interactions between cTnI and actin-tropomyosin remain unresolved<sup>14</sup>. Chapter 2 of this thesis determines the secondary structure of the cTnI<sub>135-209</sub> by NMR backbone and side-chain chemical shift assignments<sup>365</sup>. The segment is primarily disordered but has some degree of  $\alpha$ -helical propensity in certain regions. We observed the same regions to interact with actin, which we studied using a monomeric actin-DNase I complex that was tractable to solution NMR. The cryo-EM structure of the cardiac thin filament was unable to provide more details of the interaction due to the intrinsic flexibility of the cTnI segment. It could be possible to study the interaction of cTnI<sub>135-209</sub> with tropomyosin fragments and solubilized actin monomers by NMR to determine more structural details.

In addition to structural studies, we also investigated the proteolytic susceptibilities of the cTnI<sub>135-209</sub> tail because many animal studies and clinical observations identified degradation products from this region during myocardial I/R injury (see section 1.5.2.4). We mapped the exact cleavage sites for MMP-2 and calpain using *in vitro* proteolysis and mass spectrometry and were surprised to find many of them in the cTnI switch region. Given the importance of the cTnI switch region in muscle contraction, we concluded that this could be a possible mechanism of the contractile dysfunction seen in myocardial stunning as a result of myocardial I/R injury. While this

is an interesting conjecture, many more experiments are needed to determine if cTnI proteolysis truly contributes to myocardial stunning.

A major shortcoming of this work is that the cTnI cleavage mapping was done in *in vitro* which does not capture the innate complexity of the biological system. Cleavage mapping of cTnI needs to be verified by *in vivo* and *ex vivo* studies under I/R conditions. In the future, it would be worthwhile studying the proteolysis of cTnI in different experimental models of I/R injury. Troponin I proteolysis has been studied previously in isolated perfused hearts<sup>85,136</sup>, and in transgenic mouse hearts<sup>137</sup>. We could use lysate samples from isolated perfused mouse hearts subjected to I/R injury. We can utilize N-terminal degradomics which uses mass spectrometry techniques to analyze these samples and map protease-specific cTnI cleavage sites<sup>366</sup>. Another approach would be evaluating I/R injury and cTnI proteolysis in MMP-2 or calpain knockout mouse models of I/R injury<sup>367,368</sup>. Attenuating MMP-2 and calpain activity using specific inhibitors may be a potential therapeutic approach for treating I/R injury. It is probable that there are many other proteases involved in I/R injury and cTnI proteolysis. Another interesting piece of future work would be to confirm partial protection of cTnI proteolysis in the presence of either cTnC or actin, identified in our *in vitro* proteolysis experiments<sup>365</sup>. We could use reconstituted troponin complex subjected to MMP-2 or calpain-mediated digestion to observe whether the number of cleavage fragments of cTnI are reduced when it is complexed with cTnC and cTnT. A study published in 1989 by Tsunekawa *et al* reported that a cardiac/skeletal troponin T homologue protein in smooth muscle named calponin showed markedly decreased calpain 1-mediated proteolysis when bound to reconstituted filamentous actin or native thin filament<sup>369</sup>. Thus, it would be useful to study cTnI degradation by MMP-2 or calpain in reconstituted thin filaments by combining the cTn complex with actin and tropomyosin.

From a technical aspect, Chapter 3 represents a major leap forward our lab in the successful reconstitution of the ternary complex of cTn, a feat that took me several years to accomplish. The main challenge of producing reconstituted cTn was the precipitation of either cTnI or cTnT as these disordered proteins naturally aggregate on their own. A number of solubilizing mutations were introduced into cTnI. As well, we found that cTnT was more soluble in the presence of high concentration of magnesium ions, and magnesium was also effective in increasing the thermal stability of the reconstituted complex. Our methodology for producing stable, soluble forms of cTn complex will be an asset for future biophysical and structural biology studies.

In Chapter 3, we were able to demonstrate how some phosphomimetic and DCM-associated mutations in cTnC and cTnI could indirectly decrease the calcium affinity of the cTn complex through destabilization of the active orientation of the cNTnC domain<sup>355</sup>. We also showed evidence a new “dormant” orientation of cNTnC when both N and C-terminal flexible tails were removed in the reconstructed cTn<sup>355</sup>. We need to further explore our newly discovered dormant orientation of cTnC. A limitation of this finding is that we do not know the details of this proposed orientation. Knowing the exact binding sites of cNTnC with the proposed IT arm will be critical to understanding the dormant orientation. A three-dimensional structure determination by NMR spectroscopy or X-ray crystallography would be ideal for revealing the interaction between cNTnC and the IT arm in the dormant orientation. It is also possible to identify residues of the IT arm binding with cNTnC by doing the NMR chemical shift perturbation experiment. Using this technique, the IT arm will be <sup>15</sup>N isotopically labeled and produced a ternary complex with either cCTnC (deletion of cNTnC) or full length cTnC. The difference in the chemical shift perturbation between these two ternary complexes will be monitored by <sup>15</sup>N-<sup>1</sup>H HSQC experiments. If there is any chemical shift perturbation observed in <sup>15</sup>N-<sup>1</sup>H HSQC spectra, this would be due to the

interaction of cNTnC with the IT arm. It will verify our proposed dormant orientation hypothesis and identify residues of the IT arm that are involved in this orientation.

Another limitation of this chapter is not having functional data (calcium binding affinity of cTnC) that correlates with our structural findings. For instance, we demonstrated how domains of cTnC become flexible in the presence of DCM mutations and/or phosphorylation but did not have confirmation of their effects on cTn's calcium binding affinity. However, all of DCM mutations and phosphorylation that we examined in this study previously showed decreased calcium binding affinity (see sections 3.2.2 and 3.2.3). In the future, we could utilize fluorescence spectroscopy to assess the functional impact of DCM mutations and phosphorylation by measuring changes in overall calcium-binding affinity in reconstituted cTn.

In Chapter 4, we identify a promising small molecule, RPI-194, that acts as a cardiac troponin activator after screening 47 compounds. It is well established that troponin activators bind to the cNTnC and cTnI switch peptide interface to activate cNTnC. Our lab has used chimeric proteins for many years to represent this cNTnC-cTnI switch peptide binding interface for screening drug molecules. The previous NMR structure of the chimeric protein confirms that it successfully reproduces this drug binding interface<sup>187</sup>. RPI-194 was selected as a potential calcium sensitizer during the drug screening process because of its binding affinity for gChimera calculated by NMR and fluorescence spectroscopy. Subsequent experiments in stopped-flow fluorescence and an isolated perfused hearts also confirmed it as a potential calcium sensitizer. Although RPI-194 demonstrated increased cardiac output, glucose utilization, and oxygen consumption in an isolated mouse heart, however, the major drawback of this experiment is that it was tested in only one heart. We need to increase the replicates for this experiment. Fluorescence data for RPI-194 was promising which showed that it does not compete with the switch peptide of cTnI for cNTnC

but facilitates its binding. However, it did not show cardiac muscle specificity, but it acts as a calcium sensitizer also for both slow skeletal and fast skeletal muscle. There are two possible experiments that can be explored from these results. One experiment would be to investigate whether targeting slow skeletal muscle has any detrimental effects. The second experiment would be the evaluation of this compound as a potential fast skeletal troponin activator. Another concerning result caused by RPI-194 was reduced velocity and amplitude of unloaded shortening in individual mouse cardiomyocytes. It could be due to cross-reaction of RPI-194 with other proteins or cTn by itself. We could also test previously identified troponin activators in individual mouse cardiomyocytes to see whether they also demonstrate similar effects. That would tell us whether the effects we have seen in our cardiomyocyte experiments are unique to RPI-194 or not. Previously, most of the calcium sensitizers like levosimendan and pimobendan had cross-reactivity with PDE3 in addition to cTnC. RPI-194 also needs to be tested against PDE3 to rule out any cross-reactivity. We could also investigate the potential toxicity of RPI-194 by doing cytotoxicity tests in cardiomyocytes.

Developing a drug for a beating heart is very challenging. It becomes even more difficult when targeting cTnC because it shares the same isoform with slow skeletal TnC. It is nearly impossible to get a cardiac-specific troponin activator by targeting cTnC for drug binding, due to this similarity. However, the switch region of cTnI is distinct from the switch region of slow skeletal TnI. Therefore, we need to have a better understanding of the cTnC-cTnI switch region interface (represented by gChimera). A three-dimensional structure of RPI-194 bound to gChimera by either NMR or X-ray crystallography would be helpful in understanding RPI-194 binding sites in gChimera.

Despite some negative functional data, RPI-194 will be an exciting tool to develop a more cardiac-specific calcium sensitizer like the fast skeletal only calcium sensitizer, tirasemtiv. For developing a successful cardiac troponin activator, three things needed to be solved: 1) the drug compound cannot compete with the cTnI switch region binding to; 2) that it targets cardiac-specific binding sites; and 3) the drug should not cross-react with other proteins like PDE3, myosin or other EF hand proteins like calmodulin.

The six years of my PhD were heavily invested in the troponin complex to understand its structural role in cardiac diseases like myocardial stunning, dilated cardiomyopathy, and systolic heart failure. The common factor in these cardiac diseases is impaired contraction of the heart. We targeted the troponin complex to tackle this impairment because of its fundamental role in the regulation of heart muscle contraction. However, a vast number of proteins and signaling pathways are involved in this process. To effectively develop therapies against cardiac diseases, we require a better understanding of the very complex biological system of the heart. This thesis will assist researchers in investigating protease-specific cleavage products in myocardial infarction patients and testing protease-specific inhibitors to improve contractile function. Our work will also contribute to the basic understanding of DCM mutations and their consequences to the structural rearrangement of the troponin complex. These discoveries could provide the potential ability to control the function and shape of the beating heart. Our attempt to develop a calcium sensitizer for troponin will also add a valuable tool in correcting and reshaping dysfunctional hearts not only in patients with heritable cardiomyopathies but in other systolic heart failure patients as well.



## BIBLIOGRAPHY

1. Kühne, W. Untersuchungen über das protoplasma und die contractilitat. *W. Engelmann, Leipzig* (1864).
2. Szent-Gyorgyi, A.G. The early history of the biochemistry of muscle contraction. *J Gen Physiol* **123**, 631-41 (2004).
3. Banga, I., and A. Szent-Györgyi. Preparation and properties of myosin A and B. *Stud. Inst. Med. Chem. Univ. Szeged*, I:5-15 (1942).
4. Straub, F.B. Actin. *Stud. Inst. Med. Chem. Univ. Szeged*, II:3–15 (1942).
5. Huxley, A.F. & Niedergerke, R. Structural changes in muscle during contraction; interference microscopy of living muscle fibres. *Nature* **173**, 971-3 (1954).
6. Huxley, H.E. X-ray analysis and the problem of muscle. *Proc R Soc Lond B Biol Sci* **141**, 59-62 (1953).
7. Bailey, K. Tropomyosin: a new asymmetric protein component of the muscle fibril. *Biochem J* **43**, 271-9 (1948).
8. Bailey, K. Tropomyosin: a new asymmetric protein component of muscle. *Nature* **157**, 368 (1946).
9. Ebashi, S. Third component participating in the superprecipitation of 'Natural Actomyosin'. *Nature* **200**, 1010 (1963).
10. Ebashi, S. & Ebashi, F. A new protein component participating in the superprecipitation of myosin B. *J Biochem* **55**, 604-13 (1964).
11. Greaser, M.L. & Gergely, J. Reconstitution of troponin activity from three protein components. *J Biol Chem* **246**, 4226-33 (1971).

12. Greaser, M.L. & Gergely, J. Purification and properties of the components from troponin. *J Biol Chem* **248**, 2125-33 (1973).
13. Takeda, S., Yamashita, A., Maeda, K. & Maeda, Y. Structure of the core domain of human cardiac troponin in the Ca<sup>2+</sup>-saturated form. *Nature* **424**, 35-41 (2003).
14. Yamada, Y., Namba, K. & Fujii, T. Cardiac muscle thin filament structures reveal calcium regulatory mechanism. *Nat Commun* **11**, 153 (2020).
15. Cheng, Y. & Regnier, M. Cardiac troponin structure-function and the influence of hypertrophic cardiomyopathy associated mutations on modulation of contractility. *Arch Biochem Biophys* **601**, 11-21 (2016).
16. Tobacman, L.S. Thin filament-mediated regulation of cardiac contraction. *Annu Rev Physiol* **58**, 447-81 (1996).
17. Sheng, J.J. & Jin, J.P. Gene regulation, alternative splicing, and posttranslational modification of troponin subunits in cardiac development and adaptation: a focused review. *Front Physiol* **5**, 165 (2014).
18. Yang, S., Barbu-Tudoran, L., Orzechowski, M., Craig, R., Trinick, J., White, H. & Lehman, W. Three-dimensional organization of troponin on cardiac muscle thin filaments in the relaxed state. *Biophys J* **106**, 855-64 (2014).
19. Wang, L., Geist, J., Grogan, A., Hu, L.R. & Kontrogianni-Konstantopoulos, A. Thick filament protein network, functions, and disease association. *Compr Physiol* **8**, 631-709 (2018).
20. Li, M.X. & Hwang, P.M. Structure and function of cardiac troponin C (TNNC1): Implications for heart failure, cardiomyopathies, and troponin modulating drugs. *Gene* **571**, 153-66 (2015).

21. Sheng, J.J. & Jin, J.P. TNNI1, TNNI2 and TNNI3: Evolution, regulation, and protein structure-function relationships. *Gene* **576**, 385-94 (2016).
22. Wei, B. & Jin, J.P. TNNT1, TNNT2, and TNNT3: Isoform genes, regulation, and structure-function relationships. *Gene* **582**, 1-13 (2016).
23. Mahmud, Z. & Hwang, P.M. Cardiac Troponin Complex: Cardiac troponin C (TNNC1), cardiac troponin I (TNNI3), and cardiac troponin T (TNNT2). *Encyclopedia of Signaling Molecules, 2nd Edition*. S. Choi (ed.). 692-701 (2018).
24. de Lemos, J.A., Drazner, M.H., Omland, T., Ayers, C.R., Khera, A., Rohatgi, A., Hashim, I., Berry, J.D., Das, S.R., Morrow, D.A. & McGuire, D.K. Association of troponin T detected with a highly sensitive assay and cardiac structure and mortality risk in the general population. *JAMA* **304**, 2503-12 (2010).
25. Gaponenko, V., Abusamhadneh, E., Abbott, M.B., Finley, N., Gasmi-Seabrook, G., Solaro, R.J., Rance, M. & Rosevear, P.R. Effects of troponin I phosphorylation on conformational exchange in the regulatory domain of cardiac troponin C. *J Biol Chem* **274**, 16681-4 (1999).
26. Gordon, A.M., Homsher, E. & Regnier, M. Regulation of contraction in striated muscle. *Physiol Rev* **80**, 853-924 (2000).
27. Herzberg, O., Moulton, J. & James, M.N. A model for the Ca<sup>2+</sup>-induced conformational transition of troponin C. A trigger for muscle contraction. *J Biol Chem* **261**, 2638-44 (1986).
28. Takeda, S. Crystal structure of troponin and the molecular mechanism of muscle regulation. *J Electron Microsc (Tokyo)* **54 Suppl 1**, i35-41 (2005).

29. Sia, S.K., Li, M.X., Spyrapoulos, L., Gagne, S.M., Liu, W., Putkey, J.A. & Sykes, B.D. Structure of cardiac muscle troponin C unexpectedly reveals a closed regulatory domain. *J Biol Chem* **272**, 18216-21 (1997).
30. Solaro, R.J., Moir, A.J. & Perry, S.V. Phosphorylation of troponin I and the inotropic effect of adrenaline in the perfused rabbit heart. *Nature* **262**, 615-7 (1976).
31. Moir, A.J., Solaro, R.J. & Perry, S.V. The site of phosphorylation of troponin I in the perfused rabbit heart. The effect of adrenaline. *Biochem J* **185**, 505-13 (1980).
32. Howarth, J.W., Meller, J., Solaro, R.J., Trewhella, J. & Rosevear, P.R. Phosphorylation-dependent conformational transition of the cardiac specific N-extension of troponin I in cardiac troponin. *J Mol Biol* **373**, 706-22 (2007).
33. Hwang, P.M., Cai, F., Pineda-Sanabria, S.E., Corson, D.C. & Sykes, B.D. The cardiac-specific N-terminal region of troponin I positions the regulatory domain of troponin C. *Proc Natl Acad Sci U S A* **111**, 14412-7 (2014).
34. Talbot, J.A. & Hodges, R.S. Synthesis and biological activity of an icosapeptide analog of the actomyosin ATPase inhibitory region of troponin I. *J Biol Chem* **254**, 3720-3 (1979).
35. Lindhout, D.A. & Sykes, B.D. Structure and dynamics of the C-domain of human cardiac troponin C in complex with the inhibitory region of human cardiac troponin I. *J Biol Chem* **278**, 27024-34 (2003).
36. McKillop, D.F. & Geeves, M.A. Regulation of the interaction between actin and myosin subfragment 1: evidence for three states of the thin filament. *Biophys J* **65**, 693-701 (1993).
37. Rarick, H.M., Tu, X.H., Solaro, R.J. & Martin, A.F. The C terminus of cardiac troponin I is essential for full inhibitory activity and Ca<sup>2+</sup> sensitivity of rat myofibrils. *J Biol Chem* **272**, 26887-92 (1997).

38. Talbot, J.A. & Hodges, R.S. Synthetic studies on the inhibitory region of rabbit skeletal troponin I. Relationship of amino acid sequence to biological activity. *J Biol Chem* **256**, 2798-802 (1981).
39. Jackson, P., Amphlett, G.W. & Perry, S.V. The primary structure of troponin T and the interaction with tropomyosin. *Biochem J* **151**, 85-97 (1975).
40. Pearlstone, J.R., Carpenter, M.R. & Smillie, L.B. Primary structure of rabbit skeletal muscle troponin-T. Sequence determination of four cyanogen bromide fragments, CB4, CB6, and CB7. *J Biol Chem* **252**, 978-82 (1977).
41. Pearlstone, J.R. & Smillie, L.B. Identification of a second binding region on rabbit skeletal troponin-T for alpha-tropomyosin. *FEBS Lett* **128**, 119-22 (1981).
42. Pearlstone, J.R. & Smillie, L.B. The interaction of rabbit skeletal muscle troponin-T fragments with troponin-I. *Can J Biochem Cell Biol* **63**, 212-8 (1985).
43. Jin, J.P. & Chong, S.M. Localization of the two tropomyosin-binding sites of troponin T. *Arch Biochem Biophys* **500**, 144-50 (2010).
44. Tanokura, M., Tawada, Y., Ono, A. & Ohtsuki, I. Chymotryptic subfragments of troponin T from rabbit skeletal muscle. Interaction with tropomyosin, troponin I and troponin C. *J Biochem* **93**, 331-7 (1983).
45. Franklin, A.J., Baxley, T., Kobayashi, T. & Chalovich, J.M. The C-terminus of troponin T is essential for maintaining the inactive state of regulated actin. *Biophys J* **102**, 2536-44 (2012).
46. Jin, J.P. Evolution, Regulation, and Function of N-terminal Variable Region of Troponin T: Modulation of Muscle Contractility and Beyond. *Int Rev Cell Mol Biol* **321**, 1-28 (2016).

47. Solaro, R.J. & van der Velden, J. Why does troponin I have so many phosphorylation sites? Fact and fancy. *J Mol Cell Cardiol* **48**, 810-6 (2010).
48. Zhang, R., Zhao, J., Mandveno, A. & Potter, J.D. Cardiac troponin I phosphorylation increases the rate of cardiac muscle relaxation. *Circ Res* **76**, 1028-35 (1995).
49. Swiderek, K., Jaquet, K., Meyer, H.E., Schachtele, C., Hofmann, F. & Heilmeyer, L.M., Jr. Sites phosphorylated in bovine cardiac troponin T and I. Characterization by <sup>31</sup>P-NMR spectroscopy and phosphorylation by protein kinases. *Eur J Biochem* **190**, 575-82 (1990).
50. Haworth, R.S., Cuello, F., Herron, T.J., Franzen, G., Kentish, J.C., Gautel, M. & Avkiran, M. Protein kinase D is a novel mediator of cardiac troponin I phosphorylation and regulates myofilament function. *Circ Res* **95**, 1091-9 (2004).
51. Blumenthal, D.K., Stull, J.T. & Gill, G.N. Phosphorylation of cardiac troponin by guanosine 3':5'-monophosphate-dependent protein kinase. *J Biol Chem* **253**, 324-6 (1978).
52. Burkart, E.M., Sumandea, M.P., Kobayashi, T., Nili, M., Martin, A.F., Homsher, E. & Solaro, R.J. Phosphorylation or glutamic acid substitution at protein kinase C sites on cardiac troponin I differentially depress myofilament tension and shortening velocity. *J Biol Chem* **278**, 11265-72 (2003).
53. Zhang, P., Kirk, J.A., Ji, W., dos Remedios, C.G., Kass, D.A., Van Eyk, J.E. & Murphy, A.M. Multiple reaction monitoring to identify site-specific troponin I phosphorylated residues in the failing human heart. *Circulation* **126**, 1828-37 (2012).
54. Lu, Q.W., Wu, X.Y. & Morimoto, S. Inherited cardiomyopathies caused by troponin mutations. *J Geriatr Cardiol* **10**, 91-101 (2013).
55. Maron, B.J. & Maron, M.S. Hypertrophic cardiomyopathy. *Lancet* **381**, 242-55 (2013).

56. Gomes, A.V., Liang, J. & Potter, J.D. Mutations in human cardiac troponin I that are associated with restrictive cardiomyopathy affect basal ATPase activity and the calcium sensitivity of force development. *J Biol Chem* **280**, 30909-15 (2005).
57. Gomes, A.V., Harada, K. & Potter, J.D. A mutation in the N-terminus of troponin I that is associated with hypertrophic cardiomyopathy affects the Ca<sup>2+</sup>-sensitivity, phosphorylation kinetics and proteolytic susceptibility of troponin. *J Mol Cell Cardiol* **39**, 754-65 (2005).
58. Organization, W.H. Cardiovascular diseases (CVDs). Vol. 2021 (2021).
59. Statistics Canada. Table 102-0561 – The ten leading causes of death, C.d.d.I.O.O.S.C.D.c.
60. Smith, E.R. The Canadian heart health strategy and action plan. *Can J Cardiol* **25**, 451-2 (2009).
61. Statistics Canada. Table 102-0561 - Leading causes of death, t.p., by age group and sex, Canada, annual, CANSIM (database). [Internet]. Ottawa (ON): Statistics Canada; 2018. Available at: <http://www5.statcan.gc.ca/cansim/a26?lang=eng&id=1020561>
62. Public Health Agency of Canada, Report from the Canadian Chronic Disease Surveillance System: Heart Disease in Canada, 2018. Available at: <https://www.canada.ca/en/public-health/services/publications/diseases-conditions/report-heart-disease-Canada-2018.html>. (2018).
63. Heusch, G. Cardioprotection: chances and challenges of its translation to the clinic. *Lancet* **381**, 166-75 (2013).
64. Mechanic, O.J., Gavin, M. & Grossman, S.A. Acute myocardial infarction. in *StatPearls* (Treasure Island (FL), 2021).
65. Eisen, A., Giugliano, R.P. & Braunwald, E. Updates on acute coronary syndrome: A review. *JAMA Cardiol* **1**, 718-30 (2016).

66. Hausenloy, D.J. & Yellon, D.M. Myocardial ischemia-reperfusion injury: a neglected therapeutic target. *J Clin Invest* **123**, 92-100 (2013).
67. Jennings, R.B., Sommers, H.M., Smyth, G.A., Flack, H.A. & Linn, H. Myocardial necrosis induced by temporary occlusion of a coronary artery in the dog. *Arch Pathol* **70**, 68-78 (1960).
68. Frank, A., Bonney, M., Bonney, S., Weitzel, L., Koeppen, M. & Eckle, T. Myocardial ischemia reperfusion injury: from basic science to clinical bedside. *Semin Cardiothorac Vasc Anesth* **16**, 123-32 (2012).
69. Murry, C.E., Jennings, R.B. & Reimer, K.A. Preconditioning with ischemia: a delay of lethal cell injury in ischemic myocardium. *Circulation* **74**, 1124-36 (1986).
70. Verma, S., Fedak, P.W., Weisel, R.D., Butany, J., Rao, V., Maitland, A., Li, R.K., Dhillon, B. & Yau, T.M. Fundamentals of reperfusion injury for the clinical cardiologist. *Circulation* **105**, 2332-6 (2002).
71. Vaidya, Y., Cavanaugh, S.M. & Dhamoon, A.S. Myocardial stunning and hibernation. in *StatPearls* (Treasure Island (FL), 2021).
72. Heyndrickx, G.R., Baig, H., Nellens, P., Leusen, I., Fishbein, M.C. & Vatner, S.F. Depression of regional blood flow and wall thickening after brief coronary occlusions. *Am J Physiol* **234**, H653-9 (1978).
73. Heyndrickx, G.R., Millard, R.W., McRitchie, R.J., Maroko, P.R. & Vatner, S.F. Regional myocardial functional and electrophysiological alterations after brief coronary artery occlusion in conscious dogs. *J Clin Invest* **56**, 978-85 (1975).
74. Marban, E. Myocardial stunning and hibernation. The physiology behind the colloquialisms. *Circulation* **83**, 681-8 (1991).



75. Braunwald, E. & Kloner, R.A. The stunned myocardium: prolonged, postischemic ventricular dysfunction. *Circulation* **66**, 1146-9 (1982).
76. Bolli, R. Myocardial 'stunning' in man. *Circulation* **86**, 1671-91 (1992).
77. Wu, M.Y., Yiang, G.T., Liao, W.T., Tsai, A.P., Cheng, Y.L., Cheng, P.W., Li, C.Y. & Li, C.J. Current mechanistic concepts in ischemia and reperfusion injury. *Cell Physiol Biochem* **46**, 1650-1667 (2018).
78. Xia, Z., Li, H. & Irwin, M.G. Myocardial ischaemia reperfusion injury: the challenge of translating ischaemic and anaesthetic protection from animal models to humans. *Br J Anaesth* **117 Suppl 2**, ii44-ii62 (2016).
79. Becker, L.B. New concepts in reactive oxygen species and cardiovascular reperfusion physiology. *Cardiovasc Res* **61**, 461-70 (2004).
80. Ferdinandy, P. & Schulz, R. Nitric oxide, superoxide, and peroxynitrite in myocardial ischaemia-reperfusion injury and preconditioning. *Br J Pharmacol* **138**, 532-43 (2003).
81. Yasmin, W., Strynadka, K.D. & Schulz, R. Generation of peroxynitrite contributes to ischemia-reperfusion injury in isolated rat hearts. *Cardiovasc Res* **33**, 422-32 (1997).
82. Beckman, J.S. Parsing the effects of nitric oxide, S-nitrosothiols, and peroxynitrite on inducible nitric oxide synthase-dependent cardiac myocyte apoptosis. *Circ Res* **85**, 870-1 (1999).
83. Cheung, P.Y., Sawicki, G., Wozniak, M., Wang, W., Radomski, M.W. & Schulz, R. Matrix metalloproteinase-2 contributes to ischemia-reperfusion injury in the heart. *Circulation* **101**, 1833-9 (2000).

84. Ali, M.A., Cho, W.J., Hudson, B., Kassiri, Z., Granzier, H. & Schulz, R. Titin is a target of matrix metalloproteinase-2: implications in myocardial ischemia/reperfusion injury. *Circulation* **122**, 2039-47 (2010).
85. Wang, W., Schulze, C.J., Suarez-Pinzon, W.L., Dyck, J.R., Sawicki, G. & Schulz, R. Intracellular action of matrix metalloproteinase-2 accounts for acute myocardial ischemia and reperfusion injury. *Circulation* **106**, 1543-9 (2002).
86. Sawicki, G., Leon, H., Sawicka, J., Sariahmetoglu, M., Schulze, C.J., Scott, P.G., Szczesna-Cordary, D. & Schulz, R. Degradation of myosin light chain in isolated rat hearts subjected to ischemia-reperfusion injury: a new intracellular target for matrix metalloproteinase-2. *Circulation* **112**, 544-52 (2005).
87. Gunata, M. & Parlakpinar, H. A review of myocardial ischaemia/reperfusion injury: Pathophysiology, experimental models, biomarkers, genetics and pharmacological treatment. *Cell Biochem Funct* **39**, 190-217 (2021).
88. Smith, G.L., Donoso, P., Bauer, C.J. & Eisner, D.A. Relationship between intracellular pH and metabolite concentrations during metabolic inhibition in isolated ferret heart. *J Physiol* **472**, 11-22 (1993).
89. Hartmann, M. & Decking, U.K. Blocking  $\text{Na}^+\text{-H}^+$  exchange by cariporide reduces  $\text{Na}^+$ -overload in ischemia and is cardioprotective. *J Mol Cell Cardiol* **31**, 1985-95 (1999).
90. Murphy, E., Perlman, M., London, R.E. & Steenbergen, C. Amiloride delays the ischemia-induced rise in cytosolic free calcium. *Circ Res* **68**, 1250-8 (1991).
91. Anzawa, R., Seki, S., Nagoshi, T., Taniguchi, I., Feuvray, D. & Yoshimura, M. The role of  $\text{Na}^+\text{/H}^+$  exchanger in  $\text{Ca}^{2+}$  overload and ischemic myocardial damage in hearts from type 2 diabetic db/db mice. *Cardiovasc Diabetol* **11**, 33 (2012).

92. Turer, A.T. & Hill, J.A. Pathogenesis of myocardial ischemia-reperfusion injury and rationale for therapy. *Am J Cardiol* **106**, 360-8 (2010).
93. Matsumura, Y., Saeki, E., Inoue, M., Hori, M., Kamada, T. & Kusuoka, H. Inhomogeneous disappearance of myofilament-related cytoskeletal proteins in stunned myocardium of guinea pig. *Circ Res* **79**, 447-54 (1996).
94. Steinberg, S.F. Oxidative stress and sarcomeric proteins. *Circ Res* **112**, 393-405 (2013).
95. Kandasamy, A.D., Chow, A.K., Ali, M.A. & Schulz, R. Matrix metalloproteinase-2 and myocardial oxidative stress injury: beyond the matrix. *Cardiovasc Res* **85**, 413-23 (2010).
96. Gross, J. & Lapiere, C.M. Collagenolytic activity in amphibian tissues: a tissue culture assay. *Proc Natl Acad Sci U S A* **48**, 1014-22 (1962).
97. Loffek, S., Schilling, O. & Franzke, C.W. Series "matrix metalloproteinases in lung health and disease": Biological role of matrix metalloproteinases: a critical balance. *Eur Respir J* **38**, 191-208 (2011).
98. Morgunova, E., Tuuttila, A., Bergmann, U., Isupov, M., Lindqvist, Y., Schneider, G. & Tryggvason, K. Structure of human pro-matrix metalloproteinase-2: activation mechanism revealed. *Science* **284**, 1667-70 (1999).
99. Tallant, C., Marrero, A. & Gomis-Ruth, F.X. Matrix metalloproteinases: fold and function of their catalytic domains. *Biochim Biophys Acta* **1803**, 20-8 (2010).
100. Spinale, F.G., Coker, M.L., Bond, B.R. & Zellner, J.L. Myocardial matrix degradation and metalloproteinase activation in the failing heart: a potential therapeutic target. *Cardiovasc Res* **46**, 225-38 (2000).
101. Birkedal-Hansen, H. Proteolytic remodeling of extracellular matrix. *Curr Opin Cell Biol* **7**, 728-35 (1995).

102. Saarialho-Kere, U.K., Chang, E.S., Welgus, H.G. & Parks, W.C. Distinct localization of collagenase and tissue inhibitor of metalloproteinases expression in wound healing associated with ulcerative pyogenic granuloma. *J Clin Invest* **90**, 1952-7 (1992).
103. Spinale, F.G., Coker, M.L., Thomas, C.V., Walker, J.D., Mukherjee, R. & Hebbar, L. Time-dependent changes in matrix metalloproteinase activity and expression during the progression of congestive heart failure: relation to ventricular and myocyte function. *Circ Res* **82**, 482-95 (1998).
104. Strongin, A.Y., Collier, I., Bannikov, G., Marmer, B.L., Grant, G.A. & Goldberg, G.I. Mechanism of cell surface activation of 72-kDa type IV collagenase. Isolation of the activated form of the membrane metalloprotease. *J Biol Chem* **270**, 5331-8 (1995).
105. Sawicki, G. Intracellular regulation of matrix metalloproteinase-2 activity: new strategies in treatment and protection of heart subjected to oxidative stress. *Scientifica (Cairo)* **2013**, 130451 (2013).
106. Cao, J., Sato, H., Takino, T. & Seiki, M. The C-terminal region of membrane type matrix metalloproteinase is a functional transmembrane domain required for pro-gelatinase A activation. *J Biol Chem* **270**, 801-5 (1995).
107. Sato, H., Takino, T., Okada, Y., Cao, J., Shinagawa, A., Yamamoto, E. & Seiki, M. A matrix metalloproteinase expressed on the surface of invasive tumour cells. *Nature* **370**, 61-5 (1994).
108. Visse, R. & Nagase, H. Matrix metalloproteinases and tissue inhibitors of metalloproteinases: structure, function, and biochemistry. *Circ Res* **92**, 827-39 (2003).
109. Dollery, C.M., McEwan, J.R. & Henney, A.M. Matrix metalloproteinases and cardiovascular disease. *Circ Res* **77**, 863-8 (1995).

110. Schulze, C.J., Wang, W., Suarez-Pinzon, W.L., Sawicka, J., Sawicki, G. & Schulz, R. Imbalance between tissue inhibitor of metalloproteinase-4 and matrix metalloproteinases during acute myocardial [correction of myoctardial] ischemia-reperfusion injury. *Circulation* **107**, 2487-92 (2003).
111. Okamoto, T., Akaike, T., Nagano, T., Miyajima, S., Suga, M., Ando, M., Ichimori, K. & Maeda, H. Activation of human neutrophil procollagenase by nitrogen dioxide and peroxyntirite: a novel mechanism for procollagenase activation involving nitric oxide. *Arch Biochem Biophys* **342**, 261-74 (1997).
112. Okamoto, T., Akaike, T., Sawa, T., Miyamoto, Y., van der Vliet, A. & Maeda, H. Activation of matrix metalloproteinases by peroxyntirite-induced protein S-glutathiolation via disulfide S-oxide formation. *J Biol Chem* **276**, 29596-602 (2001).
113. Viappiani, S., Nicolescu, A.C., Holt, A., Sawicki, G., Crawford, B.D., Leon, H., van Mulligen, T. & Schulz, R. Activation and modulation of 72kDa matrix metalloproteinase-2 by peroxyntirite and glutathione. *Biochem Pharmacol* **77**, 826-34 (2009).
114. Rouet-Benzineb, P., Buhler, J.M., Dreyfus, P., Delcourt, A., Dorent, R., Perennec, J., Crozatier, B., Harf, A. & Lafuma, C. Altered balance between matrix gelatinases (MMP-2 and MMP-9) and their tissue inhibitors in human dilated cardiomyopathy: potential role of MMP-9 in myosin-heavy chain degradation. *Eur J Heart Fail* **1**, 337-52 (1999).
115. Zatz, M. & Starling, A. Calpains and disease. *N Engl J Med* **352**, 2413-23 (2005).
116. Goll, D.E., Thompson, V.F., Li, H., Wei, W. & Cong, J. The calpain system. *Physiol Rev* **83**, 731-801 (2003).
117. Carafoli, E. & Molinari, M. Calpain: a protease in search of a function? *Biochem Biophys Res Commun* **247**, 193-203 (1998).

118. Molinari, M. & Carafoli, E. Calpain: a cytosolic proteinase active at the membranes. *J Membr Biol* **156**, 1-8 (1997).
119. Arthur, J.S., Elce, J.S., Hegadorn, C., Williams, K. & Greer, P.A. Disruption of the murine calpain small subunit gene, *Capn4*: calpain is essential for embryonic development but not for cell growth and division. *Mol Cell Biol* **20**, 4474-81 (2000).
120. Ono, Y., Sorimachi, H. & Suzuki, K. Structure and physiology of calpain, an enigmatic protease. *Biochem Biophys Res Commun* **245**, 289-94 (1998).
121. Inserte, J., Hernando, V. & Garcia-Dorado, D. Contribution of calpains to myocardial ischaemia/reperfusion injury. *Cardiovasc Res* **96**, 23-31 (2012).
122. Hood, J.L., Brooks, W.H. & Roszman, T.L. Subcellular mobility of the calpain/calpastatin network: an organelle transient. *Bioessays* **28**, 850-9 (2006).
123. Sorimachi, Y., Harada, K., Saido, T.C., Ono, T., Kawashima, S. & Yoshida, K. Downregulation of calpastatin in rat heart after brief ischemia and reperfusion. *J Biochem* **122**, 743-8 (1997).
124. Hernando, V., Inserte, J., Sartorio, C.L., Parra, V.M., Poncelas-Nozal, M. & Garcia-Dorado, D. Calpain translocation and activation as pharmacological targets during myocardial ischemia/reperfusion. *J Mol Cell Cardiol* **49**, 271-9 (2010).
125. Melloni, E., Aversa, M., Salamino, F., Sparatore, B., Minafra, R. & Pontremoli, S. Acyl-CoA-binding protein is a potent m-calpain activator. *J Biol Chem* **275**, 82-6 (2000).
126. Shulga, N. & Pastorino, J.G. Acyl coenzyme A-binding protein augments bid-induced mitochondrial damage and cell death by activating mu-calpain. *J Biol Chem* **281**, 30824-33 (2006).

127. Wijnker, P.J., Li, Y., Zhang, P., Foster, D.B., dos Remedios, C., Van Eyk, J.E., Stienen, G.J., Murphy, A.M. & van der Velden, J. A novel phosphorylation site, Serine 199, in the C-terminus of cardiac troponin I regulates calcium sensitivity and susceptibility to calpain-induced proteolysis. *J Mol Cell Cardiol* **82**, 93-103 (2015).
128. Ho, C.Y., Stromer, M.H. & Robson, R.M. Identification of the 30 kDa polypeptide in post mortem skeletal muscle as a degradation product of troponin-T. *Biochimie* **76**, 369-75 (1994).
129. Suzuki, A., Kim, K. & Ikeuchi, Y. Proteolytic cleavage of connectin/titin. *Adv Biophys* **33**, 53-64 (1996).
130. Papp, Z., van der Velden, J. & Stienen, G.J. Calpain-I induced alterations in the cytoskeletal structure and impaired mechanical properties of single myocytes of rat heart. *Cardiovasc Res* **45**, 981-93 (2000).
131. Maekawa, A., Lee, J.K., Nagaya, T., Kamiya, K., Yasui, K., Horiba, M., Miwa, K., Uzzaman, M., Maki, M., Ueda, Y. & Kodama, I. Overexpression of calpastatin by gene transfer prevents troponin I degradation and ameliorates contractile dysfunction in rat hearts subjected to ischemia/reperfusion. *J Mol Cell Cardiol* **35**, 1277-84 (2003).
132. Gao, W.D., Atar, D., Liu, Y., Perez, N.G., Murphy, A.M. & Marban, E. Role of troponin I proteolysis in the pathogenesis of stunned myocardium. *Circ Res* **80**, 393-9 (1997).
133. Martin-Garrido, A., Biesiadecki, B.J., Salhi, H.E., Shaifta, Y., Dos Remedios, C.G., Ayaz-Guner, S., Cai, W., Ge, Y., Avkiran, M. & Kentish, J.C. Monophosphorylation of cardiac troponin-I at Ser-23/24 is sufficient to regulate cardiac myofibrillar Ca<sup>2+</sup> sensitivity and calpain-induced proteolysis. *J Biol Chem* **293**, 8588-8599 (2018).

134. Ali, M.A., Stepanko, A., Fan, X., Holt, A. & Schulz, R. Calpain inhibitors exhibit matrix metalloproteinase-2 inhibitory activity. *Biochem Biophys Res Commun* **423**, 1-5 (2012).
135. Van Eyk, J.E., Powers, F., Law, W., Larue, C., Hodges, R.S. & Solaro, R.J. Breakdown and release of myofilament proteins during ischemia and ischemia/reperfusion in rat hearts: identification of degradation products and effects on the pCa-force relation. *Circ Res* **82**, 261-71 (1998).
136. McDonough, J.L., Arrell, D.K. & Van Eyk, J.E. Troponin I degradation and covalent complex formation accompanies myocardial ischemia/reperfusion injury. *Circ Res* **84**, 9-20 (1999).
137. Murphy, A.M., Kogler, H., Georgakopoulos, D., McDonough, J.L., Kass, D.A., Van Eyk, J.E. & Marban, E. Transgenic mouse model of stunned myocardium. *Science* **287**, 488-91 (2000).
138. McDonough, J.L., Labugger, R., Pickett, W., Tse, M.Y., MacKenzie, S., Pang, S.C., Atar, D., Ropchan, G. & Van Eyk, J.E. Cardiac troponin I is modified in the myocardium of bypass patients. *Circulation* **103**, 58-64 (2001).
139. Canty, J.M. & Lee, T.C. Troponin I proteolysis and myocardial stunning: Now you see it- now you don't. *J Mol Cell Cardiol* **34**, 375-7 (2002).
140. Thomas, S.A., Fallavollita, J.A., Lee, T.C., Feng, J. & Canty, J.M., Jr. Absence of troponin I degradation or altered sarcoplasmic reticulum uptake protein expression after reversible ischemia in swine. *Circ Res* **85**, 446-56 (1999).
141. Luss, H., Meissner, A., Rolf, N., Van Aken, H., Boknik, P., Kirchhefer, U., Knapp, J., Laer, S., Linck, B., Luss, I., Muller, F.U., Neumann, J. & Schmitz, W. Biochemical



- mechanism(s) of stunning in conscious dogs. *Am J Physiol Heart Circ Physiol* **279**, H176-84 (2000).
142. Sherman, A.J., Klocke, F.J., Decker, R.S., Decker, M.L., Kozlowski, K.A., Harris, K.R., Hedjbeli, S., Yaroshenko, Y., Nakamura, S., Parker, M.A., Checchia, P.A. & Evans, D.B. Myofibrillar disruption in hypocontractile myocardium showing perfusion-contraction matches and mismatches. *Am J Physiol Heart Circ Physiol* **278**, H1320-34 (2000).
143. Kim, S.J., Kudej, R.K., Yatani, A., Kim, Y.K., Takagi, G., Honda, R., Colantonio, D.A., Van Eyk, J.E., Vatner, D.E., Rasmusson, R.L. & Vatner, S.F. A novel mechanism for myocardial stunning involving impaired Ca<sup>2+</sup> handling. *Circ Res* **89**, 831-7 (2001).
144. Feng, J., Schaus, B.J., Fallavollita, J.A., Lee, T.C. & Canty, J.M., Jr. Preload induces troponin I degradation independently of myocardial ischemia. *Circulation* **103**, 2035-7 (2001).
145. Inamdar, A.A. & Inamdar, A.C. Heart Failure: Diagnosis, management and utilization. *J Clin Med* **5**(2016).
146. Tomasoni, D., Adamo, M., Lombardi, C.M. & Metra, M. Highlights in heart failure. *ESC Heart Fail* **6**, 1105-1127 (2019).
147. Hajouli, S. & Ludhwani, D. Heart failure and ejection fraction. in *StatPearls* (Treasure Island (FL), 2021).
148. Writing committee members., Yancy, C.W., Jessup, M., Bozkurt, B., Butler, J., Casey, D.E., Jr., Drazner, M.H., Fonarow, G.C., Geraci, S.A., Horwich, T., Januzzi, J.L., Johnson, M.R., Kasper, E.K., Levy, W.C., Masoudi, F.A., McBride, P.E., McMurray, J.J., Mitchell, J.E., Peterson, P.N., Riegel, B., Sam, F., Stevenson, L.W., Tang, W.H., Tsai, E.J., Wilkoff, B.L. & American College of Cardiology Foundation/American Heart Association Task

- Force on Practice, G. 2013 ACCF/AHA guideline for the management of heart failure: a report of the American College of Cardiology Foundation/American Heart Association Task Force on practice guidelines. *Circulation* **128**, e240-327 (2013).
149. Heran, B.S., Musini, V.M., Bassett, K., Taylor, R.S. & Wright, J.M. Angiotensin receptor blockers for heart failure. *Cochrane Database Syst Rev*, CD003040 (2012).
150. Group, C.T.S. Effects of enalapril on mortality in severe congestive heart failure. Results of the Cooperative North Scandinavian Enalapril Survival Study (CONSENSUS). *N Engl J Med* **316**, 1429-35 (1987).
151. Investigators, S., Yusuf, S., Pitt, B., Davis, C.E., Hood, W.B. & Cohn, J.N. Effect of enalapril on survival in patients with reduced left ventricular ejection fractions and congestive heart failure. *N Engl J Med* **325**, 293-302 (1991).
152. Garg, R. & Yusuf, S. Overview of randomized trials of angiotensin-converting enzyme inhibitors on mortality and morbidity in patients with heart failure. Collaborative Group on ACE Inhibitor Trials. *JAMA* **273**, 1450-6 (1995).
153. Granger, C.B., McMurray, J.J., Yusuf, S., Held, P., Michelson, E.L., Olofsson, B., Ostergren, J., Pfeffer, M.A., Swedberg, K., Investigators, C. & Committees. Effects of candesartan in patients with chronic heart failure and reduced left-ventricular systolic function intolerant to angiotensin-converting-enzyme inhibitors: the CHARM-Alternative trial. *Lancet* **362**, 772-6 (2003).
154. Waagstein, F., Hjalmarson, A., Varnauskas, E. & Wallentin, I. Effect of chronic beta-adrenergic receptor blockade in congestive cardiomyopathy. *Br Heart J* **37**, 1022-36 (1975).

155. The Cardiac Insufficiency Bisoprolol Study II (CIBIS-II): a randomised trial. *Lancet* **353**, 9-13 (1999).
156. Packer, M., Gheorghiade, M., Young, J.B., Costantini, P.J., Adams, K.F., Cody, R.J., Smith, L.K., Van Voorhees, L., Gourley, L.A. & Jolly, M.K. Withdrawal of digoxin from patients with chronic heart failure treated with angiotensin-converting-enzyme inhibitors. RADIANCE Study. *N Engl J Med* **329**, 1-7 (1993).
157. Digitalis Investigation, G. The effect of digoxin on mortality and morbidity in patients with heart failure. *N Engl J Med* **336**, 525-33 (1997).
158. Amin, A. & Maleki, M. Positive inotropes in heart failure: a review article. *Heart Asia* **4**, 16-22 (2012).
159. Hwang, P.M. & Sykes, B.D. Targeting the sarcomere to correct muscle function. *Nat Rev Drug Discov* **14**, 313-28 (2015).
160. Sonnenblick, E.H., Frishman, W.H. & LeJemtel, T.H. Dobutamine: a new synthetic cardioactive sympathetic amine. *N Engl J Med* **300**, 17-22 (1979).
161. Movsesian, M., Wever-Pinzon, O. & Vandeput, F. PDE3 inhibition in dilated cardiomyopathy. *Curr Opin Pharmacol* **11**, 707-13 (2011).
162. Nony, P., Boissel, J.P., Lievre, M., Leizorovicz, A., Haugh, M.C., Fareh, S. & de Breyne, B. Evaluation of the effect of phosphodiesterase inhibitors on mortality in chronic heart failure patients. A meta-analysis. *Eur J Clin Pharmacol* **46**, 191-6 (1994).
163. Tacon, C.L., McCaffrey, J. & Delaney, A. Dobutamine for patients with severe heart failure: a systematic review and meta-analysis of randomised controlled trials. *Intensive Care Med* **38**, 359-67 (2012).

164. Kono, T., Sabbah, H.N., Rosman, H., Shimoyama, H., Alam, M. & Goldstein, S. Divergent effects of intravenous dobutamine and nitroprusside on left atrial contribution to ventricular filling in dogs with chronic heart failure. *Am Heart J* **127**, 874-80 (1994).
165. Chou, C.C., Zhou, S., Hayashi, H., Nihei, M., Liu, Y.B., Wen, M.S., Yeh, S.J., Fishbein, M.C., Weiss, J.N., Lin, S.F., Wu, D. & Chen, P.S. Remodelling of action potential and intracellular calcium cycling dynamics during subacute myocardial infarction promotes ventricular arrhythmias in Langendorff-perfused rabbit hearts. *J Physiol* **580**, 895-906 (2007).
166. Ruegg, J.C. Effects of new inotropic agents on  $\text{Ca}^{2+}$  sensitivity of contractile proteins. *Circulation* **73**, III78-84 (1986).
167. Solaro, R.J. & Ruegg, J.C. Stimulation of  $\text{Ca}^{2+}$  binding and ATPase activity of dog cardiac myofibrils by AR-L 115BS, a novel cardiotonic agent. *Circ Res* **51**, 290-4 (1982).
168. Ruegg, J.C., Pfitzer, G., Eubler, D. & Zeugner, C. Effect on contractility of skinned fibres from mammalian heart and smooth muscle by a new benzimidazole derivative, 4,5-dihydro-6-[2-(4-methoxyphenyl)-1H-benzimidazol-5-yl]-5-methyl-3(2H)-pyridazinone. *Arzneimittelforschung* **34**, 1736-8 (1984).
169. Solaro, R.J., Fujino, K. & Sperelakis, N. The positive inotropic effect of pimobendan involves stereospecific increases in the calcium sensitivity of cardiac myofilaments. *J Cardiovasc Pharmacol* **14 Suppl 2**, S7-12 (1989).
170. Pollesello, P., Papp, Z. & Papp, J.G. Calcium sensitizers: What have we learned over the last 25 years? *Int J Cardiol* **203**, 543-8 (2016).

171. Sorsa, T., Pollesello, P. & Solaro, R.J. The contractile apparatus as a target for drugs against heart failure: interaction of levosimendan, a calcium sensitiser, with cardiac troponin C. *Mol Cell Biochem* **266**, 87-107 (2004).
172. Pollesello, P., Ovaska, M., Kaivola, J., Tilgmann, C., Lundstrom, K., Kalkkinen, N., Ulmanen, I., Nissinen, E. & Taskinen, J. Binding of a new Ca<sup>2+</sup> sensitizer, levosimendan, to recombinant human cardiac troponin C. A molecular modelling, fluorescence probe, and proton nuclear magnetic resonance study. *J Biol Chem* **269**, 28584-90 (1994).
173. Mebazaa, A., Nieminen, M.S., Packer, M., Cohen-Solal, A., Kleber, F.X., Pocock, S.J., Thakkar, R., Padley, R.J., Poder, P., Kivikko, M. & Investigators, S. Levosimendan vs dobutamine for patients with acute decompensated heart failure: the SURVIVE Randomized Trial. *JAMA* **297**, 1883-91 (2007).
174. Packer, M., Colucci, W., Fisher, L., Massie, B.M., Teerlink, J.R., Young, J., Padley, R.J., Thakkar, R., Delgado-Herrera, L., Salon, J., Garratt, C., Huang, B., Sarapohja, T. & Group, R.H.F.S. Effect of levosimendan on the short-term clinical course of patients with acutely decompensated heart failure. *JACC Heart Fail* **1**, 103-11 (2013).
175. Papp, Z., Edes, I., Fruhwald, S., De Hert, S.G., Salmenpera, M., Leppikangas, H., Mebazaa, A., Landoni, G., Grossini, E., Caimmi, P., Morelli, A., Guarracino, F., Schwinger, R.H., Meyer, S., Algotsson, L., Wikstrom, B.G., Jorgensen, K., Filippatos, G., Parissis, J.T., Gonzalez, M.J., Parkhomenko, A., Yilmaz, M.B., Kivikko, M., Pollesello, P. & Follath, F. Levosimendan: molecular mechanisms and clinical implications: consensus of experts on the mechanisms of action of levosimendan. *Int J Cardiol* **159**, 82-7 (2012).
176. Sorsa, T., Heikkinen, S., Abbott, M.B., Abusamhadneh, E., Laakso, T., Tilgmann, C., Serimaa, R., Annala, A., Rosevear, P.R., Drakenberg, T., Pollesello, P. & Kilpelainen, I.

- Binding of levosimendan, a calcium sensitizer, to cardiac troponin C. *J Biol Chem* **276**, 9337-43 (2001).
177. Morgan, B.P., Muci, A., Lu, P.P., Qian, X., Tochimoto, T., Smith, W.W., Garard, M., Kraynack, E., Collibee, S., Suehiro, I., Tomasi, A., Valdez, S.C., Wang, W., Jiang, H., Hartman, J., Rodriguez, H.M., Kawas, R., Sylvester, S., Elias, K.A., Godinez, G., Lee, K., Anderson, R., Sueoka, S., Xu, D., Wang, Z., Djordjevic, N., Malik, F.I. & Morgans, D.J., Jr. Discovery of omecamtiv mecarbil the first, selective, small molecule activator of cardiac Myosin. *ACS Med Chem Lett* **1**, 472-7 (2010).
178. Malik, F.I., Hartman, J.J., Elias, K.A., Morgan, B.P., Rodriguez, H., Brejc, K., Anderson, R.L., Sueoka, S.H., Lee, K.H., Finer, J.T., Sakowicz, R., Baliga, R., Cox, D.R., Garard, M., Godinez, G., Kawas, R., Kraynack, E., Lenzi, D., Lu, P.P., Muci, A., Niu, C., Qian, X., Pierce, D.W., Pokrovskii, M., Suehiro, I., Sylvester, S., Tochimoto, T., Valdez, C., Wang, W., Katori, T., Kass, D.A., Shen, Y.T., Vatner, S.F. & Morgans, D.J. Cardiac myosin activation: a potential therapeutic approach for systolic heart failure. *Science* **331**, 1439-43 (2011).
179. Teerlink, J.R., Clarke, C.P., Saikali, K.G., Lee, J.H., Chen, M.M., Escandon, R.D., Elliott, L., Bee, R., Habibzadeh, M.R., Goldman, J.H., Schiller, N.B., Malik, F.I. & Wolff, A.A. Dose-dependent augmentation of cardiac systolic function with the selective cardiac myosin activator, omecamtiv mecarbil: a first-in-man study. *Lancet* **378**, 667-75 (2011).
180. Teerlink, J.R., Diaz, R., Felker, G.M., McMurray, J.J.V., Metra, M., Solomon, S.D., Adams, K.F., Anand, I., Arias-Mendoza, A., Biering-Sorensen, T., Bohm, M., Bonderman, D., Cleland, J.G.F., Corbalan, R., Crespo-Leiro, M.G., Dahlstrom, U., Echeverria, L.E., Fang, J.C., Filippatos, G., Fonseca, C., Goncalvesova, E., Goudev, A.R., Howlett, J.G.,

- Lanfear, D.E., Li, J., Lund, M., Macdonald, P., Mareev, V., Momomura, S.I., O'Meara, E., Parkhomenko, A., Ponikowski, P., Ramires, F.J.A., Serpytis, P., Sliwa, K., Spinar, J., Suter, T.M., Tomcsanyi, J., Vandekerckhove, H., Vinereanu, D., Voors, A.A., Yilmaz, M.B., Zannad, F., Sharpsten, L., Legg, J.C., Varin, C., Honarpour, N., Abbasi, S.A., Malik, F.I., Kurtz, C.E. & Investigators, G.-H. Cardiac myosin activation with omecantiv mecarbil in systolic heart failure. *N Engl J Med* **384**, 105-116 (2021).
181. Collibee, S.E., Bergnes, G., Muci, A., Browne, W.F.t., Garard, M., Hinken, A.C., Russell, A.J., Suehiro, I., Hartman, J., Kawas, R., Lu, P.P., Lee, K.H., Marquez, D., Tomlinson, M., Xu, D., Kennedy, A., Hwee, D., Schaletzky, J., Leung, K., Malik, F.I., Morgans, D.J., Jr. & Morgan, B.P. Discovery of tirasemtiv, the first direct fast skeletal muscle troponin activator. *ACS Med Chem Lett* **9**, 354-358 (2018).
182. Shefner, J.M., Cudkowicz, M.E., Hardiman, O., Cockcroft, B.M., Lee, J.H., Malik, F.I., Meng, L., Rudnicki, S.A., Wolff, A.A., Andrews, J.A. & Group, V.-A.S. A phase III trial of tirasemtiv as a potential treatment for amyotrophic lateral sclerosis. *Amyotroph Lateral Scler Frontotemporal Degener* **0**, 1-11 (2019).
183. Li, M.X., Mercier, P., Hartman, J.J. & Sykes, B.D. Structural basis of tirasemtiv activation of fast skeletal Muscle. *J Med Chem* **64**, 3026-3034 (2021).
184. Solaro, R.J., Bousquet, P. & Johnson, J.D. Stimulation of cardiac myofilament force, ATPase activity and troponin C  $Ca^{2+}$  binding by bepridil. *J Pharmacol Exp Ther* **238**, 502-7 (1986).
185. Li, Y., Love, M.L., Putkey, J.A. & Cohen, C. Bepridil opens the regulatory N-terminal lobe of cardiac troponin C. *Proc Natl Acad Sci U S A* **97**, 5140-5 (2000).

186. Wang, X., Li, M.X. & Sykes, B.D. Structure of the regulatory N-domain of human cardiac troponin C in complex with human cardiac troponin I147-163 and bepridil. *J Biol Chem* **277**, 31124-33 (2002).
187. Cai, F., Li, M.X., Pineda-Sanabria, S.E., Gelozia, S., Lindert, S., West, F., Sykes, B.D. & Hwang, P.M. Structures reveal details of small molecule binding to cardiac troponin. *J Mol Cell Cardiol* **101**, 134-144 (2016).
188. Thomas, J.M. Centenary: The birth of X-ray crystallography. *Nature* **491**, 186-7 (2012).
189. Smyth, M.S. & Martin, J.H. X ray crystallography. *Mol Pathol* **53**, 8-14 (2000).
190. Kachala, M., Valentini, E. & Svergun, D.I. Application of SAXS for the structural characterization of IDPs. *Adv Exp Med Biol* **870**, 261-89 (2015).
191. Ota, M., Koike, R., Amemiya, T., Tenno, T., Romero, P.R., Hiroaki, H., Dunker, A.K. & Fukuchi, S. An assignment of intrinsically disordered regions of proteins based on NMR structures. *J Struct Biol* **181**, 29-36 (2013).
192. Houdusse, A., Love, M.L., Dominguez, R., Grabarek, Z. & Cohen, C. Structures of four Ca<sup>2+</sup>-bound troponin C at 2.0 Å resolution: further insights into the Ca<sup>2+</sup>-switch in the calmodulin superfamily. *Structure* **5**, 1695-711 (1997).
193. Vogel, H.J. & Zhang, M. Protein engineering and NMR studies of calmodulin. *Mol Cell Biochem* **149-150**, 3-15 (1995).
194. Barbato, G., Ikura, M., Kay, L.E., Pastor, R.W. & Bax, A. Backbone dynamics of calmodulin studied by <sup>15</sup>N relaxation using inverse detected two-dimensional NMR spectroscopy: the central helix is flexible. *Biochemistry* **31**, 5269-78 (1992).



195. Ikura, M., Spera, S., Barbato, G., Kay, L.E., Krinks, M. & Bax, A. Secondary structure and side-chain  $^1\text{H}$  and  $^{13}\text{C}$  resonance assignments of calmodulin in solution by heteronuclear multidimensional NMR spectroscopy. *Biochemistry* **30**, 9216-28 (1991).
196. Babu, Y.S., Bugg, C.E. & Cook, W.J. Structure of calmodulin refined at 2.2 Å resolution. *J Mol Biol* **204**, 191-204 (1988).
197. Spyropoulos, L., Li, M.X., Sia, S.K., Gagne, S.M., Chandra, M., Solaro, R.J. & Sykes, B.D. Calcium-induced structural transition in the regulatory domain of human cardiac troponin C. *Biochemistry* **36**, 12138-46 (1997).
198. Service, R.F. Flexing muscle with just one amino acid. *Science* **271**, 31 (1996).
199. Hoffman, R.M. & Sykes, B.D. Structure of the inhibitor W7 bound to the regulatory domain of cardiac troponin C. *Biochemistry* **48**, 5541-52 (2009).
200. Ebashi, S. & Ebashi, F. A new protein factor promoting contraction of actomyosin. *Nature* **203**, 645-6 (1964).
201. Ebashi, S., Ebashi, F. & Kodama, A. Troponin as the  $\text{Ca}^{2+}$ -receptive protein in the contractile system. *J Biochem* **62**, 137-8 (1967).
202. Biesiadecki, B.J., Tachampa, K., Yuan, C., Jin, J.P., de Tombe, P.P. & Solaro, R.J. Removal of the cardiac troponin I N-terminal extension improves cardiac function in aged mice. *J Biol Chem* **285**, 19688-98 (2010).
203. Wattanapermpool, J., Guo, X. & Solaro, R.J. The unique amino-terminal peptide of cardiac troponin I regulates myofibrillar activity only when it is phosphorylated. *J Mol Cell Cardiol* **27**, 1383-91 (1995).
204. Li, M.X., Spyropoulos, L. & Sykes, B.D. Binding of cardiac troponin-I147-163 induces a structural opening in human cardiac troponin-C. *Biochemistry* **38**, 8289-98 (1999).

205. Suskiewicz, M.J., Sussman, J.L., Silman, I. & Shaul, Y. Context-dependent resistance to proteolysis of intrinsically disordered proteins. *Protein Sci* **20**, 1285-97 (2011).
206. Liu, Z. & Huang, Y. Advantages of proteins being disordered. *Protein Sci* **23**, 539-50 (2014).
207. Katrukha, I.A., Kogan, A.E., Vylegzhanina, A.V., Kharitonov, A.V., Tamm, N.N., Filatov, V.L., Bereznikova, A.V., Koshkina, E.V. & Katrukha, A.G. Full-size cardiac troponin I and its proteolytic fragments in blood of patients with acute myocardial infarction: antibody selection for assay development. *Clin Chem* **64**, 1104-1112 (2018).
208. Solaro, R.J. Troponin I, stunning, hypertrophy, and failure of the heart. *Circ Res* **84**, 122-4 (1999).
209. Bolli, R. & Marban, E. Molecular and cellular mechanisms of myocardial stunning. *Physiol Rev* **79**, 609-34 (1999).
210. Miyamae, M., Camacho, S.A., Weiner, M.W. & Figueredo, V.M. Attenuation of postischemic reperfusion injury is related to prevention of  $[Ca^{2+}]_m$  overload in rat hearts. *Am J Physiol* **271**, H2145-53 (1996).
211. Marban, E., Kitakaze, M., Kusuoka, H., Porterfield, J.K., Yue, D.T. & Chacko, V.P. Intracellular free calcium concentration measured with  $^{19}F$  NMR spectroscopy in intact ferret hearts. *Proc Natl Acad Sci U S A* **84**, 6005-9 (1987).
212. Hughes, B.G. & Schulz, R. Targeting MMP-2 to treat ischemic heart injury. *Basic Res Cardiol* **109**, 424 (2014).
213. Bolli, R., Patel, B.S., Jeroudi, M.O., Lai, E.K. & McCay, P.B. Demonstration of free radical generation in "stunned" myocardium of intact dogs with the use of the spin trap alpha-phenyl N-tert-butyl nitron. *J Clin Invest* **82**, 476-85 (1988).

214. Vander Heide, R.S. & Steenbergen, C. Cardioprotection and myocardial reperfusion: pitfalls to clinical application. *Circ Res* **113**, 464-77 (2013).
215. Franco, S.J. & Huttenlocher, A. Regulating cell migration: calpains make the cut. *J Cell Sci* **118**, 3829-38 (2005).
216. Lebart, M.C. & Benyamin, Y. Calpain involvement in the remodeling of cytoskeletal anchorage complexes. *FEBS J* **273**, 3415-26 (2006).
217. Siegmund, B., Ladilov, Y.V. & Piper, H.M. Importance of sodium for recovery of calcium control in reoxygenated cardiomyocytes. *Am J Physiol* **267**, H506-13 (1994).
218. Neri, M., Riezzo, I., Pascale, N., Pomara, C. & Turillazzi, E. Ischemia/reperfusion injury following acute myocardial infarction: a critical issue for clinicians and forensic pathologists. *Mediators Inflamm* **2017**, 7018393 (2017).
219. McCartney, C.E., MacLeod, J.A., Greer, P.A. & Davies, P.L. An easy-to-use FRET protein substrate to detect calpain cleavage in vitro and in vivo. *Biochim Biophys Acta* **1865**, 221-230 (2018).
220. Kelly, J.C., Cuerrier, D., Graham, L.A., Campbell, R.L. & Davies, P.L. Profiling of calpain activity with a series of FRET-based substrates. *Biochim Biophys Acta* **1794**, 1505-9 (2009).
221. Yoshida, K., Inui, M., Harada, K., Saido, T.C., Sorimachi, Y., Ishihara, T., Kawashima, S. & Sobue, K. Reperfusion of rat heart after brief ischemia induces proteolysis of caldesmon (nonerythroid spectrin or fodrin) by calpain. *Circ Res* **77**, 603-10 (1995).
222. Chen, M., Won, D.J., Krajewski, S. & Gottlieb, R.A. Calpain and mitochondria in ischemia/reperfusion injury. *J Biol Chem* **277**, 29181-6 (2002).

223. Katrukha, A.G., Bereznikova, A.V., Filatov, V.L., Esakova, T.V., Kolosova, O.V., Pettersson, K., Lovgren, T., Bulargina, T.V., Trifonov, I.R., Gratsiansky, N.A., Pulkki, K., Voipio-Pulkki, L.M. & Gusev, N.B. Degradation of cardiac troponin I: implication for reliable immunodetection. *Clin Chem* **44**, 2433-40 (1998).
224. Polzar, B., Nowak, E., Goody, R.S. & Mannherz, H.G. The complex of actin and deoxyribonuclease I as a model system to study the interactions of nucleotides, cations and cytochalasin D with monomeric actin. *Eur J Biochem* **182**, 267-75 (1989).
225. Hwang, P.M., Pan, J.S. & Sykes, B.D. A PagP fusion protein system for the expression of intrinsically disordered proteins in Escherichia coli. *Protein Expr Purif* **85**, 148-51 (2012).
226. Zahran, S., Pan, J.S., Liu, P.B. & Hwang, P.M. Combining a PagP fusion protein system with nickel ion-catalyzed cleavage to produce intrinsically disordered proteins in E. coli. *Protein Expr Purif* **116**, 133-8 (2015).
227. Delaglio, F., Grzesiek, S., Vuister, G.W., Zhu, G., Pfeifer, J. & Bax, A. NMRPipe: a multidimensional spectral processing system based on UNIX pipes. *J Biomol NMR* **6**, 277-93 (1995).
228. Johnson, B.A. Using NMRView to visualize and analyze the NMR spectra of macromolecules. *Methods Mol Biol* **278**, 313-52 (2004).
229. De Simone, A., Cavalli, A., Hsu, S.T., Vranken, W. & Vendruscolo, M. Accurate random coil chemical shifts from an analysis of loop regions in native states of proteins. *J Am Chem Soc* **131**, 16332-3 (2009).
230. Camilloni, C., De Simone, A., Vranken, W.F. & Vendruscolo, M. Determination of secondary structure populations in disordered states of proteins using nuclear magnetic resonance chemical shifts. *Biochemistry* **51**, 2224-31 (2012).

231. Kabsch, W., Mannherz, H.G., Suck, D., Pai, E.F. & Holmes, K.C. Atomic structure of the actin:DNase I complex. *Nature* **347**, 37-44 (1990).
232. Baghirova, S., Hughes, B.G., Poirier, M., Kondo, M.Y. & Schulz, R. Nuclear matrix metalloproteinase-2 in the cardiomyocyte and the ischemic-reperfused heart. *J Mol Cell Cardiol* **94**, 153-61 (2016).
233. Elce, J.S., Hegadorn, C., Gauthier, S., Vince, J.W. & Davies, P.L. Recombinant calpain II: improved expression systems and production of a C105A active-site mutant for crystallography. *Protein Eng* **8**, 843-8 (1995).
234. Sheterline, P., Clayton, J. & Sparrow, J. Actin. *Protein Profile* **2**, 1-103 (1995).
235. Gasteiger, E., Gattiker, A., Hoogland, C., Ivanyi, I., Appel, R.D. & Bairoch, A. ExPASy: The proteomics server for in-depth protein knowledge and analysis. *Nucleic Acids Res* **31**, 3784-8 (2003).
236. Tripet, B., Van Eyk, J.E. & Hodges, R.S. Mapping of a second actin-tropomyosin and a second troponin C binding site within the C terminus of troponin I, and their importance in the Ca<sup>2+</sup>-dependent regulation of muscle contraction. *J Mol Biol* **271**, 728-50 (1997).
237. Ramos, C.H. Mapping subdomains in the C-terminal region of troponin I involved in its binding to troponin C and to thin filament. *J Biol Chem* **274**, 18189-95 (1999).
238. Blumenschein, T.M., Stone, D.B., Fletterick, R.J., Mendelson, R.A. & Sykes, B.D. Dynamics of the C-terminal region of TnI in the troponin complex in solution. *Biophys J* **90**, 2436-44 (2006).
239. Murakami, K., Yumoto, F., Ohki, S.Y., Yasunaga, T., Tanokura, M. & Wakabayashi, T. Structural basis for Ca<sup>2+</sup>-regulated muscle relaxation at interaction sites of troponin with actin and tropomyosin. *J Mol Biol* **352**, 178-201 (2005).

240. Van Eyk, J.E., Thomas, L.T., Tripet, B., Wiesner, R.J., Pearlstone, J.R., Farah, C.S., Reinach, F.C. & Hodges, R.S. Distinct regions of troponin I regulate  $\text{Ca}^{2+}$ -dependent activation and  $\text{Ca}^{2+}$  sensitivity of the acto-S1-TM ATPase activity of the thin filament. *J Biol Chem* **272**, 10529-37 (1997).
241. Mogensen, J., Hey, T. & Lambrecht, S. A systematic review of phenotypic features associated with cardiac troponin I mutations in hereditary cardiomyopathies. *Can J Cardiol* **31**, 1377-85 (2015).
242. Kumar, S., Ratnikov, B.I., Kazanov, M.D., Smith, J.W. & Cieplak, P. CleavPredict: a platform for reasoning about matrix metalloproteinases proteolytic events. *PLoS One* **10**, e0127877 (2015).
243. Eckhard, U., Huesgen, P.F., Schilling, O., Bellac, C.L., Butler, G.S., Cox, J.H., Dufour, A., Goebeler, V., Kappelhoff, R., Auf dem Keller, U., Klein, T., Lange, P.F., Marino, G., Morrison, C.J., Prudova, A., Rodriguez, D., Starr, A.E., Wang, Y. & Overall, C.M. Active site specificity profiling datasets of matrix metalloproteinases (MMPs) 1, 2, 3, 7, 8, 9, 12, 13 and 14. *Data Brief* **7**, 299-310 (2016).
244. Eckhard, U., Huesgen, P.F., Schilling, O., Bellac, C.L., Butler, G.S., Cox, J.H., Dufour, A., Goebeler, V., Kappelhoff, R., Keller, U.A., Klein, T., Lange, P.F., Marino, G., Morrison, C.J., Prudova, A., Rodriguez, D., Starr, A.E., Wang, Y. & Overall, C.M. Active site specificity profiling of the matrix metalloproteinase family: Proteomic identification of 4300 cleavage sites by nine MMPs explored with structural and synthetic peptide cleavage analyses. *Matrix Biol* **49**, 37-60 (2016).
245. Turk, B.E., Huang, L.L., Piro, E.T. & Cantley, L.C. Determination of protease cleavage site motifs using mixture-based oriented peptide libraries. *Nat Biotechnol* **19**, 661-7 (2001).

246. Eckhard, U., Huesgen, P.F., Schilling, O., Bellac, C.L., Butler, G.S., Cox, J.H., Dufour, A., Goebeler, V., Kappelhoff, R., Keller, U.A.D., Klein, T., Lange, P.F., Marino, G., Morrison, C.J., Prudova, A., Rodriguez, D., Starr, A.E., Wang, Y. & Overall, C.M. Active site specificity profiling of the matrix metalloproteinase family: Proteomic identification of 4300 cleavage sites by nine MMPs explored with structural and synthetic peptide cleavage analyses. *Matrix Biol* **49**, 37-60 (2016).
247. Cuerrier, D., Moldoveanu, T. & Davies, P.L. Determination of peptide substrate specificity for mu-calpain by a peptide library-based approach: the importance of primed side interactions. *J Biol Chem* **280**, 40632-41 (2005).
248. Ward, D.G., Cornes, M.P. & Trayer, I.P. Structural consequences of cardiac troponin I phosphorylation. *J Biol Chem* **277**, 41795-801 (2002).
249. Li, Y., Zhu, G., Paolocci, N., Zhang, P., Takahashi, C., Okumus, N., Heravi, A., Keceli, G., Ramirez-Correa, G., Kass, D.A. & Murphy, A.M. Heart failure-related hyperphosphorylation in the cardiac troponin I C terminus has divergent effects on cardiac function in vivo. *Circ Heart Fail* **10**(2017).
250. Colantonio, D.A., Van Eyk, J.E. & Przyklenk, K. Stunned peri-infarct canine myocardium is characterized by degradation of troponin T, not troponin I. *Cardiovasc Res* **63**, 217-25 (2004).
251. Schwartz, S.M., Duffy, J.Y., Pearl, J., Goins, S., Wagner, C.J. & Nelson, D.P. Glucocorticoids preserve calpastatin and troponin I during cardiopulmonary bypass in immature pigs. *Pediatr Res* **54**, 91-7 (2003).

252. Communal, C., Sumandea, M., de Tombe, P., Narula, J., Solaro, R.J. & Hajjar, R.J. Functional consequences of caspase activation in cardiac myocytes. *Proc Natl Acad Sci U S A* **99**, 6252-6 (2002).
253. Eberli, F.R. Stunned myocardium- an unfinished puzzle. *Cardiovasc Res* **63**, 189-91 (2004).
254. Bolli, R., Zhu, W.X., Thornby, J.I., O'Neill, P.G. & Roberts, R. Time course and determinants of recovery of function after reversible ischemia in conscious dogs. *Am J Physiol* **254**, H102-14 (1988).
255. Heusch, G. & Schulz, R. Characterization of hibernating and stunned myocardium. *Eur Heart J* **18 Suppl D**, D102-10 (1997).
256. Ehring, T., Schulz, R. & Heusch, G. Characterization of "hibernating" and "stunned" myocardium with focus on the use of calcium antagonists in "stunned" myocardium. *J Cardiovasc Pharmacol* **20 Suppl 5**, S25-33 (1992).
257. Gao, W.D., Atar, D., Backx, P.H. & Marban, E. Relationship between intracellular calcium and contractile force in stunned myocardium. Direct evidence for decreased myofilament  $Ca^{2+}$  responsiveness and altered diastolic function in intact ventricular muscle. *Circ Res* **76**, 1036-48 (1995).
258. Gao, W.D., Liu, Y., Mellgren, R. & Marban, E. Intrinsic myofilament alterations underlying the decreased contractility of stunned myocardium. A consequence of  $Ca^{2+}$ -dependent proteolysis? *Circ Res* **78**, 455-65 (1996).
259. McDonald, K.S., Moss, R.L. & Miller, W.P. Incorporation of the troponin regulatory complex of post-ischemic stunned porcine myocardium reduces myofilament calcium sensitivity in rabbit psoas skeletal muscle fibers. *J Mol Cell Cardiol* **30**, 285-96 (1998).



260. Foster, D.B., Noguchi, T., VanBuren, P., Murphy, A.M. & Van Eyk, J.E. C-terminal truncation of cardiac troponin I causes divergent effects on ATPase and force: implications for the pathophysiology of myocardial stunning. *Circ Res* **93**, 917-24 (2003).
261. Davis, J.P., Norman, C., Kobayashi, T., Solaro, R.J., Swartz, D.R. & Tikunova, S.B. Effects of thin and thick filament proteins on calcium binding and exchange with cardiac troponin C. *Biophys J* **92**, 3195-206 (2007).
262. Shah, S., Yogasundaram, H., Basu, R., Wang, F., Paterson, D.I., Alastalo, T.P. & Oudit, G.Y. Novel dominant-negative mutation in cardiac troponin I causes severe restrictive cardiomyopathy. *Circ Heart Fail* **10**(2017).
263. Hamdani, N., Paulus, W.J., van Heerebeek, L., Borbely, A., Boontje, N.M., Zuidwijk, M.J., Bronzwaer, J.G., Simonides, W.S., Niessen, H.W., Stienen, G.J. & van der Velden, J. Distinct myocardial effects of beta-blocker therapy in heart failure with normal and reduced left ventricular ejection fraction. *Eur Heart J* **30**, 1863-72 (2009).
264. Sequeira, V., Wijnker, P.J., Nijenkamp, L.L., Kuster, D.W., Najafi, A., Witjas-Paalberends, E.R., Regan, J.A., Boontje, N., Ten Cate, F.J., Germans, T., Carrier, L., Sadayappan, S., van Slegtenhorst, M.A., Zaremba, R., Foster, D.B., Murphy, A.M., Poggesi, C., Dos Remedios, C., Stienen, G.J., Ho, C.Y., Michels, M. & van der Velden, J. Perturbed length-dependent activation in human hypertrophic cardiomyopathy with missense sarcomeric gene mutations. *Circ Res* **112**, 1491-505 (2013).
265. Di Lisa, F., De Tullio, R., Salamino, F., Barbato, R., Melloni, E., Siliprandi, N., Schiaffino, S. & Pontremoli, S. Specific degradation of troponin T and I by mu-calpain and its modulation by substrate phosphorylation. *Biochem J* **308 ( Pt 1)**, 57-61 (1995).

266. Thygesen, K., Alpert, J.S., Jaffe, A.S., Simoons, M.L., Chaitman, B.R., White, H.D., Joint, E.S.C.A.A.H.A.W.H.F.T.F.f.U.D.o.M.I., Authors/Task Force Members, C., Thygesen, K., Alpert, J.S., White, H.D., Biomarker, S., Jaffe, A.S., Katus, H.A., Apple, F.S., Lindahl, B., Morrow, D.A., Subcommittee, E.C.G., Chaitman, B.R., Clemmensen, P.M., Johanson, P., Hod, H., Imaging, S., Underwood, R., Bax, J.J., Bonow, J.J., Pinto, F., Gibbons, R.J., Classification, S., Fox, K.A., Atar, D., Newby, L.K., Galvani, M., Hamm, C.W., Intervention, S., Uretsky, B.F., Steg, P.G., Wijns, W., Bassand, J.P., Menasche, P., Ravkilde, J., Trials, Registries, S., Ohman, E.M., Antman, E.M., Wallentin, L.C., Armstrong, P.W., Simoons, M.L., Trials, Registries, S., Januzzi, J.L., Nieminen, M.S., Gheorghiade, M., Filippatos, G., Trials, Registries, S., Luepker, R.V., Fortmann, S.P., Rosamond, W.D., Levy, D., Wood, D., Trials, Registries, S., Smith, S.C., Hu, D., Lopez-Sendon, J.L., Robertson, R.M., Weaver, D., Tendera, M., Bove, A.A., Parkhomenko, A.N., Vasilieva, E.J., Mendis, S., Guidelines, E.S.C.C.f.P., Bax, J.J., Baumgartner, H., Ceconi, C., Dean, V., Deaton, C., Fagard, R., Funck-Brentano, C., Hasdai, D., Hoes, A., Kirchhof, P., Knuuti, J., Kolh, P., McDonagh, T., Moulin, C., Popescu, B.A., Reiner, Z., Sechtem, U., Sirnes, P.A., Tendera, M., Torbicki, A., Vahanian, A., Windecker, S., Document, R., Morais, J., Aguiar, C., Almahmeed, W., Arnar, D.O., Barili, F., Bloch, K.D., Bolger, A.F., Botker, H.E., Bozkurt, B., Bugiardini, R., Cannon, C., de Lemos, J., Eberli, F.R., Escobar, E., Hlatky, M., James, S., Kern, K.B., Moliterno, D.J., Mueller, C., Neskovic, A.N., Pieske, B.M., Schulman, S.P., Storey, R.F., Taubert, K.A., Vranckx, P. & Wagner, D.R. Third universal definition of myocardial infarction. *J Am Coll Cardiol* **60**, 1581-98 (2012).
267. Babuin, L. & Jaffe, A.S. Troponin: the biomarker of choice for the detection of cardiac injury. *CMAJ* **173**, 1191-202 (2005).

268. Zahran, S., Figueiredo, V.P., Graham, M.M., Schulz, R., Hwang, P.M. Proteolytic digestion of serum cardiac troponin I a marker of ischemic severity. *Journal Applied Lab Med, In press* (2018).
269. Lee, C.S., Chien, C.V., Bidwell, J.T., Gelow, J.M., Denfeld, Q.E., Masterson Creber, R., Buck, H.G. & Mudd, J.O. Comorbidity profiles and inpatient outcomes during hospitalization for heart failure: an analysis of the U.S. nationwide inpatient sample. *BMC Cardiovasc Disord* **14**, 73 (2014).
270. McNally, E.M., Golbus, J.R. & Puckelwartz, M.J. Genetic mutations and mechanisms in dilated cardiomyopathy. *J Clin Invest* **123**, 19-26 (2013).
271. Gomes, A.V. & Potter, J.D. Molecular and cellular aspects of troponin cardiomyopathies. *Ann N Y Acad Sci* **1015**, 214-24 (2004).
272. Yang, Z., Yamazaki, M., Shen, Q.W. & Swartz, D.R. Differences between cardiac and skeletal troponin interaction with the thin filament probed by troponin exchange in skeletal myofibrils. *Biophys J* **97**, 183-94 (2009).
273. Ferrieres, G., Pugniere, M., Mani, J.C., Villard, S., Laprade, M., Doutre, P., Pau, B. & Granier, C. Systematic mapping of regions of human cardiac troponin I involved in binding to cardiac troponin C: N- and C-terminal low affinity contributing regions. *FEBS Lett* **479**, 99-105 (2000).
274. Hwang, P.M., Pan, J.S. & Sykes, B.D. Targeted expression, purification, and cleavage of fusion proteins from inclusion bodies in Escherichia coli. *FEBS Lett* **588**, 247-52 (2014).
275. Raran-Kurussi, S., Cherry, S., Zhang, D. & Waugh, D.S. Removal of Affinity Tags with TEV Protease. *Methods Mol Biol* **1586**, 221-230 (2017).

276. Lakomek, N.A., Ying, J. & Bax, A. Measurement of  $^{15}\text{N}$  relaxation rates in perdeuterated proteins by TROSY-based methods. *J Biomol NMR* **53**, 209-21 (2012).
277. Liu, Q., Shi, C., Yu, L., Zhang, L., Xiong, Y. & Tian, C. General order parameter based correlation analysis of protein backbone motions between experimental NMR relaxation measurements and molecular dynamics simulations. *Biochem Biophys Res Commun* **457**, 467-72 (2015).
278. Volkman, B.F., Lipson, D., Wemmer, D.E. & Kern, D. Two-state allosteric behavior in a single-domain signaling protein. *Science* **291**, 2429-33 (2001).
279. Gagne, S.M., Tsuda, S., Spyropoulos, L., Kay, L.E. & Sykes, B.D. Backbone and methyl dynamics of the regulatory domain of troponin C: anisotropic rotational diffusion and contribution of conformational entropy to calcium affinity. *J Mol Biol* **278**, 667-86 (1998).
280. van der Velden, J. Diastolic myofilament dysfunction in the failing human heart. *Pflugers Arch* **462**, 155-63 (2011).
281. Zhang, J., Guy, M.J., Norman, H.S., Chen, Y.C., Xu, Q., Dong, X., Guner, H., Wang, S., Kohmoto, T., Young, K.H., Moss, R.L. & Ge, Y. Top-down quantitative proteomics identified phosphorylation of cardiac troponin I as a candidate biomarker for chronic heart failure. *J Proteome Res* **10**, 4054-65 (2011).
282. Biesiadecki, B.J. & Westfall, M.V. Troponin I modulation of cardiac performance: Plasticity in the survival switch. *Arch Biochem Biophys* **664**, 9-14 (2019).
283. Salhi, H.E., Walton, S.D., Hassel, N.C., Brundage, E.A., de Tombe, P.P., Janssen, P.M., Davis, J.P. & Biesiadecki, B.J. Cardiac troponin I tyrosine 26 phosphorylation decreases myofilament  $\text{Ca}^{2+}$  sensitivity and accelerates deactivation. *J Mol Cell Cardiol* **76**, 257-64 (2014).

284. Marston, S.B. & Redwood, C.S. Modulation of thin filament activation by breakdown or isoform switching of thin filament proteins: physiological and pathological implications. *Circ Res* **93**, 1170-8 (2003).
285. Layland, J., Solaro, R.J. & Shah, A.M. Regulation of cardiac contractile function by troponin I phosphorylation. *Cardiovasc Res* **66**, 12-21 (2005).
286. Solaro, R.J., Henze, M. & Kobayashi, T. Integration of troponin I phosphorylation with cardiac regulatory networks. *Circ Res* **112**, 355-66 (2013).
287. Robertson, S.P., Johnson, J.D., Holroyde, M.J., Kranias, E.G., Potter, J.D. & Solaro, R.J. The effect of troponin I phosphorylation on the  $\text{Ca}^{2+}$ -binding properties of the  $\text{Ca}^{2+}$ -regulatory site of bovine cardiac troponin. *J Biol Chem* **257**, 260-3 (1982).
288. Feng, H.Z., Chen, M., Weinstein, L.S. & Jin, J.P. Removal of the N-terminal extension of cardiac troponin I as a functional compensation for impaired myocardial beta-adrenergic signaling. *J Biol Chem* **283**, 33384-93 (2008).
289. Zhang, R., Zhao, J. & Potter, J.D. Phosphorylation of both serine residues in cardiac troponin I is required to decrease the  $\text{Ca}^{2+}$  affinity of cardiac troponin C. *J Biol Chem* **270**, 30773-80 (1995).
290. McConnell, B.K., Moravec, C.S. & Bond, M. Troponin I phosphorylation and myofilament calcium sensitivity during decompensated cardiac hypertrophy. *Am J Physiol* **274**, H385-96 (1998).
291. Yu, Z.B., Zhang, L.F. & Jin, J.P. A proteolytic NH<sub>2</sub>-terminal truncation of cardiac troponin I that is up-regulated in simulated microgravity. *J Biol Chem* **276**, 15753-60 (2001).

292. Barbato, J.C., Huang, Q.Q., Hossain, M.M., Bond, M. & Jin, J.P. Proteolytic N-terminal truncation of cardiac troponin I enhances ventricular diastolic function. *J Biol Chem* **280**, 6602-9 (2005).
293. Garvey, J.L., Kranias, E.G. & Solaro, R.J. Phosphorylation of C-protein, troponin I and phospholamban in isolated rabbit hearts. *Biochem J* **249**, 709-14 (1988).
294. England, P.J. Studies on the phosphorylation of the inhibitory subunit of troponin during modification of contraction in perfused rat heart. *Biochem J* **160**, 295-304 (1976).
295. Mope, L., McClellan, G.B. & Winegrad, S. Calcium sensitivity of the contractile system and phosphorylation of troponin in hyperpermeable cardiac cells. *J Gen Physiol* **75**, 271-82 (1980).
296. Hofmann, P.A. & Lange, J.H., 3rd. Effects of phosphorylation of troponin I and C protein on isometric tension and velocity of unloaded shortening in skinned single cardiac myocytes from rats. *Circ Res* **74**, 718-26 (1994).
297. Noland, T.A., Jr. & Kuo, J.F. Protein kinase C phosphorylation of cardiac troponin I and troponin T inhibits  $Ca^{2+}$ -stimulated MgATPase activity in reconstituted actomyosin and isolated myofibrils, and decreases actin-myosin interactions. *J Mol Cell Cardiol* **25**, 53-65 (1993).
298. Noland, T.A., Jr., Raynor, R.L., Jideama, N.M., Guo, X., Kazanietz, M.G., Blumberg, P.M., Solaro, R.J. & Kuo, J.F. Differential regulation of cardiac actomyosin S-1 MgATPase by protein kinase C isozyme-specific phosphorylation of specific sites in cardiac troponin I and its phosphorylation site mutants. *Biochemistry* **35**, 14923-31 (1996).
299. Wijnker, P.J., Sequeira, V., Witjas-Paalberends, E.R., Foster, D.B., dos Remedios, C.G., Murphy, A.M., Stienen, G.J. & van der Velden, J. Phosphorylation of protein kinase C sites

- Ser42/44 decreases  $\text{Ca}^{2+}$ -sensitivity and blunts enhanced length-dependent activation in response to protein kinase A in human cardiomyocytes. *Arch Biochem Biophys* **554**, 11-21 (2014).
300. Carballo, S., Robinson, P., Otway, R., Fatkin, D., Jongbloed, J.D., de Jonge, N., Blair, E., van Tintelen, J.P., Redwood, C. & Watkins, H. Identification and functional characterization of cardiac troponin I as a novel disease gene in autosomal dominant dilated cardiomyopathy. *Circ Res* **105**, 375-82 (2009).
301. Lim, C.C., Yang, H., Yang, M., Wang, C.K., Shi, J., Berg, E.A., Pimentel, D.R., Gwathmey, J.K., Hajjar, R.J., Helmes, M., Costello, C.E., Huo, S. & Liao, R. A novel mutant cardiac troponin C disrupts molecular motions critical for calcium binding affinity and cardiomyocyte contractility. *Biophys J* **94**, 3577-89 (2008).
302. Mogensen, J., Murphy, R.T., Shaw, T., Bahl, A., Redwood, C., Watkins, H., Burke, M., Elliott, P.M. & McKenna, W.J. Severe disease expression of cardiac troponin C and T mutations in patients with idiopathic dilated cardiomyopathy. *J Am Coll Cardiol* **44**, 2033-40 (2004).
303. Preston, L.C., Lipscomb, S., Robinson, P., Mogensen, J., McKenna, W.J., Watkins, H., Ashley, C.C. & Redwood, C.S. Functional effects of the DCM mutant Gly159Asp troponin C in skinned muscle fibres. *Pflugers Arch* **453**, 771-6 (2007).
304. Preston, L.C., Ashley, C.C. & Redwood, C.S. DCM troponin C mutant Gly159Asp blunts the response to troponin phosphorylation. *Biochem Biophys Res Commun* **360**, 27-32 (2007).

305. Biesiadecki, B.J., Kobayashi, T., Walker, J.S., Solaro, R.J. & de Tombe, P.P. The troponin C G159D mutation blunts myofilament desensitization induced by troponin I Ser23/24 phosphorylation. *Circ Res* **100**, 1486-93 (2007).
306. Dong, W.J., Xing, J., Ouyang, Y., An, J. & Cheung, H.C. Structural kinetics of cardiac troponin C mutants linked to familial hypertrophic and dilated cardiomyopathy in troponin complexes. *J Biol Chem* **283**, 3424-32 (2008).
307. Johnston, J.R., Landim-Vieira, M., Marques, M.A., de Oliveira, G.A.P., Gonzalez-Martinez, D., Moraes, A.H., He, H., Iqbal, A., Wilnai, Y., Birk, E., Zucker, N., Silva, J.L., Chase, P.B. & Pinto, J.R. The intrinsically disordered C terminus of troponin T binds to troponin C to modulate myocardial force generation. *J Biol Chem* **294**, 20054-20069 (2019).
308. Szczesna, D., Zhang, R., Zhao, J., Jones, M., Guzman, G. & Potter, J.D. Altered regulation of cardiac muscle contraction by troponin T mutations that cause familial hypertrophic cardiomyopathy. *J Biol Chem* **275**, 624-30 (2000).
309. Watkins, H., McKenna, W.J., Thierfelder, L., Suk, H.J., Anan, R., O'Donoghue, A., Spirito, P., Matsumori, A., Moravec, C.S., Seidman, J.G. & et al. Mutations in the genes for cardiac troponin T and alpha-tropomyosin in hypertrophic cardiomyopathy. *N Engl J Med* **332**, 1058-64 (1995).
310. Lassalle, M.W. Defective dynamic properties of human cardiac troponin mutations. *Biosci Biotechnol Biochem* **74**, 82-91 (2010).
311. Yang, J., Liu, W.L., Hu, D.Y., Zhu, T.G., Yang, S.N., Li, C.L., Li, L., Sun, Y.H., Xie, W.L., Yang, J.G., Li, T.C., Bian, H., Tong, Q.G. & Xiao, J. Novel mutations of cardiac



- troponin T in Chinese patients with hypertrophic cardiomyopathy. *Zhonghua Xin Xue Guan Bing Za Zhi* **39**, 909-14 (2011).
312. Lopez Davila, A.J., Zhu, L., Fritz, L., Kraft, T. & Chalovich, J.M. The positively charged C-terminal region of human skeletal troponin T retards activation and decreases calcium sensitivity. *Biochemistry* **59**, 4189-4201 (2020).
313. Li, M.X., Spyrapoulos, L., Beier, N., Putkey, J.A. & Sykes, B.D. Interaction of cardiac troponin C with Ca<sup>2+</sup> sensitizer EMD 57033 and cardiac troponin I inhibitory peptide. *Biochemistry* **39**, 8782-90 (2000).
314. Li, M.X., Gelozia, S., Danmaliki, G.I., Wen, Y., Liu, P.B., Lemieux, M.J., West, F.G., Sykes, B.D. & Hwang, P.M. The calcium sensitizer drug MCI-154 binds the structural C-terminal domain of cardiac troponin C. *Biochem Biophys Res* **16**, 145-151 (2018).
315. Tikunova, S.B., Cuesta, A., Price, M., Li, M.X., Belevych, N., Biesiadecki, B.J., Reiser, P.J., Hwang, P.M. & Davis, J.P. 3-Chlorodiphenylamine activates cardiac troponin by a mechanism distinct from bepridil or TFP. *J Gen Physiol* **151**, 9-17 (2019).
316. Hooijman, P., Stewart, M.A. & Cooke, R. A new state of cardiac myosin with very slow ATP turnover: a potential cardioprotective mechanism in the heart. *Biophys J* **100**, 1969-76 (2011).
317. Naber, N., Cooke, R. & Pate, E. Slow myosin ATP turnover in the super-relaxed state in tarantula muscle. *J Mol Biol* **411**, 943-50 (2011).
318. Stewart, M.A., Franks-Skiba, K., Chen, S. & Cooke, R. Myosin ATP turnover rate is a mechanism involved in thermogenesis in resting skeletal muscle fibers. *Proc Natl Acad Sci USA* **107**, 430-5 (2010).

319. Murphy, S.P., Ibrahim, N.E. & Januzzi, J.L., Jr. Heart failure with reduced ejection fraction: A review. *JAMA* **324**, 488-504 (2020).
320. Curtis, J.P., Sokol, S.I., Wang, Y., Rathore, S.S., Ko, D.T., Jadbabaie, F., Portnay, E.L., Marshalko, S.J., Radford, M.J. & Krumholz, H.M. The association of left ventricular ejection fraction, mortality, and cause of death in stable outpatients with heart failure. *J Am Coll Cardiol* **42**, 736-42 (2003).
321. Bourge, R.C., Fleg, J.L., Fonarow, G.C., Cleland, J.G., McMurray, J.J., van Veldhuisen, D.J., Gheorghiu, M., Patel, K., Aban, I.B., Allman, R.M., White-Williams, C., White, M., Filippatos, G.S., Anker, S.D. & Ahmed, A. Digoxin reduces 30-day all-cause hospital admission in older patients with chronic systolic heart failure. *Am J Med* **126**, 701-8 (2013).
322. Wolska, B.M., Kitada, Y., Palmiter, K.A., Westfall, M.V., Johnson, M.D. & Solaro, R.J. CGP-48506 increases contractility of ventricular myocytes and myofilaments by effects on actin-myosin reaction. *Am J Physiol* **270**, H24-32 (1996).
323. Brixius, K., Mehlhorn, U., Bloch, W. & Schwinger, R.H. Different effect of the Ca<sup>2+</sup> sensitizers EMD 57033 and CGP 48506 on cross-bridge cycling in human myocardium. *J Pharmacol Exp Ther* **295**, 1284-90 (2000).
324. Kitada, Y., Kobayashi, M., Narimatsu, A. & Ohizumi, Y. Potent stimulation of myofilament force and adenosine triphosphatase activity of canine cardiac muscle through a direct enhancement of troponin C Ca<sup>2+</sup> binding by MCI-154, a novel cardiotonic agent. *J Pharmacol Exp Ther* **250**, 272-7 (1989).
325. Planelles-Herrero, V.J., Hartman, J.J., Robert-Paganin, J., Malik, F.I. & Houdusse, A. Mechanistic and structural basis for activation of cardiac myosin force production by omecamtiv mecarbil. *Nat Commun* **8**, 190 (2017).

326. Woody, M.S., Greenberg, M.J., Barua, B., Winkelmann, D.A., Goldman, Y.E. & Ostap, E.M. Positive cardiac inotrope omecamtiv mecarbil activates muscle despite suppressing the myosin working stroke. *Nat Commun* **9**, 3838 (2018).
327. Teerlink, J.R., Felker, G.M., McMurray, J.J.V., Ponikowski, P., Metra, M., Filippatos, G.S., Ezekowitz, J.A., Dickstein, K., Cleland, J.G.F., Kim, J.B., Lei, L., Knusel, B., Wolff, A.A., Malik, F.I., Wasserman, S.M. & Investigators, A.-A. Acute Treatment with omecamtiv mecarbil to increase contractility in acute heart failure: The ATOMIC-AHF study. *J Am Coll Cardiol* **67**, 1444-1455 (2016).
328. Metzger, J.M. & Westfall, M.V. Covalent and noncovalent modification of thin filament action: the essential role of troponin in cardiac muscle regulation. *Circ Res* **94**, 146-58 (2004).
329. Li, M.X., Wang, X. & Sykes, B.D. Structural based insights into the role of troponin in cardiac muscle pathophysiology. *J Muscle Res Cell Motil* **25**, 559-79 (2004).
330. Li, M.X., Saude, E.J., Wang, X., Pearlstone, J.R., Smillie, L.B. & Sykes, B.D. Kinetic studies of calcium and cardiac troponin I peptide binding to human cardiac troponin C using NMR spectroscopy. *Eur Biophys J* **31**, 245-56 (2002).
331. Oda, T., Yanagisawa, H. & Wakabayashi, T. Cryo-EM structures of cardiac thin filaments reveal the 3D architecture of troponin. *J Struct Biol* **209**, 107450 (2020).
332. Shefner, J.M., Andrews, J.A., Genge, A., Jackson, C., Lechtzin, N., Miller, T.M., Cockroft, B.M., Meng, L., Wei, J., Wolff, A.A., Malik, F.I., Bodkin, C., Brooks, B.R., Caress, J., Dionne, A., Fee, D., Goutman, S.A., Goyal, N.A., Hardiman, O., Hayat, G., Heiman-Patterson, T., Heitzman, D., Henderson, R.D., Johnston, W., Karam, C., Kiernan, M.C., Kolb, S.J., Korngut, L., Ladha, S., Matte, G., Mora, J.S., Needham, M., Oskarsson, B.,

- Pattee, G.L., Pioro, E.P., Pulley, M., Quan, D., Rezania, K., Schellenberg, K.L., Schultz, D., Shoesmith, C., Simmons, Z., Statland, J., Sultan, S., Swenson, A., Berg, L., Vu, T., Vucic, S., Weiss, M., Whyte-Rayson, A., Wymer, J., Zinman, L. & Rudnicki, S.A. A phase 2, double-blind, randomized, dose-ranging trial of reldesemtiv in patients with ALS. *Amyotroph Lateral Scler Frontotemporal Degener* **22**, 287-299 (2021).
333. Rudnicki, S.A., Andrews, J.A., Duong, T., Cockroft, B.M., Malik, F.I., Meng, L., Wei, J., Wolff, A.A., Genge, A., Johnson, N.E., Tesi-Rocha, C., Connolly, A.M., Darras, B.T., Felice, K., Shieh, P.B., Mah, J.K., Statland, J., Campbell, C., Habib, A.A., Kuntz, N.L., Oskoui, M. & Day, J.W. Reldesemtiv in patients with spinal muscular atrophy: a phase 2 hypothesis-generating study. *Neurotherapeutics* (2021).
334. Orstavik, O., Manfra, O., Andressen, K.W., Andersen, G.O., Skomedal, T., Osnes, J.B., Levy, F.O. & Krobert, K.A. The inotropic effect of the active metabolite of levosimendan, OR-1896, is mediated through inhibition of PDE3 in rat ventricular myocardium. *PLoS One* **10**, e0115547 (2015).
335. Bohm, M., Morano, I., Pieske, B., Ruegg, J.C., Wankerl, M., Zimmermann, R. & Erdmann, E. Contribution of cAMP-phosphodiesterase inhibition and sensitization of the contractile proteins for calcium to the inotropic effect of pimobendan in the failing human myocardium. *Circ Res* **68**, 689-701 (1991).
336. Bethke, T., Meyer, W., Schmitz, W., Scholz, H., Wenzlaff, H., Armah, B.I., Bruckner, R. & Raap, A. High selectivity for inhibition of phosphodiesterase III and positive inotropic effects of MCI-154 in guinea pig myocardium. *J Cardiovasc Pharmacol* **21**, 847-55 (1993).
337. Waudby, C.A., Ramos, A., Cabrita, L.D. & Christodoulou, J. Two-dimensional NMR lineshape analysis. *Sci Rep* **6**, 24826 (2016).

338. Reiser, P.J., Welch, K.C., Jr., Suarez, R.K. & Altshuler, D.L. Very low force-generating ability and unusually high temperature dependency in hummingbird flight muscle fibers. *J Exp Biol* **216**, 2247-56 (2013).
339. Tikunova, S.B., Rall, J.A. & Davis, J.P. Effect of hydrophobic residue substitutions with glutamine on Ca<sup>2+</sup> binding and exchange with the N-domain of troponin C. *Biochemistry* **41**, 6697-705 (2002).
340. Black, D.J., Tikunova, S.B., Johnson, J.D. & Davis, J.P. Acid pairs increase the N-terminal Ca<sup>2+</sup> affinity of CaM by increasing the rate of Ca<sup>2+</sup> association. *Biochemistry* **39**, 13831-7 (2000).
341. Tikunova, S., Belevych, N., Doan, K. & Reiser, P.J. Desensitizing mouse cardiac troponin C to calcium converts slow muscle towards a fast muscle phenotype. *J Physiol* **596**, 4651-4663 (2018).
342. Edman, K.A. The velocity of unloaded shortening and its relation to sarcomere length and isometric force in vertebrate muscle fibres. *J Physiol* **291**, 143-59 (1979).
343. Sah, R., Oudit, G.Y., Nguyen, T.T., Lim, H.W., Wickenden, A.D., Wilson, G.J., Molkentin, J.D. & Backx, P.H. Inhibition of calcineurin and sarcolemmal Ca<sup>2+</sup> influx protects cardiac morphology and ventricular function in K<sub>v</sub>4.2N transgenic mice. *Circulation* **105**, 1850-6 (2002).
344. Crackower, M.A., Oudit, G.Y., Kozieradzki, I., Sarao, R., Sun, H., Sasaki, T., Hirsch, E., Suzuki, A., Shioi, T., Irie-Sasaki, J., Sah, R., Cheng, H.Y., Rybin, V.O., Lembo, G., Fratta, L., Oliveira-dos-Santos, A.J., Benovic, J.L., Kahn, C.R., Izumo, S., Steinberg, S.F., Wymann, M.P., Backx, P.H. & Penninger, J.M. Regulation of myocardial contractility and cell size by distinct PI3K-PTEN signaling pathways. *Cell* **110**, 737-49 (2002).

345. Kuang, M., Febbraio, M., Wagg, C., Lopaschuk, G.D. & Dyck, J.R. Fatty acid translocase/CD36 deficiency does not energetically or functionally compromise hearts before or after ischemia. *Circulation* **109**, 1550-7 (2004).
346. Kovacic, S., Soltys, C.L., Barr, A.J., Shiojima, I., Walsh, K. & Dyck, J.R. Akt activity negatively regulates phosphorylation of AMP-activated protein kinase in the heart. *J Biol Chem* **278**, 39422-7 (2003).
347. Swenson, A.M., Tang, W., Blair, C.A., Fetrow, C.M., Unrath, W.C., Previs, M.J., Campbell, K.S. & Yengo, C.M. Omecantiv mecarbil enhances the duty ratio of human beta-cardiac myosin resulting in increased calcium sensitivity and slowed force development in cardiac muscle. *J Biol Chem* **292**, 3768-3778 (2017).
348. Tang, W., Unrath, W.C., Desetty, R. & Yengo, C.M. Dilated cardiomyopathy mutation in the converter domain of human cardiac myosin alters motor activity and response to omecantiv mecarbil. *J Biol Chem* **294**, 17314-17325 (2019).
349. Pineda-Sanabria, S.E., Julien, O. & Sykes, B.D. Versatile cardiac troponin chimera for muscle protein structural biology and drug discovery. *ACS Chem Biol* **9**, 2121-30 (2014).
350. McKay, R.T., Saltibus, L.F., Li, M.X. & Sykes, B.D. Energetics of the induced structural change in a  $\text{Ca}^{2+}$  regulatory protein:  $\text{Ca}^{2+}$  and troponin I peptide binding to the E41A mutant of the N-domain of skeletal troponin C. *Biochemistry* **39**, 12731-8 (2000).
351. Paakkonen, K., Sorsa, T., Drakenberg, T., Pollesello, P., Tilgmann, C., Permi, P., Heikkinen, S., Kilpelainen, I. & Annala, A. Conformations of the regulatory domain of cardiac troponin C examined by residual dipolar couplings. *Eur J Biochem* **267**, 6665-72 (2000).

352. Feldkamp, M.D., O'Donnell, S.E., Yu, L. & Shea, M.A. Allosteric effects of the antipsychotic drug trifluoperazine on the energetics of calcium binding by calmodulin. *Proteins* **78**, 2265-82 (2010).
353. Robertson, I.M., Sun, Y.B., Li, M.X. & Sykes, B.D. A structural and functional perspective into the mechanism of Ca<sup>2+</sup>-sensitizers that target the cardiac troponin complex. *J Mol Cell Cardiol* **49**, 1031-41 (2010).
354. Lindert, S., Li, M.X., Sykes, B.D. & McCammon, J.A. Computer-aided drug discovery approach finds calcium sensitizer of cardiac troponin. *Chem Biol Drug Des* **85**, 99-106 (2015).
355. Mahmud, Z., Dhimi, P.S., Rans, C., Liu, P.B. & Hwang, P.M. Dilated Cardiomyopathy Mutations and Phosphorylation disrupt the Active Orientation of Cardiac Troponin C. *J Mol Biol* **433**, 167010 (2021).
356. Russell, A.J., Hartman, J.J., Hinken, A.C., Muci, A.R., Kawas, R., Driscoll, L., Godinez, G., Lee, K.H., Marquez, D., Browne, W.F.t., Chen, M.M., Clarke, D., Collibee, S.E., Garard, M., Hansen, R., Jia, Z., Lu, P.P., Rodriguez, H., Saikali, K.G., Schaletzky, J., Vijayakumar, V., Albertus, D.L., Clafin, D.R., Morgans, D.J., Morgan, B.P. & Malik, F.I. Activation of fast skeletal muscle troponin as a potential therapeutic approach for treating neuromuscular diseases. *Nat Med* **18**, 452-5 (2012).
357. Hwee, D.T., Kennedy, A., Ryans, J., Russell, A.J., Jia, Z., Hinken, A.C., Morgans, D.J., Malik, F.I. & Jasper, J.R. Fast skeletal muscle troponin activator tirasemtiv increases muscle function and performance in the B6SJL-SOD1G93A ALS mouse model. *PLoS One* **9**, e96921 (2014).

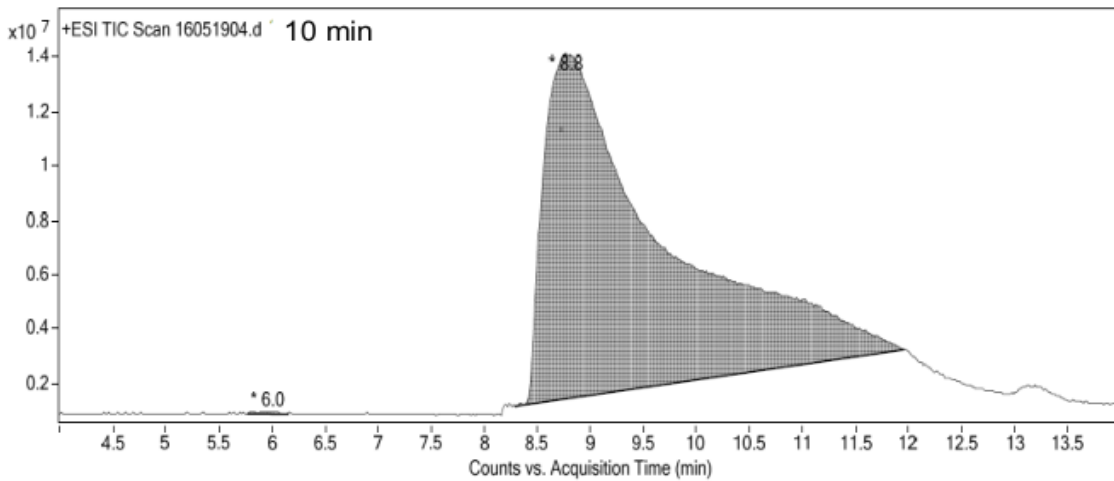
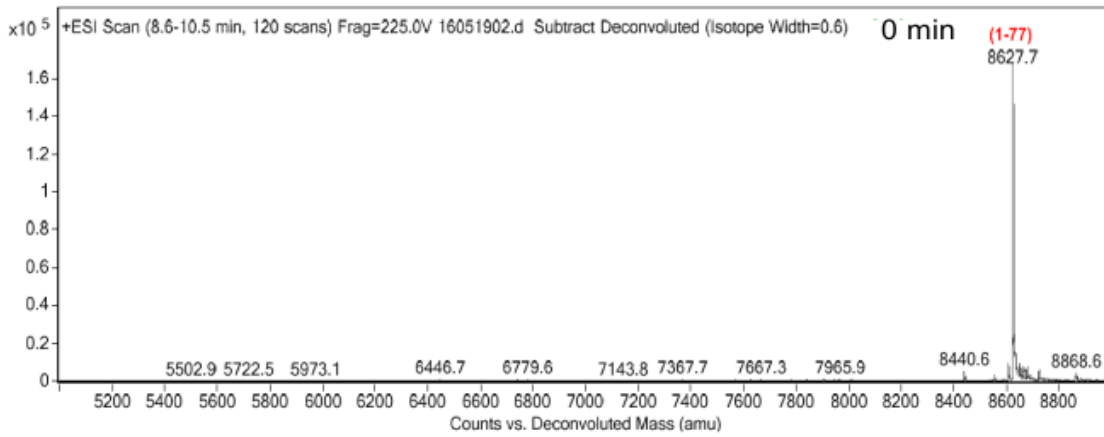
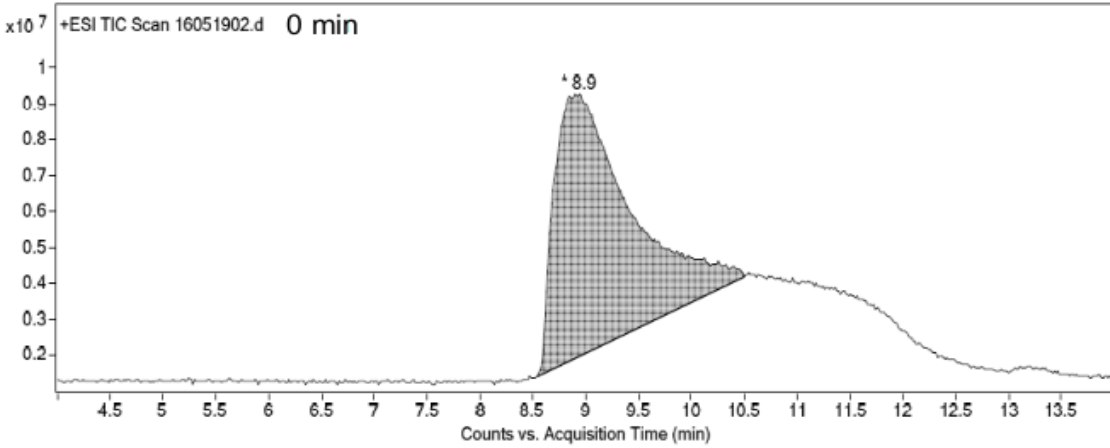
358. Calder, A.N., Androphy, E.J. & Hodgetts, K.J. Small molecules in development for the treatment of spinal muscular atrophy. *J Med Chem* **59**, 10067-10083 (2016).
359. Hwee, D.T., Kennedy, A.R., Hartman, J.J., Ryans, J., Durham, N., Malik, F.I. & Jasper, J.R. The small-molecule fast skeletal troponin activator, CK-2127107, improves exercise tolerance in a rat model of heart failure. *J Pharmacol Exp Ther* **353**, 159-68 (2015).
360. Parvatiyar, M.S., Pinto, J.R., Dweck, D. & Potter, J.D. Cardiac troponin mutations and restrictive cardiomyopathy. *J Biomed Biotechnol* **2010**, 350706 (2010).
361. Brizendine, R.K., Alcalá, D.B., Carter, M.S., Haldeman, B.D., Facemyer, K.C., Baker, J.E. & Cremo, C.R. Velocities of unloaded muscle filaments are not limited by drag forces imposed by myosin cross-bridges. *Proc Natl Acad Sci U S A* **112**, 11235-40 (2015).
362. O'Connell, C.B., Tyska, M.J. & Mooseker, M.S. Myosin at work: motor adaptations for a variety of cellular functions. *Biochim Biophys Acta* **1773**, 615-30 (2007).
363. Mickelson, A.V. & Chandra, M. Hypertrophic cardiomyopathy mutation in cardiac troponin T (R95H) attenuates length-dependent activation in guinea pig cardiac muscle fibers. *Am J Physiol Heart Circ Physiol* **313**, H1180-H1189 (2017).
364. Graether, S.P. Troubleshooting Guide to Expressing Intrinsically Disordered Proteins for Use in NMR Experiments. *Front Mol Biosci* **5**, 118 (2018).
365. Mahmud, Z., Zahran, S., Liu, P.B., Reiz, B., Chan, B.Y.H., Roczковский, A., McCartney, C.E., Davies, P.L., Li, L., Schulz, R. & Hwang, P.M. Structure and proteolytic susceptibility of the inhibitory C-terminal tail of cardiac troponin I. *Biochim Biophys Acta Gen Subj* **1863**, 661-671 (2019).
366. Luo, S.Y., Araya, L.E. & Julien, O. Protease substrate identification using N-terminomics. *ACS Chem Biol* **14**, 2361-2371 (2019).

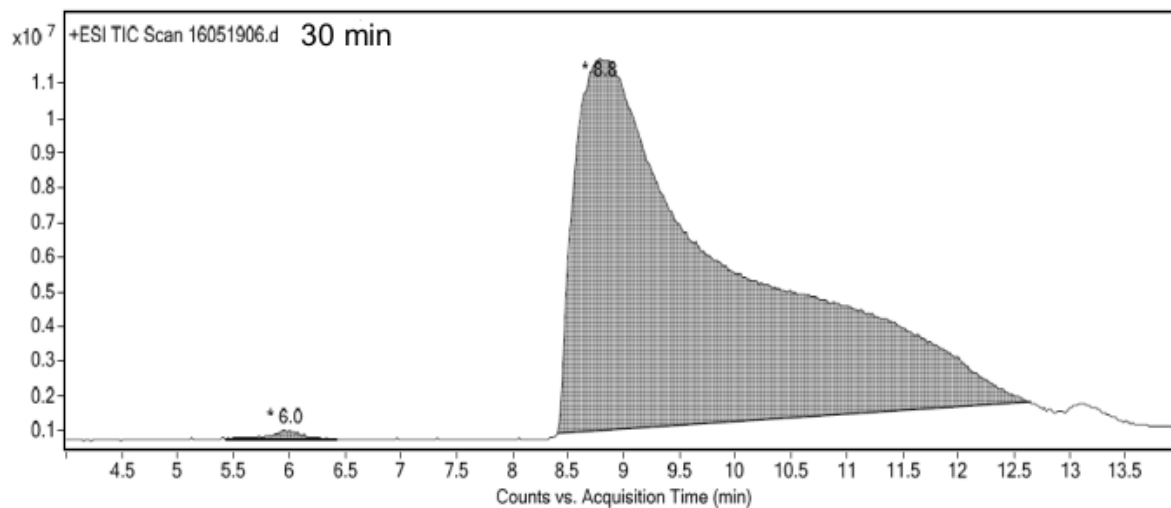
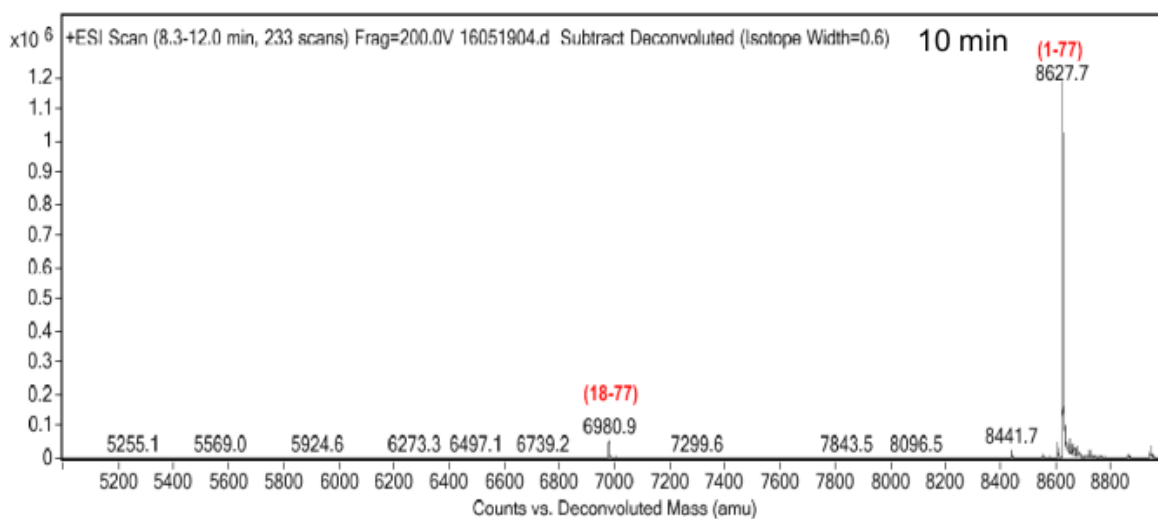
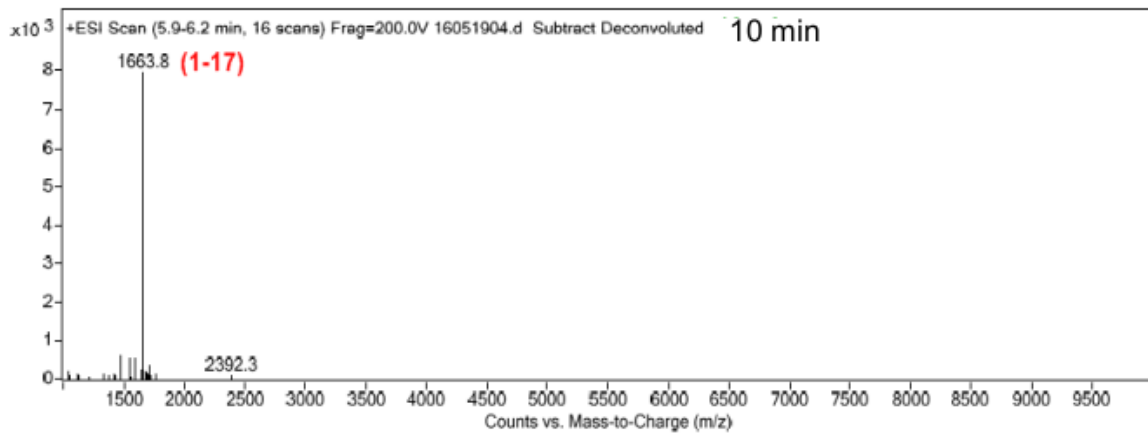


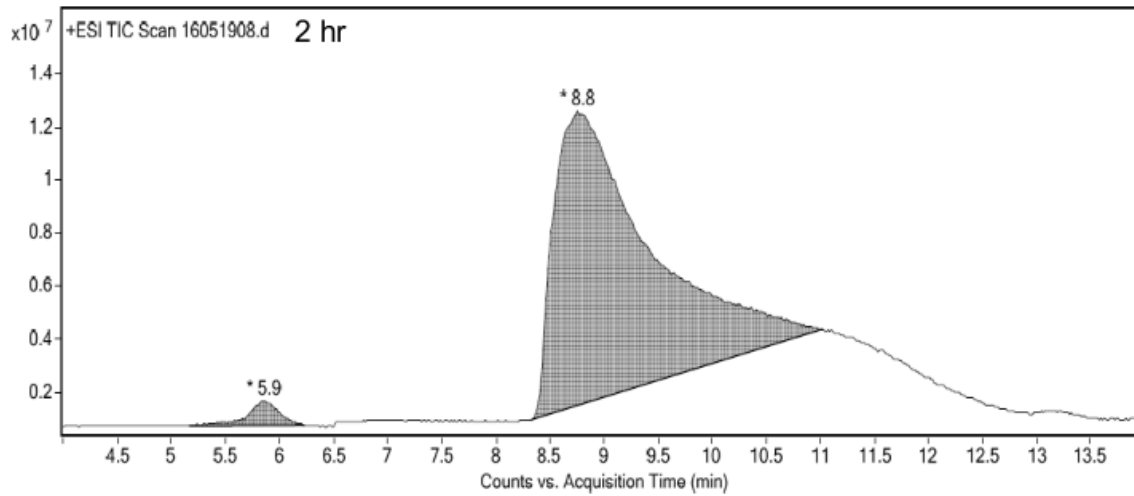
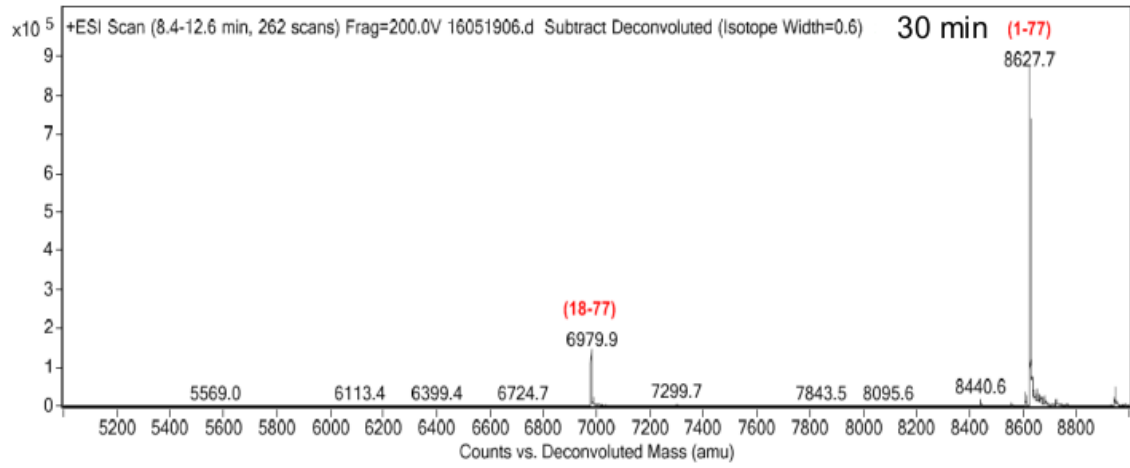
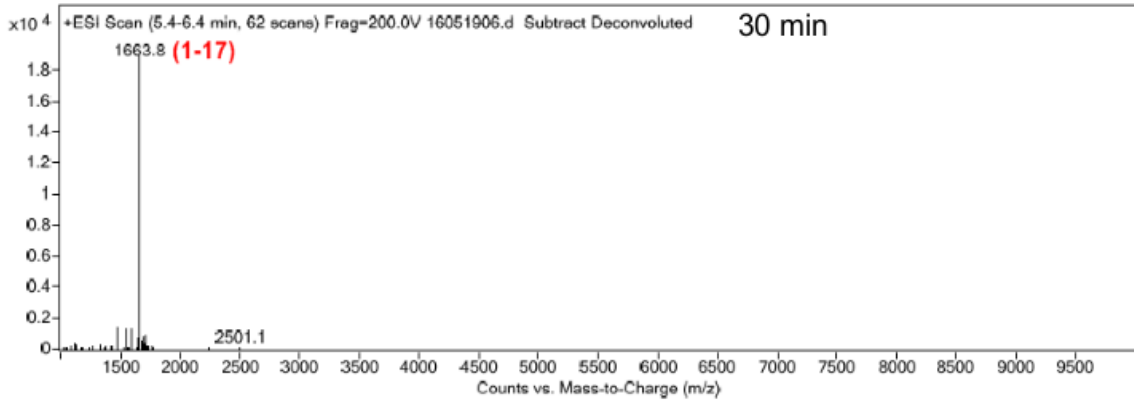
367. Azam, M., Andrabi, S.S., Sahr, K.E., Kamath, L., Kuliopulos, A. & Chishti, A.H. Disruption of the mouse mu-calpain gene reveals an essential role in platelet function. *Mol Cell Biol* **21**, 2213-20 (2001).
368. Matsusaka, H., Ide, T., Matsushima, S., Ikeuchi, M., Kubota, T., Sunagawa, K., Kinugawa, S. & Tsutsui, H. Targeted deletion of matrix metalloproteinase 2 ameliorates myocardial remodeling in mice with chronic pressure overload. *Hypertension* **47**, 711-7 (2006).
369. Tsunekawa, S., Takahashi, K., Abe, M., Hiwada, K., Ozawa, K. & Murachi, T. Calpain proteolysis of free and bound forms of calponin, a troponin T-like protein in smooth muscle. *FEBS Lett* **250**, 493-6 (1989).

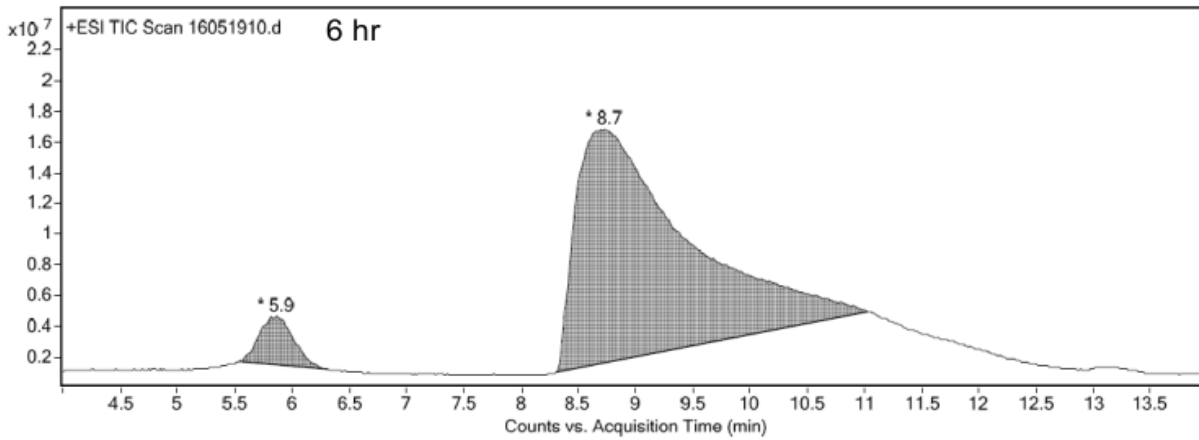
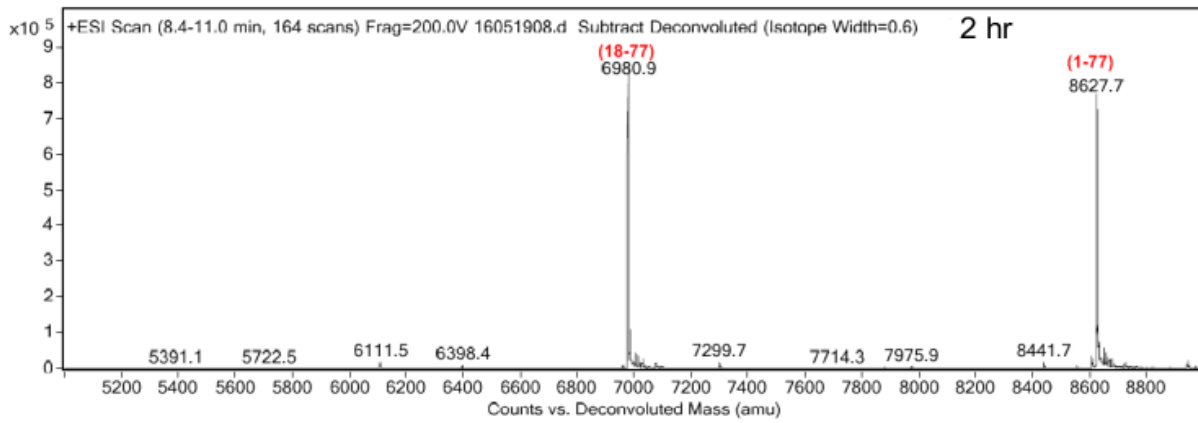
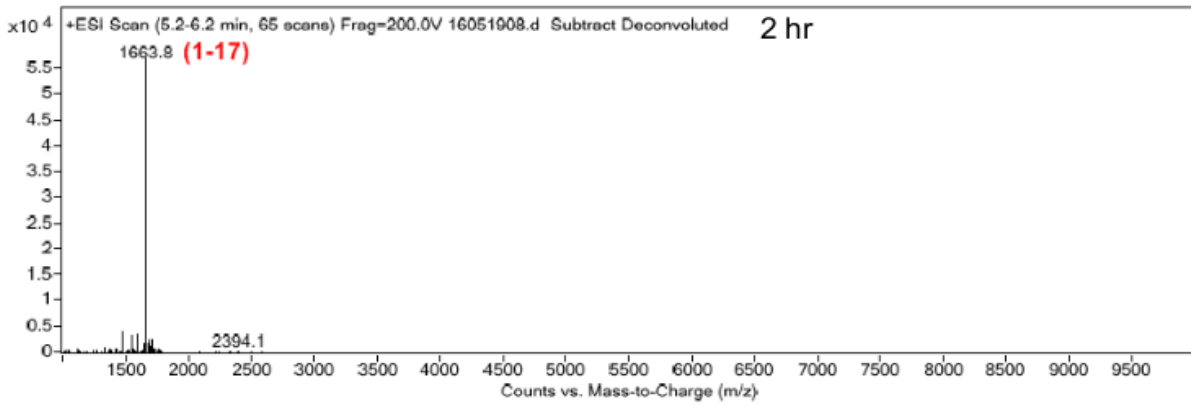
**Appendix 1:** Mass spectrometry data of cTnI<sub>1-77</sub> and cTnI<sub>135-209</sub> proteolysed by MMP-2 at time points from 0 min to 24 h

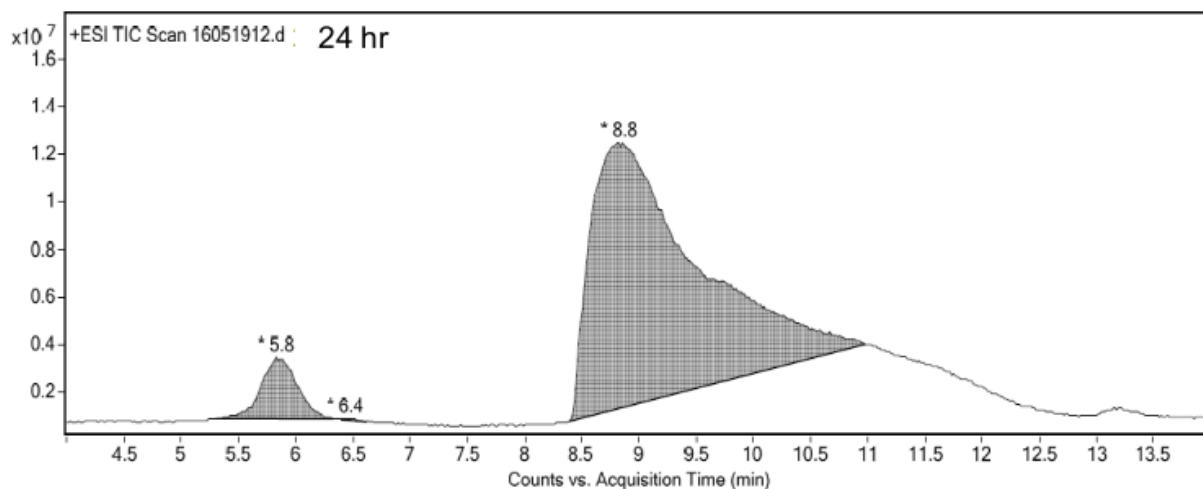
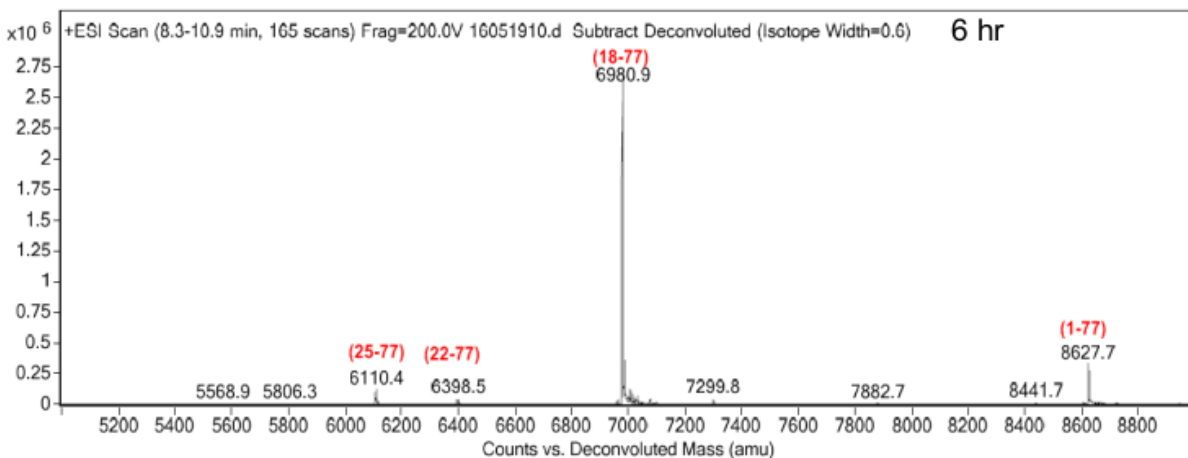
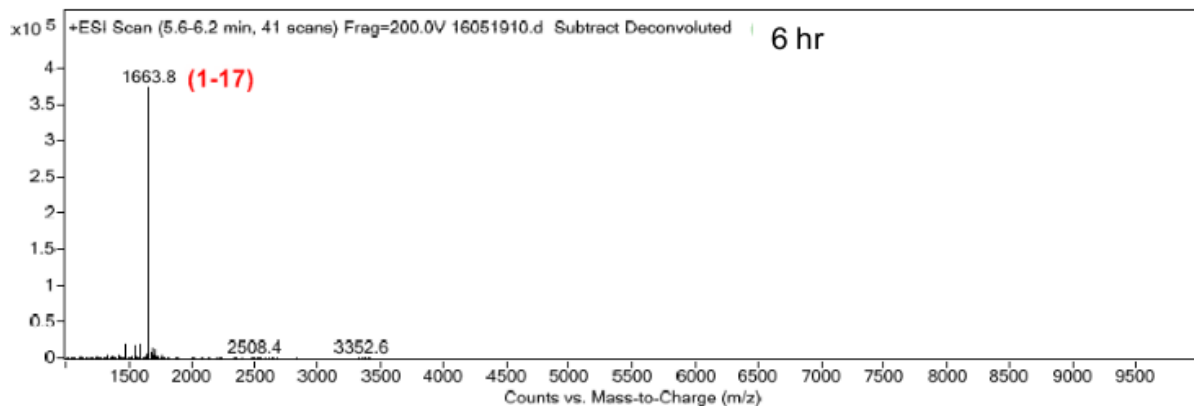
**Proteolysis of cTnI<sub>1-77</sub> by MMP-2**

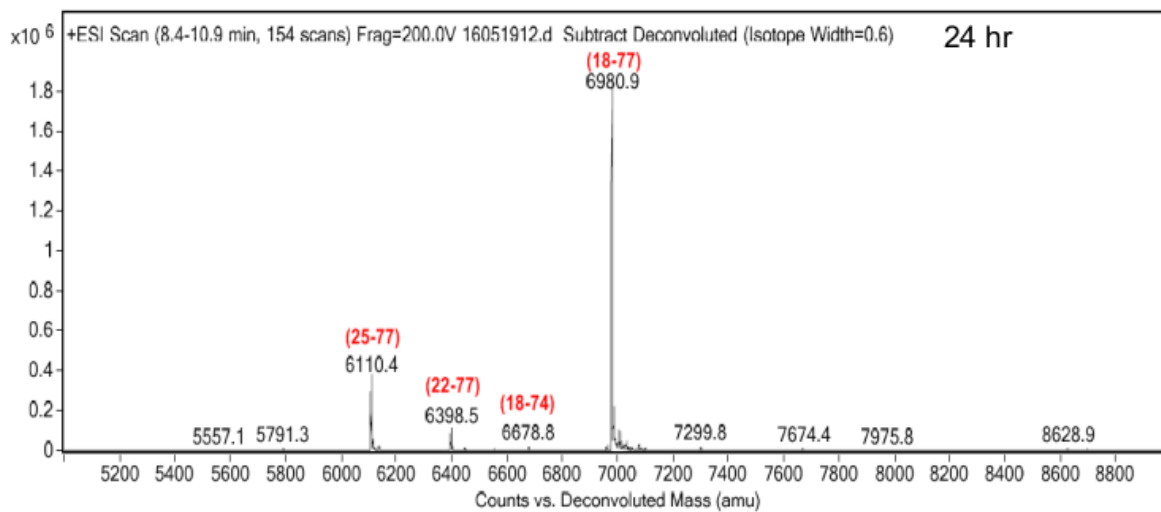
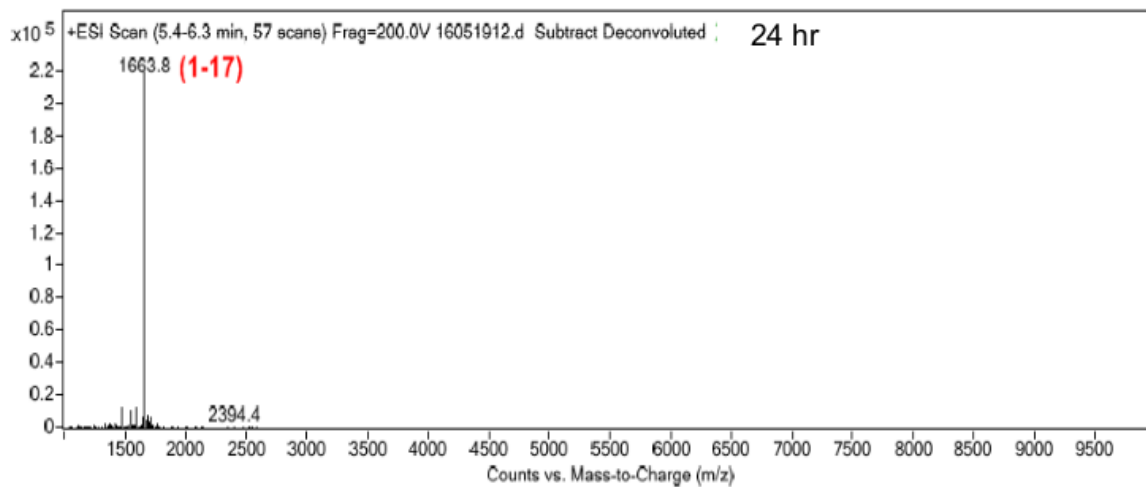




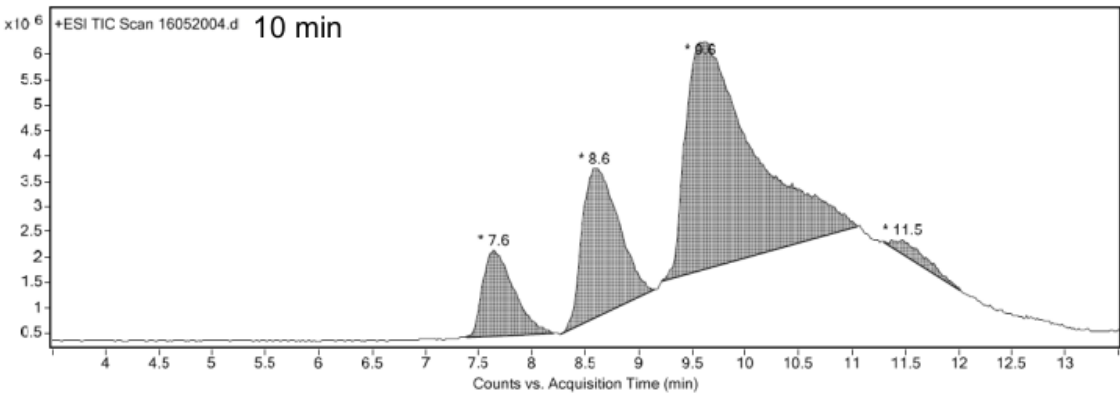
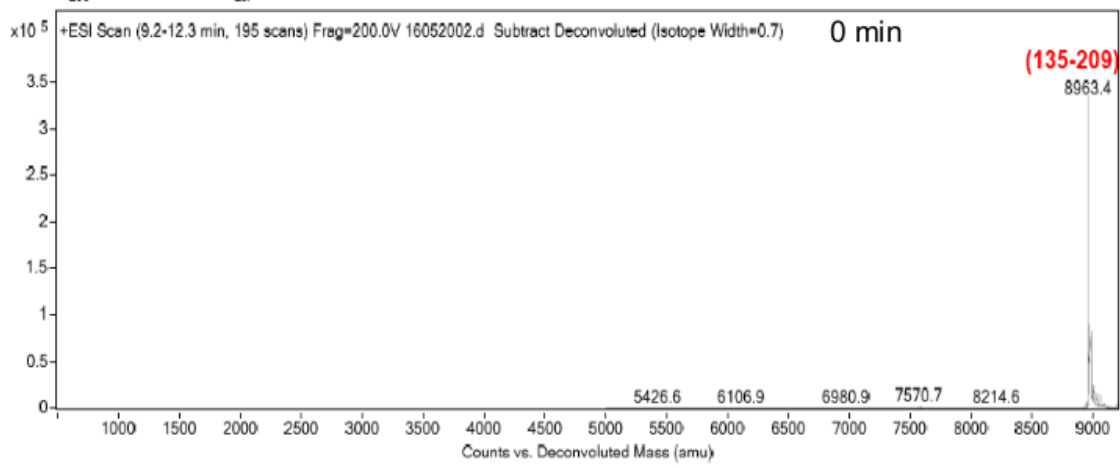
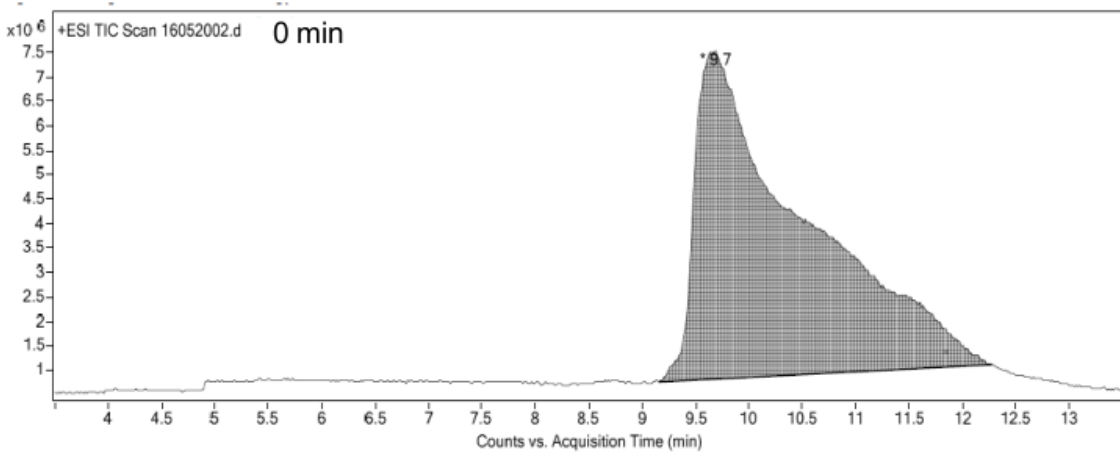




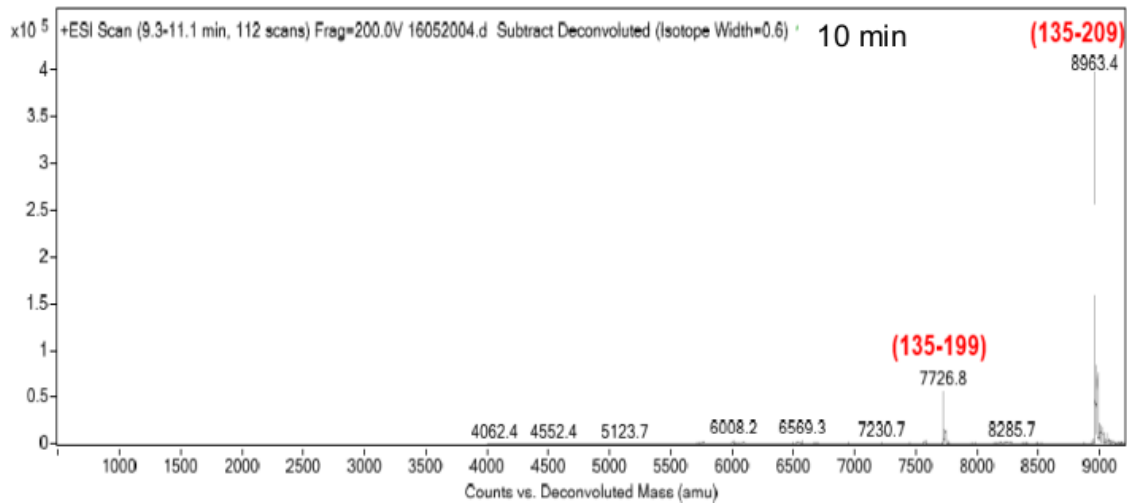
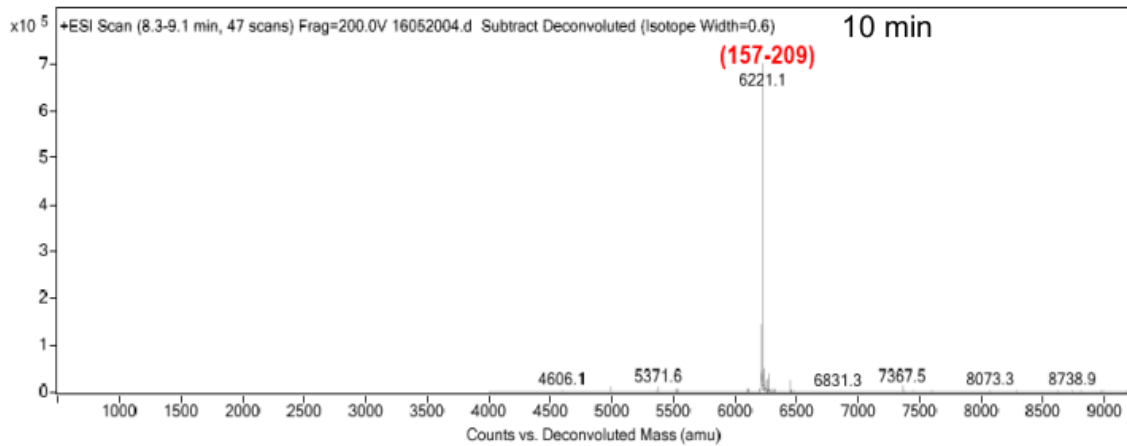
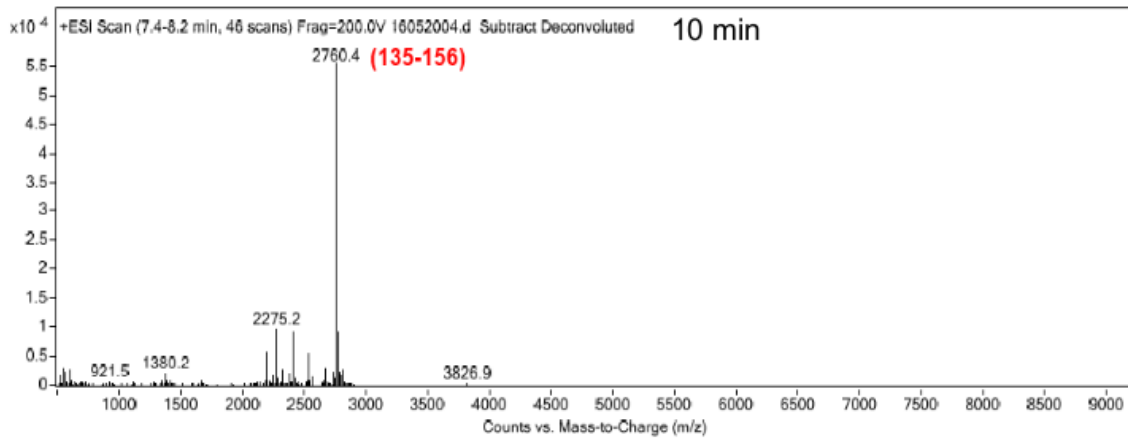


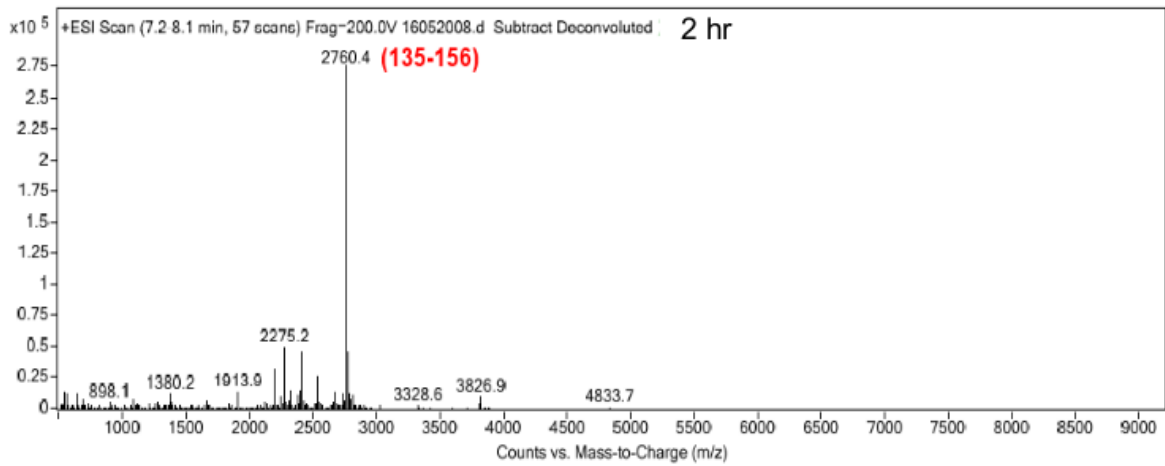
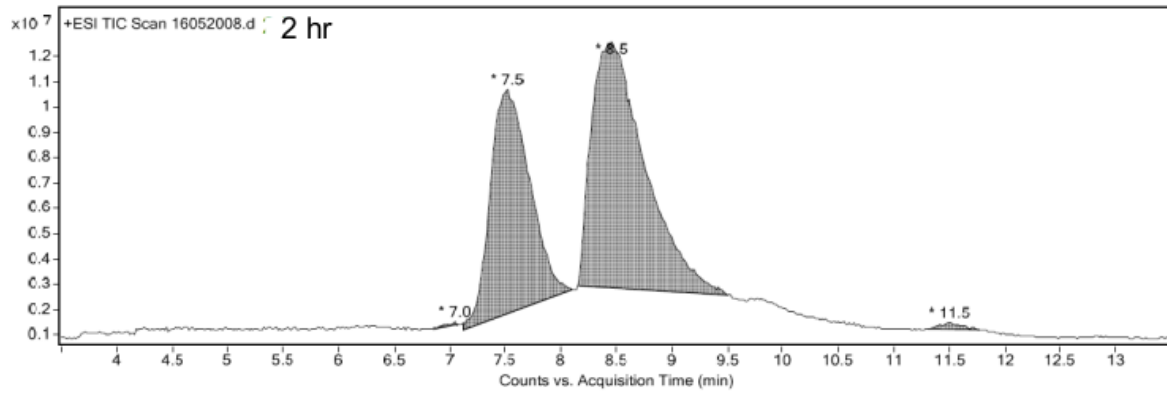
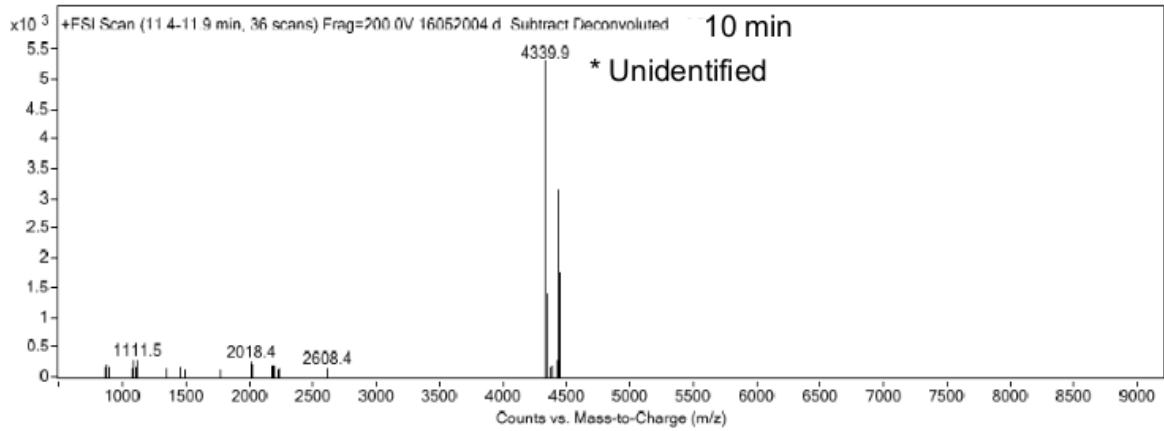


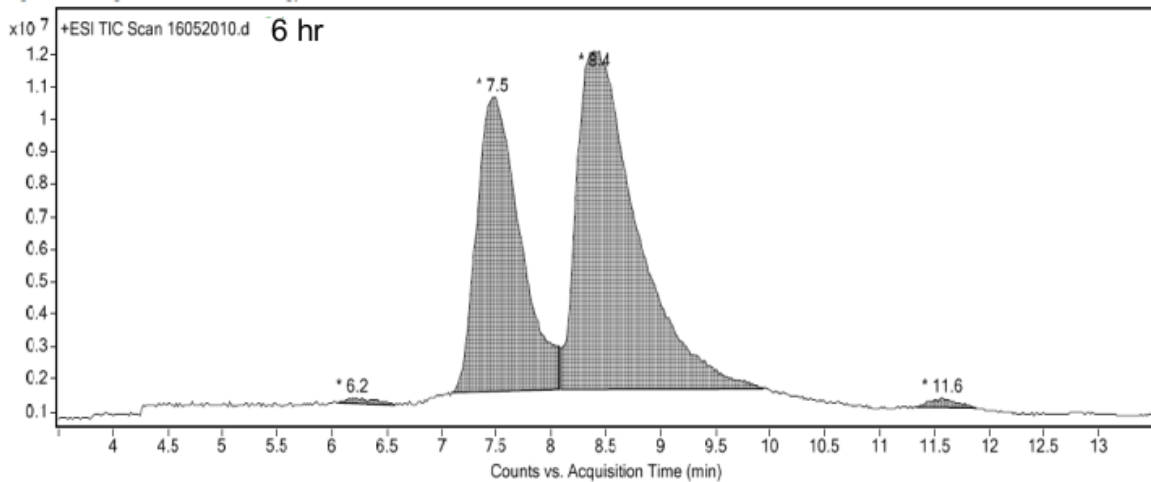
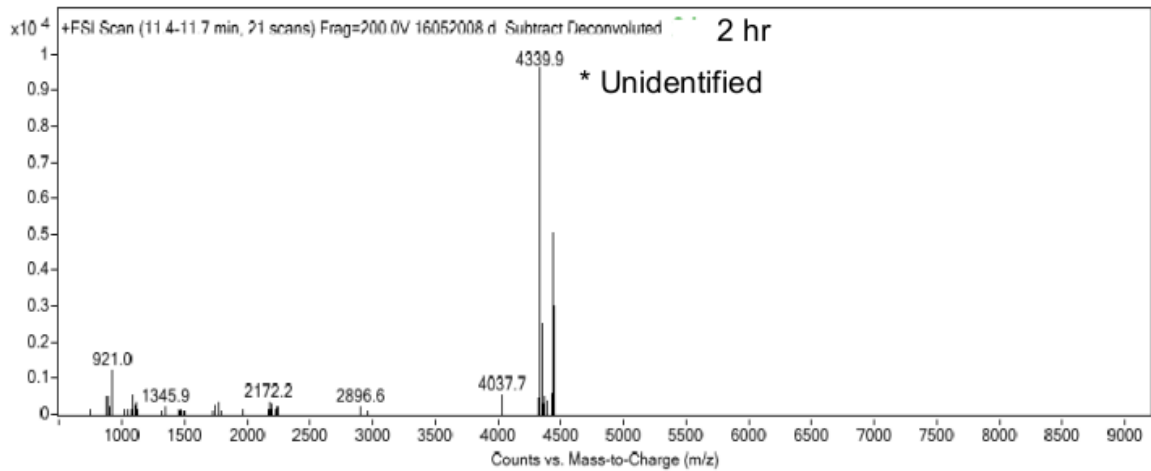
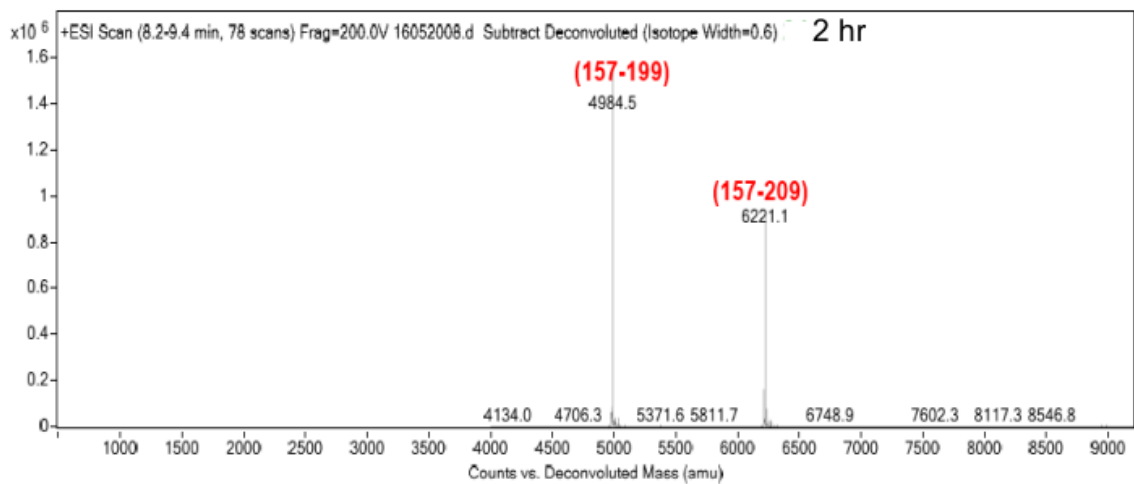
# Proteolysis of cTnI<sub>135-209</sub> by MMP-2

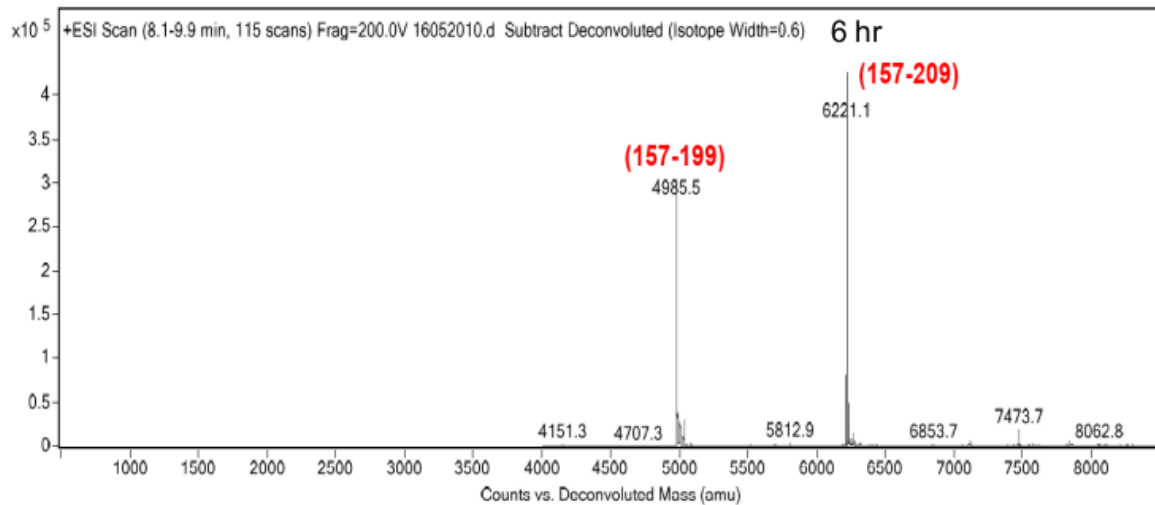
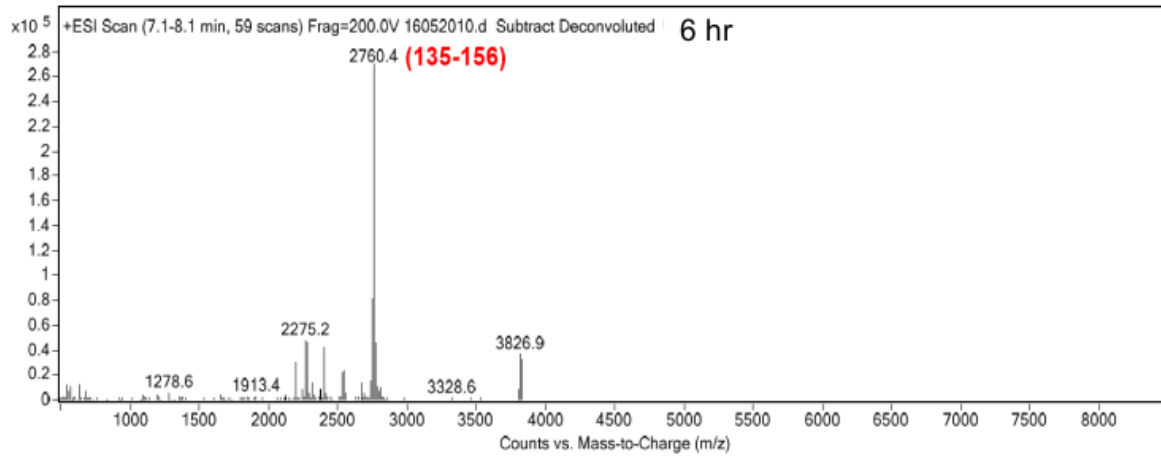
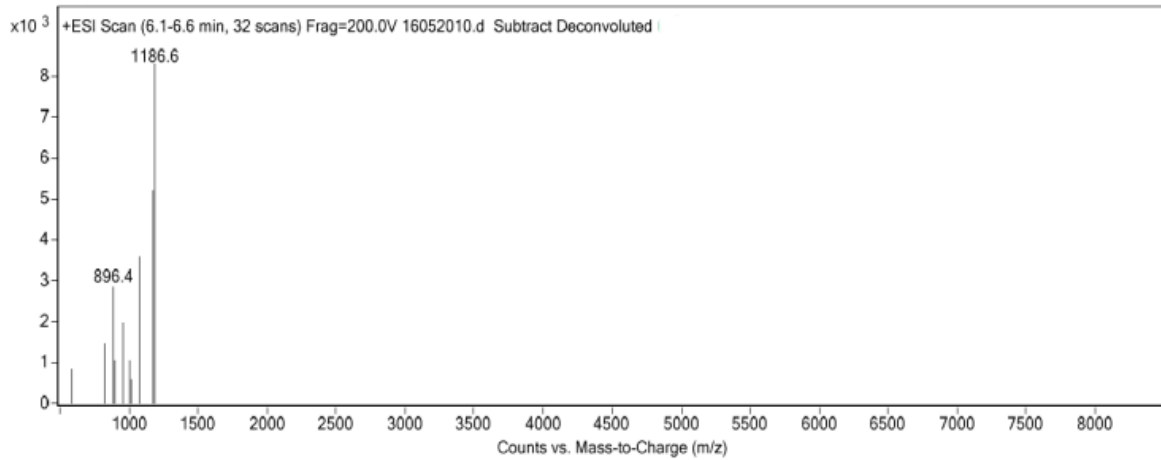


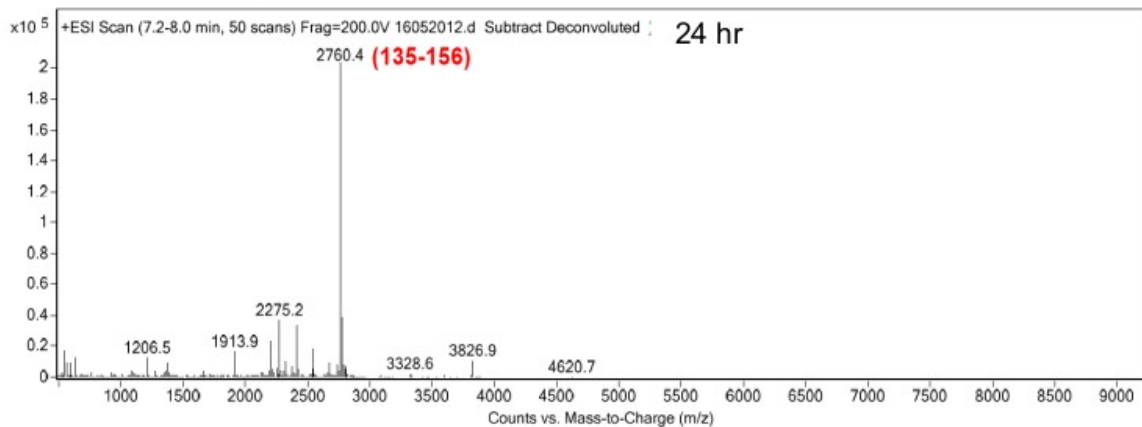
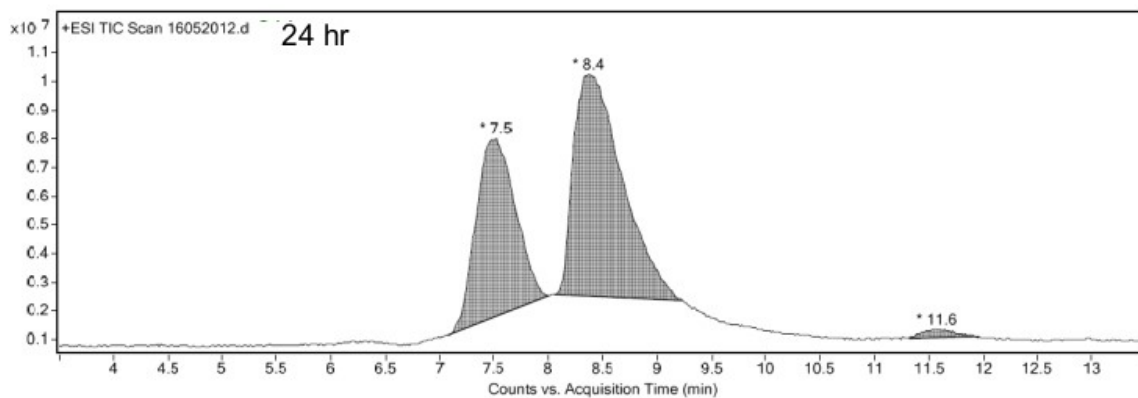
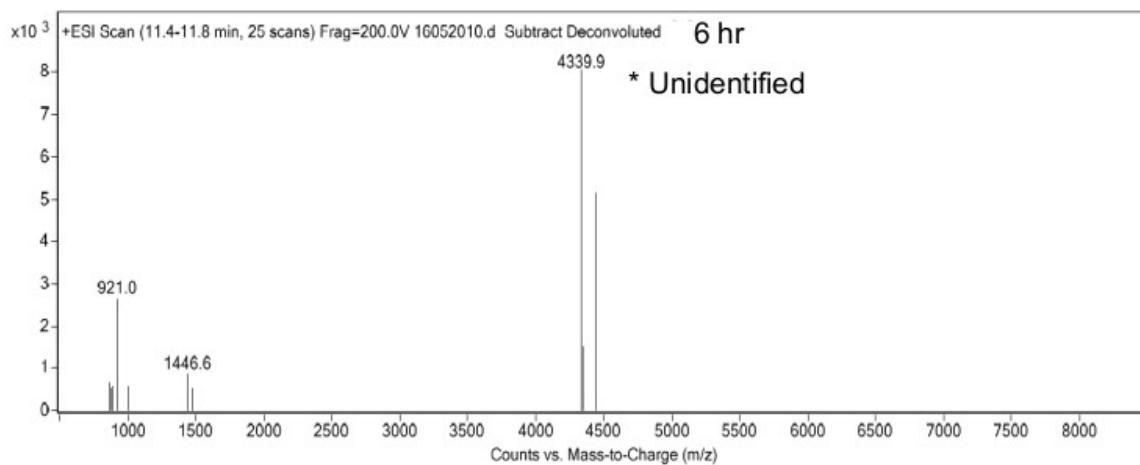


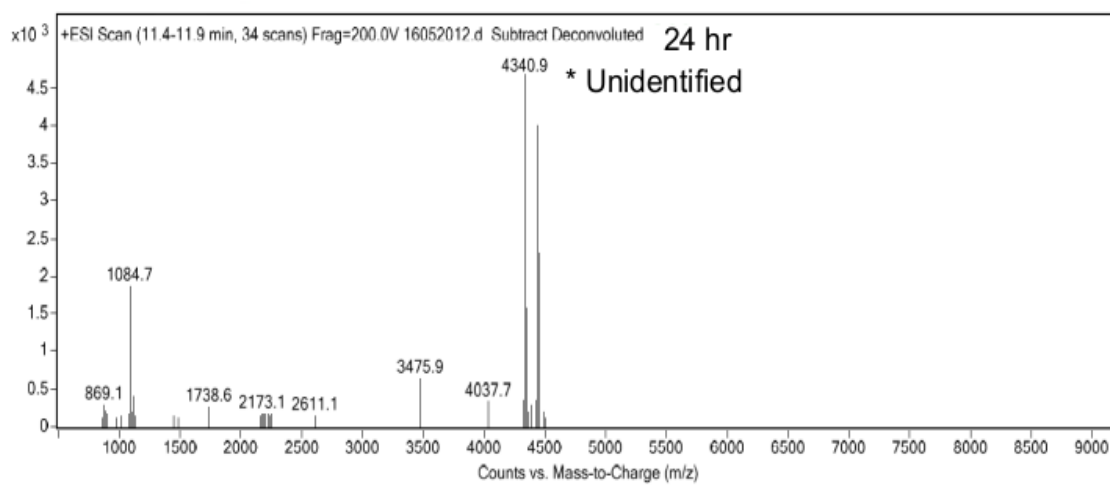
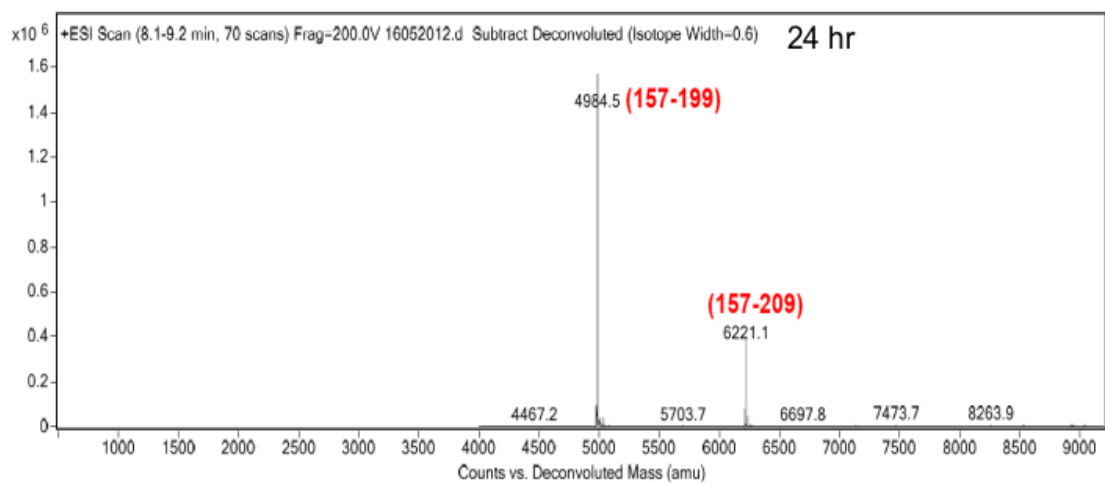






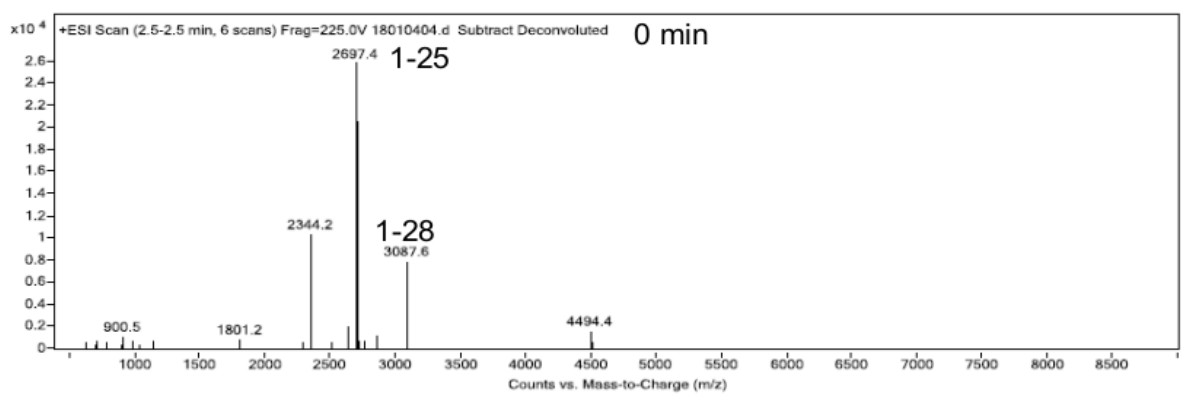
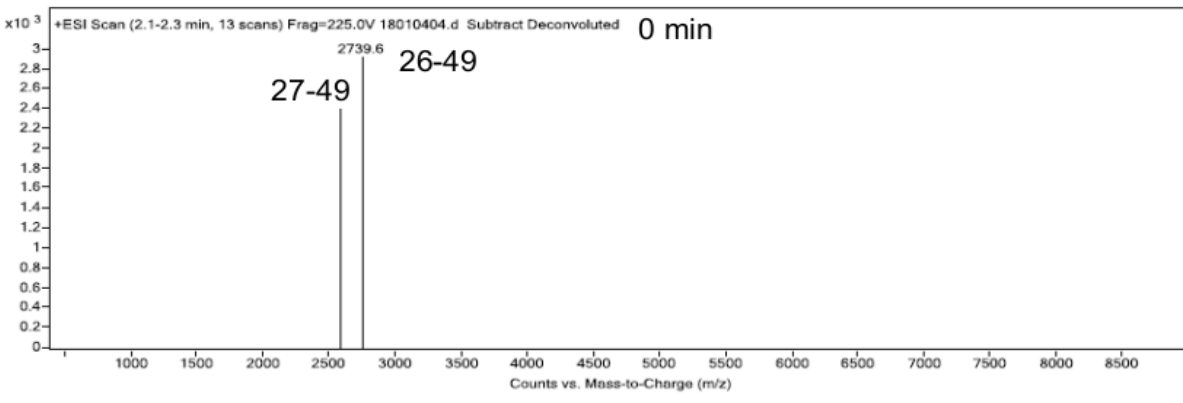
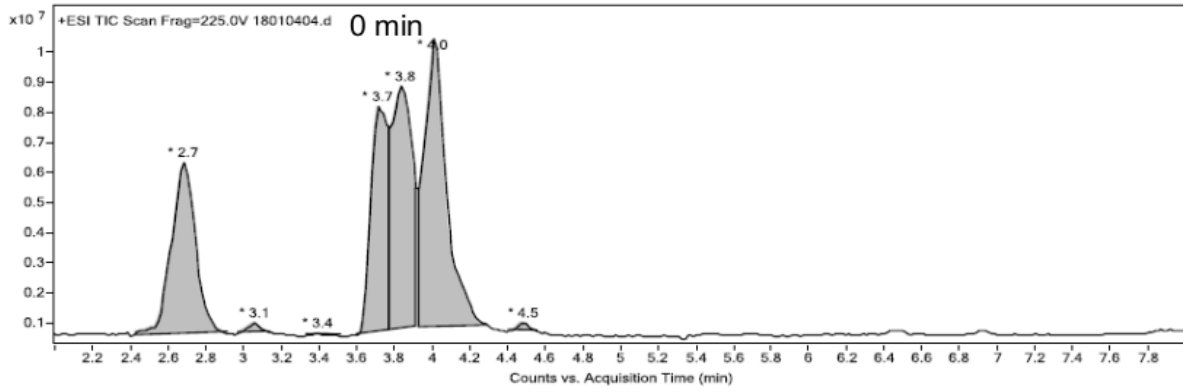


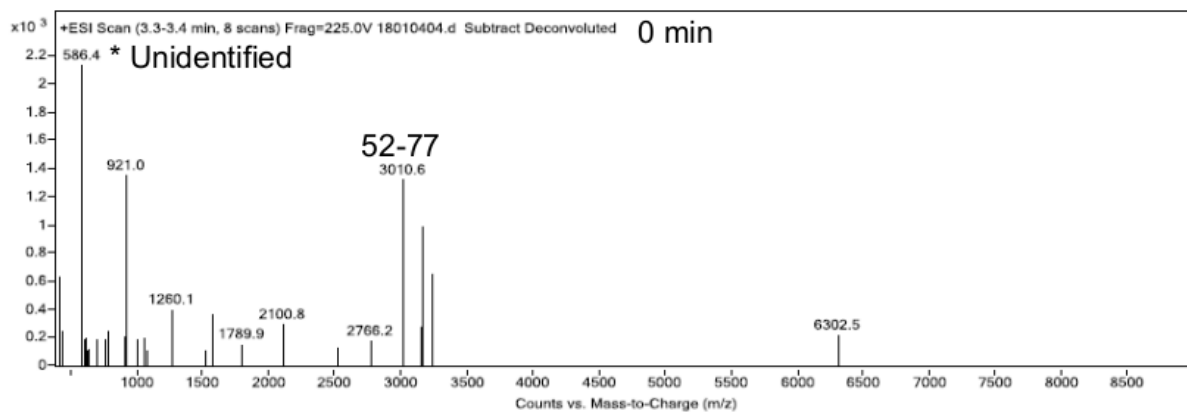
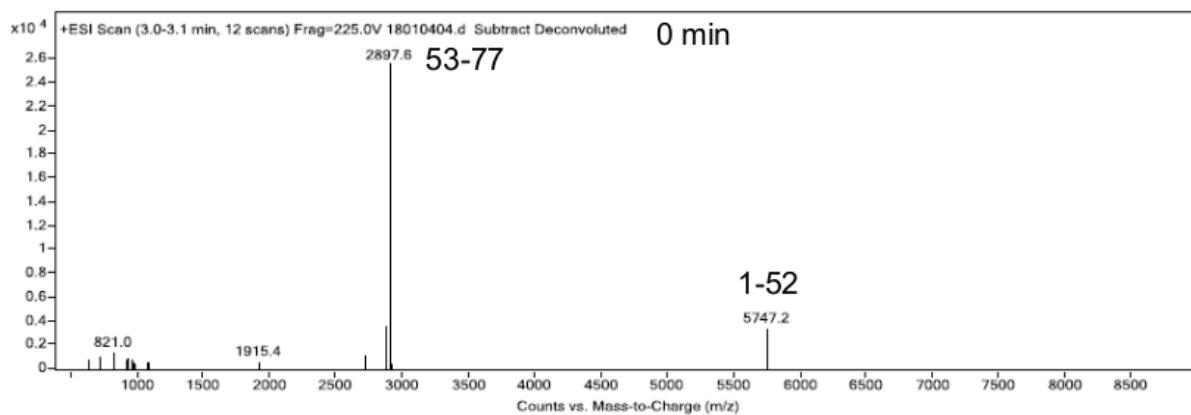
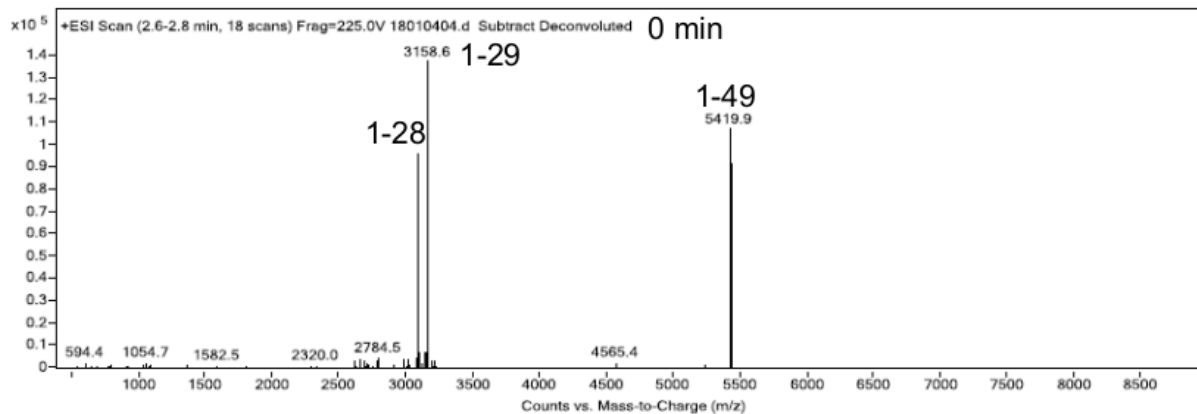




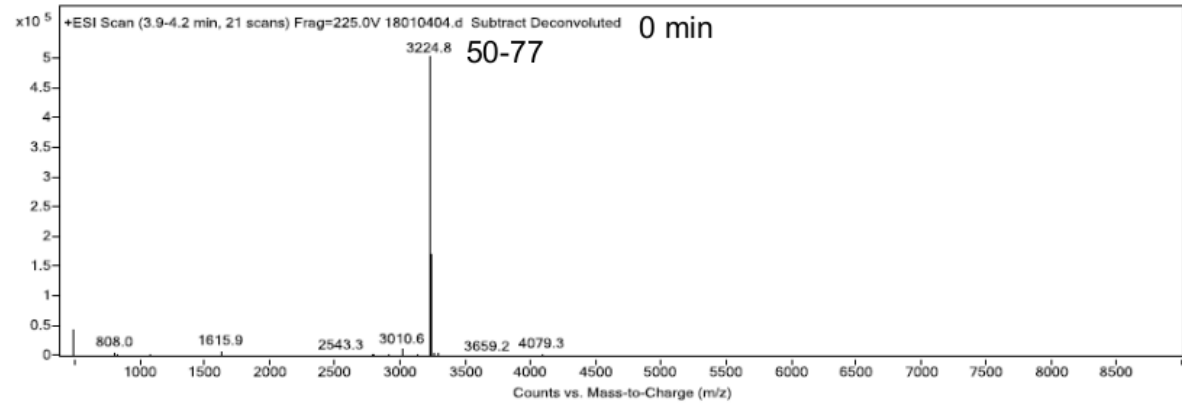
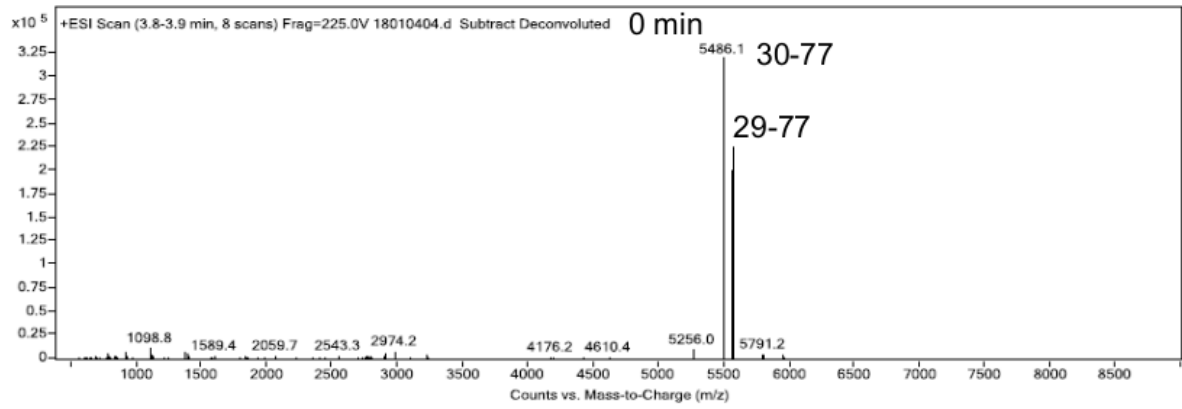
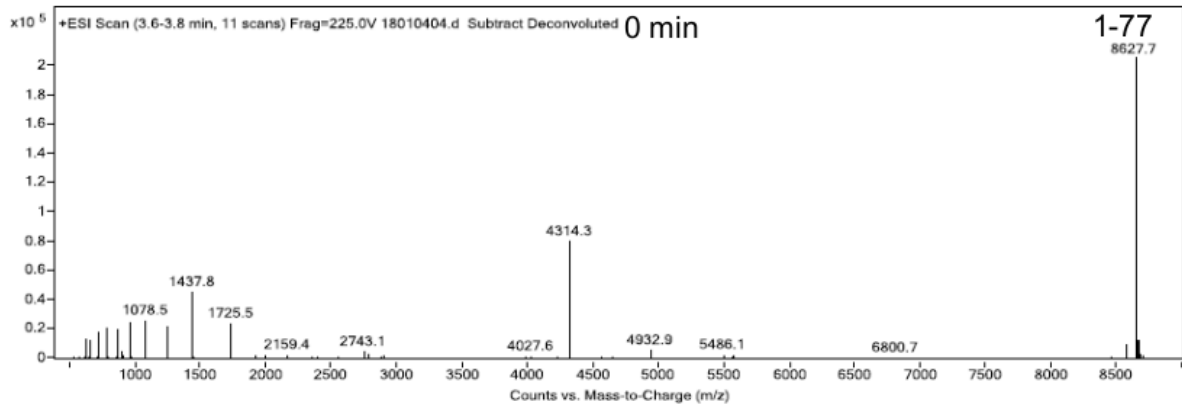
**Appendix 2:** Mass spectrometry data of cTnI<sub>1-77</sub> proteolysed by calpain-2 at time points from 0 min to 24 h.

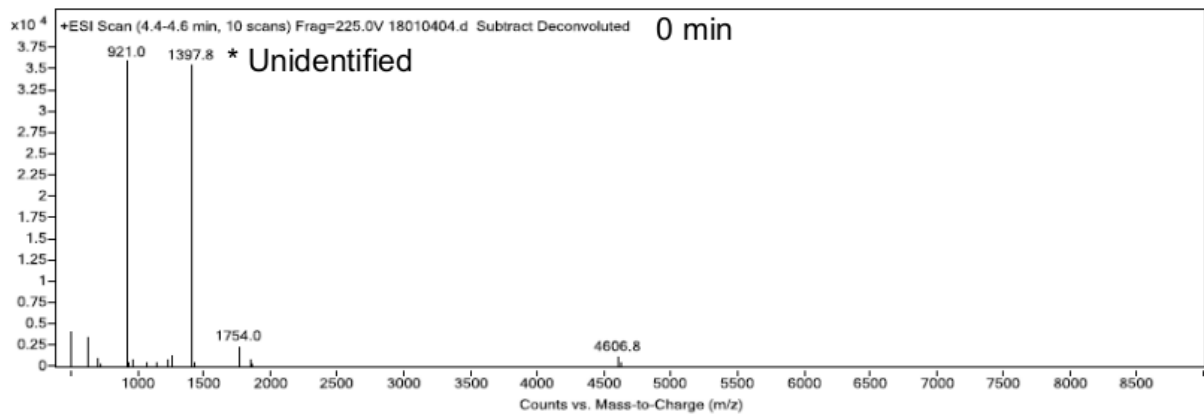
### Proteolysis of cTnI<sub>1-77</sub> by calpain-2

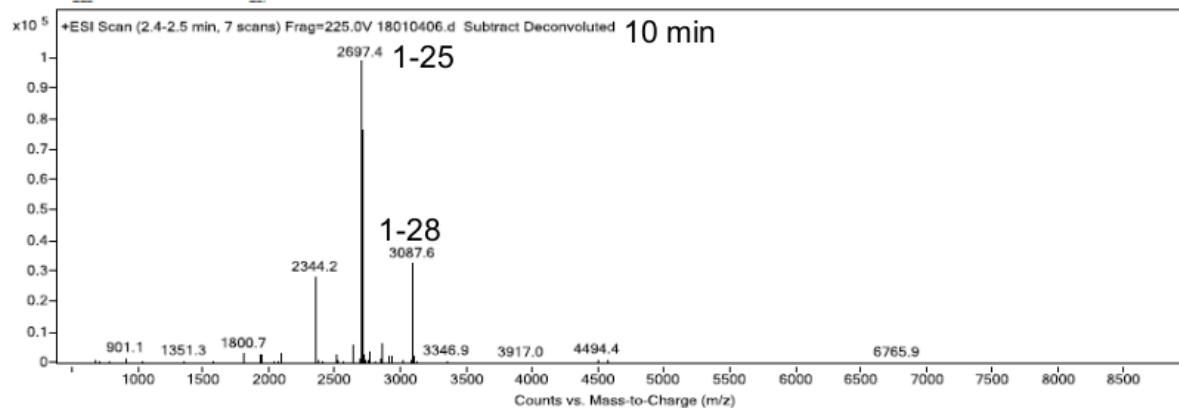
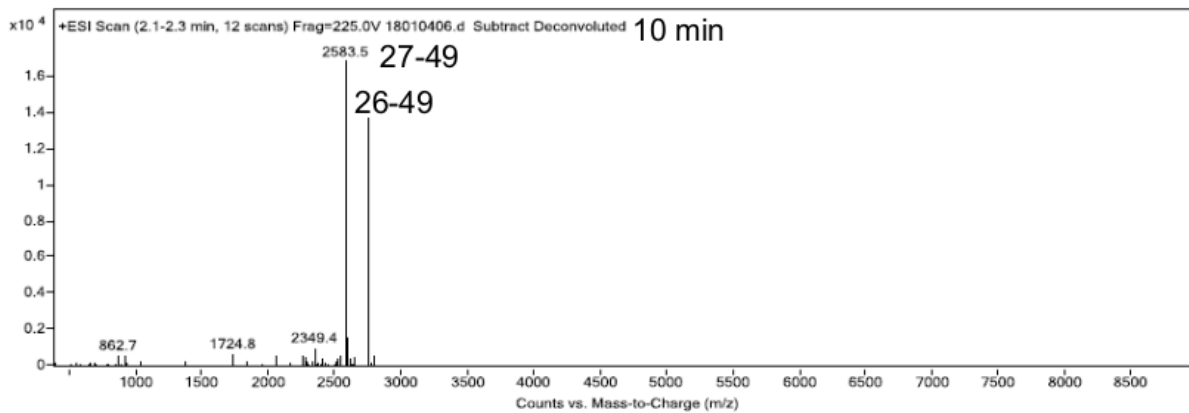
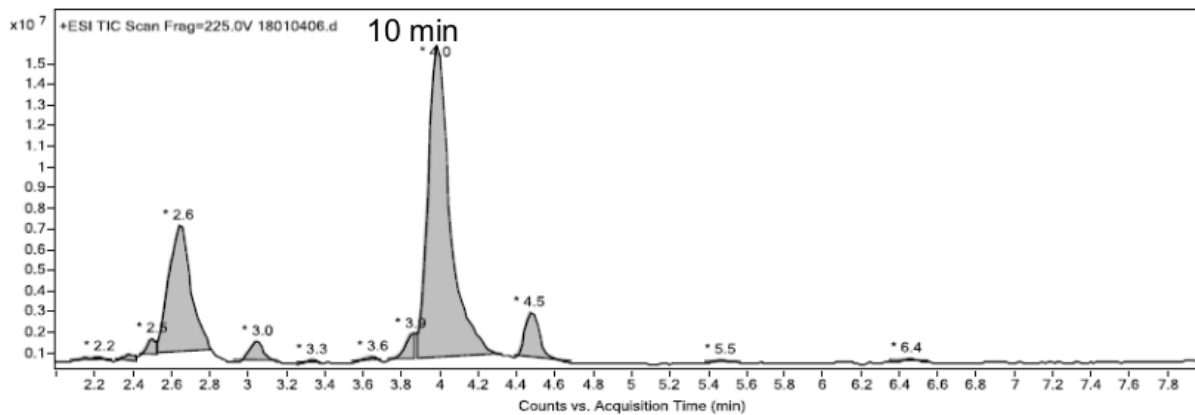


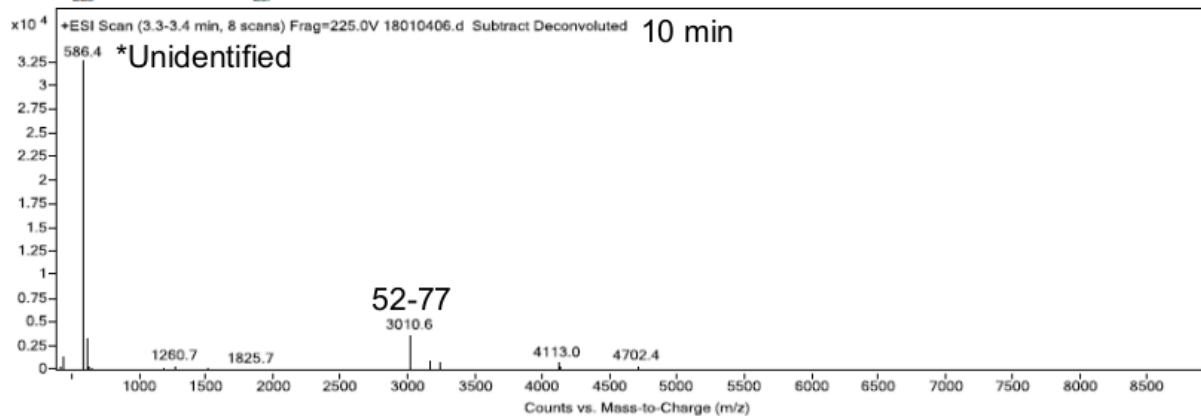
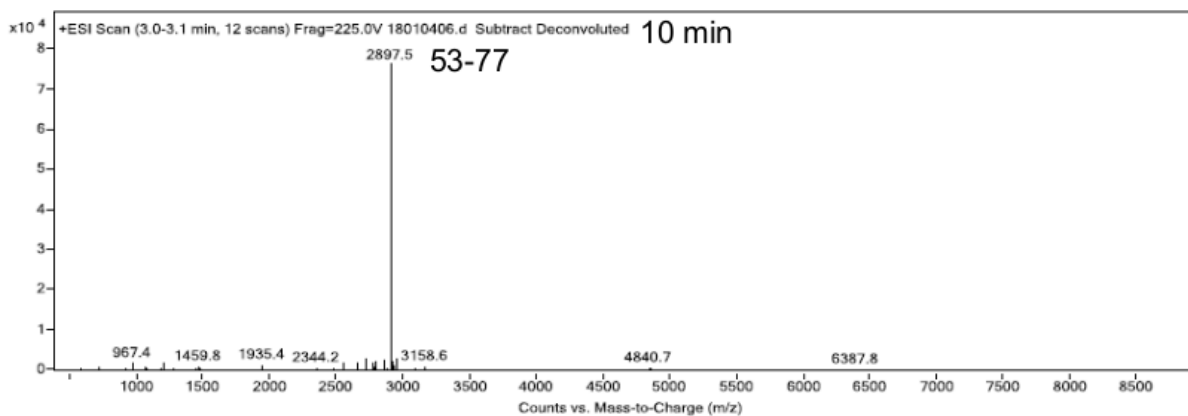
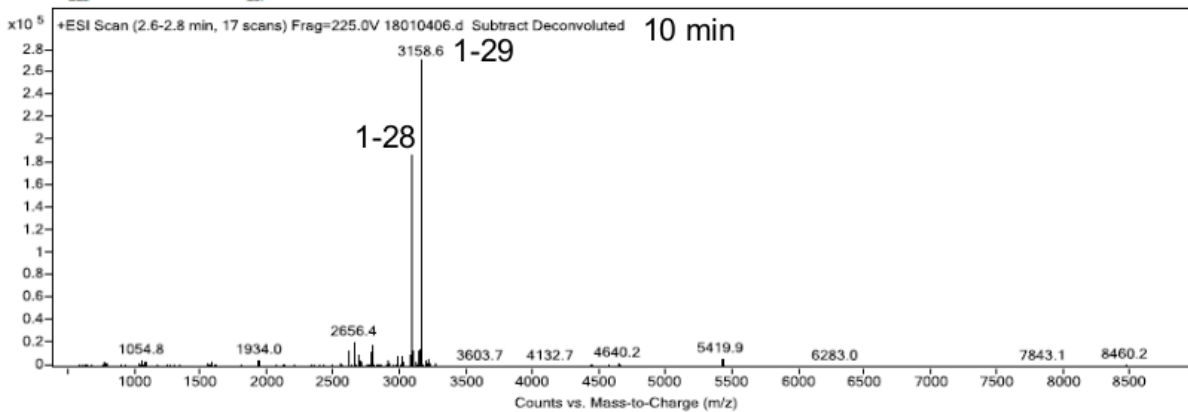


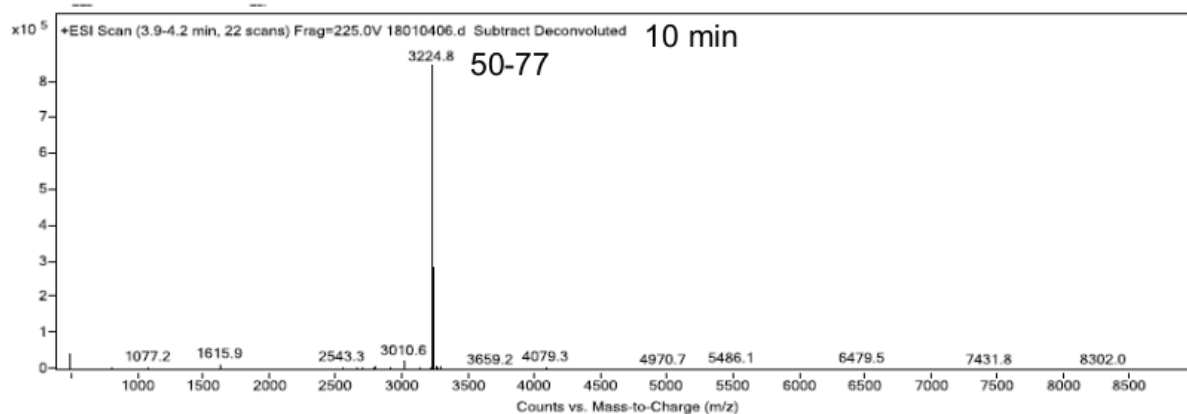
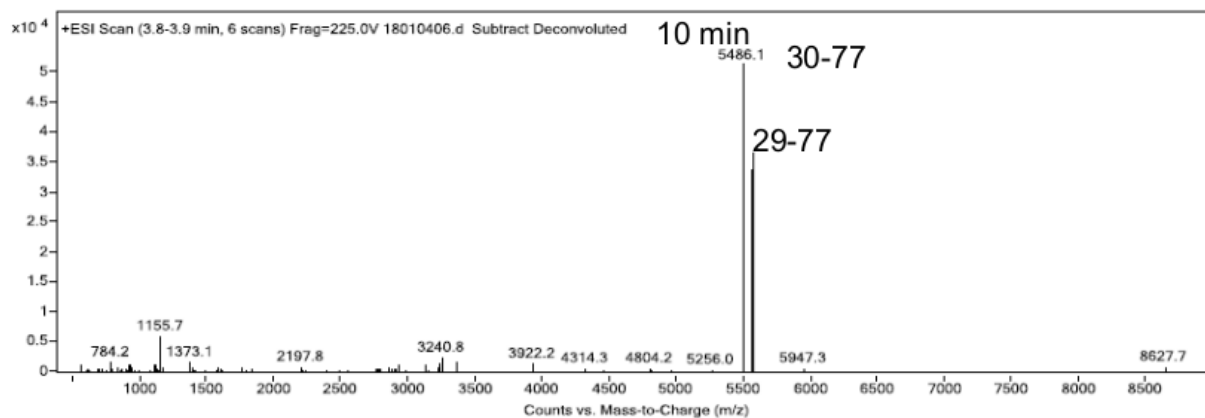
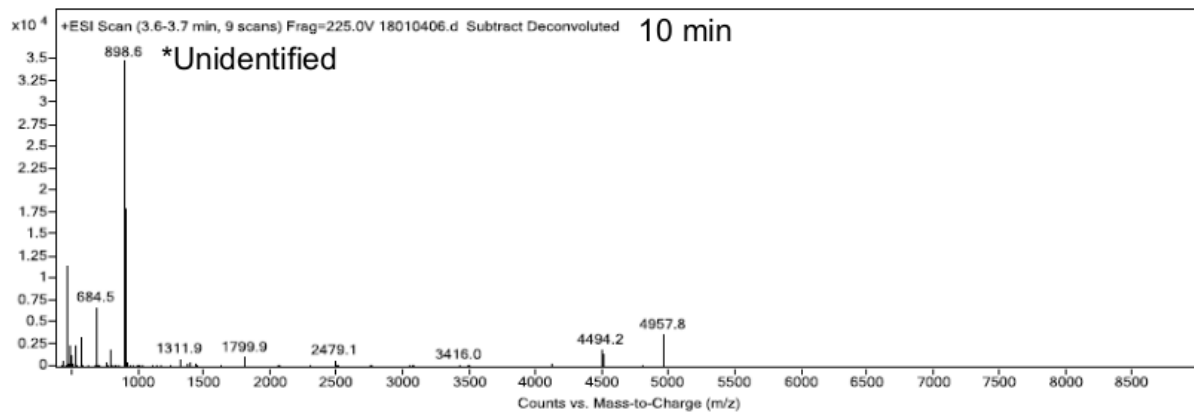


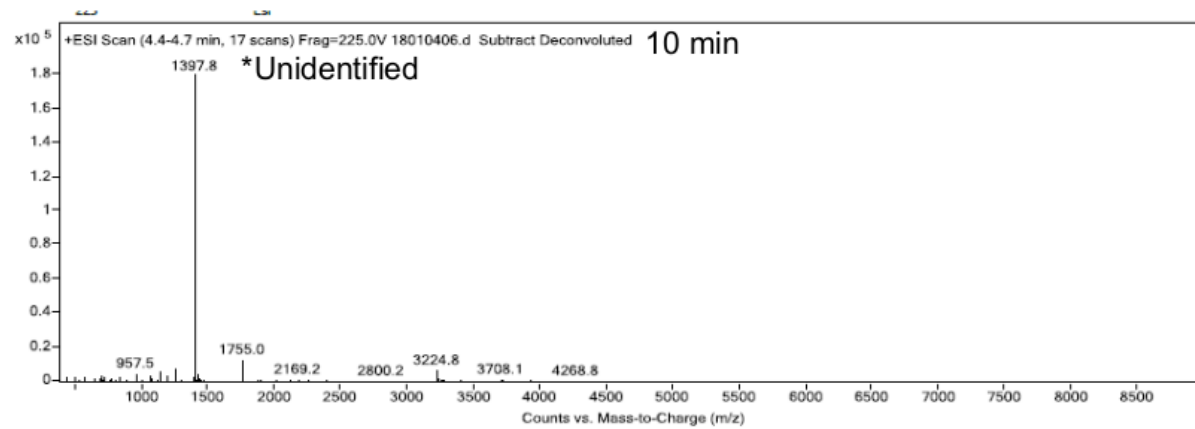


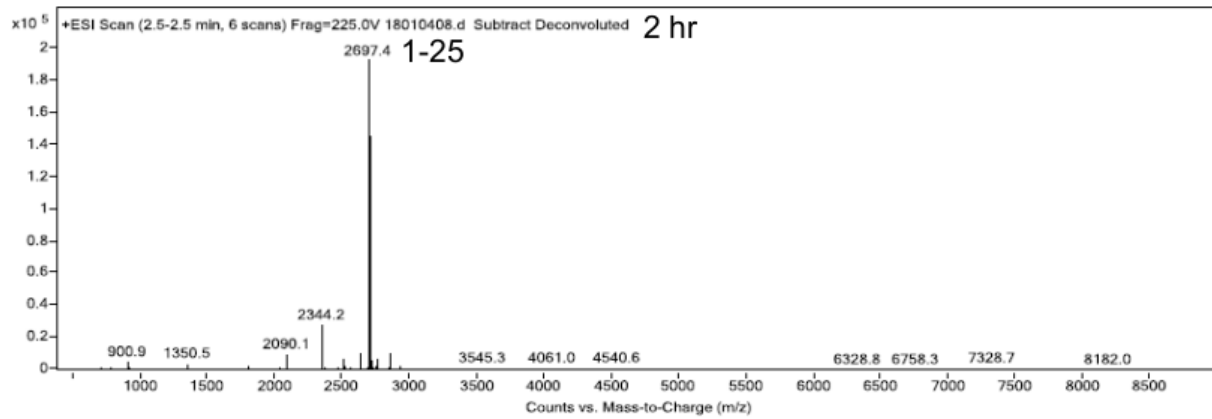
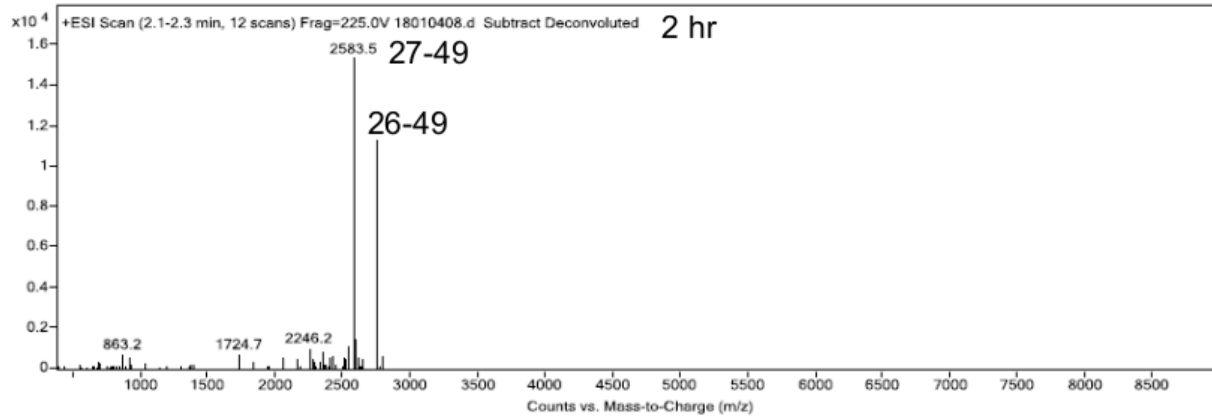
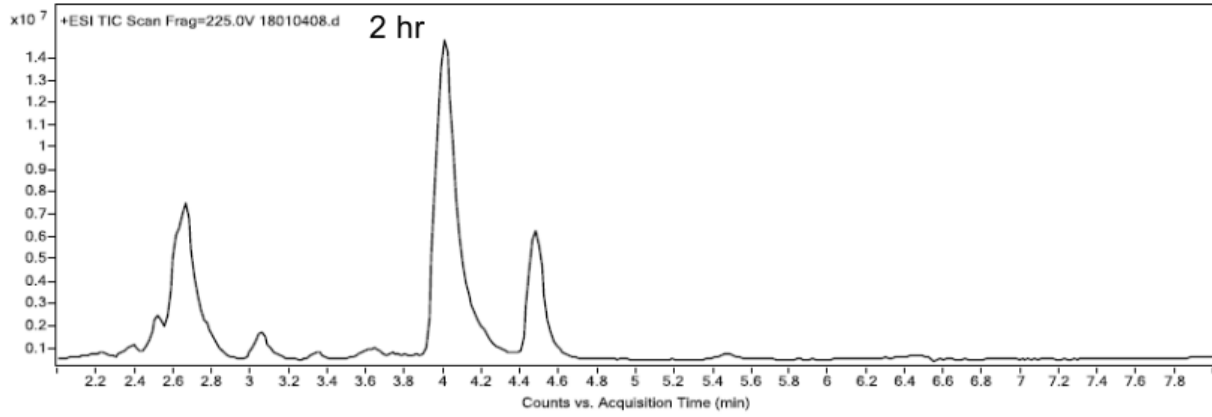


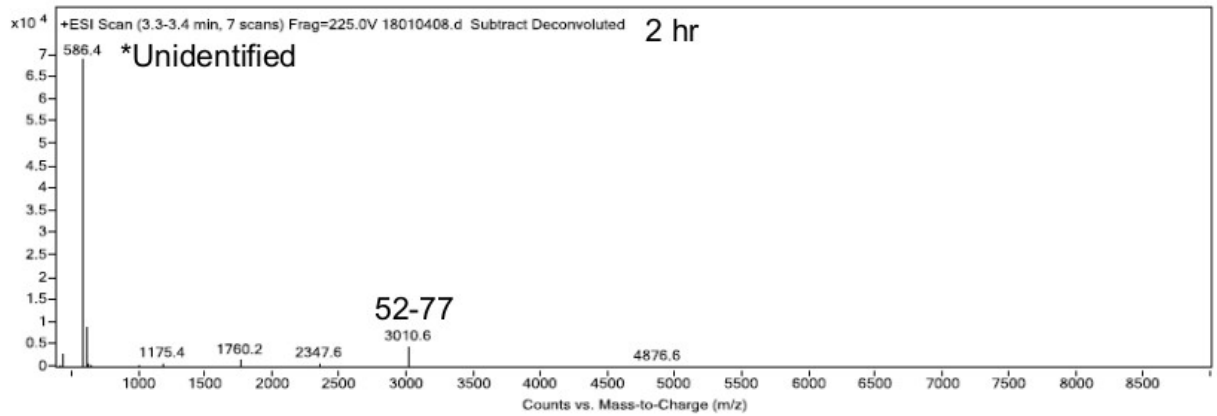
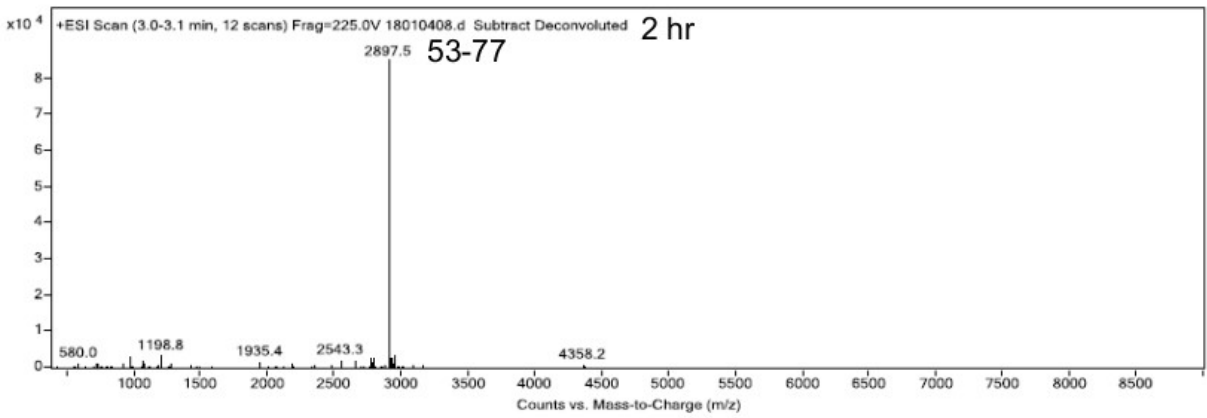
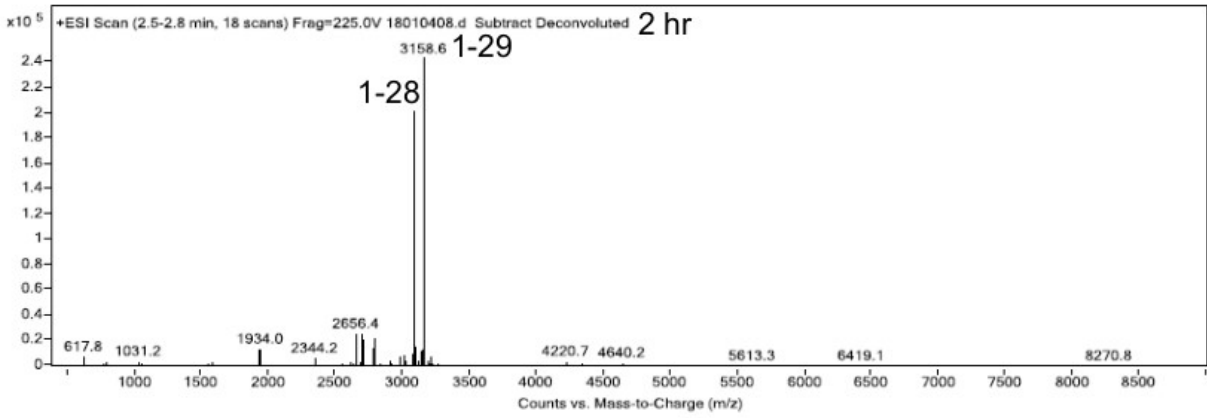




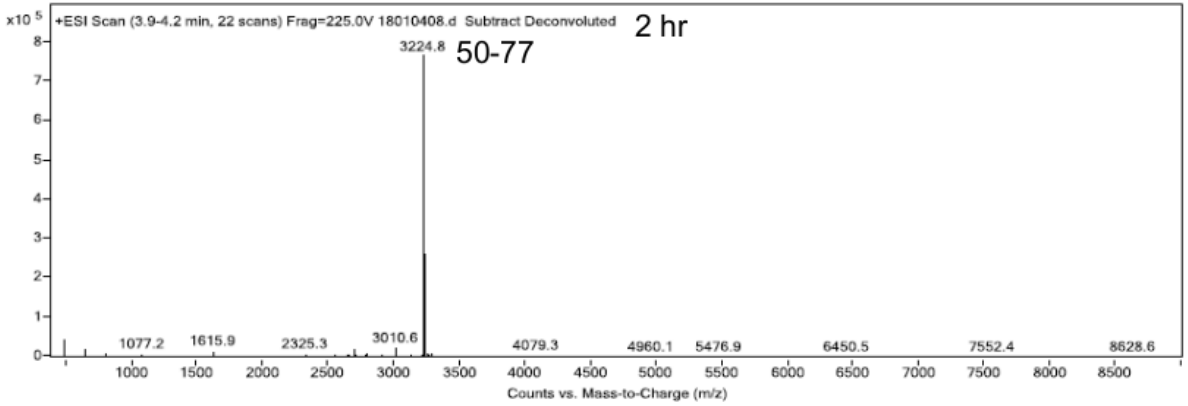
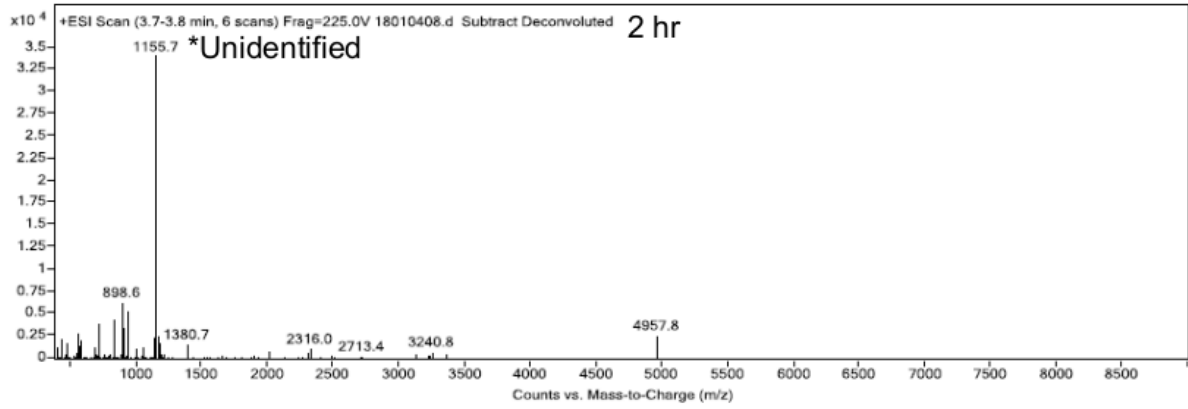
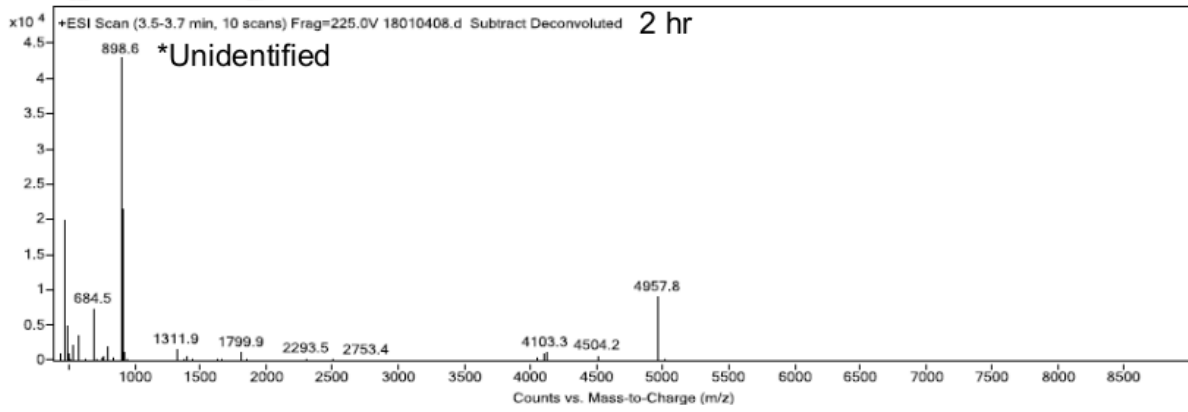


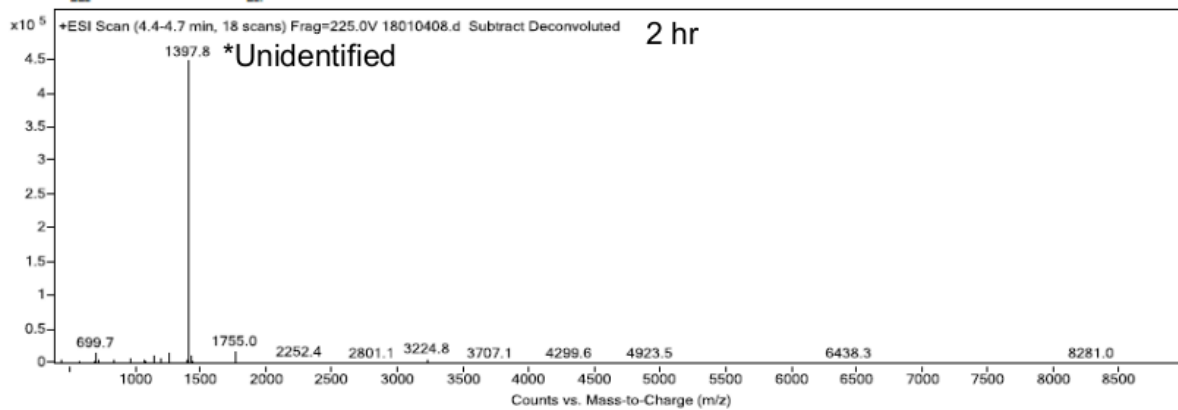


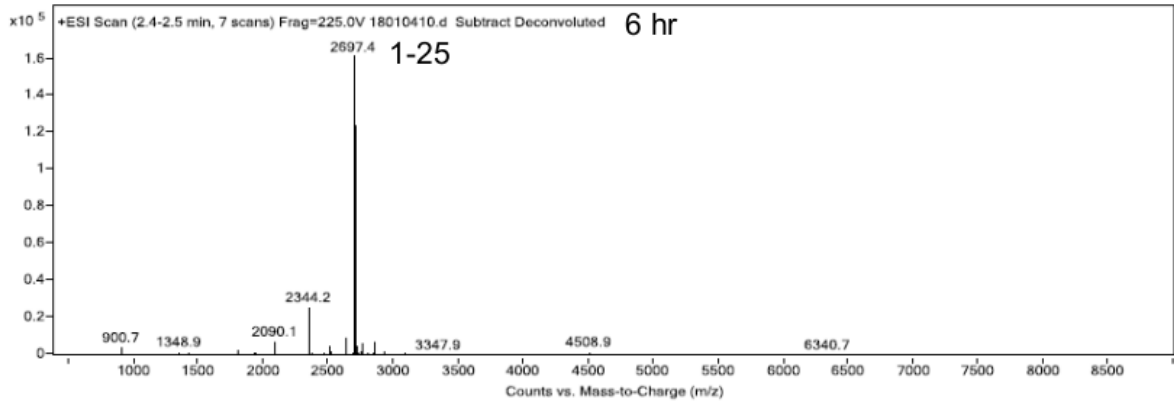
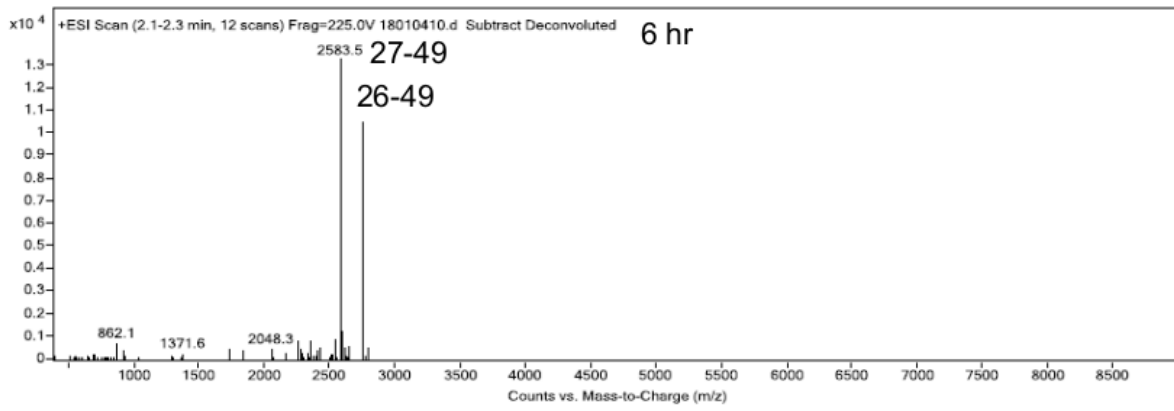
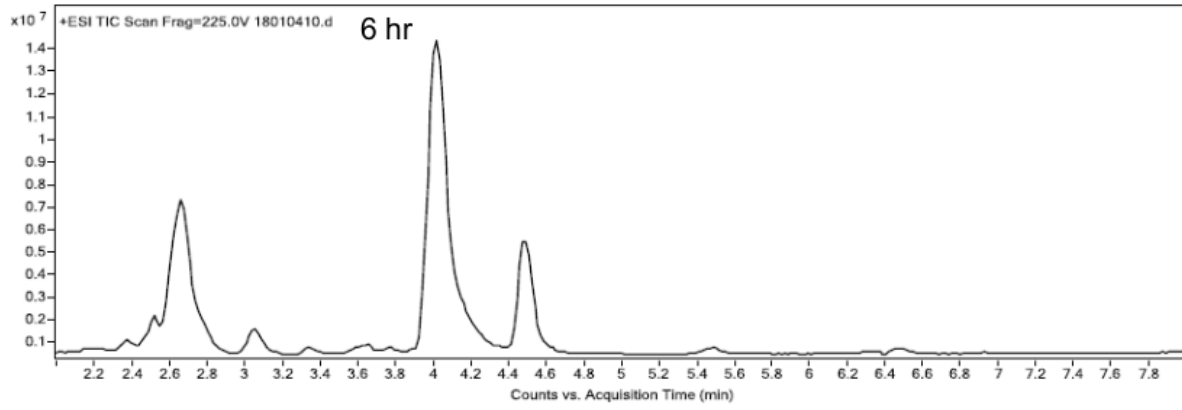


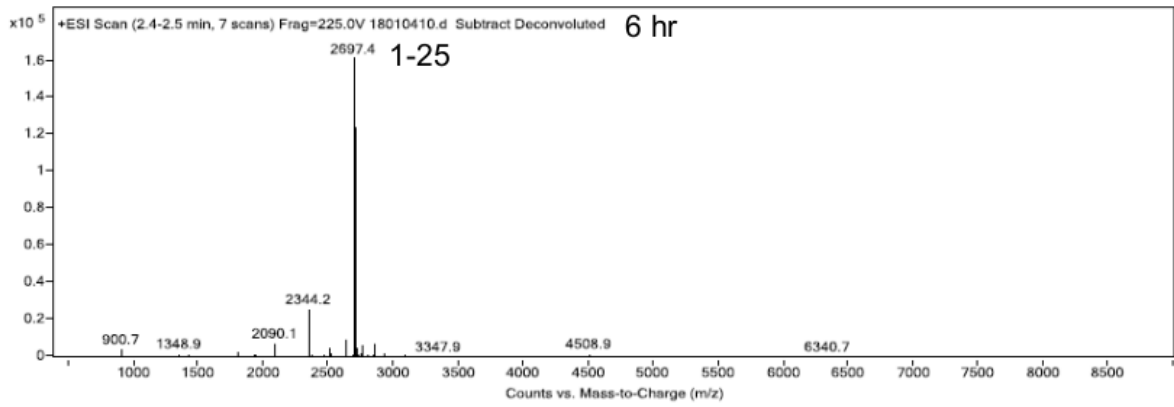
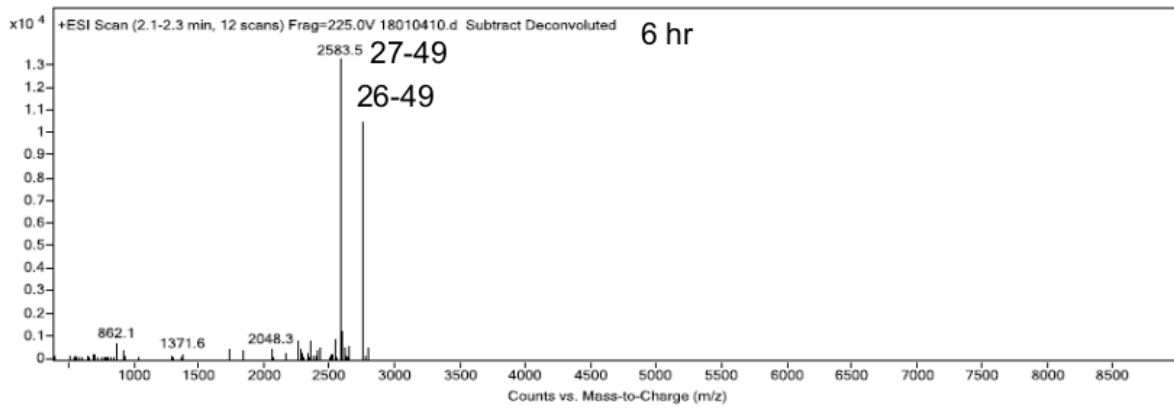
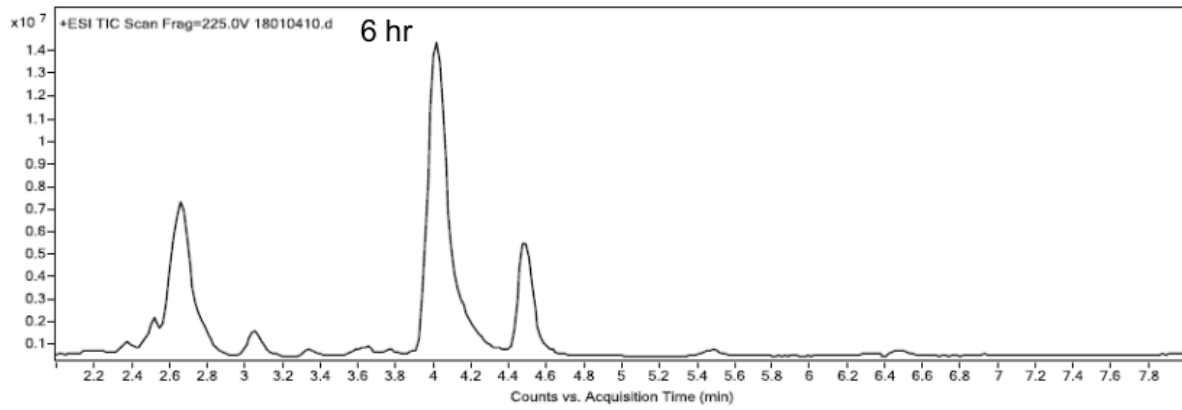


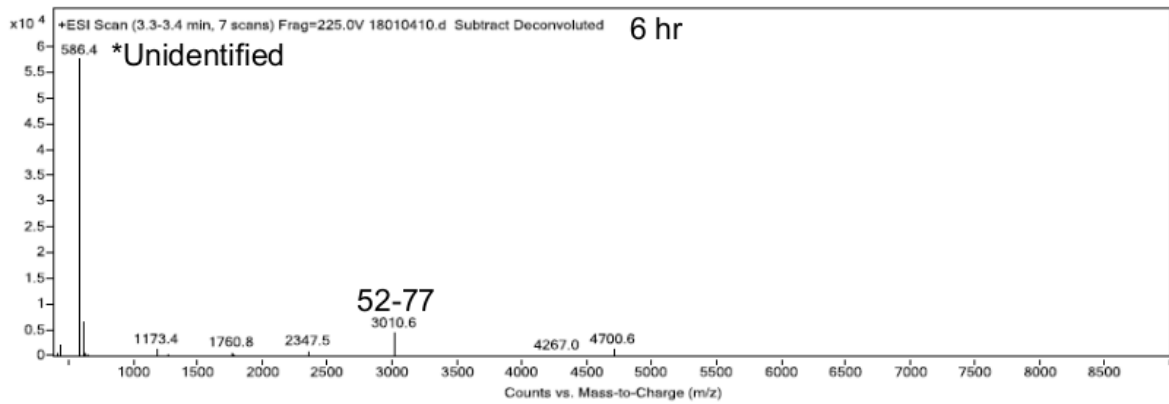
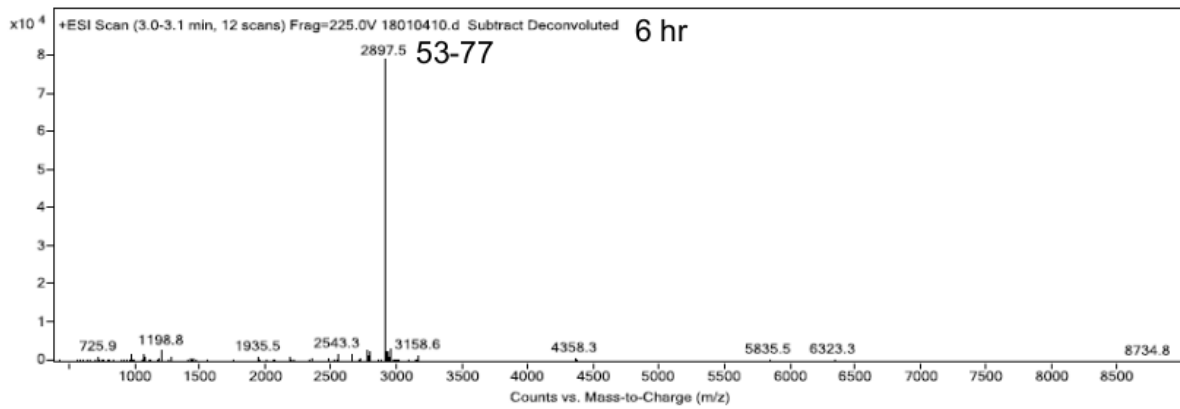
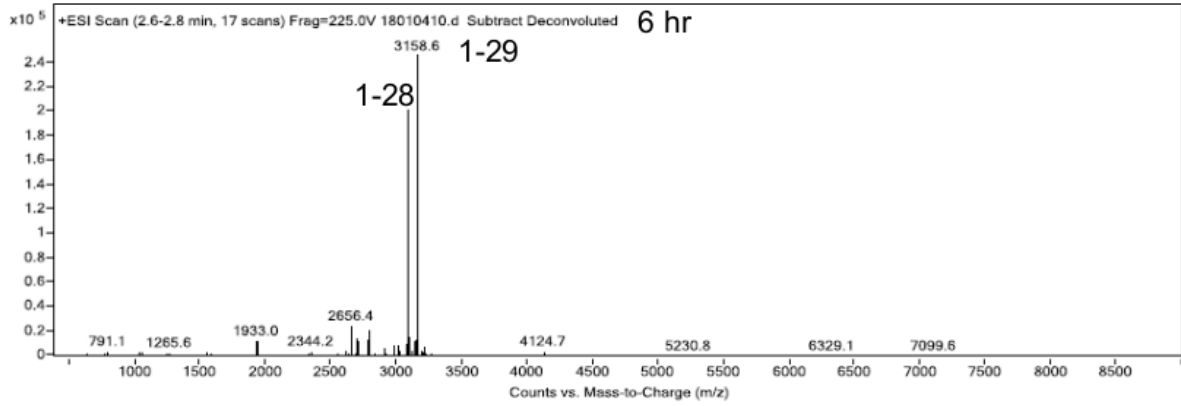


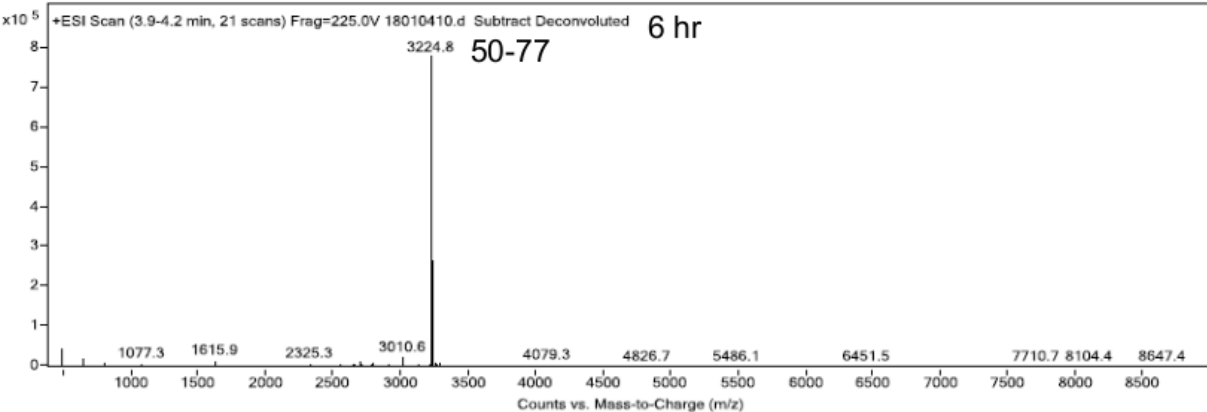
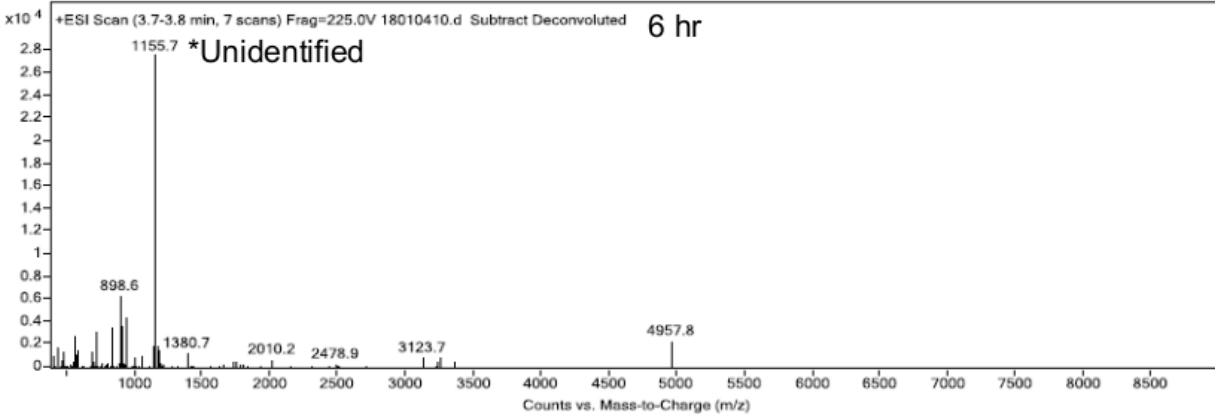
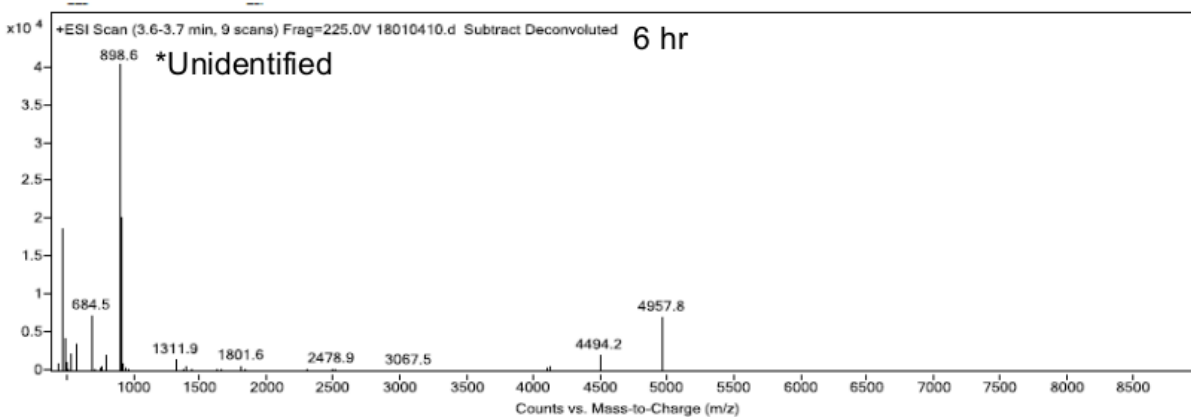


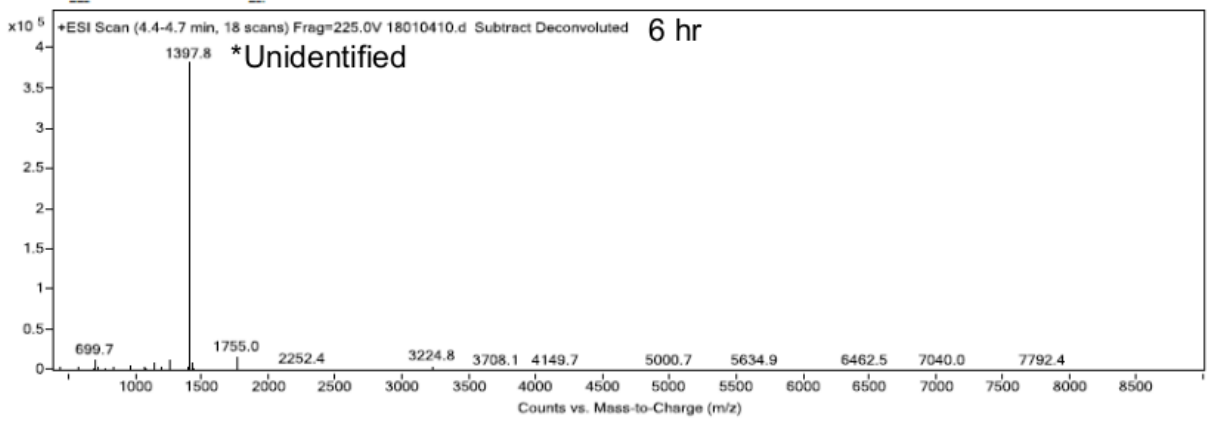


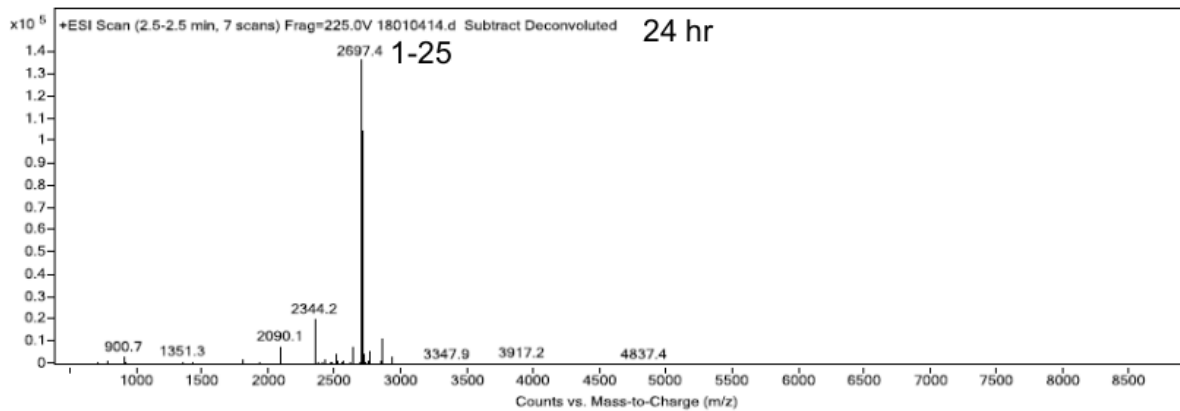
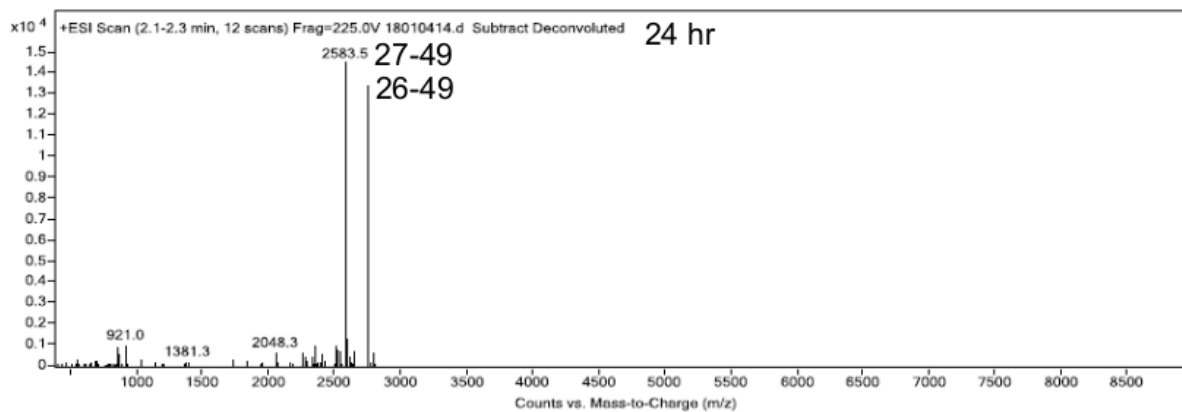
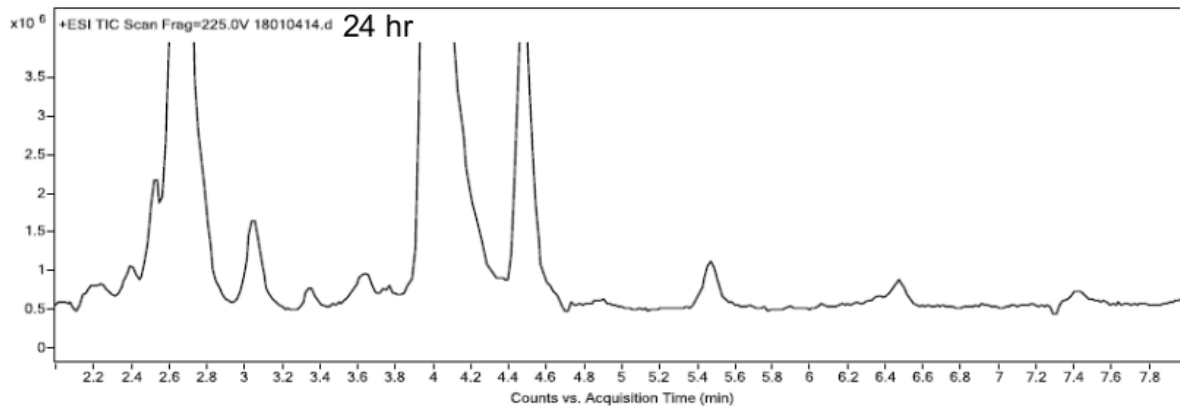




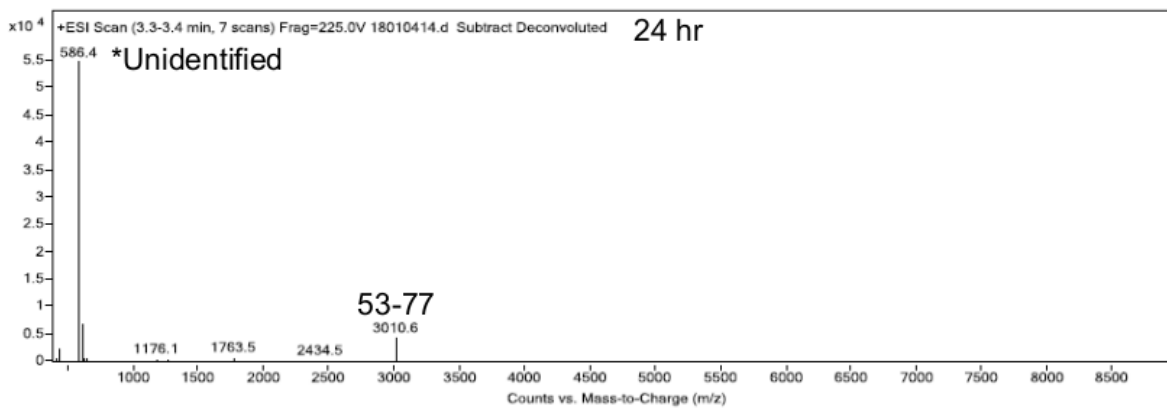
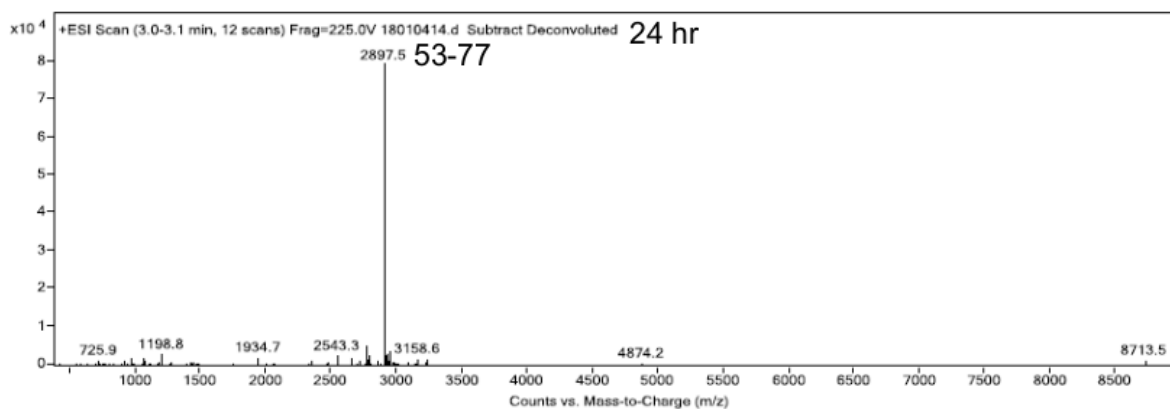
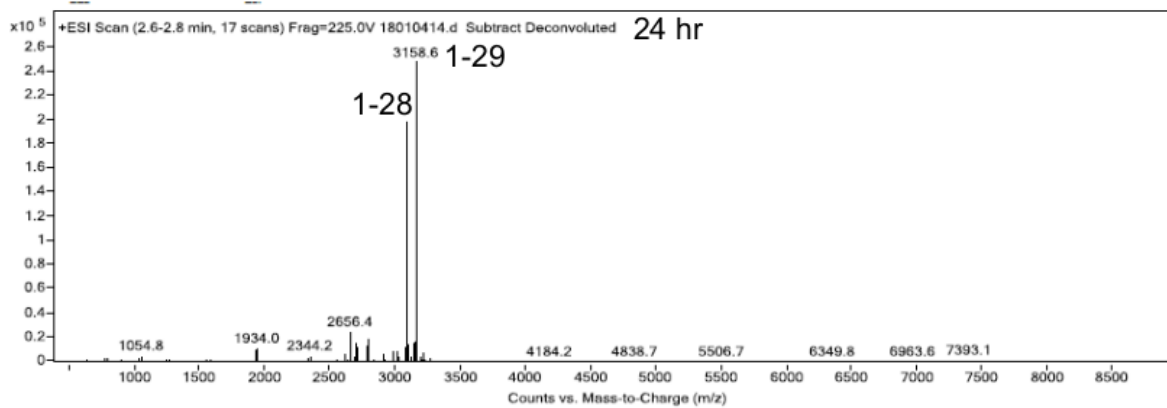


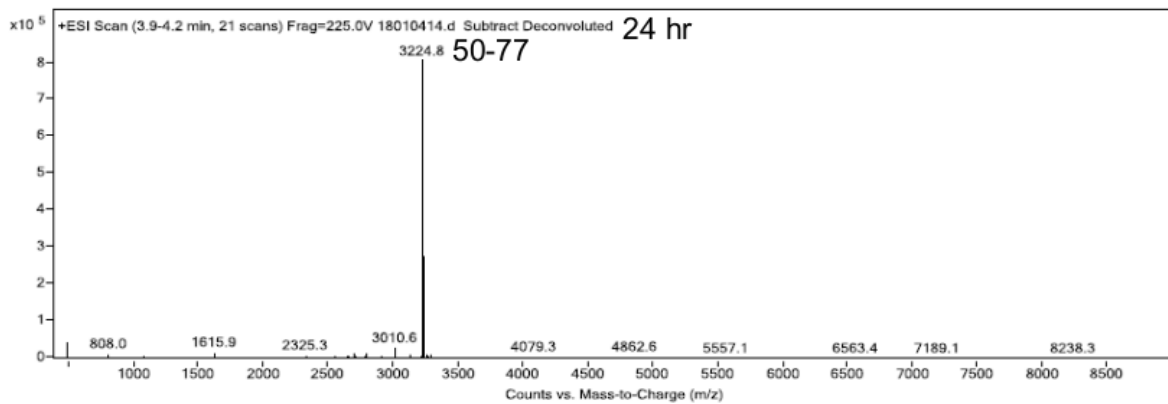
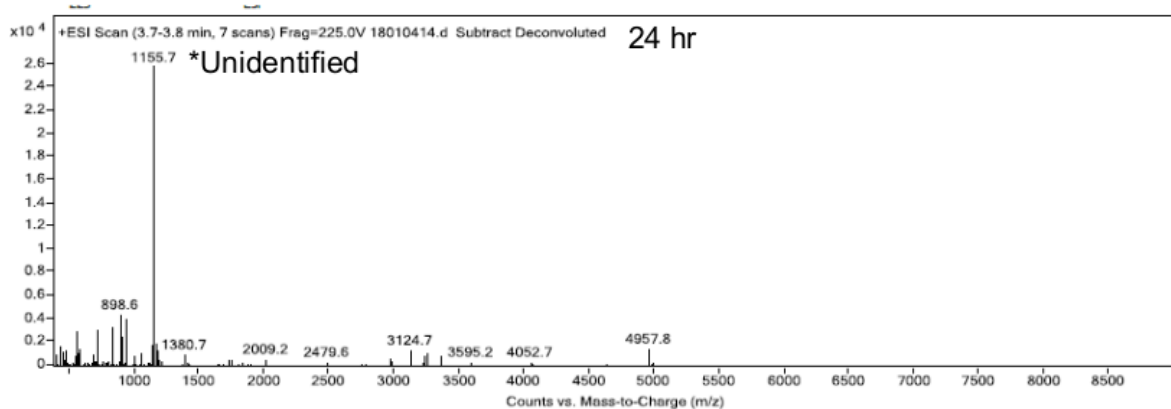
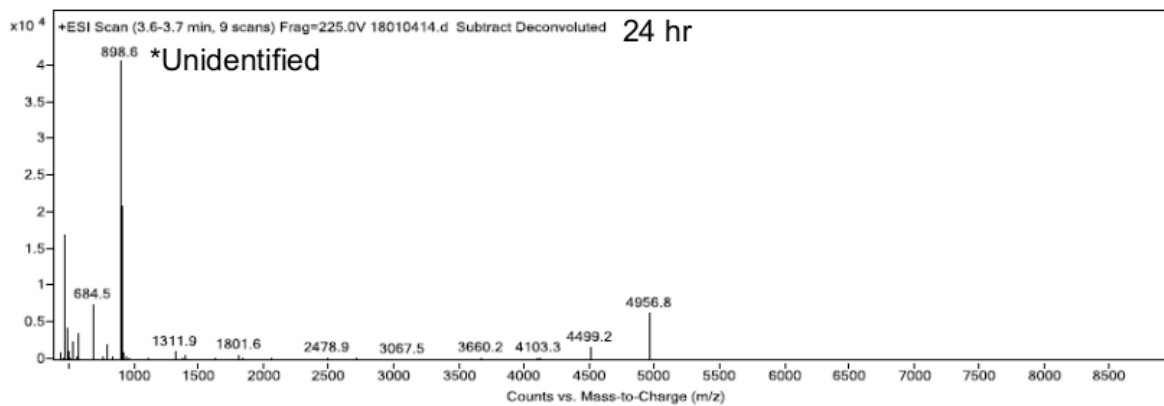


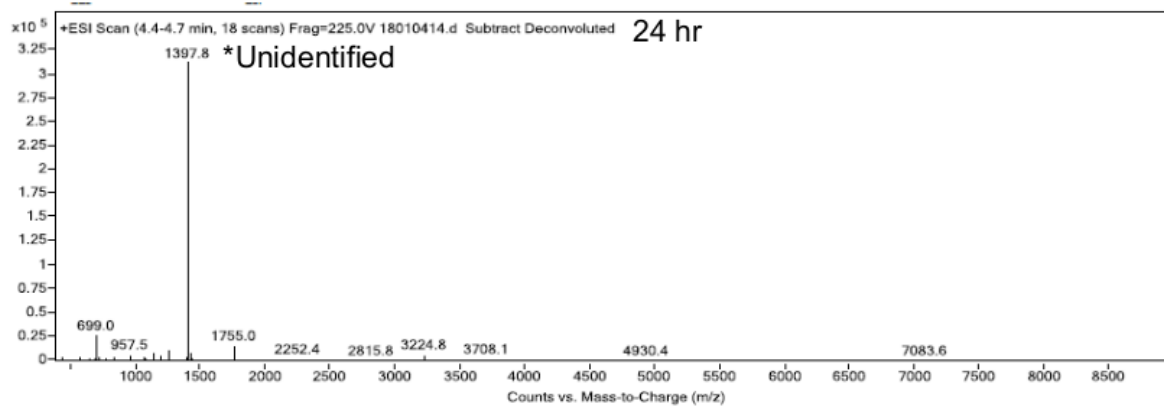












**Appendix 3:** Mass spectrometry data of cTnI<sub>135-209</sub> proteolysed by calpain-2 at time points from 0 min to 24 h.

**Proteolysis of cTnI<sub>135-209</sub> by calpain-2**

